UNIVERSITY OF SOUTHAMPTON

FACULTY OF MEDICINE

Cancer Sciences Unit

Volume 1 of 1

The Role of Fc Gamma Receptors in the Activity of Therapeutic Monoclonal Antibodies

by

Robert James Oldham

Thesis for the degree of Doctor of Philosophy

September 2016

UNIVERSITY OF SOUTHAMPTON

ABSTRACT

FACULTY OF MEDICINE

Biomedicine

Thesis for the degree of Doctor of Philosophy

THE ROLE OF FC GAMMA RECEPTORS IN THE ACTIVITY OF THERAPEUTIC MONOCLONAL ANTIBODIES

Robert James Oldham

Fc gamma receptors (FcγRs) are the major family of receptors responsible for interacting with immunoglobulin G (IgG). They are known to be required for the anti-tumour activity of direct targeting mAbs through expression on NK cells and macrophages. Furthermore, recent work has suggested that cross-linking via FcγRs is required for the activity of agonistic, immune modulatory mAb. This thesis sought to investigate the requirement for these receptors for different aspects of mAb activity; from T cell activation to tumour depletion, using a combination of *in vitro* and *in vivo* systems.

A panel of CHO-K1 cells were generated and transfected to express the polymorphic variants of human FcγRs. These were characterised for their ability to bind IgG before being used as feeder cells in T cell proliferation assays. The assays found that cross-linking of the anti-CD28 mAb, TGN1412 by FcγRIIb (CD32b) or FcγRIIa (CD32a) but not FcγRIIIa (CD16a) transfected cells induced T cell proliferation. Furthermore, this was accompanied by the release of pro-inflammatory cytokines including TNF-α, IFN-γ and IL-2. With the importance of cross-linking via CD32b demonstrated, experiments probed the mechanism of expression using Ramos and Raji cells. These experiments investigated the gene and promoter sequences as well as the effect of epigenetic inhibitors, however further investigation is required.

Next a novel mouse model was developed to investigate the efficacy of anti-human (h)CD20 mAbs. The type II mAb obinutuzumab was found to give prolonged tumour clearance compared to the type I rituximab in a fully syngeneic model with the target antigen expressed on malignant and normal B cells. The use of immune compromised mice confirmed that activatory FcγRs were required for efficient anti-CD20 mediated tumour clearance. Further experiments demonstrated that anti-CD20 mAbs could be combined with the PI3Kδ inhibitor, GS9820, to prolong tumour clearance. These experiments unexpectedly revealed that hIgG1 had an abnormally short half-life in NOD SCID mice, causing the basis for this to be examined as NOD SCID mice are widely used for immunotherapy experiments, particularly patient derived xenografts. Further investigations found that half-life could be restored through genetic deletion of mouse CD32 or by reconstitution with IgG. The polymorphic variant of CD32 found in NOD SCID mice had a higher affinity for hIgG1 which could explain the short half-life.

Overall the results presented here demonstrate the multiple roles played by FcγRs in the many aspects of mAb immunotherapy, from effector cell activation to cross-linking and altering mAb half-life. This knowledge will help guide the next generation of therapeutic mAbs

Table of contents

List of figures

List of tables

Declaration of Authorship

I, **Robert James Oldham** declare that this thesis and the work presented in it are my own and has been generated by me as the result of my own original research.

The Role of Fc Gamma Receptors in the Activity of Therapeutic Monoclonal Antibodies

I confirm that:

1. This work was done wholly or mainly while in candidature for a research degree at this University;
2. Where any part of this thesis has previously been submitted for a degree or any other qualification at this University or any other institution, this has been clearly stated;
3. Where I have consulted the published work of others, this is always clearly attributed;
4. Where I have quoted from the work of others, the source is always given. With the exception of such quotations, this thesis is entirely my own work;
5. I have acknowledged all main sources of help;
6. Where the thesis is based on work done by myself jointly with others, I have made clear exactly what was done by others and what I have contributed myself;
7. Parts of this work have been published as stated below

Work investigating the Tcl-1 model in hCD20 Tg mice:
Tipton TR, Roghanian A, Oldham RJ, Carter MJ, Cox KL, Mockridge CI, et al. Antigenic modulation limits the effector cell mechanisms employed by type I anti-CD20 monoclonal antibodies. Blood. 2015;125(12):1901-9.

T cell proliferation assays and CHO-K1 assays contributed towards data in:
Hussain K, Hargreaves CE, Roghanian A, Oldham RJ, Chan HT, Mockridge CI, et al. Upregulation of FcgammaRIIb on monocytes is necessary to promote the superagonist activity of TGN1412. Blood. 2015;125(1):102-10.

Signed: .....

Date: .....

Acknowledgements

I would firstly like to thank my supervisors; Prof Mark Cragg without whose guidance this work would not have come together. Thank you for your thorough and constructive proof reading of this thesis, I will always be proud of the 1 paragraph out of the ~250 pages in this thesis commented with 'good stuff'! Also to Dr Ali Roghanian for guiding me through lab work, particularly when starting out. I would also like to thank Dr Kirsty Harper and Huntingdon Life Sciences/Enivgo as well as Jakob, Barbara and the rest of the CMC bioassay team for making me feel welcome during my placement. Without the funding from the MRC and HLS I would not have been able to carry out this project.

Thanks also go to everyone in Tenovus who has helped over the years, particularly to the BRF staff for their training and technical assistance, even if I did get bitten to…..! Additionally I would like to thank Dr Kam Hussain for teaching me the proliferation assays in this thesis as well as providing reagents and samples used throughout. Thanks also go to Dr Chantal Hargreaves for help with qPCR, Dr Ian Mockridge for Biacore, Dr Claude Chan for molecular biology guidance and to Dr Patrick Duriez for help in protein production and purification. Finally thanks to Dr Matt Carter for help with all things Tcl-1 and to Kerry Cox for doing countless injections and palpations.

The last 4 years haven't always been easy and I must mention both my Grandads and Alex, my lifelong friend who were there at the start of this journey but sadly passed away before the end and are much missed. Most importantly, I would also like to thank all those people who have kept me sane, particularly to Ruth, Kirstie and Muchaala for providing the laughs and emergency cupcakes needed to get me through, as well as to everyone else I have shared an office with. I also thank my family for all their support and encouragement, even if they don't really understand much of what I do! Finally, A huge thank you must go to my wife, Hannah for putting up with me during the writing of this thesis, even during some of my more grumpy days, as well as for though proof reading and (mostly) helpful comments and suggestions.

Definitions and Abbreviations

2-ME	2-MercaptoEthanol
6xHIS	6x Histidine tag
ADCC	Antibody dependent cellular cytotoxicity
ADCP	Antibody dependent cellular phagocytosis
AID	Activation induced cytidine deaminase
AML	Acute myeloid leukaemia
ANOVA	Analysis of variance
APC	Allophycocyanin
BCR	B cell receptor
BMDMs	Bone marrow derived macrophages
BSA	Bovine serum albumin
BTK	Brutons tyrosine kinase
CAR	Chimeric antigen receptor
CDC	Complement mediated cytotoxicity
cDNA	Complementary DNA
CDR	Complementarity determining region
Cetux	Cetuximab
CFSE	Carboxyfluorescein succinimidyl ester
$C_{H/L}$	Heavy/light chain constant domain
CHO-K1 (cells)	Chinese Hamster Ovary-K1
CLL	Chronic lymphocytic leukaemia
CML	Chronic myeloid leukaemia
CNV	Copy number variation
CO_2	Carbon Dioxide
Cp	Crossing point
CTL	Cellular Technologies Limited
CVF	Cobra venom factor
Da	Daltons
DC	Dendritic cell
DLBCL	Diffuse large B cell lymphoma
DMSO	Dimethyl sulfoxide
DNA	Deoxyribose nucleic acid
dNTPs	Deoxynucleotide triphosphate
DTT	Dithiothreitol
E. coli	Escherichia coli
EDTA	Ethylenediaminetetraacetic acid
EGFR	Epidermal growth factor receptor
ELISA	Enzyme linked immunosorbent assay
ERK	Extracellular signal-related kinase

F(ab)	Fragment antigen-binding
FACS	Fluorescence activated cell sorting
FAM	6-fluorescein amidite
Fc	Fragment crystallisable
FcRn	Neonatal Fc receptor
FCS	Foetal calf serum
FcγR	Fcγ Receptor
FDA	US Food and Drug Administration
FITC	Fluorescein isothiocyanate
FL	Follicular lymphoma
FSC	Forward scatter (in flow cytometry)
FT	Flowthrough
GM-CSF	Granulocyte-macrophage colony-stimulating factor
GP	L-Glutamine and Sodium pyruvate
GTP	Guanosine triphosphate
GVHD	Graft versus host disease
hCD_	Human CD molecule
HEK	Human embryonic kidney
hIgG	Human immunoglobulin G
HLS	Huntingdon Life Sciences
HPLC	High performance liquid chromatography
HPV	Human papilloma virus
HRP	Horseradish peroxidase
i.p	intraperitoneally
i.v.	Intravenously
IC	Immune complex
IFN-γ	Interferon gamma
IgG	Immunoglobulin G
IL-_	Interleukin_
IPF	Idiopathic pulmonary fibrosis
ITAM	Immunoreceptor tyrosine-based activation motif
ITIM	Immunoreceptor tyrosine-based inhibitory motif
ITP	Immune thrombocytopenic purpura
IVC	Individually ventilated cages
IVIG	Intravenous immunoglobulin
K_A	Affinity constant
KD	Dissociation constant
LB	Lysogeny broth
LPS	Lipopolysaccharide
mAb	Monoclonal antibody
MAC	Membrane attack complex
MAPK	Mitogen-activated protein kinase

mCD_	Mouse CD molecule
MCP-1	Monocyte chemotaxic protein 1
M-CSF	Macrophage colony-stimulating factor
MFI	Mean fluorescence intensity
MHC	Major histocompatibility complex
MIP1	Macrophage inflammatory protein 1
MMP	Matrix metalloprotease
mRNA	Messenger RNA
MSD	Meso scale discovery
n.s	Non-significant
NHL	Non-hodgkin lymphoma
NK (cell)	Natural Killer cell
NOD	Non-obese diabetic
NOTAM	FcR γ-chain signalling deficient mice
NQ	N297Q mutated IgG1
NSG (mice)	NOD SCID IL2 γ-/-
OBZ	Obinutuzumab (GA101)
PBMCs	Peripheral blood mononuclear cells
PBS	Phosphate buffered saline
PCR	Polymerase chain reaction
PDX	Patient derived xenograft
PE	Phycoerythrin
PEI	polyethylenimine
PI	Propidium Iodide
PI3Kδ	Phosphoinositide 3-kinase, delta isoform
PKC	Protein kinase C
PLCγ	Phospholipase C-gamma
PMN	Polymorphic mononuclear cell
PNGase F	Peptide -*N*-Glycosidase F
PS	Penicillin and Streptomycin
qPCR	Quantitative PCR
RA	Rheumatoid arthritis
RNA	Ribose nucleic acid
RPMI (media)	Roswell Park Memorial Institute
RS	Recombination signal
RT PCR	Reverse transcription PCR
RTX	Rituximab
SCF	Stem cell factor
SCID	Severe combined immune deficient
SD	Standard deviation
SDS	Sodium dodecyl sulphate
SDS-PAGE	Sodium dodecyl sulphate polyacrylamide gel electrophoresis

SEM	Standard error of the mean
SLE	Systemic lupus erythematosus
SLL	Small lymphocytic leukaemia
SOC	Superoptimal broth with catabolite repression
SPR	Surface plasmon resonance (Biacore)
SSC	Side scatter (in flow cytometry)
TAE	Tris-acetate EDTA
Tcl-1	T cell leukaemia 1
TCR	T cell receptor
TE	Trypsin Ethylenediaminetetraacetic acid
Tg	Transgenic
TLR	Toll-like receptor
TNF-α	Tumour necrosis factor alpha
UV	Ultraviolet
VEGF	Vascular endothelial growth factor
$V_{H/L}$	Heavy/light chain variable domain
WBC	White blood cell

Chapter 1 Literature Review

1.1 Cancer as a disease

Cancer is one of the most prevalent conditions in the western world, with more than 1 in 3 people in the UK predicted to develop the disease during their lifetime.[1] In the early 1970's, the one year survival rate for newly diagnosed cancer patients was 50%; in 2011, the same percentage survived for more than 10 years following diagnosis.[2] This improvement in survival has been largely due to improved early diagnosis, as well as the development of more effective treatments. However, this broad increase in survival hides the heterogeneity of the disease and its survival rates which can vary from weeks to decades according to tumour type.

Cancer is an umbrella term used to encompass a broad range of malignancies which can occur throughout the body, resulting from an accumulation of mutations which leads to dysregulated cell behaviour. Each of these diseases arises from a specific tissue or cell type and has its own clinical course and pathology with the classification of a tumour identified by its tissue of origin. Moreover, the tumour cells often retain the identity of the tissue from which they derive, even if they have metastasised elsewhere. Even within a particular cancer type, there can be considerable variation between patients, both in the way the disease progresses and how they respond to treatment. This is often dependent on the stage of diagnosis and the specific mutations accumulated by the tumour, as well as the microenvironment in which the tumour resides. Approaches have been developed to categorise the severity of tumours. In the case of solid malignancies the TMN system is used which independently assesses the size of primary tumour (T), spread into local lymph nodes (N) and presence of metastases (M).[3] Taking into account all these factors, as well as the age and general health of the patient, an informed decision as to the best treatment option can be made.

Despite an increase in the cancer survival rate, the incidence of cancer is increasing. This is largely due to the increase in life expectancy across the world, including in developing countries. Approximately 89% of new cancer diagnoses occur in adults over the age of 50, with 36% of cases in those over the age of 75.[4] Moreover, as life expectancy increases, the incidence of cancer is expected to increase further. As a risk factor, age cannot be prevented, similar to inherited genetic risk factors. Inherited mutations, in particular genes, can increase the likelihood of cancer

developing. For instance, the BRCA1 protein normally functions as a DNA repair protein; when mutated, such as in certain types of breast cancer, DNA cannot be repaired efficiently, allowing the accumulation of further mutations.[5]

Mutated genes such as BRCA1 can be inherited, but mutations commonly occur from exposure to carcinogens over time. Whilst background levels of exposure to carcinogens (such as natural, background radiation) can be difficult to avoid, certain factors such as smoking (lung cancer), exposure to asbestos (mesothelioma) and exposure to UV light (skin cancer) all increase cancer risk. These carcinogens are capable of causing DNA lesions; when these lesions occur in genes that control cell growth and division, tumours can develop.[6] Finally, some cancers are associated with viral infection; for example 70% of cervical cancer cases are thought to be caused by just two types (16 and 18) of human papillomavirus (HPV).[7] HPV proteins can accelerate the cell cycle leading to rapid division, with the HPV E6 protein able to inactivate p53, a key regulator of the cell cycle which will be discussed further in section 1.1.1 .[8] This is just one of a number of mechanisms by which HPV infection can lead to aberrant cell division, ultimately resulting in the formation of tumours.[9]

1.1.1 The Hallmarks of Cancer

Despite a huge degree of heterogeneity in the mechanisms of cancer development, mutational burden and the tissue from which a cancer develops, there are certain features that are common to all cancers. In 2000, Hanahan and Weinberg published their seminal paper describing 'The Hallmarks of Cancer' where they sought to identify and describe the six basic capabilities common to all cancers.[10] The hallmarks are summarised in Table 1.1 and focus on the ability for a tumour to divide rapidly, to modify the microenvironment and to form metastases. The first hallmark is the ability for a tumour to become self-sufficient in growth signals, allowing for rapid growth without relying on signals from other cells. One common example of this is Philidelphia chromosome positive chronic myeloid leukaemia, where patients have a chromosomal translocation resulting in a BCR-Abl fusion protein.[11] This gives an increase in Abl kinase activity, which allows cells to enter the cell cycle even in the absence of the growth factors, granulocyte-colony stimulating factor (G-CSF) and stem cell factor (SCF).[12] This self-sufficiency is accompanied by cells having limitless replication potential, another of the six hallmarks. Combined, these factors allow for sustained rapid cell division.

On the opposite side of cell division is cell death; these two processes normally occur in balance to achieve homeostasis. Typically, this cell death takes the form of apoptosis which functions to remove cells which are damaged or no longer required in a controlled way without damaging the surrounding tissue.[13] However, tumour cells are able to evade normal cell death pathways through the overexpression of anti-apoptotic proteins, such as Bcl-2 and its related proteins, or through the down regulation of pro-apoptotic proteins such as Bim and Puma.[10] It is common in follicular lymphoma (FL) for Bcl-2 to translocate to the IgHV locus, resulting in an overexpression of Bcl-2, promoting cell survival.[14] Consequentially, when this evasion of cell death is combined with accelerated growth, tumour cells will rapidly accumulate.

Original Hallmarks of cancer	Emerging Hallmarks
Self-sufficiency in growth signals	Avoiding immune destruction
Evading growth suppressors	Deregulating cellular energetics
Resisting cell death	Genomic instability and mutation
Tissue invasion and metastasis	Tumour-promoting inflammation
Limitless replicative potential	
Sustained angiogenesis	

Table 1.1 ***The hallmarks of cancer.***
The original 6 hallmarks of cancer were proposed by Hanahan and Weinberg in 2000. These hallmarks focus on the ability for the tumour to overcome normal, regulated cell cycle progression, alter the microenvironment and promote tumour metastases. 11 years later the follow-up paper proposed 4 additional 'emerging hallmarks' which included the ability for a tumour to evade detection and destruction by the immune system.(Hanahan, 2011)

The fast rate of cell division requires a large amount of energy, therefore tumours require an extensive blood supply. Accordingly, serum levels of the pro-angiogenic vascular endothelial growth factor (VEGF) were found to be higher in melanoma patients compared to healthy controls, highlighting the importance of a robust blood supply in tumourigenesis.[15] Despite this increase in blood supply, the availability of oxygen can limit tumour growth. Under these circumstances tumour cells adapt by changing their metabolism through a process known as the Warburg effect.[16] Tumour cells undergo a high rate of glycolysis which generates pyruvate. Rather than

entering the TCA cycle, pyruvate is metabolised to lactate which can be detected within the tumour.[16] Metabolism via this route is thought to occur as a result of low oxygen availability or as a consequence of mitochondrial damage, whilst it has been proposed more recently that production of lactate generates the building blocks required for cell growth and division.[17] Furthermore, this high rate of glycolysis allows for the imaging of tumours through positron emission topography (PET) scanning.

A key step in overcoming the normal control of the cell cycle is the accumulation of mutations in key regulatory proteins. One of the most widely studied proteins is p53; this has been described as the 'guardian of the genome' due to its ability to transduce anti-proliferative signals in response to DNA damage and hypoxia.[18] This is an important regulatory function as it prevents DNA replication and cell division when DNA is damaged and so potentially limits the accumulation of mutations. Mutations in p53 can result in a loss of this suppressive function and therefore rapid proliferation of malignant cells develops, potentially with further DNA damage, through the cell cycle.[19] This was first demonstrated in experiments where tumour cell lines with dysfunctional p53 proceeded through the cell cycle following radiation damage.[20] p53 has been found to be mutated in 31% of all tumours, with mutation rates as high as 50% in colorectal cancer samples.[21, 22] p53 and functionally related proteins, such as the Retinoblastoma protein (Rb) and phosphatase and tensin homolog (PTEN), are known as tumour suppressors; they normally function to prevent cell cycle progression, particularly in response to cellular stress. In contrast, K-RAS is a proto-oncogene which, when bound to GTP, is active and propagates a diverse range of signalling that can promote cell cycle progression. It is believed that 17-25% of human tumours have mutated K-RAS, where gain of function mutations prevent the self-inactivation of the protein (via GTP hydrolysis), leading to increased cell cycle progression.[23] These mutations are representative of those that commonly accumulate in oncogenes and tumour suppressors that allow a cell to proceed uncontrolled through the cell cycle.

When published in 2000, these six hallmarks summarised the knowledge to date regarding the features common to all tumours. However, 11 years after the original paper, a follow-up proposed four additional emerging hallmarks, reflecting the progress made in understanding tumourigenesis over the intervening decade.[24] One of these emerging hallmarks was the ability for a tumour to promote inflammation. It is now known that the inflammatory environment can contribute to tumour progression by providing growth and survival factors to the tumour.[25] One of the best illustrations of the role of inflammation comes from the association between infection and tumour formation. *Bacteroides fragelis* colonises a proportion of the human population, with

toxin gene present in the colon mucosa of colorectal cancer patients compared to controls.[26] Moreover, *Bacteroides fragelis* infection in mice results in rapid inflammation of the colon and the formation of colon tumours. Interestingly, this could be inhibited by blocking the pro-inflammatory cytokine interleukin-17 (IL-17) or by deleting $CD4^+$ T cells.[27] Moreover, pro-inflammatory cytokines including tumour necrosis factor-alpha (TNF-α) can upregulate the expression of matrix metalloproteases (MMPs).[28] This is significant as MMPs promote matrix remodelling which can support tumour cell growth and promote the formation of metastases. For example, MCF7 tumour cells grew slower *in vivo* when injected with MMP11 deficient fibroblasts compared to MMP11 competent fibroblasts.[29]

A further hallmark added to the revised paper was the ability to accumulate mutation; a pre-requisite to many of the other hallmarks discussed. Finally, the revised paper highlighted the capability of tumours to evade the immune system as an emerging hallmark. Immune deficient mice were found to be more susceptible to carcinogen induced tumours than wild type, immune competent mice.[30] When investigating colon cancer in humans, patients with a high number of tumour infiltrating cytotoxic T cells have an improved prognosis compared to patients who lack infiltration of these cells.[31] In addition, there is evidence that tumour cells become adapted to avoid detection by the immune system. One study of colorectal cancer patients found that those whose tumours had low expression of major histocompatibility complex (MHC) class I had a poorer outcome, presumably due to reduced tumour recognition by the immune system.[32] In contrast, patients whose tumours were completely negative for MHC class I had a better outcome as a result of NK cell mediated lysis (missing self hypothesis; see section 1.4). It is clear that the immune system plays a role in limiting the expansion of tumour cells. However as mutations accumulate, those cells best able to escape immune surveillance are positively selected for and therefore persist. This process of immunoediting results in an increasingly less immunogenic tumour as mutations accumulate over time.[33] Taken together, these early experiments paved the way for future research into the mechanisms behind this process and into therapies to re-engage the immune system against cancer.

1.1.2 B cell malignancies

As already described, malignancies can occur in almost any tissue in the body, including blood cells. Blood born malignancies can be divided into two broad categories; leukaemias and lymphomas.

Leukaemias tend to present in the blood and bone marrow, whilst lymphomas form as a solid tumour in the secondary lymphoid organs. In 2013, leukaemias accounted for 3% of all UK cancers, with 9,301 new cases each year compared to 13,413 new diagnoses of Non-Hodgkin lymphoma (NHL) per annum.[1] Leukaemias and lymphomas can derive from a number of blood borne cell types, however malignancies derived from some cell types are more common than others. T cell leukaemia is rare, however malignancies arising from myeloid cells are more common with acute myeloid leukaemia (AML) accounting for 34% of all leukaemias in 2011.[1]

B cell malignancies derive from an expansion of B cells which can occur at various stages during their development and can be divided into several distinct categories, depending on the pathology of the cells involved. For example, FL is characterised by an expansion in germinal centre B cells which reside in the primary and secondary lymphoid follicles.[34] This leads to the formation of tumours within the lymph nodes and spleen. With regard to chronic lymphocytic leukaemia (CLL), it is the most common adult B cell malignancy in the western world and is characterised by circulating $CD5^{+}CD19^{+}$ B cells. The cells themselves are often small in size and readily infiltrate the bone marrow.[35] CLL is most prevalent in later life, however it can be exceptionally heterogeneous in its clinical course; some patients experience indolent disease that does not require treatment whereas others develop a more aggressive disease.[36] CLL has become an exceptionally well-studied disease, fuelled by its commonality, easily accessible malignant cells and its potentially long disease course. In contrast to CLL, diffuse large B cell lymphoma (DLBCL) normally presents as a rapidly enlarging lymph node with little evidence of normal lymph node architecture.[37] Whilst the cell morphology can be highly variable between individual cases, DLBCL cells are normally large in size with large nuclei. Also in contrast to CLL, DLBCL cells are rarely found in the circulation.[38] Whilst there are many other types of B cell malignancies, these two examples effectively highlight the heterogeneity observed both within and between the different classes. This heterogeneity is reflected in the diverse range of treatments available, from surgery and chemotherapy to more targeted radiotherapy and monoclonal antibodies (mAbs).

1.2 Approaches to cancer therapy

Four main approaches have been developed for the treatment of malignant tumours: surgery, radiotherapy, chemotherapy and immunotherapy. Typically, treatment will involve a number of therapeutic approaches in combination, with the regime selected on the basis of the nature and

location of the tumour involved. Surgery is often an effective strategy for the removal of solid, bulk tumours, such as in breast cancer. However, surgery often leaves residual disease surrounding the bulk tumour and is not effective against metastases at distant sites. For this reason, surgery is most effective when the disease is at an early stage when the likelihood of metastasis having formed is reduced. Additionally, surgery often involves removal of a large amount of healthy tissue surrounding the tumour which can have a negative effect on patients. In some cases, surgery is impractical due to excessive trauma to the surrounding tissue, such as with some brain tumours.

A treatment that can be used when surgery is not an option is radiotherapy. This makes use of high energy x-rays to permanently damage DNA, which can result in death of the tumour cell. Additionally, radiation can be used as an adjuvant after surgery with the aim of targeting tumour cells in the tissue surrounding the original tumour. Interestingly, the damage caused by radiation can be affected by oxygen levels, with the hypoxic environment in a solid tumour reducing radiation induced killing.[39] Hypoxia initiates a DNA damage response within cells; this makes them more resistant to radiotherapy induced DNA damage. Therefore, the tumour is less likely to be killed by the therapy.[40, 41] Whilst radiotherapy can be administered in a highly focused way, it does not specifically target tumour cells, consequentially this can result in significant damage to the surrounding tissue. Furthermore, the ionising radiation used in radiotherapy is itself a carcinogen, which can lead to mutations and subsequently, the formation of new primary tumours. Recent advances have sought to minimise side effects through the development of image guided radiotherapy, allowing the more precise localisation of radiation.[42]

An important component of treatment for many patients is the use of chemotherapeutic agents to specifically kill rapidly dividing cells. These agents can work in a number of ways to exert a similar response. Alkylating agents such as chlorambucil non-specifically cause DNA damage; this activates the DNA damage response, resulting in arrest of the cell cycle and eventually apoptosis.[43] Another class of chemotherapy agents are the purine analogues such as fludarabine. These are structurally similar to the purine bases found normally in DNA and become incorporated in their place during DNA replication. However, once incorporated into the DNA, these agents prevent normal DNA replication and accordingly, cell division.[44] Additionally, purine analogues can directly inhibit the enzyme ribonuclease reductase, which is normally responsible for maintaining the pools of dNTPs required for DNA synthesis.[45] Pyrimidine analogues such as 5-fluorouracin have also been developed, which function via a similar mechanism. Often, several chemotherapy agents of different classes are used in combination to increase their efficacy though targeting multiple

cell processes whilst minimising side effects caused by high doses of a single agent. The use of multiple agents is also able to minimise the risk of resistance to treatment. The primary disadvantage of chemotherapy is that dividing, non-malignant cells are also targeted. This leads to wide ranging side effects as a result of targeting other cell types. For example, hair loss as a result of cell death in hair follicles is a common side effect as well as anaemia, nausea and fatigue.[46] Despite this, the systemic administration of these drugs has the advantage that they can also be active against metastases, the primary source of relapse in cancer patients.

In order to limit the side effects of chemotheraprutic drugs, more targeted therapies are being increasingly developed and used. These often involve the use of small molecules to specifically inhibit biological pathways important in tumour cells. The phosphoinositide 3-kinase (PI3K) family is a group of enzymes which mediate intracellular signalling leading to, amongst other things, cell growth, proliferation and survival. Members of the PI3K family are expressed in most cells of the body, however the δ isoform is mostly restricted to leukocytes.[47] This has led to the development of the PI3Kδ inhibitor idelalisib. As a single agent, idelalisib achieved an overall response rate of 56% and median progression free survival of 17 months in relapsed CLL patients.[48] However, where the drug is thought to have real benefit is in conjunction with the mAb rituximab, where a 24 week progression free survival of 93% was obtained in relapsed CLL cases.[49] Similarly, the small molecule inhibitor ibrutinib, which is an inhibitor of brutons tyrosine kinase (BTK), has also been widely studied. This enzyme normally plays a crucial role in B cell development and signals downstream of the B cell receptor (BCR).[50] Disruption of this signalling therefore prevents B cell proliferation. The use of idelalisib, ibrutinib and related molecules allows for malignant cells to be targeted with much greater specificity than traditional chemotherapy, reducing side effects. The final and most recent strategy used to treat cancer is immunotherapy, which is discussed in detail below.

1.3 Immunotherapy

As detailed above, immune evasion is a hallmark of cancer, as described by Hanahan and Weinberg.[24] This has resulted in several strategies aimed at redirecting the immune system against cancer. These can be broken down into two broad categories: passive and active immunotherapy. Passive immunotherapy involves the administration of components generated externally such as antibodies to deplete tumour cells directly or factors aimed at transiently boosting an on-going

immune response. In comparison, active immunotherapy uses the endogenous immune system to generate an anti-tumour response *in situ*.

1.3.1 Active immunotherapy

One class of active immunotherapy is the use of vaccines against a tumour antigen, this relies on finding tumour-specific targets to mount an immune response to. B cells express a BCR with a unique antigen binding site, known as an idiotype. This can therefore serve as a tumour specific antigen for a B cell malignancy, provided that the cells are unique, clonally evolved B cells. Vaccinating against this idiotype can stimulate the generation of immune cells recognising the unique antigen receptor on a malignant clone. This approach has been investigated in the clinic. In one study, FL patients had their tumour idiotype sequenced and a vaccine against it developed. This resulted in durable tumour regression with a progression-free survival of 44.2 months, compared to 30.6 months for the control arm.[51] In this study, the vaccine was conjugated to keyhole limpit hemocyanin and administered with GM-CSF to boost the immune response. Whilst this treatment strategy has been shown to have an effect, the benefits are relatively minor and come at a large cost. Each patient needs to have a personalised vaccine developed based on the individual idiotype of their tumour. Moreover, further mutation of the BCR renders the vaccine redundant. An alternative vaccination approach is the use of DNA vaccines. The protein to be vaccinated against is encoded in a DNA plasmid along with CpG motifs. It is thought that these motifs are recognised by toll-like receptor 9 (TLR-9), therefore acting to have an adjuvant effect.[52] However, the method of delivery has proven to be a challenge for DNA vaccines and, as a result, they have not been widely used clinically.[53]

An alternative approach to inducing an anti-tumour response has been to pulse patient derived dendritic cells (DCs) with lysates from autologous tumour samples. The dendritic cells can take up and present the non-defined, tumour antigens in the context of MHC. Subsequently, the pulsed cells are returned to the patient where they can present the antigens to T cells, eliciting a significant $CD4^+$ and $CD8^+$ response.[54] As with idiotype vaccinations, this does not provide an 'off the shelf' treatment and has to be developed individually for each patient. However, this approach has been used clinically in a limited number of glioma patients where the treatment was found to be feasible with a good response to the therapy.[54]

As has previously been described, the development of some cancers is attributable to a known pathogen. Vaccinating against this pathogen can therefore provide protection against the cancer it is associated with. Perhaps the best known example is the HPV vaccine Cervarix/Gardasil.[55] The vaccine contains the major capsid proteins from HPV types 6, 11, 16 and 18.[55] This induces immunity against these strains of HPV. By preventing infection, the opportunity for the virus to induce cervical carcinoma is reduced. Whilst it is too early to determine the effects of the vaccine on cervical cancer rates, there has been a marked decrease in the prevalence of HPV 7, 11, 16 and 18 infection. In the 6 years following the introduction of a vaccination program in the USA infection rates decreased 64% in females aged 14-19.[56]

1.3.2 Passive immunotherapy – immune modulation

One strategy of passive immunotherapy has been to administer factors known to manipulate and stimulate the immune system. For example, a number of early studies investigated the administration of exogenous IL-2, a cytokine which normally stimulates proliferation of T cells as well as well as acting as a growth factor for NK cells.[57] In one study of metastatic melanoma patients, 12-15 doses of IL-2 were administered every 8 hours with two courses 14 days apart; this gave an overall response of 13%.[58] Whilst this is a low response, those who were disease free for 18 months after treatment tended to remain so for over 10 years.[58] When combined with a GP100 peptide vaccine, the response was improved to 16%, demonstrating how treatment strategies can be combined to improve patient outcome, albeit modestly in this case.[58]

Whilst vaccines aim to generate an immune response from the endogenous immune system, other strategies have also been employed to genetically engineer T cells *ex vivo* to recognise tumour antigens before returning them to the patient. This approach uses chimeric antigen receptors (CARs) which are comprised of single chain variable fragments derived from antibodies specifically recognising the tumour antigen conjugated to potent activatory T cell signalling domains. The DNA encoding for a CAR is virally transduced into a patient's T cells before the cells are expanded and then returned to the patient (reviewed in[59]). Whilst this strategy can result in potent anti-tumour responses, it is a time consuming and therefore expensive process which has to be tailored to each individual patient. In a trial of 25 patients with acute lymphoblastic leukaemia receiving CARs targeting the B cell marker CD19, 90% achieved complete remission with a 78% survival rate 6 months after treatment.[60] Similar results have been obtained for other forms of leukaemia

including CLL.[61] Nevertheless, one significant drawback of CAR therapy has been the toxic levels of pro-inflammatory cytokines in patients undergoing therapy which has, in some cases, resulted in death.[62, 63] The majority of CARs developed to date have targeted CD19, however it has been reported that CD19 can be lost from the surface of ALL cells and can be alternatively spliced, preventing killing by CARs.[64] Overcoming this resistance and reducing toxic cytokine release remain key challenges in the field.

One of the most recent breakthroughs in cancer immunotherapy has been the development of oncolytic viruses which can replicate in and kill cancer cells without causing any damage to normal cells. T-VEC, the first oncolytic virus to be approved by the FDA, achieved a 26% overall response rate in a trial of late stage melanoma patients, with a one year survival rate of 58%, compared to a typical 25% for this stage of patients under previous treatments.[65, 66] This therapy makes use of a modified herpes simplex virus. In order for a virus to replicate, the hosts natural anti-viral response must be blocked using genes encoded by the virus. Modified tumour cells lack an anti-viral response, therefore viruses that are modified to be unable to block the response can replicate inside tumour cells but not healthy cells which maintain an anti-viral response.[67] Additionally, the virus contains the gene encoding for GM-CSF. This promotes dendritic cell differentiation and therefore antigen presentation to the cells of the adaptive immune system following tumour lysis.[67]

Whilst oncolytic viruses are still emerging as a cancer therapy, the most extensively used form of immunotherapy to treat cancer comes in the form of mAbs. This involves the administration of laboratory produced antibodies to elicit tumour cell clearance. This will be discussed at length in section 1.7; briefly, there are three major strategies employed by therapeutic antibodies: targeting cells for depletion, blocking signalling and immune modulation. Direct targeting mAbs recognise tumour specific antigens and signal for deletion of the target cells via activation of immune effector cells. Signal blocking mAbs either block the receptor for a signalling molecule or sequester the signalling molecule itself, preventing it exerting an effect. Finally immune modulating mAbs block inhibitory receptors or agonise activatory receptors on the surface of immune cells. Whilst these therapies have been shown to be successful against certain tumours, their effects are often transient with the molecules being cleared from the body. This means that multiple, regular doses are required which increases the cost of treatment. Before discussing how mAbs are generated and elicit their function, it is important to understand antibody development and its place within the immune system.

1.4 B cells within the human immune system

The human immune system provides defence against pathogens that enter the body. This has arisen as a result of the immune system evolving alongside the pathogens themselves. The human immune system can be divided into two broad arms; the innate and the adaptive immune responses. The innate immune system is restricted to recognition of a limited repertoire of simple molecules and regular structural patterns on pathogens, using receptors known as pattern recognition receptors.[68] These receptors are present on macrophages, neutrophils and dendritic cells where they broadly distinguish between self and non-self molecules and provide the first line of defence against pathogens. The cells of the innate immune system secrete inflammatory cytokines following activation. These act to establish a barrier around the site of infection as well as to recruit other immune cells, particularly neutrophils, which have the ability to capture and phagocytose pathogens. Another important cell type in the innate immune response are NK cells. These cytotoxic cells express a variety of activatory and inhibitory receptors. Self peptide, presented in the context of MHC I binds to inhibitory receptors on the NK cell. However, viral infection can result in a downregulation of MHC I expression on an infected cell. This reduces NK cell inhibition and results in killing of the target cell through a process known as the missing self hypothesis, which is summarised in Figure 1.1.[69, 70]

B and T cells form the basis of the adaptive immune system. When generated, each T or B cell carries a single unique receptor on its surface, allowing a specific response against a pathogen through the induction of memory, B and T cells that are able to provide more rapid responses and long-lived specific immunity against a particular antigen. Other cell types can be required for an effective adaptive response; dendritic cells in the circulation are able to engulf pathogens and present peptide fragments on their surface to lymphocytes. This activates T cells which are capable of specifically recognising the peptide being presented, using their unique T cell receptor (TCR) and allowing them to proliferate and enter the circulation.[71] Once in the circulation, T cells can recognise the target antigen on the surface of the pathogen and facilitate its destruction. However, stimulation through the TCR alone is not sufficient on its own to cause full T cell activation. Co-stimulation is required from the antigen presenting cell through one of a number of molecules including CD28 and CD137.[72] Additionally, T cells express a number of co-inhibitory molecules which, upon interaction with their ligands on antigen presenting cells, inhibit T cell activation. These inhibitory surface molecules include CTLA-4, OX40, PD-1 and are thought to be important in promoting tolerance to self-antigens, therefore reducing autoimmunity.[73] Furthermore, these

inhibitory molecules have been found to be upregulated on tumour infiltrating T cells compared to normal circulating T cells, with PD-1 found to be upregulated in a number of cancers including melanoma.[74] This has given rise to the so called check-point blocking antibodies to reactivate these T cells, as will be discussed in detail in section 1.7.

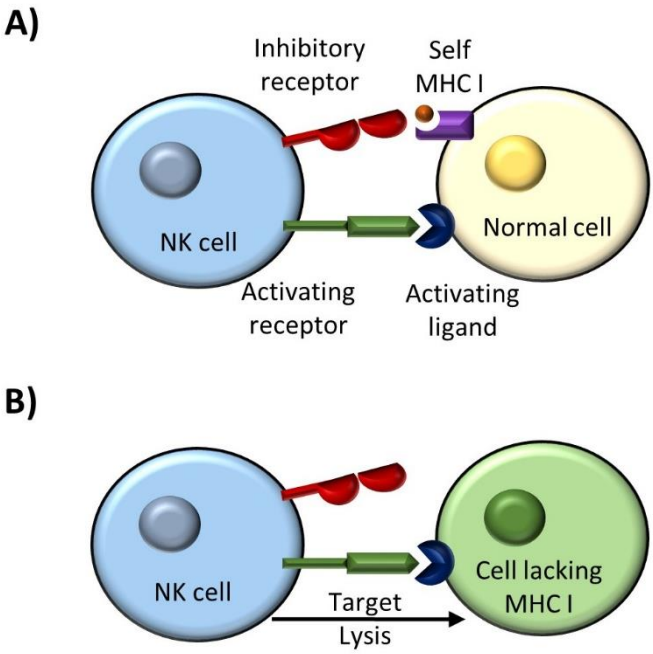

Figure 1.1 ***The missing self hypothesis.***
A) Normal cells express self peptide in the context of MHC I, this is recognised by inhibitory receptors on the surface of the NK cell and prevents activation despite signals through activatory receptors. B) when MHC is lost, for example following viral infection, inhibitory signalling is lost but activating signals remain, allowing the NK cell to lyse the target.

B cells form the other major arm of the adaptive immune system; they develop and mature in the bone marrow where they undergo clonal selection to give cells capable of producing a diverse range of reactivity to different antigens and pathogens. As with T cells, each B cell has a receptor that recognises a single, unique chemical structure; these are known as the BCR. The BCR consists of a membrane bound immunoglobulin of the IgM isotype which acts as an antigen binding subunit.[75] This is linked non-covalently to the intracellular signalling subunits CD79a and CD79b which allow the B cells to become activated in response to antigen engagement. [76] Activation through the BCR can lead to differentiation of the cell as well as the secretion of immunoglobulin, a process which can be regulated through a tightly controlled negative feedback loop to prevent autoimmunity. The function of B cells is largely to differentiate into plasma cells and secrete antibodies; these are proteins that are highly specific to a single antigen and function to link the specificity of the adaptive immune system to the potent killing of the effector cells of the innate

immune system. Crucially, each plasma cell comes from a unique B cell and produces a single, secreted immmunoglobulin of the same specificity as the original B cell.

The BCR have to develop a huge amount of diversity during their generation in order to respond to the repertoire of potential antigens they need to encounter. The specific recognition of an antigen is achieved through the complementarity determining regions (CDR) loops.[77] The combination of light and heavy chains leads to a high degree of diversity, however the diversity can also come from within the chains themselves. Each light chain is formed from a rearrangement between two gene segments (V and J) and each heavy chain from three gene segments (V, D and J).[78] The process of V(D)J recombination is tightly controlled and can only occur between conserved recombination signal (RS) sequences, consisting of a 12 or 23 nucleotide spacer.[79] The RS sequences are recognised by the RAG1 and RAG2 proteins which bring these sequences close together via the formation of hairpin loops and breaks between gene segments.[80] The ends are then precisely joined by nonhomologous end-joining (NHEJ) proteins to link the V D and J segment.[79] These combinations lead to at least 6000 possible rearranged heavy chains and 320 light chains. Therefore, there are a theoretical $1.9x10^6$ possible unique antibody binding sites.[75]

However the number of antigen binding sites generated is greater than this due to steps that introduce further diversity. The first step is in the V(D)J recombination process. Whist recombination occurs within the RS sequence, the precise cutting site is not specific, resulting in variation in variable region length.[81] Further variation in segment length can occur through the removal of additional bases by exonucleases as well as the insertion of bases during the ligation step.[82] The result is greater diversity in both the sequence and the length of the variable regions.

The final step in developing BCR diversity is somatic hypermutation, which occurs as activated B cells rapidly divide in the germinal centres.[78] When activated by BCR, there is upregulation of the enzyme activation induced deaminase (AID). Due to its function as a DNA mutator, expression is tightly controlled both transcriptionally and post-translationally in the form of phosphorylation.[83] The enzyme functions to convert cytosine to uracil in the transcribed V region; the resulting mismatch is repaired by the cellular machinery, ultimately resulting in a C:G pair becoming converted to T:A. This further increases the diversity of the antibodies that can be produced by a cell.[84, 85] Overall, this diversity means that in response to a given antigen, B cells can secrete a highly specific, high affinity antibody. Such is the diversity generated, several B cell clones can become activated against a single antigen, allowing the targeting of multiple epitopes on any given antigen.

1.5 B cell origins and development in humans

The idea of B cell development by clonal selection was first proposed in 1957 by F. Macfarlane Burnet, with the basic principle being that a vast number of lymphocytes are randomly generated, each with BCRs of differing specificity, before selecting those that can react with the antigens that are encountered.[75, 86] The development of B cells in humans is summarised in Figure 1.2, highlighting the key surface markers expressed at each stage of development. B cells initially develop in the bone marrow where the B cell receptor begins to form; pro-B cells only express μ-chains which become associated with surrogate light chains as the cell matures to a pre-B cell. Those heavy chains which successfully pair with surrogate light chain are selected for by out-proliferating those cells where successful pairing has not been achieved.[87] This process of signalling through the surrogate BCR confirms that the receptor can recognise antigen. If successful, the cell will begin to produce full mature chains which will associate with the heavy chains to form surface IgM in the plasma membrane.[88]

Subsequently, a B cell is able to leave the bone marrow where it starts producing surface IgD.[75] B cells move to the germinal centres of secondary lymphoid organs where they undergo somatic hypermutation as previously described. At this stage it is able to respond to foreign antigens but is yet to encounter self-antigens, so is known as a mature naïve B cell.[75] It is vital that B cells reactive to self antigens are eliminated to prevent immune responses against self. The first described method to achieve this was clonal deletion. It was demonstrated using transgenic mice that autoreactive B cells encountering antigen undergo apoptosis within 2-3 days, following developmental arrest.[89] This clonal deletion was originally thought to be the major mechanism of tolerance however it has subsequently been found to be a default mechanism employed when receptor editing fails.[90] Receptor editing occurs when autoreactive BCR bind to their antigen, this was initially found to result in the reactivation of the immunoglobulin gene rearrangement mechanism at the light chain locus.[91] Subsequently, editing has been shown to occur at the heavy chain locus, albeit to a lesser extent.[92] This process prevents the development of autoreactive B cells without deleting the cell itself.[90] However, receptor editing is not always successful. Those cells that continue to be autoreactive are removed by clonal deletion, as already described, or selected via anergy. Sustained BCR stimulation as a result of self-antigen results in a cell no longer being able to react to an antigen, often with an accompanying downregulation of IgM.[68] These three processes together ensure that self-reactive B cells do not propagate and reduce the chance of B cell mediated autoimmunity.

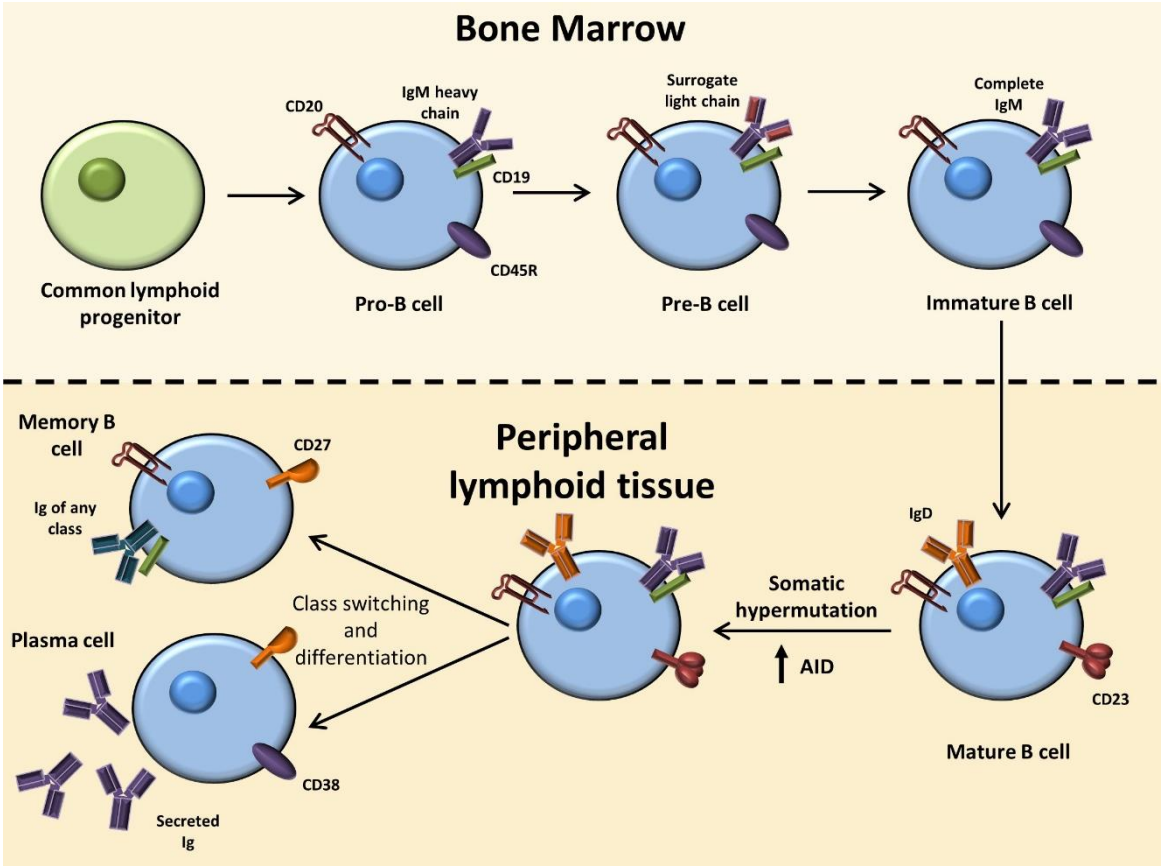

Figure 1.2 ***Human B cell development.***

B and T cells develop from a common lymphoid progenitor cell in the bone marrow. Pro-B cells express IgG heavy chain before expressing surrogate light chains as part of the transition to pre-B cell. Activation causes true light chains to replace the surrogates and the cell enters the peripheral lymphoid tissue. At this point B cells begin to express IgD at the cell surface and undergo somatic hypermutation to increase the affinity of the expressed IgM, facilitated by expression of the enzyme AID. Cells can then enter class switching before differentiating into plasma cells or memory B cells. Notable markers expressed at different stage of development are highlighted. Information is adapted from reviews by Allman (2008) and Pieper (2013)

Once activated, a B cell can undergo class switching (discussed below) to produce IgG. Following class switching, the cell can differentiate in the germinal centres of peripheral lymphoid organs into memory or plasma cells. Memory B cells are long lived and allow a rapid immune response to subsequent exposure to antigen whilst plasma cells are the major IgG secreting cell in the body.[93] This survival and differentiation of affinity matured B cell clones requires signalling through the canonical nuclear factor kappa-light-chain enhancer of activated B cells (NF-κB) pathway; evidenced by germinal centre specific deletion of the RELA component of the pathway which prevents the generation of germinal centre plasma cells.[94] Yet RELA deficiency did not impair the formation of germinal centres or affinity maturation suggesting that NFκB signalling is not required at this earlier stage of development.

1.5.1 Antibody structure and diversity

The primary role of B cells is to generate plasma cells to produce and secrete antibodies which are capable of recognising and binding to target antigens with a high affinity in order to activate the effector cells of the immune system. Each antibody is a homodimer of two identical heavy and light chains. The antigen specificity of an antibody comes from its complementarity determining regions (CDRs) which are located within the variable domain found on each immunoglobulin chain (V_L for light chain and V_h for heavy chain) followed by the constant domain(s) (C_L for light chain and C_H for heavy chains).[75] The variable domains and first constant domains are known collectively as a F(ab), whilst the remaining constant domains of the heavy chain are known as the Fc region.

The antibodies secreted by B cells can be one of several classes depending on the specific cell being engaged. The first antibodies often released after encountering an antigen are IgM. These are formed from two light and two heavy chains to make a monomeric IgM which, in turn, join to form homopentamers with a mushroom-like structure joined together by a single J-chain, as shown in Figure 1.3. Alternative antibody isotypes are produced through class switching which occurs in the light zone of the germinal centres. Each constant region gene segment is flanked by a switch sequence which allows intervening segments to be spliced out. This process is initiated by AID, repair of uracil residues leads to single strand breaks which are subsequently converted to the double strand breaks required for class switching.[95, 96] Importantly, once a segment is removed it can not be re-expressed by a cell, therefore a cell can not revert to an earlier class of immunoglobulin.[96] The focus of this study is on IgG antibodies which are produced by mature B cells following class switching.

The various forms of human IgG are illustrated in Figure 1.3, indicating that there are four isotypes of IgG in humans; all homodimers formed of two heavy and light chains varying in their arrangement of disulphide bonds around the hinge region. This alters the flexibility of the antibody and the angles between F(ab) arms.[68] The mean angle between F(ab) arms was found to be highest for IgG3 (136°) and lowest for IgG1 (117°).[97] Moreover, the same study ranked the flexibility of IgG isotypes from most to least flexible as follows: IgG3>IgG1>IgG4>IgG2.[97] It is important that antibodies have flexibility about the hinge as this is required for bivalent binding to epitopes.[77] Recently, it has been shown that the formation of the disulphide bonds in the hinge of human IgG2 can influence the agonistic propertied of an antibody.[98] In summary the antibody hinge angle may be important in antigen binding as well as modifying its function.

Humans also produce IgA, IgE and IgD. As previously mentioned, membrane bound IgD is produced during B cell development along with IgM. The function of secreted IgD has remained relatively unclear however the isotype has been shown to bind to respiratory bacteria and viruses, including the measles virus. IgD thought to be able to activate innate immune cells, particularly basophils and mast cells.[99, 100] IgA can be secreted as a dimer held together with a J chain; it is mostly secreted in the mucosal membranes where it plays a role in protection against microorganisms.[101] Finally, the main function of IgE is in protection against parasites such as helminths, however the isotype is also responsible for the symptoms of allergic reactions.[102] In addition to structural variation, immunoglobulins also vary in their glycosylation, as can be seen in Figure 1.3. The sugars present at these glycosylated residues are known to influence antigen binding and effector function; mutation of residue N297 in IgG prevents glycosylation of this site and prevents interaction with the main elements of the immune effector systems.[103, 104] The exact nature of the carbohydrate moiety attached to each glycosylated residue is extremely heterogeneous and is dependent on the glycan processing in the antibodies cell of origin.[105]

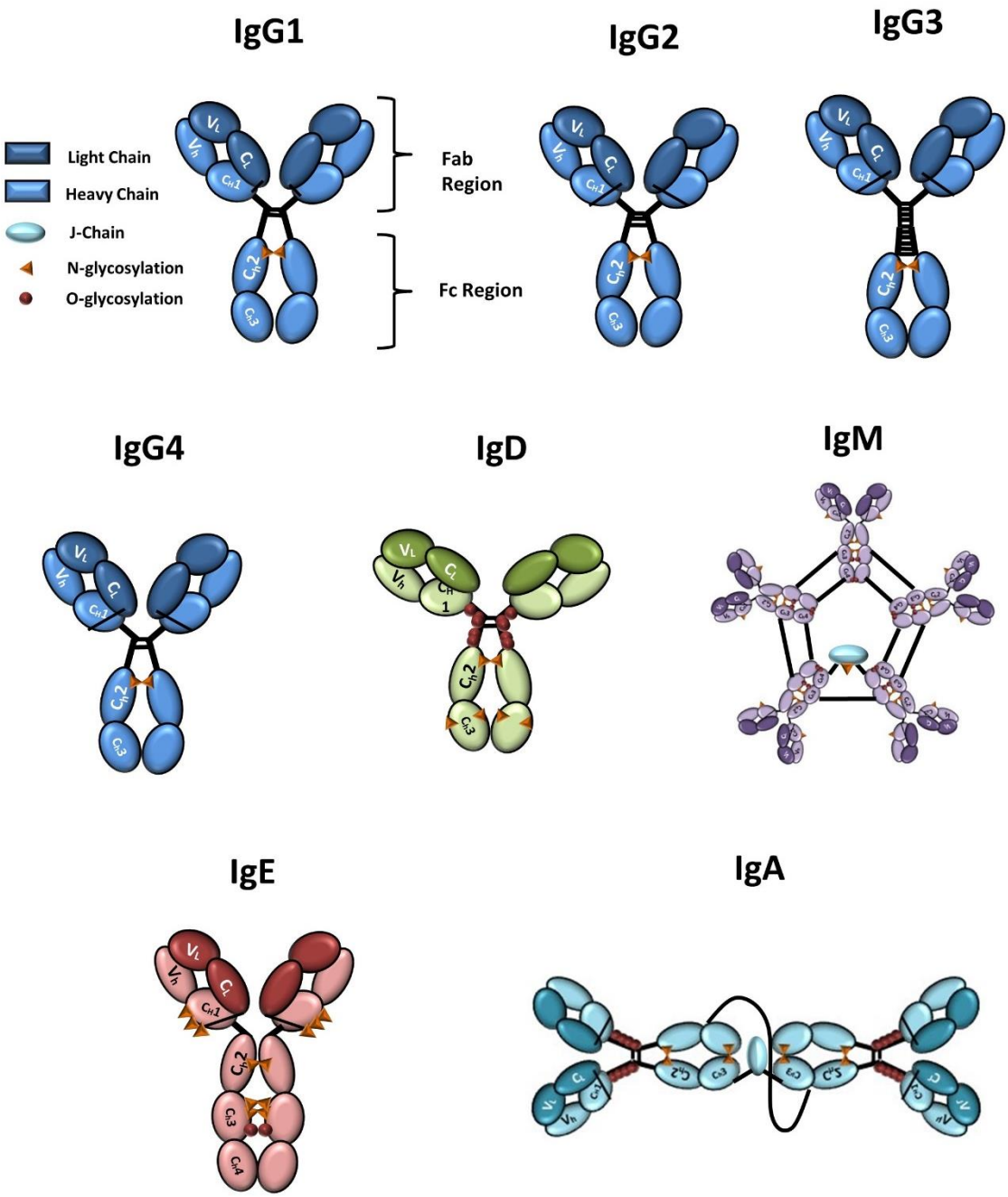

Figure 1.3 ***Structures of human immunoglobulins.***

The monomers of human immunoglobulin contain two light chains and two heavy chains. For IgG, IgA and IgD the C_h2 and C_h3 domains form the Fc region which is able to interact with Fc receptors. The antigen binding regions are on the V_L and V_h domains. IgG has four subclasses which primarily vary in their hinge region, with alternative arrangements of disulphide bonds. IgG contains a single N-linked glycosylation site on heavy chain residue N297 where as IgD has considerable N-linked and O-linked glycosylation and forms a more open structure. IgM and IgE monomers have an additional C_h4 domain and a shorter hinge region than the other classes. IgM monomers form a pentamer joined by a J-chain. IgA also contains a J-chain which is required for the formation of dimers. Information is adapted from a review by Vidarsson (2014)

1.6 Production of monoclonal antibodies

The specificity of antibodies for their target and the size of the potential repertoire available makes them attractive for use as therapeutics capable of targeting a vast array of molecules or cells. This property led to the search for a method of generating them in the lab and industrialise their production. In 1975 Georges Köhler and César Milstein created the first hybridomas, a fusion of a B cell (from an immunised sheep in the first instance) and a myeloma cell to make an immortal cell that could produce a single antibody.[106] These were the first so called monoclonal antibodies and were key to the commercialisation of antibodies produced on a large scale. The first mAb approved for use by the FDA was muromonab (OKT3) in 1986 designed to prevent organ rejection in transplant patients who had become resistant to steroids.[107, 108] The mechanism of action for therapeutic antibodies will be discussed in detail later.

There are three main approaches employed to generate mAbs against a specific antigen. The first is to generate antibodies *in vivo;* animals are injected with an antigen, antigen peptide fragment or cells expressing the antigen. This is typically a non-self molecule such as a human protein in a mouse and as such is recognised by the host as being foreign, invoking an immune response. Often, the antigen is coupled with an adjuvant; this non-specifically boosts the immune system of the recipient animal resulting in a stronger immune response against the target antigen.[109] Additionally, these adjuvants can protect the antigen from degradation and improve antigen presentation, as well as improving immune activation.[110] One of the most widely used adjuvants in mice is Freund's adjuvant, which can either be incomplete (comprised of non-metabolisable oils) or complete (with the addition of heat inactivated mycobacteria).[111] Immunisation causes the animal to produce antibodies against the target antigen, albeit in small quantities. Multiple antibodies will be produced, each from a unique B cell clone, therefore these antibodies against the same antigen but from different B cell clones are termed polyclonal. Multiple rounds of immunisation can be performed in the same animal to boost the immune response and increase the yield of specific antibody forming cells. Spleen cells are subsequently harvested from immunised animals and fused to myeloma cells to create the hybridoma secreting a single mAb.[112] Following rounds of subcloning to isolate single cells, this can lead to the generation of a hybridoma line, capable of continuously producing a single, antigen specific mAb. This strategy of immunisation was employed in mice in order to generate muromonab.

One of the major problems with muromonab was that it is a murine IgG2a isotype. Following administration to humans, the antibody itself is recognised as being foreign, effectively vaccinating the patient against the mAb. It has been demonstrated that, following initial administration, 40-80% of patients develop anti-muromonab antibodies.[113] This results in the clearance of the mAb from the circulation, particularly following repeated dosing, limiting its efficacy. In order to overcome this immunogenicity, mAbs have been genetically engineered to attach the murine V_L and V_H domains onto a human IgG scaffold containing the human constant domains, as depicted in Figure 1.4. These reagents are known as chimeric mAbs and the first one approved for use by the FDA was rituximab in 1997, for use in NHL. At the same time, rituximab became the first mAb specifically approved for use in cancer.[114] These chimeric mAbs still contain a significant amount of mouse framework and there have been numerous reports of patients, particularly those with autoimmune conditions, developing anti-rituximab antibodies.[115, 116] In order to reduce immunogenicity further, mAbs have subsequently been humanised; complementarity determining regions (CDRs) from antibodies raised in an animal are engrafted onto a human antibody scaffold, minimising the amount of host sequence.

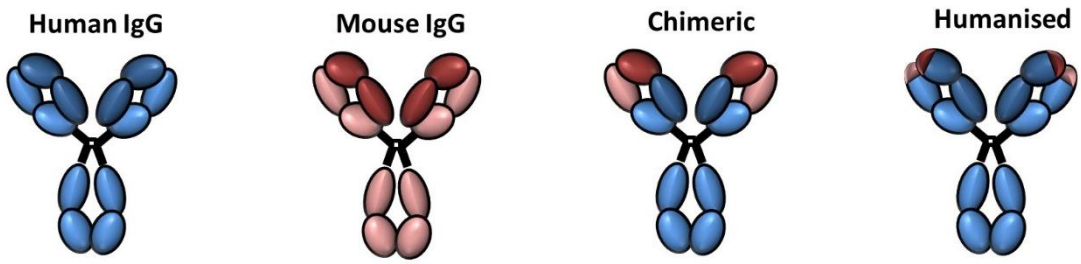

Figure 1.4 ***Development of therapeutic monoclonal antibodies.***
Human and mouse IgG share the same basic structure. Chimeric mAbs graft the V_L and V_H domains from a mouse antibody onto the human backbone. For humanised mAbs, only the complementarity determining regions (CDRs) are transferred on the human IgG scaffold. Reducing the amount of murine sequences reduces the potential immunogenicity of the mAb.

An alternative method for generating mAbs is phage display, a technique which selects antibodies of the desired specificity from libraries of bacteriophage. These libraries are created by amplifying the mRNA of heavy and light chain genes from spleen cells, before combining them randomly to generates single chains.[117] These can be expressed by bacteriophage, each expressing a unique antibody single chain. Multiple rounds of screening are performed against the target antigen. At each stage, the bacteriophages capable of binding the antigens are selected with increased stringency at each stage; this results in the selection single clones with high affinity.[118] Additionally, negative selection can be performed to exclude clones which bind to structurally related, non-target molecules. The plasmid encoding the single chain in selected bacteriophages can be isolated and the variable region fused onto an antibody backbone of the desired isotype, and tested to

ensure biological activity.[119, 120] This generates a fully human mAb with human variable and constant regions. Once the mAb encoding plasmid has been generated, site directed mutagenesis can be performed, targeting the CDRs with the aim of increasing the affinity of the mAb for its target in a process known as affinity maturation.[121] Crucially, this process does not exclude the production of self-reactive antibodies, a process which occurs during *in vivo* immunisation. This potentially offers an increase in the available antibody repertoire, depending on the size of the library used.

A final method for mAb production is through the use of humanised mice. This makes use of genetically altered mice which express human immunoglobulin heavy and light chain genes with the loss of the corresponding mouse genes.[122] This results in mice which, following immunisation, produce human antibodies against the antigen. However, these initial mice were restricted by the length of human DNA that could be inserted into the mouse genome, resulting in a restricted repertoire of human antibodies. More recently, mouse models have been produced where the full complement of human Ig genes has been inserted which respond to antigens by producing high affinity antibodies with human variable regions.[123] Finally, rather than genetically modify mice, immune deficient strains can be reconstituted with bone marrow from humans. This allows mice to produce human IgM, and more recently IgG in response to antigens in a system that also reconstitutes mice with human effector cells.[124] All these methods have been used to successfully generate therapeutic mAbs against a range of targets.

1.7 Current therapeutic monoclonal antibodies

Since the development of muromonab, there has be a steady increase in the number of mAbs approved by clinical use, targeting a variety of molecules. A selection of these mAbs is shown in Table 1.2, identifying their targets and the diseases for which they are indicated.[125, 126] It is clear from this that clinical mAbs can be split into three primary groups, depending on their mechanism of action: immune modulators, signal blockers and deleting antibodies. In some cases, mAbs can fulfil more than one of these functions (see below).

Antibody (trade name)	Target	Source and isotype	Selected indications	Mechanism
Rituximab (Rituxan/ Mabthera)[127]	CD20	Chimeric IgG1	Low grade/follicular NHL CLL Rheumatoid Arthritis	B cell deletion by ADCC, ADCP and CDC[128]
Trastuzumab (Herceptin)[129]	Her-2	Humanised IgG1	Her-2^{+} breast cancer Her-2^{+} gastric or oesophageal cancer	Her-2 signalling inhibition ADCC[130]
Cetuximab (Erbitux)[131]	EGFR	Chimeric IgG1	Colorectal cancer Non-small cell lung carcinoma Head and neck cancer	Blocking EGFR signalling ADCC[132]
Bevacizumab (Avastin)[133]	VEGF-A	Humanised IgG1	Colorectal cancer Glioblastoma Non-small cell lung carcinoma	Blocking VEGF signalling to reduce angiogenesis[134]
Alemtuzumab (Campath)[135]	CD52	Humanised IgG1	Withdrawn, previously- CLL T cell lymphoma	Cell deletion by direct killing and ADCC[136]
Obinutuzumab (Gazyva)[137]	CD20	Humanised IgG1	CLL	B cell deletion by ADCC, ADCP and direct cell death[138]
Ipilimumab (Yervoy)[139]	CTLA-4	Human IgG1	Melanoma Bladder cancer Prostate cancer Non-small cell lung carcinoma	Blocking inhibitory T cell signalling through CTLA-4[140]
Nivolumab (Opdivo)[141]	PD-1	Human IgG4	Metastatic melanoma Non-small cell lung carcinoma Renal cell carcinoma	Blocking inhibitory t cell signalling through PD-1[142]

Table 1.2 ***Selected antibodies approved by the FDA for use in cancer.***

The targets of the antibodies are listed as well as selected key indications for which they are approved. Alemtuzumab has since been withdrawn from use pending revised approval for use in multiple sclerosis. The proposed mechanisms of action are stated and will be discussed in more detail later (ADCC/P = antibody dependent cellular cytotoxicity/phagocytosis; CDC = complement dependent cytotoxicity). Additional information adapted from Reichart, 2015 and Scott, 2012

Signal blocking mAbs can engage a cell surface receptor or its ligand to prevent interactions that would otherwise lead to proliferative signals in the tumour cell. One such example is the anti-epidermal growth factor receptor (EGFR) antibody cetuximab (Erbitux), approved by the FDA for use in a number of cancers, including colorectal.[131] Cetuximab binds to the extracellular domain

of EGFR to prevent the binding of its ligand.[143, 144] The binding of EGF to its receptor initiates an intracellular signalling cascade through the MAPK pathway.[145] The ERK protein in the MAPK pathway is capable of translocating to the cell nucleus, where it is able to phosphorylate transcription factors such as c-myc which plays an important role in cell cycle progression[146, 147] This pathway is inhibited with cetuximab, blocking the proliferative signalling and therefore EGF dependent tumour growth.[148] Initial experiments in human xenograft models found that, when combined with chemotherapy, cetuximab was able to elicit potent anti-tumour activity.[149] Subsequent studies in metastatic colorectal cancer patients concluded that the addition of cetuximab to irinotecan treatment improved progression free survival compared to irinotecan monotherapy (4 months vs 2.6 months).[150]

Whilst cetuximab is able to bind to a receptor to stop growth signals, mAbs have also been developed which can sequester the signalling molecules themselves. The most commonly used example of this is bevacizumab (Avastin), an anti-vascular endothelial growth factor A (VEGF-A) antibody which is approved for use in several metastatic cancers including colorectal, lung and breast.[133] VEGF-A induces angiogenesis through endothelial cell proliferation and migration. Inhibiting the interaction between VEGF-A and its receptor reduces angiogenesis, a key hallmark of cancer.[134] By reducing angiogenesis, the blood supply to the tumour is restricted, limiting its growth. This is reflected in clinical trials where the addition of Avastin to capecitabine treatment resulted in improved progression-free survival in elderly metastatic colorectal cancer patients (9.1 months vs 5.1 months for capecitabine alone).[151]

As has been previously discussed, checkpoint blocking antibodies prevent the propagation of inhibitory signals received by T cells, strategies have also been developed that agonise costimulatory molecules. One such example is CD28, which is able to engage CD80 and CD86.[152] Once engaged, CD28 can activate Rho family GTPases, leading to actin cytoskeleton rearrangements and the production of IL-2, promoting T cell differentiation and signalling.[153] This requirement for costimulation ensures that only professional antigen presenting cells can initiate a T cell response. Agonistic anti-CD28 mAbs were developed which were found to drive the expansion of functional T cells *in vitro* and *in vivo.*[154] One of the most studied anti-CD28 mAbs is TGN1412, a human IgG4 (hIgG4) mAb designed to stimulate T cell anti-tumour activity, primarily developed for use in CLL. [155] This antibody proved to be promising in pre-clinical studies, causing a rapid proliferation of T cells without the need for engagement of the TCR. Moreover, subsequent safety and toxicity studies in cynomolgus macaques did not identify any toxicity, even at doses as high as 50mg/kg.[156] Based on these results, a phase I clinical trial was conducted in healthy

volunteers; within 60 minutes of infusion, all volunteers began experiencing side effects which rapidly progressed in to hypertension, tachycardia and life threatening systemic cytokine release.[157] Later investigations found that this toxicity was not predicted in primate studies as cynomolgus macaques do not express CD28 on the relevant memory T cell populations, which were found to be responsible for the effects observed in the trial volunteers.[158]

The catastrophic results of the TGN1412 trial has led to an impetus to develop more accurate *in vitro* assays for predicting toxicity. Current efforts have deduced that cross-linking of TGN1412 at the cell surface is required to give T cell proliferation. This was originally demonstrated through immobilising TGN1412 onto plastic or by using an anti-IgG cross linking antibody.[158, 159] Neither of these techniques gives a biologically relevant explanation for the activity and subsequent toxicity of TGN1412 in humans. However, more recent work has demonstrated that the high density preculture of human peripheral blood mononuclear cells (PBMCs) prior to antibody treatment was able to facilitate TGN1412 induced T cell proliferation and cytokine release.[160] It has since been shown that high density culture results in the upregulation of CD32b on monocytes; blocking this receptor prevents TGN1412 mediated proliferation.[161] This provides a biologically relevant explanation for the activity of TGN1412 and the subsequent induction of cytokine release which is summarised in Figure 1.5

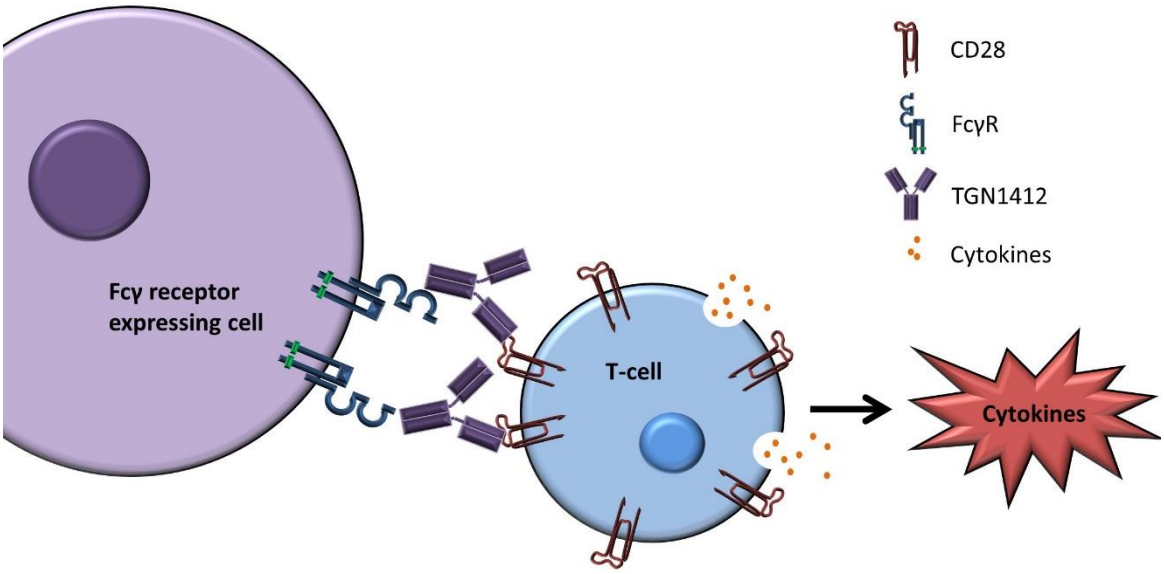

Figure 1.5 ***The proposed mechanism for cytokine release by TGN1412.***
It is thought that the mAb TGN1412 engages CD28 on T cells through tis F(ab) regions whilst the Fc region engages FcγRs on other cell populations. This results in cross-linking of CD28 which can cause T cells proliferation as well as cytokine release

The final group of antibodies is those that actively deplete tumour cells through the engagement of cytotoxic effector cell mechanisms. In order to limit off-target effects, these mAbs typically target antigens which are present on tumour cells but have limited expression on normal. For example, the mAb Herceptin is widely used to treat $Her2^{+}$ breast cancer where, as well as modulating Her2 mediated signalling, it targets tumour cells for destruction by effector cell populations.[162, 163] One of the most widely studied and targeted antigens for depleting mAbs is CD20; mAbs raised against this antigen are used in the treatment of a wide range of B cell malignancies and autoimmune conditions. This is as a result of CD20 being expressed exclusively in B cells from an early stage. Anti-CD20 mAbs will be the focus of a large part of this study, however before discussing the mechanisms by which these mAbs function, it is important to understand CD20 as a target.

1.8 CD20 structure and function

CD20 was discovered as a marker of B cells more than three decades ago (then termed B1).[164] As well as being the first B cell specific antigen to be identified, it was also the first antigen known to regulate B cell function, with different anti-CD20 mAbs found to have opposing effects on cell cycle progression (reviewed by Beers[165], Tedder[166] and Cragg[167]). Since its identification, CD20 has had a major impact on our understanding of B cell biology. However, the focus of CD20 has now shifted to its properties as an antibody target after it was identified as being expressed on the majority of B cell malignancies. Furthermore, identification of its B cell specific nature has also proven to be important in the treatment of autoimmune conditions such as rheumatoid arthritis, where deletion of B cells has been shown to improve symptoms.

Despite its success as a mAb target, the function of CD20 has remained unclear, especially as the natural ligand for CD20 is either unknown or not present, meaning that all functional data to date comes from engagement with antibodies. Co-precipitation studies suggested that human CD20 exists in the plasma membrane of B cells as a homo-tetramer, a feature consistent with the structure of ion channels, sparking studies to explore the possible function of CD20 in regulating calcium flux.[168, 169] CD20 is now known to belong to the MS4A family of proteins, containing four membrane spanning domains as well as cytoplasmic amino and carboxy termini.[170] The evidence for CD20 as an ion channel appeared to be supported by experiments demonstrating that cell lines transfected with CD20 had an increased ionic conductance, an effect that was eliminated in the presence of a calcium chelator.[171] However, more recent evidence suggests that CD20 does not function directly in mediating calcium flux, but instead modulates BCR signalling. This evidence comes from Ramos B cells lacking the BCR. Engagement of CD20 in these cells was not able to induce calcium flux.[169] This is consistent with work showing that CD20 is physically associated with a subpopulation of BCR in the membrane, a phenomena that is reversed rapidly after BCR cross-linking, with CD20 instead becoming associated with calmodulin binding proteins.[169, 172]

In vivo studies have only provided limited evidence as to the physiological function of CD20. The first description of a CD20 deficient mouse in 1998 described the mice as having no major defects in B cell maturation, proliferation or IgG production.[173] This result was subsequently corroborated by an independent mouse knockout line, although it was noted that mice lacking CD20 expression (CD20 -/-) had reduced calcium influx following BCR cross-linking.[174] In addition, a case report has described a patient deficient in CD20. Despite B cell lines generated from this patient having no

impairment in BCR signalling, there was a reduced antibody production in response to vaccination with T-independent antigens.[175] These results were subsequently confirmed in CD20 deficient mice, which also had impaired T-independent responses to polysaccharide antigens.[175] Furthermore, recent work by Morsy and colleagues found that CD20 deficient mice had reduced levels of neutralising antibodies to adeno-associated virus; which are likely T-dependent. Taken together, the evidence suggests that CD20 may play a subtle, indirect role in mediating BCR signalling to achieve optimal humoral responses that are dose, time and antigen dependent.

1.8.1 Classification of anti-CD20 mAbs

Since the generation of 1F5, the first anti-CD20 mAb, many more have been raised and characterised *in vitro* and in the clinic. It was clear from the outset that not all anti-CD20 mAbs are the same; as detailed earlier, different mAbs were found to have opposing effects on cell cycle progression. For instance, 1F5 was found to induce the entry of resting B cells into the G_1 phase of the cell cycle, as evidenced by a rapid increase in RNA synthesis, whilst the antibody B1 did not.[176] However, both mAbs inhibited the differentiation of B cells to secrete immunoglobulin. The identification of these differences led to efforts to classify anti-CD20 mAbs in order to understand their functional differences. Initially, Deans et al proposed five groups, based on the ability of mAbs to recognise a chimeric mouse:human CD20 molecule incorporating the extracellular loop of murine CD20 but with the AxP-binding motif from human CD20.[177] More recently, mAbs have been classified into just two groups, based on their ability to redistribute CD20 into detergent-insoluble lipid rafts in the plasma membrane.[178] The majority of anti-CD20 mAbs generated to date, including rituximab, are classed as type I and can induce efficient redistribution of CD20 into lipid rafts.[179] Conversely, the rarer type II antibodies such as obinutuzumab do not induce CD20 redistribution.

Further comparisons between the two classes of mAb have revealed clear differences in their binding to CD20. Studies investigating the binding of radiolabelled $F(ab')_2$ to $CD20^+$ cell lines revealed that type I mAbs bind, on average, to twice as many CD20 molecules compared to type II.[180, 181] Niederfellner and colleagues subsequently compared the crystal structures of the obinutuzumab and rituximab F(ab) molecules complexed with a cyclical CD20 peptide, revealing the type II mAb to be more tilted in relation to the mimitope binding.[182, 183] Combining these observations, one possible explanation is that type II mAbs are able to bind to the CD20 tetramer,

but due to the altered angle of binding, engagement prevents another mAb from binding the same tetramer, thereby reducing the number of available binding sites by 50%.[184] However, a definitive explanation for this 2:1 binding ratio is still to be deduced, with other possible explanations including differential recognition of the CD20 tetramer conformations or differences in binding, either within or between tetramers.[165, 182]

The mechanisms by which anti-CD20 mAbs exert their effect will be discussed in detail in the next section, however type I and type II mAbs have been found to differ in the mechanisms of target cell killing they can perform. Type I mAbs are able to induce potent complement dependent cytotoxicity (CDC) whereas type II mAbs do not.[180] Conversely, only type II mAbs have been shown to induce potent homotypic adhesion of B cells, which can result in target cell death.[185] Further work demonstrated that the direct killing induced by type II mAbs was dependent on actin polymerisation and was the result of lysosomal membrane permeabilisation.[138] It has been proposed that redistribution into lipid rafts could directly influence the effector mechanisms engaged, however all the evidence presented thus far has been based on *in vitro* data rather than investigating the *in vivo* mechanisms of action.[186]

1.9 Effector mechanisms of monoclonal antibodies

Investigations into the mechanism of action have found that anti-CD20 mAbs can engage multiple mechanisms of action, with the reliance on each of these mechanisms variable between mAbs. These mechanisms have been studied in great detail with opinion as to the most important mechanism changing as our understanding has increased. The primary mechanisms, as summarised in Figure 1.6 are: CDC, direct cell death, antibody dependent cellular cytotoxicity (ADCC) and antibody dependent cellular phagocytosis (ADCP). Whilst these mechanisms have been proposed for deleting antibodies against a number of targets, here they will be explored in the context of anti-CD20 mAbs.

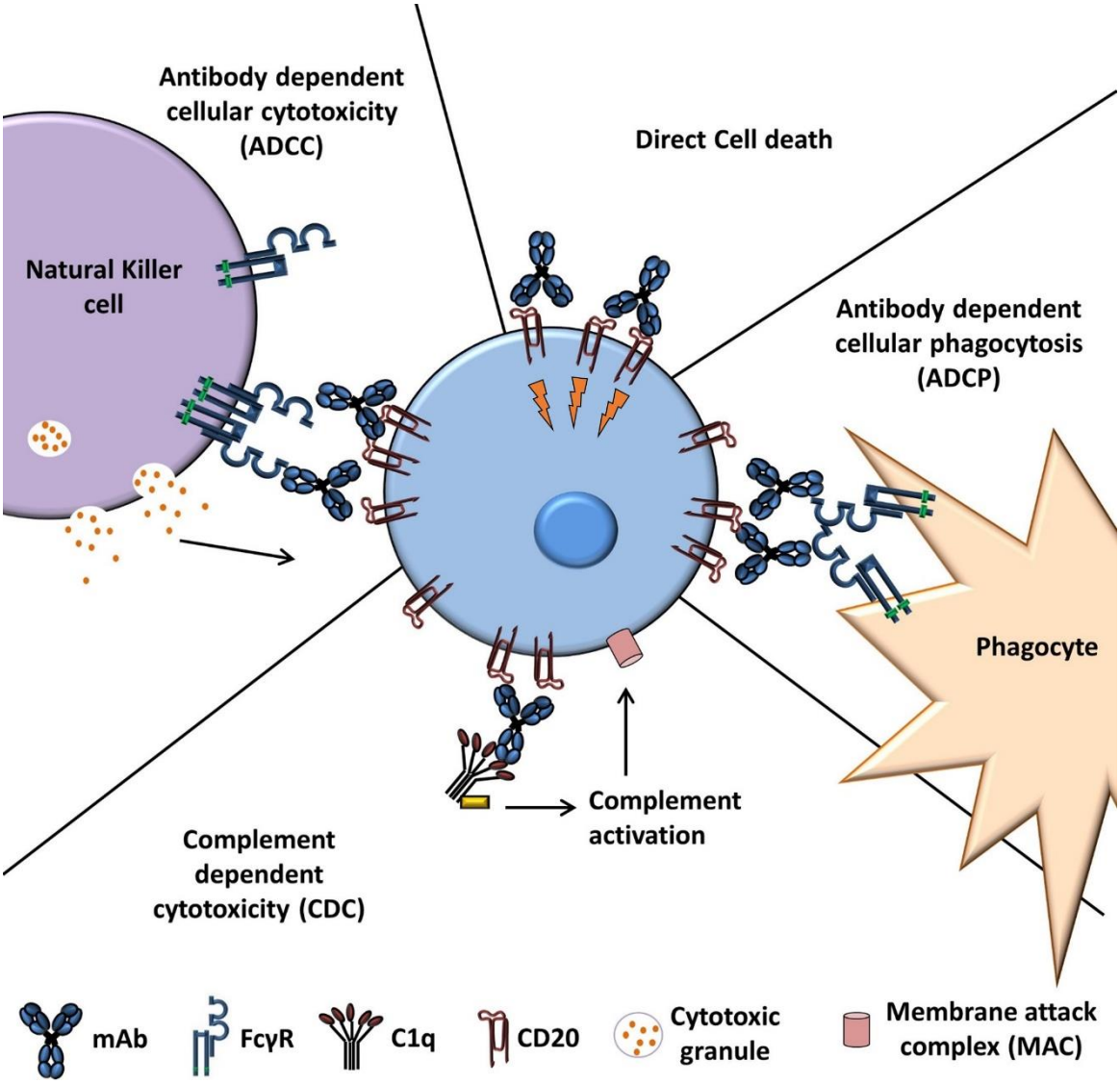

Figure 1.6 ***Proposed mechanisms for the anti-tumour activity of anti-CD20 mAbs.***

Antibody binding to CD20 can result in direct signalling for target cell death through the propagation of intracellular signals. Antibody can bind to CD20 through it F(ab) arms, allowing the Fc portion to interact with components of the immune system. For example it can engage the complement cascade to ultimately result in the death of the target cell through the formation of the membrane attack complex (MAC). Alternatively the antibody can cross-link Fcγ receptors (FcγR) on effector cells, resulting in phagocytosis or cytotoxic granule release by NK cells.

1.9.1 Complement dependent cytotoxicity

The complement pathway contains a cascade of molecules that can become activated by an antibody bound to its target, leading to the death of the target cell and recruitment of inflammatory cells.[68] Rituximab can result in the death of a $CD20^{+}$ cell via the classical complement pathway, an overview of which is presented in Figure 1.7. The C1 component of the complement cascade can bind to several antibodies in close proximity opsonising a cell; this in turn activates

the C4 and C2 components, which together form C3 convertase. As the cascade progresses, molecules such as C3b and C4b are deposited on the cell surface; these help target the cell for ingestion by phagocytes.[68] Ultimately, the complement cascade can result in the formation of the membrane attack complex, a channel comprising multiple copies of C9 as well as C6, C7 and C8, which forms through the plasma membrane of the target cell and results in its lysis through the accumulation of extracellular fluid.[77] Interestingly, the components of the complement cascade can also induce a number of non-lytic effects; C5a has been demonstrated to be a chemotaxic agent of monocytes and has also been shown to enhance macrophage mediated phagocytosis, therefore enhancing other effector mechanisms.[187, 188] Moreover, the binding of C5a to its receptor has been shown to result in the upregulation of activatory FcγRs on Kupffer cells with an accompanied downregulation in inhibitory CD32b expression.[189]

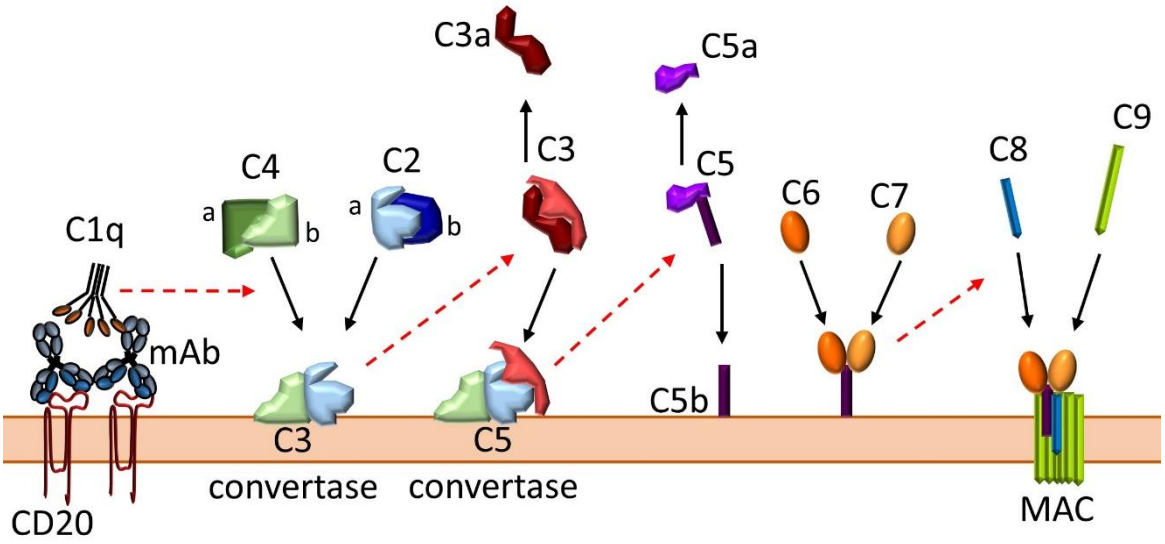

Figure 1.7 ***Overview of complement mediated cytotoxicity.***
Following engagement with CD20, the mAb Fc can bind to C1q beginning the classical complement pathway. Each complex catalyses the cleavage of the next components resulting in deposition on the plasma membrane. Lysis of C5 leads to C5b deposition which recruits components of the membrane attack complex (MAC) to result in cell death. C3a and C5a are released during complement activation and can act as mediators of inflammation

In order to activate the complement cascade, C1q must be fixated by at least two antibody Fc portions close to the plasma membrane.[190] The Fc portion of antigen complexed rituximab has been shown to activate the C1q component of the complement cascade, leading to target cell lysis as described above.[191] This has been demonstrated *in vitro* using human cell lines, however this work also highlighted that some cell lines are more resistant to rituximab induced CDC.[192, 193] It has subsequently been suggested that, in the case of rituximab, the high expression level of CD20 and the proximity of the antibody binding loop to the plasma membrane facilitates this efficient CDC.[194] Furthermore, the ability of type I mAbs to redistribute and cluster CD20 in lipid rafts is

thought to facilitate their potent CDC activity, something that type II mAbs are not capable of.[180] It is thought that this redistribution brings the Fc regions of CD20 bound antibodies close together, better recruiting and clustering C1q and subsequently activating the complement pathway.[180]

Initial *in vitro* investigations into complement defense molecules supported the importance of CDC for the activity of rituximab, with high levels of CD59 expression at the surface of cell lines found to be associated with resistance to rituximab therapy.[195] This effect could be overcome *in vitro* by using an anti-CD59 blocking mAb.[195] Similarly, the expression level of CD55 was found to be associated with resistance to rituximab therapy, but could be overcome using small-interfering RNA (siRNA) targeting CD55.[196] Further work has tried to assess how important CDC is to the activity of rituximab *in vivo.* Work using primary FL cells found that complement defense levels had no correlation to the clinical response to rituximab, in direct contrast to the *in vitro* data.[197]

In order to better understand the *in vivo* role of complement, experiments have been performed in mouse models. Cobra-venom factor (CVF) is able to deplete complement components *in vivo*; its use illustrated that complement was required for rituximab mediated depletion of subcutaneous BJAB tumours and human lymphoma cell line xenografts.[186, 198] Interestingly, the activity of the type II mAb tositumomab was unaffected by the administration of CVF, further suggesting that CDC is of limited importance to the activity of type II mAb. However, these early models, which typically lacked complement defense from mouse complement, investigated the depletion of small numbers of cells from highly passaged cell lines and were therefore not the most relevant for studying anti-CD20 immunotherapy. As a result, later studies using more biologically relevant models have challenged the role of complement; these have made use of anti-mouse CD20 mAbs or human CD20 (hCD20) transgenic (Tg) mice. These approaches more accurately model the depletion of B cells from within their correct biological niche. These models investigating depletion of normal hCD20 Tg B cells found that the requirement for complement was limited; in both C1q-/- and C3-/- mice, rituximab was still able to give efficient cell clearence.[199, 200] Additionally, it has been suggested that complement components can actually inhibit other effector mechanisms, with C3b deposits shown to block interactions between rituximab and FcγRIIIa (CD16a) on natural killer cells, adversely affecting ADCC.[201]

The importance of CDC to the activity of therapeutic mAbs in humans is controversial. Certainly, patients receiving rituximab infusion indicate that complement is consumed following treatment.[202] It is also widely discusssed that activation of the complement system is responsible for the acute side effects resulting from mAb therapy.[203] Furthermore, it has been demonstrated

that complement is consumed following rituximab administration in CLL patients.[202] Additionally, the serum from these patients requires addition of complement components before it can efficiently kill cells in response to rituximab *in vitro*.[202] On the other hand, some studies suggested that complement components may have an adverse effect on rituximab therapy. For example, a polymorphism in C1qa that corresponds to reduced C1q levels was found to be associated with an improved response to rituximab therapy.[204]

On balance it appears that, whilst rituximab is capable of inducing CDC *in vitro* and *in vivo*, it is not required for rituximab activity in the most relevant mouse models. The evidence surrounding the contribution of CDC to mAb activity in humans is limited with seemingly polar results. Despite this, current opinion based on mouse models concludes that CDC is of limited importance for rituximab activity, resulting in a change of focus towards alternative effector mechanisms.

1.9.2 Direct cell death

The second proposed mechanism for anti-CD20 cell killing is direct cell death, where the engagement of the antibody with its target results in killing of the target cell. Since the early work on anti-CD20 mAb, there has been demonstrations of anti-proliferative and apoptotic effects through the transmission of intracellular signals.[205] A number of cell lines (although importantly not all) have demonstrated growth arrest in response to CD20 cross-linking.[206] Moreover, these effects on cell growth and survival appear to vary with the antibody used. Rituximab was found to induce only weak cell death signals, however once cross-linked, these signals become more potent.[206] In contrast, the type II mAbs tositumomab and obinutuzumab can induce potent target cell death, even without additional cross-linking, in an Fc and FcγR independent manner.[185, 191]

The mechanism by which cell death occurs has been demonstrated to vary between mAbs. Rituximab has been proposed to induce apoptotic cell death with evidence that it can augment or reverse death from various types of chemotherapy.[205, 207, 208] Rituximab resistant cell lines (induced by repeated rituximab exposure) were found to have reduced expression of the proapoptotic proteins bax and bak, suggesting rituximab interference in the cell death pathway.[207] Additionally, signalling pathways induced by engagement of CD20 with rituximab have been proposed to relate to that of the BCR, with an influx of calcium.[209, 210] In a study of 10 CLL patients treated with rituximab, caspase 3 and caspase 9 were found to be activated in tumour cells, with an additional

study finding a similar result for caspase 9 in FL patients.[211, 212] However, this is in contrast to a number of studies suggesting that rituximab induces caspase independent killing.[191, 213] This is of particular relevance as caspase modulation is a major mechanism of chemotherapy resistance; if rituximab can act independently, it may be able to overcome this resistance.

In contrast, the type II mAbs obinutuzumab and tositumomab have been shown to induce homotypic adhesion and actin-dependent lysosomal cell death in lymphoma cell lines and primary CLL samples.[138] Death induced by both these mAbs cannot be prevented by the use of caspase inhibitors, suggesting that type II mAbs can induce cell death which is neither apoptotic or autophagic. It is important to reiterate that this cell death induced by type II mAbs does not require additional cross-linking, in contrast to that of type I mAbs.[191]

Despite multiple demonstrations of direct cell death mediated by anti-CD20 mAbs *in vitro*, evidence *in vivo* is limited and has been difficult to obtain. Studies have been performed in mice which express FcγRs deficient in signalling capacity. These so-called NOTAM mice were shown to be able to cross-link rituximab without activating effector cell signalling; this allows for only the signalling effects on tumour cells to be investigated.[214] When rituximab was used in these mice it was incapable of inducing potent anti-tumour activity. This implies that direct cell death induced by transient rituximab cross-linking does not play a significant role in its activity, whilst further adding to the belief that FcγR mediated mechanisms are vital for rituximab mediated anti-tumour activity.[214]

There have been demonstrations of direct killing using antibodies against targets other than CD20. The anti-CD38 mAb daratumumab has been approved by the FDA for use in multiple myeloma. Unusually for a direct targeting mAb, its therapeutic activity was not significantly diminished in mice lacking activatory FcγR, however when mCD32 was blocked in FcR γ-chain deficient mice activity was lost.[215] In contrast to rituximab, daratumumab was able to maintain anti-tumour activity in NOTAM mice even when mCD32 was blocked. These results imply that cross-linking by activatory or inhibitory FcγRs was sufficient for anti-tumour activity.[215] This demonstrates that direct cell death can be observed *in vivo* following direct targeting mAb despite appearing to be of little importance to the therapeutic activity of rituximab.

1.9.3 FcγR mediated mechanisms

The final proposed mechanism of action for the activity of anti-CD20 mAbs is through FcγR expressing effector cells. The repertoire, structure and function of these receptors will be discussed in detail in section 1.11, however their engagement can result in the degranulation of NK cells and the phagocytosis of target cells by macrophages.[216] These receptors are able to link the antigen specificity of an antibody to the potent effector cell functions of NK cells and phagocytes. Fc receptors bind to the Fc region of antibodies and are split into sub-groups depending on their specificity; for example, FcεR are specific for IgE and FcγR interact with IgG. [217] Humans express six FcγRs (five activatory and one inhibitory) whilst mice express four (three activatory and one inhibitory).[218] With the exception of CD16b in humans, all activatory FcγRs signal through immunoreceptor tyrosine-based activatory motifs (ITAMs). This signalling is counteracted by the inhibitory FcγR (CD32b in humans, CD32 in mice) which signal through an immunoreceptor tyrosine-based inhibitory motif (ITIM).[219] All activatory receptors in mice, as well as CD16a and CD64 in humans, require the expression of the FcR γ-chain for transport of the receptor to the cell surface, as well as for cell signalling.[220]

It is now widely accepted that FcγRs are an absolute requirement for effective anti-CD20 immunotherapy. Initial evidence came from mice lacking the FcR γ-chain; these mice do not express any activatory FcγRs. Raji cell xenografts were not cleared in FcR γ-chain deficient mice, in comparison to robust clearance from wild type mice.[221] These results have been supported by more recent data using anti-mouse CD20 mAbs or depletion of hCD20 Tg B cells in fully syngeneic immune competent models. In both of these cases, the FcR γ-chain was found to be an absolute requirement for the anti-tumour activity of rituximab.[199, 200, 222] There is also some evidence from human studies that FcγRs are important for anti-CD20 activity. This data comes from polymorphisms in FcγRs; these will be discussed in detail later. Two independent studies have shown that follicular lymphoma patients with a lower affinity F158 allele for the FcγR CD16a have a reduced progression free survival following rituximab therapy, compared to those homozygous for the higher affinity V158 allele.[223, 224] Rituximab is widely given in combination with cyclophosphamide, doxorubicin, vincristine and prednisone as part of the R-CHOP regime. In DLBCL patients treated with R-CHOP, the V158 allele was significantly associated with a higher complete response rate. [225-227] However, it should be noted that several studies (most notably that of Keane in DLBCL and Farag in CLL) found no correlation between CD16a polymorphisms and

patient outcome following rituximab treatment. Despite this, the majority of evidence has led to the conclusion that FcγRs are an absolute requirement for anti-CD20 mAb therapy.

With the importance of FcγRs recognised in mAb mediated immunotherapy, there have been subsequent studies to investigate the relative contributions of FcγR bearing effector cell types on therapeutic outcome. Work using anti-EpCAM antibodies on *ex vivo* colorectal cancer samples has shown that the depletion of monocytes and/or NK cells from PBMC effector samples reduced the specific lysis of tumour cells.[228] This implies that both populations can act as antibody effectors. Additionally, *in vitro* work has demonstrated that rituximab is capable of inducing the killing of B cell lymphoma samples through the activation of both macrophages and NK cells.[229] Following activation, NK cells release granules containing perforin and granzymes which form lethal pores in the membrane of the target cell.[230] Furthermore, the release of granzyme B by NK cells results in the cleavage of caspases 3 and 7, as well as the permeabilisation of the mitochondria in the target cell; both processes lead to cell death.[231] Breast cancer patients treated with the anti-HER2 antibody trastuzumab were found, compared to untreated controls, to have an increased NK cell tumour infiltrate accompanied by elevated lymphocyte granzyme B expression.[163] This suggests that NK cells are recruited to the tumour following trastuzumab therapy and become activated. Despite this, mouse models have demonstrated that depletion of NK did not affect the deleting ability of anti-CD20 mAb.[232] This has led to recent research focusing on phagocytosis by macrophages as being the primary effector mechanism for anti-CD20 mAb mediated tumour clearance.

Macrophages are present in almost all tissues and are capable of phagocytosing pathogens and necrotic cells after being activated by signals through FcγRs and TLRs.[68] macrophages can either derive from monocytes or be tissue resident. The tissue resident macrophages are thought to derive from the yolk sack where they colonise the primordial liver[233] Furthermore, macrophages are heavily influenced by their environment, causing them to divide into two broad, functionally polarised states depending on the stimuli they receive, known as M1 and M2 macrophages.[234] The differentiation and function of these polarised macrophages is summarised in Figure 1.8. M1 macrophage differentiation is simulated by IFNγ and LPS treatment; these cells function to remove intracellular pathogens whilst secreting cytokines that create a general pro-inflammatory environment.[235] Alternatively, macrophages can become polarised to an M2 phenotype by anti-inflammatory cytokines such as IL-4 and IL-13, resulting in macrophages that can recruit leukocytes and create an anti-inflammatory response.[235] M2 macrophages can be further subdivided depending on the stimulation they receive, with each class producing specific

molecules in response to activation, as shown in Figure 1.8. It is thought that tissue resident macrophages tend to be more M2-like due to their role in tissue homeostasis and resolution of inflammation.[236-238] In addition to these subsets of macrophages, there are other classes which can not be easily defined, including tumour associated macrophages (TAMs)

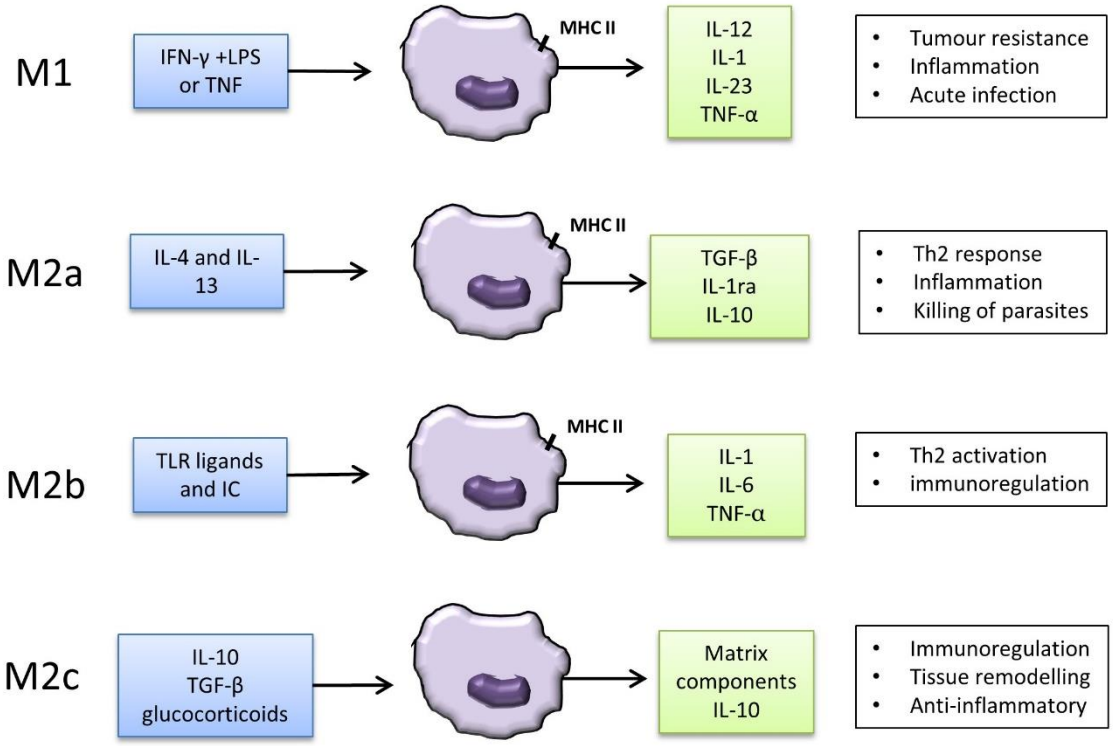

Figure 1.8 ***The polarisation of human macrophages.***
The four major groups of polarised human macrophages are shown including the stimuli that lead to their polarisation as well as components they produce in response to polarisation. M1 macrophages are thought to generally be of a pro-inflammatory phenotype whilst M2 macrophages are broadly anti-inflammatory. Adapted from Mantovani, 2004 with updated information from Mantovani, 2013 and Roszer, 2015.

In response to the binding of immune complexes (ICs) to FcγRs, macrophages become activated (through mechanisms which will be discussed later) to result in phagocytosis of opsonised target cells. There has been some work into the macrophage subsets that most effectively phagocytose target cells in cancer immunotherapy. Leidi et al found that macrophages polarised to an M2 like phenotype more efficiently phagocytose CLL cells opsonised with rituximab *in vitro.*[239] Moreover, Herter and colleagues compared three anti-CD20 antibodies and found that M2c macrophages (a subset activated by IL-10 and glucocorticoids) exhibited superior phagocytosis of Raji targets compared to M1 polarised cells with all mAbs investigated.[240]

As has already been eluded to, it is now thought that macrophages are the primary cell type responsible for anti-CD20 effector function, at least in mice. The evidence for this comes from the fact that several groups have used clodronate vesicles to deplete macrophages in mice, resulting

in a significant reduction in anti-CD20 mAb activity.[200, 222, 241] The importance of macrophages in rituximab therapy has also been highlighted by investigations into the physical location of tumour cell clearance. Mice that had received a splenectomy had no reduction in tumour cell clearance, whereas in those with restricted blood flow to the liver, tumour depletion was significantly reduced.[242] This, together with the clodronate investigations, implies that Kupffer cells (the liver resident macrophages) are important for rituximab therapy. Similar observations were made in an anti-Her2 model, where the number of liver metastases significantly increased following Kupffer cell deletion.[243] These results have been confirmed by intravital imaging studies, designed to observe cell depletion in the liver following anti-CD20 or anti-Her2 therapy. [244, 245] Importantly, it was shown that B cells could attach to Kupffer cells following rituximab treatment and that this attachment was reduced in FcR γ-/- mice, highlighting the importance of FcγRs and Kupffer cells in anti-CD20 therapy in mice.[244] In humans, evidence for the importance of macrophages comes from combination therapies with granulocyte macrophage colony-stimulating factor (GM-CSF); this is a cytokine which normally induces monocyte differentiation into M1 macrophages.[246] GM-CSF administration to follicular lymphoma patients resulted in an improved response to rituximab therapy.[247, 248] It is interesting that M1 differentiation was able to improve rituximab therapy when M2 macrophages have been described as better phagocytosing rituximab opsonised targets *in vitro.* Nonetheless, this highlights the importance macrophages in the activity of direct targeting antibodies.

1.10 Anti-CD20 resistance and new developments in mAb therapy

With mAbs now well established as a therapy in cancer, and with a good understanding as to their mechanism of action, work has gone into improving antibody therapy. This is of particular importance as resistance to mAb therapy has been widely reported. In the case of rituximab, reports of resistance emerged from an early stage, with descriptions of the loss of CD20 from the target cell, leading to resistance.[249] Subsequent work went on to show that rituximab is internalised from normal and malignant primary B cells and is targeted to the lysosome.[250, 251] An alternative mechanism proposed for rituximab resistance is shaving, where rituximab and bound CD20 are removed from the target cell surface by FcγR expressing effector cells.[252] A mechanism for rituximab induced CD20 internalisation has recently emerged, whereby the Fc of rituximab is able to act in a cis fashion with CD32b on the target cell. Furthermore this induced internalisation

in a manner that is independent of signalling through the ITIM of CD32b.[253] Importantly, type II reagents such as obinutuzumab appear to be much less sensitive to this internalisation.[253, 254] Moreover, It has since been shown in two independent clinical trials that CD32b expression on target cells limits rituximab efficacy.[254, 255]

1.10.1 Overcoming rituximab resistance

Several strategies have been employed for overcoming resistance to rituximab. One option is to block CD32b, the receptor thought to be key for rituximab internalisation. The use of a CD32b blocking antibody has been found to improve rituximab mediated depletion of CLL cells in a xenograft model.[256] Work is currently under way to explore if this strategy delivers benefit in patients. One interesting approach has been to use histone deacetylase inhibitors in combination with rituximab. These have been found to increase CD20 expression levels in cell lines and enhance the effects of rituximab in mice receiving BJAB xenografts.[257] Alternatively, the proteasome inhibitor bortezomib, in combination with rituximab, was found to increase overall survival of FL patients compared to rituximab alone.[258] Yet the mechanism for this activity remains unclear, as one study showed bortezomib to reduce CD20 expression on the cell surface.[259]

Another obvious way to avoid rituximab resistance is to make use of other anti-CD20 reagents. However, ofatumumab as a single agent only gave a clinical response in 9% of FL patients resistant to rituximab in combination with chemotherapy.[260] In contrast, ocrelizumab, which recognises an overlapping CD20 epitope as rituximab, gave a 38% response rate in rituximab exposed patients.[261] It is worth noting however that these patients were rituximab exposed and not necessarily resistant. With studies demonstrating that type II mAbs are not internalised to the same extent as rituximab, these reagents were predicted to offer hope to rituximab resistant patients. Despite this Phase I data in NHL and CLL found the response to obinutuzumab to be a relatively modest 13% in rituximab refractory patients.[262] However, when compared directly in a randomised trial of CLL patients, rituximab plus cholambucil resulted in a progression free survival of 15.2 months, this was increased to 26.7 months for obinutuzumab plus chlorambucil.[263]

Clearly, anti-CD20 mAb therapy can still be improved further; the current challenge with mAb therapy, particularly those targeting CD20, is to further improve their efficacy. This has focused on the engineering of the antibody to improve effector functions, as well as novel combination therapies.

1.10.2 Antibody engineering

With the importance of FcγR effector mechanisms clearly established, work has since investigated how Fc:FcγR interactions can be enhanced to promote improved target cell clearance. One mechanism has been through the glycoengineering of mAbs; this came to fruition with the FDA approval of the glycomodified anti-CD20 mAb obinutuzumab, an afucosylated mAb approved for use in CLL. The deficiency in fucosylation comes from the production of the mAb in a cell line overexpressing β-1,4-N-acetyl-glucosaminyltransferase III and Golgi α-mannosidase II, enriching for mAb with bisected, non-fucosylated oligosaccharides.[185] This modification was developed based on work demonstrating that the removal of fucose from IgG1 increased the affinity for the activatory FcγR CD16a approximately 50 fold.[264] Importantly, this was only accompanied by a small increase in the affinity for the inhibitory FcγR CD32b, leading to an overall increase in the activatory to inhibitory (A:I) ratio. This modified mAb resulted in increased in ADCC *in vitro*, compared to the parental nonglycomodified antibody and rituximab.[265] This appears to have translated to an improved clinical response, with a trial in CLL patients finding that those treated with obinutuzumab plus chlorambucil had an increased progression free survival compared to those treated with rituximab plus chlorambucil.[263] However, whether these results come from the glycomodification or the type II effect overcoming internalisation is not clear.

1.10.3 Combination therapies to improve anti-CD20 therapy

Combination strategies using anti-CD20 mAb have been described with the aim of overcoming rituximab resistance. However, further combinations are in development to improve the efficacy of anti-CD20 mAb by synergising with other therapeutic mechanisms. Rituximab has already been used in combination with chemotherapy, yet the recent combinations focus on more targeted drugs. Lenalidomide is an immune modulatory compound which has been shown to act through a number of mechanisms, including restoring the formation of immunological synapses via the upregulation of T cell costimulatory molecules.[266] Lenalidomide is already approved for use in multiple myeloma, however it has shown efficacy as a single agent in untreated and relapsed refractory CLL.[267-270] Whilst it is thought that lenalidomide improves autologous tumour cell recognition by T cells, it has also been demonstrated to improve NK cell function *in vitro*, leading to enhanced ADCC.[271-273] Subsequently, this observation led to the proposal that lenalidomide may

be able to enhance rituximab mediated therapy. Indeed, this has been found in a number of haematological malignancies, including one recent study in CLL where the combination gave an 83% overall response rate, compared to 56% seen previously for lenalidomide alone.[268, 274]

A number of drug molecules are under investigation which act to inhibit signalling pathways. It is hoped these may work synergistically with anti-CD20 mAbs to improve therapy. For instance, Ibrutinib is an inhibitor of BTK, indicated for use in CLL and mantle cell lymphoma (MCL).[275] This molecule has been shown to prevent CLL migration and proliferation by inhibiting a number of constitutively active pathways in CLL.[276, 277] This has been translated into clinical trials, where ibrutinib alone gave an overall response rate (ORR) of 84% in previously untreated CLL and SLL patients.[278] In a further study of high-risk CLL patients the combination of ibrutinib with rituximab gave an (ORR) of 95%.[279] Another signalling inhibitor under investigation in combination with rituximab is the PI3Kδ inhibitor, idelalisib. *In vitro*, this has been shown to influence cell survival, metabolism and proliferation.[280, 281] Moreover, rituximab alone resulted in a 14 week progression free survival in 46% of relapsed CLL patients, this was improved to 93% with the addition of idelalisib.[49] Idelalisib is of particular interest as the outcomes of treatment therapy were similarly favourable, even when patients were stratified according to key risk markers (p53 mutation, IGHV mutation status and 17p deletion) which signify poor prognosis with other treatments.[49]

One further approach under investigation for improving anti-CD20 therapy has been combination with checkpoint blockers. In a murine lymphoma model, anti-CTLA-4 combined with anti-CD20 mAb improved therapy compared to either mAb alone, as well as giving rise to stronger protection from tumour rechallenge.[282] In humans, CLL patients have been found to have a higher expression of PD-1 on their circulating T cells than healthy donors.[283] This is coupled with an increase in PD-L1 expression on malignant B cells with the interaction thought to be responsible for decreased IFN-γ production by T cells in CLL patients.[283] In a phase II trial of relapsed FL, patients the combination of rituximab and the anti-PD-1 mAb pidilizumab resulted in an objective response rate of 66%.[284] These results suggest that the direct targeting of anti-CD20 mAbs in combination with the potent T cell activation of checkpoint blockers may offer a new therapeutic option for patients with B cell malignancies.

1.11 Fcγ receptors

As has already been eluded to, FcγRs are the class of receptors responsible for linking the specificity of antibodies to the potent target cell killing by effectors. In humans there are five

activatory and one inhibitory FcγR, whilst in mice there are three activatory receptors and one inhibitory.[218] The basic structure and signalling functions of FcγRs have already been introduced, however here they will be discussed in more detail.

1.11.1 FcγR structure

All FcγRs in humans and mice consist of extracellular immunoglobulin domains which are capable of interacting with the Fc domain of an antibody.[218] The structure of human FcγRs is presented in Figure 1.9 with the equivalent mouse structures in Figure 1.10.[218, 285-289] Human FcγRI (hCD64), mouse FcγRI (mCD64) and mFcγRIV contain three extracellular immunoglobulin domains whilst all other receptors contain two. Both human and mouse CD64 are considered to be high affinity receptors for IgG, for reasons which will be discussed subsequently, mFcγRIV has an intermediate affinity for mIgG, depending on the specific isotype.[289] In contrast, the receptors with only two immunoglobulin domains have a lower affinity for IC than those with three.[290] Whilst all receptors show similarity in their extracellular regions, there is considerable variation in their intracellular signalling domains.

In both mice and humans the inhibitory FcγR (mCD32, hCD32b) contains an ITIM domain within its intracellular tail which is able to transduce inhibitory signals through the cell (see section 1.11.4).[219] Similarly, human CD32a and CD32c also contain a signalling domain on their intracellular domain, however, this takes the form of an ITAM. In response to receptor engagement these ITAMs become phosphorylated and recruit downstream signalling molecules through a process discussed below (section 1.11.4). All activatory receptors in mice, as well as hCD64 and hFcγRIIa (CD16a) do not contain signalling motifs within their extracellular regions, instead they non-covalently associate with the common FcR γ-chain in the plasma membrane; the FcR γ-chain contains two ITAM domains for signalling.[291] As well as being required for signalling, the FcR γ-chain is necessary for the associated receptors to reach the plasma membrane; therefore in mice where the FcR γ-chain has been genetically deleted, no activatory FcγRs are expressed at the cell surface. The only FcγR which does not signal through ITAMs or ITIMs is human FcγRIIb (hCD16b), a receptor with no mouse homologue. This receptor is tethered to the membrane via a GPI linker and it is currently unclear as to how this receptor signals, although it has been reported to localise into lipid rafts following engagement.[290, 292]

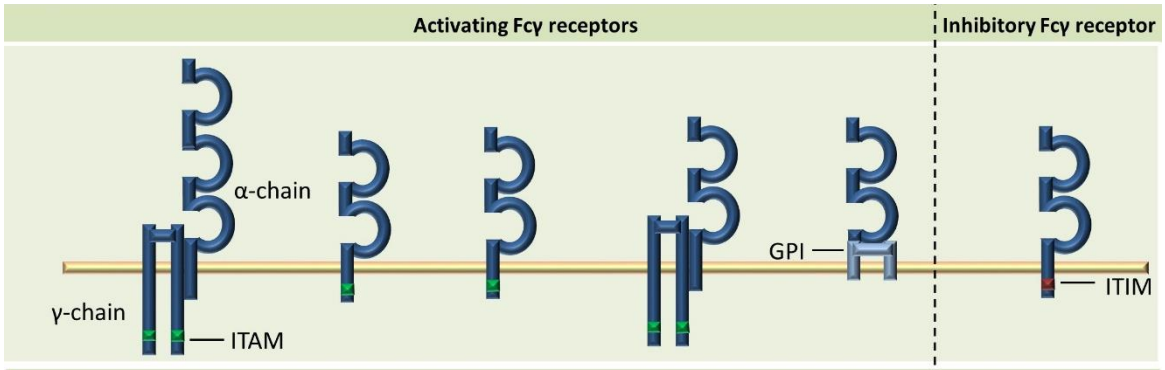

	FcγRI	FcγRIIa	FcγRIIc	FcγRIIIa	FcγRIIIb	FcγRIIb
	CD64	CD32a	CD32c	CD16a	CD16b	CD32b
B cell	---	---	+/-	---	---	+
Monocyte/ macrophage	+	+	---	+	---	+
Neutrophil	+	+	---	---	+	+
NK cell	---	---	+/-	+	---	---
Eosinophil	+	---	---	---	+	---
Basophil	---	+	---	---	+/-	+

Figure 1.9 ***Structure and expression pattern of human FcγRs.***

CD64 contains three immunoglobulin domains (represented by loops) in its extracellular domain whilst all other receptors contain two. All the activatory receptors (with the exception of CD16b) signal through ITAM sequences whilst the sole inhibitory receptor (CD32b) signals through an ITIM motif. In the case of CD64 and CD16a signalling occurs via association with the ITAM containing FcR γ-chain which is also required for transport of the receptor to the plasma membrane. CD16b is unique as it is tethered to the membrane through a GPI linker and has unknown signalling function. Information is adapted from work by Meknache (2009) Gillis (2014), Pincetic (2014) and Woolf (2014).

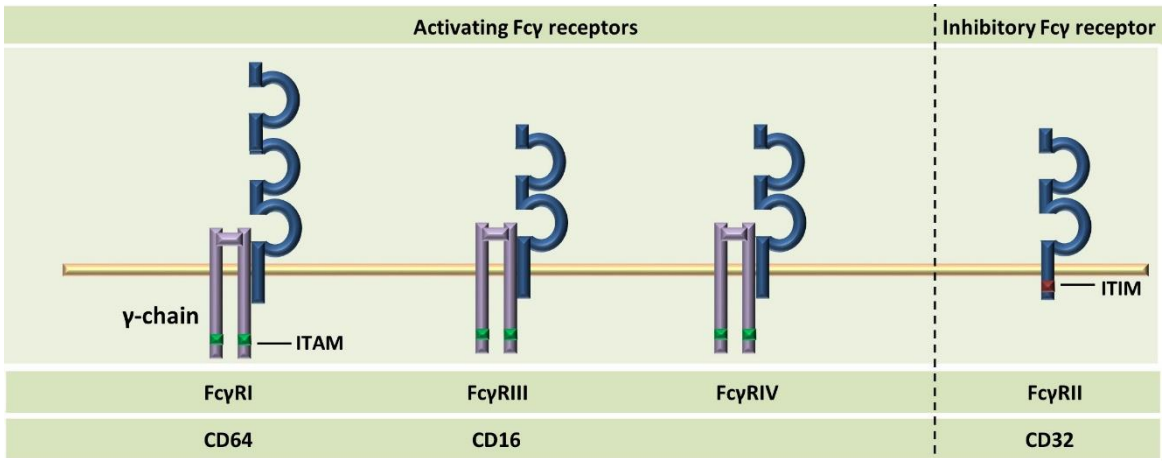

Figure 1.10 ***Structure of mouse FcγRs.***
Mice express three activatory and one inhibitory FcγR. All FcγRs contain extracellular immunoglobulin domains on their α-chains, represented by loops. CD64 has three immunoglobulin domains whilst the other receptors have two. The inhibitory receptor, CD32, has an ITIM domain in its extracellular tail for signalling. The activatory receptors have to be associated with the mouse FcR γ-chain for transport to the plasma membrane. This also contains the ITAM motifs required for activatory FcγR signalling. Information adapted from reviews by Nimmerjahn (2008) and Guilliams (2104).

1.11.2 Human FcγR specificity and function

hCD64

hCD64 is the only high affinity FcγR in humans and the only one to have three extracellular immunoglobulin domains. The receptor is capable of binding to monomeric hIgG1, hIgG3, and hIgG4 with a K_A in the range of 3.3-6.5 $x10^7M^{-1}$. On the other hand, the receptor is not capable of binding to hIgG2.[290] There has been a significant amount of work into investigating how hCD64 achieves its high affinity, with a focus on the interaction with hIgG1. This has recently been aided by two independent crystal structures of hCD64 in complex with hIgG1 being solved. The structure obtained by Kiyoshi et al is shown in Figure 1.11 with the Fc of hIgG1 interacting with the second immunoglobulin domain of CD64 as well as the interface between the second and third domains.[293] This study identified a hydrophobic pocket within hCD64, not found on the other FcγRs; this pocket was described as being suited to the binding of L235 of antibody Fc, contributing to the high affinity binding.[293] An additional report highlighted a KHR motif in the second immunoglobulin domain of hCD64. This was optimally placed to interact with the glycans on N297 of hIgG1, increasing the strength of binding.[294] This was explored further by mutational studies demonstrating that changing any of these residues resulted in a reduced affinity for hIgG1.[294] Taken together these results suggests that there are multiple mechanisms by which hCD64 achieves its high affinity.

CD64 is expressed on activated granulocytes as well as most myeloid and dendritic cells.[295] Due to its high affinity for IgG, hCD64 has been thought to act as a 'scavenger' for free IgG in the serum and to be always fully occupied by circulating IgG. However recent evidence has shown that ICs can displace free IgG from hCD64 and that the receptor is capable of mediating anti-tumour immunotherapy in a B16 mouse melanoma model.[296] Furthermore bispecific mAbs have been develop that target Her2 and hCD64. It is thought that these mAbs 'arm' neutrophils and monocytes and have given promising results in prostate cancer patients.[295, 297] It has been proposed that the preference of hCD64 for IC may arise from local cytokine stimulation, with IL-3 found to enhance IC binding to hCD64 whilst only having a minimal effect on the binding of monomeric IgG.[298] This has been postulated to occur through alterations in receptor mobility and/or clustering rather than changing expression level of the receptor itself.[298] Despite these reports, the biological importance of hCD64 in the immune system remains largely unclear.

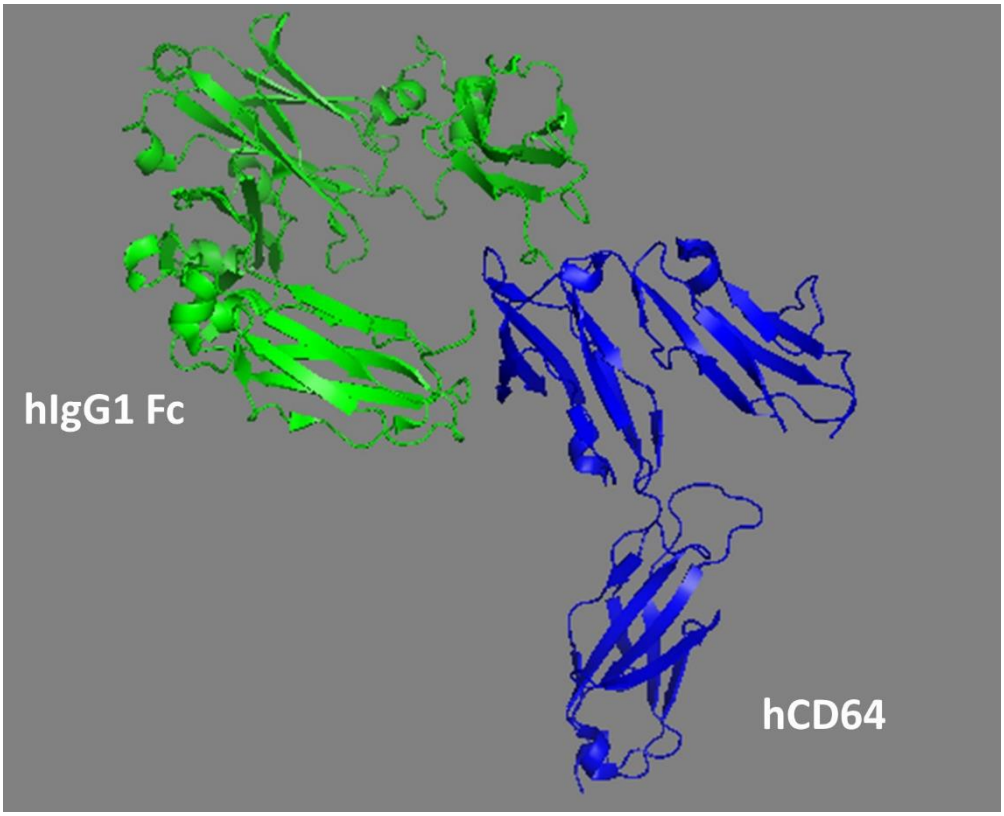

Figure 1.11 ***Structure of extracellular hCD64 in complex with the Fc of hIgG1****.*
Image produced in PyMol from PDBe submission 4w4o produced by Kiyoshi et al. 2015. Green ribbons represent the Fc from a hIgG1 whilst the blue chain presents the structure of hCD64 with the three immunoglobulin domains visible. The image is orientated so the plasma membrane would be at the bottom of the figure. The Fc interacts with CD64 in domain two and in the loop between domains two and three of hCD64.

hCD32a

hCD32a is a single chain receptor which contains its own ITAM motifs without association with the FcR γ-chain. The receptor can bind to all four human IgG isotypes, however it has the highest affinity for hIgG1 at 3.5-5.2 x$10^{6}M^{-1}$ depending on the polymorphic variant of the receptor (see section 1.11.5).[290] This polymorphic variation also affects the affinity for hIgG2 with the high affinity H131 allele having a 4.5 fold higher affinity for hIgG2 than the low affinity R131 variant.[290] hCD32a is expressed on monocytes, macrophages and neutrophils. Through its intracellular signalling it has been demonstrated to contribute to the phagocytic activity of neutrophils.[299] Additionally, experiments using a glycomodified rituximab found that blocking hCD32a reduced the *in vitro* phagocytosis of target cells by neutrophils.[300] Furthermore, mutating the antibody Fc to increase its affinity for hCD32a resulted in more efficient antibody mediated phagocytosis of beads by macrophages.[301] Taken together, these results suggest that hCD32a is important in facilitating mAb mediated phagocytosis. As mentioned previously, hCD32a is thought to form a

dimer and this dimerization is required for efficient signalling. Mutating the residues at the dimer interface in hCD32a did not interfere with ligand binding but did reduce ITAM phosphorylation.[302] This suggests that dimerization is important for hCD32a to mediate effector cell functions

Interestingly a role for hCD32a has been implied in autoimmunity. In one study hCD32a Tg mice were found to be more susceptible to collagen induced arthritis than non-Tg controls with a high incidence of spontaneous autoimmunity as mice aged.[303] Whether changes in hCD32a expression in humans relates to human disease remains to be seen.

hCD32b

The inhibitory FcγR, hCD32b has the lowest affinity out of all human FcγRs for hIgG1, hIgG2 and hIgG3 (1.2, 0.2, 1.7 $x10^5 M^{-1}$ respectively), whilst its affinity for hIgG4 is similar to that for the other low affinity receptors.[290] This receptor plays an important role in regulating immune responses; it is the only FcγR on B cells and is thought to negatively feedback on antibody production. This feedback loop may provide an important checkpoint to restrict antibody production and reduce the risk of autoimmunity.[218] Additionally, hCD32b is expressed on macrophages and neutrophils, where several activatory receptors are also expressed. It is thought that the expression of hCD32b tightly controls the pro-inflammatory response of macrophages, this is evidenced by experiments in CD32 deficient mice which display increased macrophage activity and an increased susceptibility to collagen-induced arthritis.[304] Finally, in follicular dendritic cells, hCD32b it is thought to trap immune complexes containing antigen in the germinal centre, a process important for driving a B cell response in the germinal centres.[305] This indicates the broad range of functions that can be performed by hCD32b. [306]

Two major isoforms of hCD32b exist, known as CD32b1 and CD32b2. The b1 isoform contains a 19 amino acid insertion in its intracellular domain and is expressed primarily in B cells whereas the b2 isoform is expressed in myeloid cells.[307] Whilst both isoforms of the receptor retain signalling capacity, the b1 isoform does not have the ability to localise into clathrin coated pits and, unlike CD32b2, can not mediate endocytosis.[308]

As has been demonstrated previously, as well as modulating the response of effector cells, hCD32b binding facilitates the internalisation of rituximab via a cis interaction on the target cell.[253] This was found to significantly impact ADCC and phagocytosis by removing the CD20 antigen and depleting rituximab from the circulation.[309] Furthermore, in mice lacking CD32 the activity of direct

targeting antibodies was improved, highlighting the role of the receptor in limiting mAb efficacy.[221] In addition, hCD32b has also been associated with autoimmunity. A polymorphism which encodes for an isoleucine (I) to threonine (T) substitution at position 232 results in reduced inhibitory activity, was found to be strongly associated with systemic lupus erythematosus (SLE).[310] Furthermore, expression of hCD32b was found to be reduced on memory B cells from patients with active SLE.[311] Overall, it is clear that hCD32b plays an important role in regulating the immune response and therefore defects in its function are associated with autoimmune conditions.

hCD32c

The hCD32c gene is the result of an unequal cross-over event between hCD32a and hCD32b during evolution of the low affinity FcγR gene locus, resulting in a receptor with the extracellular ligand binding domain of hCD32b and the intracellular signalling domain of hCD32a.[312] The majority of individuals contain a haplotype that contains an upstream stop codon, inherited with a polymorphism that inserts a proline residue within the gene, together resulting in a lack of hCD32c expression.[313] Just 20% out of 146 individuals tested were found to contain the open reading frame for hCD32c.[313] It was initially thought that, in these individuals, hCD32c expression was restricted to NK cells, however more recently expression has been seen on B cells. In the case of response to anthrax vaccination, individuals with expression of hCD32c gave an improved response to vaccination.[314] Despite the hCD32c open reading frame resulting in receptor expression on NK cells, there was found to be no significant difference in rituximab induced ADCC when using NK cells from donors with or without the open reading frame for hCD32c.[312] This is in contrast to earlier studies which suggested that donor NK cells expressing certain isoforms of hCD32c were able to facilitate redirected ADCC.[315] On the other hand, when using NK cells from donors lacking the open reading frame, no killing was observed in the same assay. Taken together these results suggest that hCD32c is capable of inducing ADCC *in vitro,* however how much this contributes to effector function in complete biological systems is unclear.

hCD16a

The affinity of hCD16a for hIgG subtypes varies with polymorphisms in the receptor, however CD16a has a highest affinity for monomeric hIgG1 and hIgG3, compared to the other IgG subclasses (K_A: 12-20 and 77-98 $x10^5 M^{-1}$, respectively). The receptor can still bind to hIgG2 and

hIgG4 but with a lower affinity (K_A:0.3-0.7 and 2.0-2.5 $x10^5M^{-1}$, respectively).[290] hCD16a is the only FcγR expressed on the NK cells from the majority of individuals, whilst it is also expressed on monocytes and macrophages.[218] Given that NK cells have been found to induce potent tumour-lysis *in vitro* following rituximab therapy, it seems that interaction with hCD16a may be important in anti-CD20 immunotherapy.[181] For example, it has been found that $CD56^{bright}$ NK cells, lacking hCD16a expression were less cytotoxic than $CD56^{dim}$ NK cells with a high level of hCD16a expression.[316] Moreover there is evidence that hCD16a is important for mediating ADCP. In a fibroblast cell line, lacking endogenous FcγR expression, transfection with hCD16a rendered the cells able to phagocytose opsonised erythrocytes, suggesting that this receptor in isolation is sufficient to facilitate phagocytosis.[317] In a more biologically relevant system, the blocking of hCD16a on human monocyte-derived macrophages was found to significantly reduce the phagocytosis of rituximab opsonised targets.[318] Further evidence for the importance of hCD16a in mAb therapy comes from investigations into polymorphic variation within the receptor; this will be discussed in detail in section 1.11.5. Taken together these results demonstrate that hCD16a is an important mediator of effector mechanisms that are known to be required for immunotherapy.

<u>hCD16b</u>

hCD16b is a GPI linked receptor that is structurally similar to hCD16a. Little is known about the function and signalling of the receptor however, the obinutuzumab mediated phagocytosis of CLL cells by polymorphic mononuclear cells (PMNs) was found to require the expression of hCD16b and hCD32a, suggesting that the receptor does have functional consequences.[300] It was originally thought that hCD16b expression was limited to neutrophils however its expression has since been found on basophils.[288] A meta-analysis of 16 studies found a significant association between loss of hCD16b copy number and autoimmune conditions, particularly SLE and rheumatoid arthritis.[319] One possibility is that reduced expression of hCD16b may slow the internalisation of immune complexes. This could result in the deposition of immune complexes in the tissues, a characteristic of SLE.[319, 320] Despite this the function of hCD16b remains largely unclear particularly with regard to the signalling pathways it engages to exert effector function.

1.11.3 Mouse FcγRs

As has already been mentioned, mice express three activatory and one inhibitory FcγR which broadly cover the same functions as the equivalent family of human receptors. All activatory FcγRs in mice require association with the FcR γ-chain for cell surface expression and signalling. As with humans, each FcγR has a unique binding profile for mIgG subclasses which is summarised in Table 1.3.

	mIgG1	**mIgG2a**	**mIgG2b**	**mIgG3**
mCD64 (FcγRI)[321]	-	High	Low	Very low
mCD32 (FcγRII)[322]	Low	Low	Low	-
mCD16 (FcγRIII)[322]	Low	Low	Low	-
FcγRIV[321]	-	High	High	-

Table 1.3 ***Relative binding affinities of mFcγRs for mIgG isotypes.***
Data was determined for the binding of monomeric IgG to each receptor, blacks indicate that binding was not observed. Additional information adapted from Bruhns, 2012

When comparing the mouse and human systems, the inhibitory receptor (mCD32) performs a similar function to its human homologue, as does the high affinity receptor mCD64. In contrast, mice lack an equivalent of hCD16b and hCD32c, suggesting that the gene duplication events resulting in the formation of these receptors occurred after evolutionary divergence of mice and humans.[218] In terms of extracellular sequence similarity hCD16a is considered to be the orthologue of mFcγRIV, and hCD32a the orthologue of mCD16, however fundamental differences remain between these pairs of receptors.[323] For example hCD32a contains an ITAM sequence within its extracellular tail whereas mCD16 does not and instead associates with the FcR γ-chain.[218] Further complications in comparison between the mouse and human systems arise when investigating the expression patterns of each receptor. For example hCD64 is widely expressed on myeloid cells whereas expression of the murine receptor is restricted to monocyte derived DCs.[324] Furthermore, hCD16a is expressed on NK cells whereas its mouse homologue (based on sequence), FcγRIV is not. Instead mCD16 is expressed on NK cells and displays a much broader expression profile than hCD16a.[324]

Overall the family of receptors performs a comparable role between mice and humans, this is evidenced by the use mice lacking activatory FcγRs in which rituximab mIgG2a did not have any significant anti-tumour activity.[241] However the differences in specificities and expression profile should be carefully considered when making assumptions about human FcγRs from experiments performed in mice.

1.11.4 FcγR Signalling

In order to generate effector cell function following mAb engagement, FcγRs have to be able to induce signalling within the cell expressing the receptor. This signalling occurs through the phosphorylation of the ITAM or ITIM motifs on the intracellular tails of FcγRs. ITAMs are highly conserved sequences found within numerous receptors including the BCR and the T cell co-receptor CD3.[325] The ITAM consists of the sequence YXXL/I which is found in duplicate with 6-8 amino acids between the repeats.[326, 327] Mutagenesis of the tyrosine residues within the ITAM abrogates signalling completely whereas mutation of the surrounding residues reduces the magnitude of signalling, strongly suggesting that the phosphorylation of the tyrosine residues is essential for signalling.[328] The signalling pathways downstream of activatory FcγR engagement are summarised in Figure 1.12.[218, 322]

When multiple antibodies engage antigens they can form ICs. The antibodies present in a single IC can engage multiple FcγRs present on the same cell, causing the receptors to cluster and become cross-linked. This cross-linking causes the tyrosine residues within the ITAMs to be phosphorylated by Src family kinases.[329] However the genetic deletion of individual Src kinases (Hck, Fgr and Lyn) delayed induction of phagocytosis but did not stop it, suggesting that Src kinases are important for signalling but that different family members have overlapping function.[330] The ITAM phosphorylation provides a docking site for the Src homology-2 (SH2) domains of spleen tyrosine kinase (Syk); this induces a conformational change in Syk which stabilises the complex.[331, 332] Stabilisation of Syk leads to autophosphorylation, activating Syk for phosphorylation of downstream targets.[333] Importantly CD32a cross-linking has been shown to result in phosphorylation of the receptor and Syk, suggesting that this is the pathway activated following FcγR engagement.[299] Downstream of Syk there are two distinct pathways, through Ras or PI3K. Signalling through Ras activates the ERK/MAPK pathway. This has been shown to result in the degranulation of NK cells, as well as proliferation of macrophages following FcγR cross-linking.[334,

[335] On the other hand, activation of PI3K facilitates the phosphorylation of phosphadidylinositol (4.5) phosphate (PIP_2) to form PIP_3 in the plasma membrane. The activation of PI3K has been demonstrated to be required for phagocytosis of IgG opsonised particles larger than 2µM in diameter.[336] The production of PIP_3 provides a docking site for, and activating phospholipase C-gamma (PLCγ).[337, 338] PLCγ functions to catalyse the formation of inositol 1,4,5-trisphosphate (IP_3) and diacylglycerol from PIP_2. Diacylglycerol is able to activate protein kinase C (PKC), a process which is important for phagosome formation.[339] On the other hand, IP_3 is able to increase the release of calcium from intracellular stores, although this process is not required for phagocytosis by macrophages.[340] Instead, phagocytosis is signalled through the activation of small GTPases which are activated by the activity of PI3K. The function of Rho GTPases is to reorganise F-actin, this allows the formation of the phagocytic cups required for phagocytosis.[341] The expression of CD32a in fibroblasts allowed the cells to act as phagocytes, however blocking expression of the Rho GTPases Cdc42 and Rac1 inhibited phagocytosis, highlighting the importance of this family of proteins.[342]

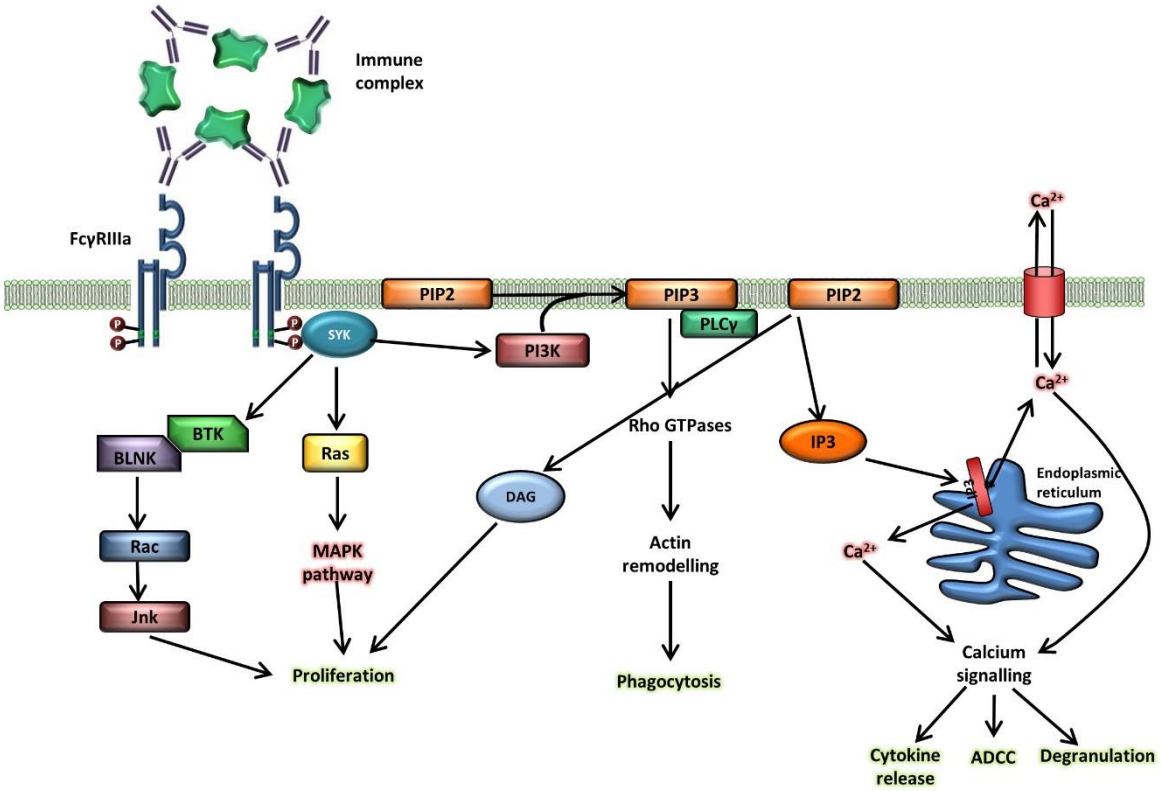

Figure 1.12 ***Pathways involved in activatory FcγR signalling.***

Crosslinking of FcγRIIIa (CD16a) by ICs results in phosphorylation of the ITAM regions on the receptor associated FcR γ-chain. This phosphorylation provides a binding site for Syk which facilitates the activation of the Ras and JNK pathways. These result in the proliferation of the cell. Syk is also able to activate PI3K which catalyses the generation of PIP_3, a molecule which can result in phagocytosis through Rho GTPase signalling. Additionally PIP_3 recruits PLCγ which can catalyse the formation of DAG and IP_3 from PIP_2 leading to the release of calcium from intracellular stores, this can lead to the degranulation of NK cells. Information adapted from Nimmerjahn (2008) and Daeron (1997)

Recent work has confirmed that phosphorylated ITAMs are required for the formation of phagocytic cups in macrophages; Nck binds to the phosphorylated ITAM, allowing the recruitment of N-WASP in the presence of Cdc42.[343] Importantly, N-WASP is required for phagocytic cup formation. This provides evidence that ITAM phosphorylation is key to driving this process. In NK cells the intracellular signalling following FcγR cross-linking is primarily mediated through calcium release from intracellular stores, resulting in the exocytosis of lysosomes containing cytotoxic proteins such as perforin.[230]

The inhibitory FcγR in both humans and mice (CD32b and CD32, respectively), signals through an intracellular ITIM domain with the sequence V/IcYxxL/V where x represents any amino acid.[344] As with the ITAM, it is the phosphorylation of the tyrosine residue within this sequence that is necessary for signalling. Tyrosine phosphorylation occurs after receptor cross linking and is mediated by Lyn or other Src family kinases; Lyn itself is activated by ITAM-containing receptors which co-locate with CD32b.[345, 346] This phosphorylation of provides a docking site for the SH2 domain of Src homology 2 containing inositol phosphatase (SHIP).[347] This stabilises and activates SHIP, allowing it to hydrolyse PIP_3, otherwise generated by ITAM signalling.[348] The mechanism of CD32b signalling is shown in Figure 1.13, demonstrating that activated SHIP can also recruit Shc and Dok which are able to downregulate MAPK signalling through inhibiting Ras.[349, 350] This further prevents effector cell activation and proliferation.[351, 352] In B cells, CD32b can further act to activatory signalling by reducing the phosphorylation of CD19, this molecule normally functions as a B cell receptor and can activate PI3K, an effect reduced by CD32b signalling.[353]

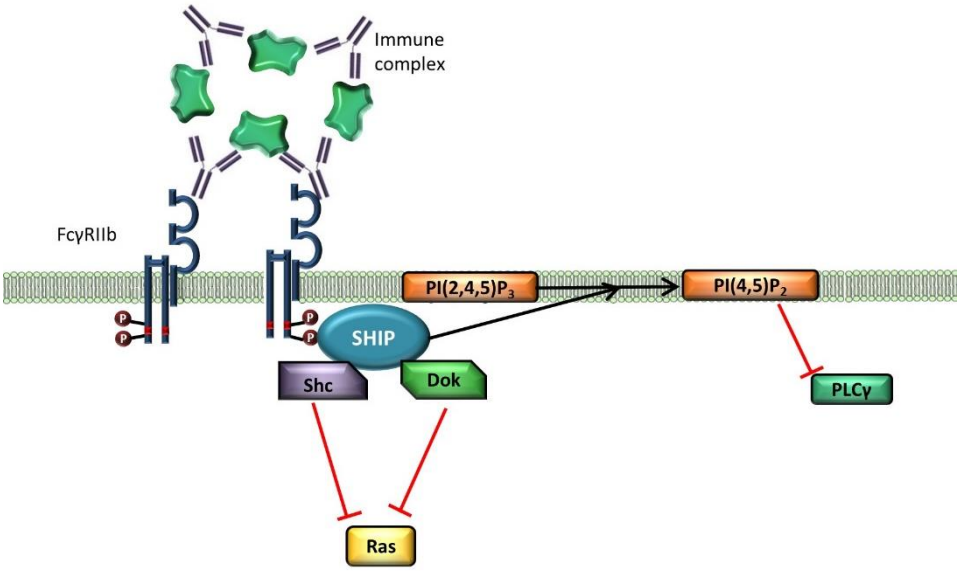

Figure 1.13 ***Signalling pathways mediated by FcγRIIb (CD32b).***
Following cross-linking, the receptor is phosphorylated, providing a docking site for SHIP. This catalyses the production of PIP_2 to inhibit PLCγ signalling. Additionally SHIP recruits Dok and Shc which can inhibit Ras mediated intracellular signalling. Information adapted from Pritchard, 2003 and Getahun, 2015

1.11.5 Human FcγR polymorphisms

The interaction between the IgG Fc region and FcγR is crucial in mediating effector cell function; however genetic analysis has revealed a number of polymorphisms within FcγR genes that affect their affinity for antibody Fc. These polymorphisms have been associated with various (particularly autoimmune) diseases as well as with altered response to mAb therapy. These are summarised in Table 1.4 .

One such polymorphism has been found in CD32a, where a single nucleotide change encodes for either a histidine (H) or arginine (R) at amino acid position 131.[354] The H allele has an approximately 1.5 fold higher binding affinity for hIgG1 ($52x10^6M^{-1}$ Vs $35x10^6M^{-1}$ for R allele) and importantly is the only receptor capable of interacting efficiently with IgG2.[290] Several studies have investigated the association between this polymorphism and disease susceptibility and progression. One such study found that, compared to healthy controls, the high affinity H allele of CD32a was found at a significantly higher frequency in patients with Guillain-Barré syndrome (GBS), an autoimmune condition characterised by autoantibodies against nerve constituents.[355] Furthermore, the H allele was associated with more severe symptoms in the same cohort of GBS patients. Similarly, the H allele was also found to be associated with development of Kawasaki disease (KD) suggesting that the high affinity allele is associated with susceptibility to autoimmune conditions.[356] Studies into FcγR polymorphisms have been extensively investigated in association with the connective tissue autoimmune condition SLE. Whilst some studies were unable to find a significant association, a recent meta-analysis of 35 articles with over 12,000 combined individuals found a significant association between the low affinity R131 allele and SLE.[357] Finally, conflicting results have been produced by studies investigating the association between CD32a polymorphisms and immune thrombocytopenic purpura (ITP) a condition where autoantibodies are produced against platelets, resulting in their depletion. A meta-analysis concluded that the H131R polymorphism in CD32a was associated with susceptibility to childhood onset ITP in Caucasian populations but was not associated with disease development in the wider population.[358] Taken together, an association has been found between CD32a polymorphisms and a number of autoimmune conditions. However the high affinity allele was found to be associated with ITP and KD whilst the low affinity allele correlated with SLE. It is possible that this relates to the pathology of the disease; in ITP the high affinity results in increased platelet deletion whereas

in SLE the removal of ICs may improve disease pathology meaning the low affinity R131 allele results in accumulation of IC, increasing disease pathology.

FcγR	Polymorphism	Frequency		Functional significance
CD32a	H131R	HH	33.2%	H allele has a higher affinity for IgG1, 2 and 3. The H allele may also be associated with some autoimmune conditions.[290, 355]
		HR	47.4%	
		RR	19.3%	
CD32b	I232T	II	66.0%	T allele has reduced signalling as a result of diminished lipid raft localisation[359]
		IT	30.4%	
		TT	3.6%	
CD16a	F158V	FF	58.6%	V allele has a higher affinity for IgG1 and may give an improved response to anti-CD20 mAbs. [223, 224, 290]
		FV	33.8%	
		VV	7.6%	
CD16b	NA1/NA2	NA1/NA1	7.3%	Haplotype with one synonymous and four non-synonymous mutations. NA1 has a higher affinity for IgG1 and IgG3[290, 360]
		NA1/NA2	43.1%	
		NA2/NA2	49.5%	

Table 1.4 ***Common human FcγR polymorphisms****.*

Polymorphisms in CD32a, CD32b and CD16a result from a single nucleic acid change whereas the variation in CD16b is encoded as a haplotype with five mutations. Variation in CD16a, CD32a and CD16b alters receptor affinity for human IgG whereas the polymorphism in CD32b affects receptor redistribution into lip rafts. Frequency data is taken from the 1000 genomes project (http://browser.1000genomes.org/index.html) with the exception of CD16b where data comes from 218 control patients in a single study, Bournazos, 2010

With CD32a known to be expressed on phagocytes, several studies have investigated the correlation between the H131R polymorphism and response to direct targeting mAb therapy. In one such study, whilst there was no difference in prognostic characteristics between genotypes in NHL patients, those with the HH genotype were more likely to have a complete response to rituximab treatment when given in conjunction with chemotherapy.[361] It should however be noted that this study was carried out on a small cohort with just 9 patients homozygous for H131. Further investigations have found that CD32a genotype does not predict response to rituximab in CLL patients or impact response to rituximab plus CHOP in DLBCL.[227, 362] These reports support a meta-analysis of 2831 colorectal cancer patients receiving cetuximab where there was no association between either allele and clinical response. Taken together, the evidence from the largest studies points to CD32a polymorphism status not impacting on response to direct targeting mAb treatment.

The inhibitory FcγR, CD32b can contain a rare I232T polymorphism. This amino acid is in the transmembrane region of the receptor.[363] One study in a south east Asian cohort found an association between the I232 allele and development of SLE, however a similar study in a Caucasian cohort found no association, suggesting that environmental factors may also be important in SLE development.[364, 365] Furthermore, this association based on ethnicity was supported by a recent meta-analysis.[357] One complication from these studies is that the T232 allele is found at lower frequencies in Caucasian populations, making it more difficult for studies to have sufficient statistical power. Additionally a study of rheumatoid arthritis patients found T232 to be associated with more severe disease, characterised by radiologic joint damage.[366] A further study identified an association between T232 and kidney deficiency in RA patients.[367] Taken together these results suggest that in a number of cases the T232 allele of CD32b is associated with susceptibility and increased severity of autoimmune conditions. This susceptibility suggested that the T232 allele may have reduced inhibitory function; this has been investigated with demonstrations that I232T does not affect ligand binding but reduces the ability of the receptor to associate with lipid rafts.[359] These lipid rafts are areas of the membrane where signalling molecules are thought to be brought together to increase the signalling efficiency. This has been highlighted by experiments where the T232 allele led to the reduced inhibition of BCR signalling, which may result in increased B cell activity, an important component of autoimmune conditions.[359]

In vitro experiments to investigate the activity of the CD32b polymorphic variants in response to mAb therapy found that a human macrophage cell line expressing T232 had a higher phagocytosis

of opsonised pneumococci than cells expressing I232; suggesting that the T allele confers reduced inhibitory signalling.[368] In the same study, T232 macrophages were found to have an increased induction of the proinflammatory factors IL-6 and TNF-α during the experiments. This implies that T232 is less active and therefore confers less inhibition on macrophage activity. Despite these results, Weng et al have demonstrated that the CD32b genotype had no effect on the clinical outcome of follicular lymphoma patients treated with rituximab, although this study lacked power due to the rarity of the T232 allele.[369] Overall, it appears that whilst the CD32 I232T polymorphism is associated with autoimmune conditions, it either does not have a significant effect on response to mAb therapy or studies with sufficient statistical power are yet to be performed.

The NA1 and NA2 haplotypes of CD16b have not been investigated to the same extend as other FcγR polymorphisms, perhaps reflecting our reduced understanding of CD16b biology. Neutrophils from donors homozygous for NA1 have been described to have increased phagocytosis of particles opsonised with IgG1 or IgG3.[360] Later studies suggested that this was due to the higher capacity of the NA1 isoform to prime CD32a, rather than being due to differences in affinity.[370] Idiopathic pulmonary fibrosis (IPF) results from lung injury, although the mechanism of this is unclear, it is postulated that there is a role for immune complex in this injury. The high affinity NA1 allele of CD16b was found at a higher frequency in IPF patients than in controls although there was no association with disease progression.[360] An additional analysis identified a modest association between CD16b haplotypoe and SLE susceptibility.[357] There has been a single study investigating the CD16b haplotypes in mAb therapy. This found no association between either variant and response to rituximab therapy.[371]

A polymorphism in CD16a was identified in 1997, where a single nucleotide change encodes for a substitution from a phenylalanine (F) to valine (V) at position 158 (sometimes referred to as position 176).[372] The same study went on to demonstrate that the V158 allele had a higher affinity for pooled human IgG1 and IgG3 than the F allele. Work has gone on to investigate the association of this polymorphism with autoimmune conditions; including analysis showing that the low affinity F158 is associated with SLE.[357] Furthermore, SLE patients homozygous for F158 were more likely to develop renal disease than V allele carriers, suggesting V allele carriers may be able to more effectively clear ICs which would otherwise cause kidney damage.[373] Interestingly, for CD16a the low affinity allele is associated with SLE, similar to the observations for CD32a, further suggesting that reduced IC clearance increases risk and severity of SLE and that activatory FcγR are central to this process.

Given the important role played by CD16a in NK cell and macrophage activation, substantial attention has been devoted to the significance of the F158V polymorphism in response to mAb therapy. In studies of FL patients, Cartron and Weng independently demonstrated that patients homozygous for V158 had an improved progression free survival compared to F allele carriers when treated with rituximab.[223, 224] In the latter study V158 homozygous patients had a progression free survival of 533 days compared to 148 days for heterozygous patients. This is thought to occur as the dissociation constant of rituximab for V1758 is 660nM compared to 2000nM for F158.[185] The increased affinity is thought to result in more efficient effector cell signalling and therefore target cell clearance. These investigations focussed on the use of rituximab as a single agent, however it is commonly given in combination with chemotherapy. Even when given as R-CHOP, Persky et al found the V158 allele to be associated with improved outcome. In FL, 100% of VV patients were still alive five years after treatment compared to 75% of the F158 homozygous patients.[374] Despite this, similar studies have been less conclusive, for example, in a study of DLBCL patients treated with R-CHOP, there was a trend towards increased progression free survival in V158 homozygotes; however this did not reach significance.[225] Furthermore a study of 460 FL patients treated with rituximab plus chemotherapy, followed by two years of rituximab maintenance therapy, concluded that the CD16a genotype had no effect on progression free survival.[375] These seemingly conflicting results may arise from differences in treatment schedule, especially the prolonged maintenance treatment in the latter study, as well as patient disease stage and differences in methodologies used for genotyping patients.[226]

Whilst rituximab has been the focus of most studies into CD16a polymorphisms, there have also been studies to investigate if CD16a genotype is a useful predictor of outcome to cetuximab therapy. In three separate studies investigating patients with metastatic colorectal cancer, patients with one or more V158 allele were found to have an increased response to cetuximab therapy, although in one of these studies the trend did not reach significance.[376-378] In contrast, a number of studies came to the opposing conclusion that patients homozygous for the V158 allele had a poorer response to cetuximab treatment[379, 380] These seemingly polar results are representative of the field and highlight the variation observed. However, in a retrospective analysis of these studies Mellor et al noted that in two of these studies, [376, 381] there was significant deviation from Hardy-Weinberg equilibrium.[226] This would suggest that there was selection pressure, copy number variation or an insufficient sample size to accurately determine gene frequencies. One technical possibility for this deviation could be down to difficulties in distinguishing between the sequences of CD16a and CD16b which are almost identical in their

extracellular region.[226] Interestingly, a meta-analysis concluded that FF patients responded better to cetuximab therapy.[382] One explanation is that F158 results in less tumour deletion and therefore reduced mAb consumption, making more mAb available to block EGFR signalling.

1.11.6 Copy number variation in human FcγRs

As well as polymorphic variation in FcγR genes, there has also been described differences in copy number as a result of gene duplication or deletion events. This is widespread with over 12% of the human genome covered by copy number variation (CNV). the FcγR locus appears to be particularly susceptible to CNV.[383] An analysis of CD16b copy number found that neutrophils from donors with more than two copies of CD16b had a greater uptake of ICs than neutrophils from those with less than two copies.[384] The same study went on to find that low CD16b copy number was associated with SLE in a UK cohort. Furthermore, in rheumatoid arthritis, CD16b deletion was associated with antibody positive disease whilst duplications were associated with antibody negative disease.[385] Similar results were found for CNV in CD16a where copy number correlated with protein expression; individuals with two or three copies of the gene had NK cells with greater activity in redirected ADCC assays than NK cells from those with only one copy.[386] This result would suggest that response to direct targeting mAb may be affected by CD16a copy number although this is yet to be determined in a clinical trial. Overall these results demonstrate that genetic variation affecting FcγRs goes beyond polymorphisms and can have an effect on effector cell activity in response to mAb.

1.12 Antibody half-life

The turnover of antibody within an organism is an important process for maintaining a constant serum concentration. Normally this process is a constant cycle of antibody production and degradation. However, when mAb are injected they are gradually removed from the serum, either as a result of binding to their target or through protein breakdown. This is an important consideration in developing therapeutic mAb as a longer half life can results in a more prolonged therapeutic benefit. The serum concentration of IgG is maintained by the neonatal Fc receptor (FcRn) which scavenges IgG from the lysosome for return to the serum.[387]

1.12.1 FcRn

Whilst FcRn is a Fc receptor by name, it differs substantially from the FcγRs in its structure and function. The crystal structure revealed the receptor to be similar to MHC with an MHC I-like heavy chain and a β_2-microglobulin light chain.[388] hFcRn has two functions: to transport IgG from mother to foetus across the placenta as well as scavenging IgG from the lysosome back into the serum. Both these functions rely on the receptors unique ability to bind IgG in a pH dependent manner.[387] The receptor is capable of binding to the Fc of IgG at an acidic pH of less than 6.5 but not at a physiological pH of 7.4.[389] The process by which hFcRn mediates IgG recycling is presented in Figure 1.14.[387, 390] Typically, serum proteins and IgG are endocytosed by monocytes and endothelial cells lining the blood vessels. The endosomes become acidified which allows binding of IgG FcRn, facilitating its transport back to the cell surface where IgG dissociates in the neutral pH.[387] Whilst this maintains serum IgG concentration, hFcRn is also able to transport IgG across the placenta from mother to foetus. This happens via a similar, pH dependent process where syncytiotrophoblasts endocytose fluid containing hIgG.[391, 392] The endosomes containing IgG are gradually acidified which allows tight binding of hIgG to hFcRn, when the vesicles fuse to the foetal side of the cell, the neutral pH causes bound IgG to be released.[387] Importantly, this transport happens down a concentration gradient, preventing release of IgG on the maternal side. Overall, this is an important process in providing immune protection to the developing foetus and is facilitated by the pH dependent binding of IgG to hFcRn.

Mice also express FcRn which is closely related to its human homologue functionally and structurally. However, in contrast to human, mFcRn primarily facilitates the transfer of IgG from mother to offspring at the neonatal phase; the receptor is expressed in the epithelia of the small intestine where it is able to transport IgG in ingested milk.[393] This can occur due to the acidic nature of the stomach contents as it enters the duodenum, this facilitates IgG binding to mFcRn. Following transcytosis the mIgG is released in the neutral pH of the extracellular space

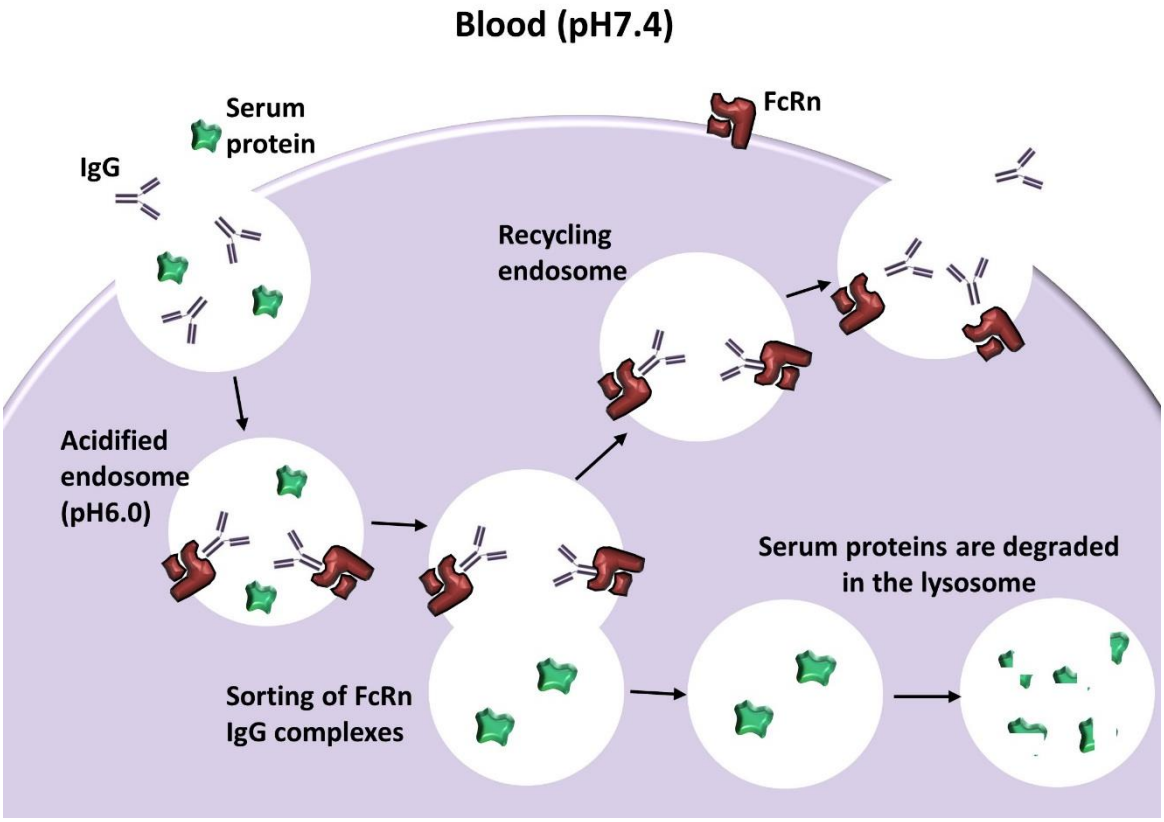

Figure 1.14 ***hFcRn mediated antibdy recycling.***
IgG and serum proteins are endocytosed by monocytes and endothelial cells. Under acidic conditions in the endosome hFcRn bings to IgG. FcRn then recycles IgG back into the circulation whilst serum proteins are broken down. hFcRn releases IgG under the neutral conditions in the blood. A similar process facilitates hFcRn mediated IgG transport from mother to foetus in the placenta. Image adapted from reviews by Roopenian (2007) and Mitragotri (2014)

The ability of FcRn to bind IgG in a pH dependent manner has been extensively investigated. It was found that upon differing pH there is no major conformational change in hFcRn which can account for the dramatic change in IgG binding.[394] Unlike the classical FcγRs, hFcRn binds to IgG in the C_H2-C_H3 hinge region, which contains several histidine residues. At an acidic pH the histidine residues are protonated, allowing interaction with acidic residues at the surface of hFcRn.[395] These results have been confirmed by mutational studies where changing the histidine residues at positions 310 and 435 in IgG to alanine severely reduced binding to hFcRn, even at an acidic pH.[396]

The importance of FcRn for extending serum IgG half-life has best been demonstrated by the use of mFcRn deficient mice. In these animals the serum half-life of mIgG was significantly reduced (9 days vs 1.4 days), with a similar reduction in half-life for hIgG. However, when mFcRn deficient mice expressed the human FcRn transgene the half-life of hIgG was restored.[397] FcRn is therefore of major significance to therapeutic mAbs where a longer half-life can lead to increased efficacy with reduced dosing. This has been demonstrated by mAb engineering with the aim of improving binding to FcRn and therefore increasing serum half-life with a large number of studies having

identified mutations in the mAb capable of increasing half-life. in one such example an N434A mutation in hIgG1 increased its half-life in hFcRn Tg mice from 5.79 days to 9.6 days, an effect achieved by a 1.6 fold increase in relative binding to hFcRn at pH 6.0.[398] In the same study a triple mutant was generated with a 3.3 fold higher affinity for hFcRn however this did not provide any extension in half-life over the single mutant.[398] Taken together these results suggest that there may be an upper limit for improving FcRn binding, reaching a point where affinity is also increased at a neutral pH, offering no further extension of half-life. In contrast, there are some cases where a reduced affinity for FcRn and therefore a shorter half-life may be beneficial. For example, when administering toxin-conjugated mAbs or when imaging antibody distribution.[387, 399]

Overall mAb half-life plays an important role in mediating function as a longer half-life for therapeutic mAbs results in an increased bioavailability which can lead to an improved therapeutic outcome. It is therefore important to understand how half-life varies between model systems in order to understand if differences in efficacy between mAbs are due to improved targeting and effector functions or a result of a more prolonged half-life due to the system selected. This is particularly important when considering the strains of mice used for experiments. These can vary significantly in their genetic make up, especially when using immune compromised mice which lack the ability to produce immunoglobulin. It has been found that administration of intravenous immunoglobulin (IVIG) saturates FcRn which can lead to shortened serum half-life.[400] It therefore stands that a lack of endogenous immunoglobulin will also alter the kinetics of mAb clearance. Understanding this as well as the impact of genetic differences is therefore an important area in the development of mAbs which has not been fully investigated.

1.13 Animal models of human disease

In order to understand disease mechanisms and to aid in the development of new therapies it is essential to be able to have *in vivo* models available. Increasing our knowledge of disease mechanism can highlight novel approaches for therapy. Furthermore, large trials in humans are expensive and time consuming. Selecting appropriate *in vivo* models can reduce the demands of a trial in humans. Despite this, even the best characterised drugs can have unpredicted side effects when used *in vivo*. Whilst animal models are often useful for identifying these off-target effects they do not negate the need for careful studies in humans. For example, as discussed earlier with TGN1412 even primate models could not predict the devastating cytokine release caused by the

drug.[157] The most common mammal for pre-clinical studies is the mouse due to its small size, relatively short generation time and the ease with which it can be genetically manipulated. It should always be remembered however that an animal model is not a direct surrogate for the human disease but rather a representation, meaning that results obtained should be interpreted with care before being applied to the human disease.[401]

There are three main approaches which will be discussed here for using mouse models to investigate anti-CD20 mAbs. The first approach is to use hCD20 Tg mice to investigate the depletion of B cells using anti-hCD20 reagents. The second approach is the use of disease models to investigate the depletion of malignant cells. These often arise from overexpression of an oncogene and provide a model of murine leukaemia that is similar to that found in humans. The final approach is to engraft leukemic cells from humans into mice. This involves using immune compromised mice, allowing for human tumour cells to be manipulated and treated in a mouse. Each of these approaches offers its own advantages and drawbacks for investigating anti-hCD20 mAbs.

1.13.1 B cell depletion in hCD20 Tg mice

One model that has been widely used to study anti-CD20 mAbs *in vivo* is the hCD20 Tg mouse.[402] In this model hCD20 is expressed on B cells as well as mouse CD20. This model means that anti-hCD20 mAbs can be studied by measuring the depletion of normal B cells from within their correct biological niche in a fully syngeneic system. Initial experiments using hCD20 Tg mice used anti-hCD20 mAbs on a mIgG2a framework in order to efficiently engage mouse effector functions to result in the depletion of circulating B cells.[242] This work highlighted the niches most resistant to B cell depletion; in the spleen of hCD20 Tg mice, marginal zone B cells were found to be more resistant to anti-hCD20 mAb therapy than follicular B cells.[242] Studies have gone on to investigate clinically relevant hIgG1 anti-hCD20 mAbs; these reagents were still able to efficiently deplete hCD20 Tg B cells as well as identifying differences in efficacy between these anti-hCD20 mAbs.[199] In addition, hCD20 Tg mice have been useful in elucidating the mechanism of action for anti-CD20 mAbs, in particular rituximab. The transfer of hCD20 Tg mouse B cells into different recipient strains was used to demonstrate that the lack of the C1q and C3 components of the complement cascade did not affect rituximab therapy, whilst depletion was abrogated in the presence of the FcR γ-chain.[199]

The hCD20 Tg mouse has therefore provided a useful system for modelling the depletion of B cells using novel anti-hCD20 mAbs and understanding their mechanism of action. However, the primary drawback of this model is that it only allows for the depletion of normal B cells rather than the malignant cells which these mAbs were designed to deplete. Models have therefore been developed to replicate human disease in mice to understand mAb therapy in the tumour setting.

1.13.2 Tcl-1 model of CLL like disease

Several models have been developed to try to replicate human CLL in mice. These have focussed around reproducing the genetic abnormalities found in human CLL. For example, the most common genetic lesion in CLL is deletion of 13q14, occurring in about 50% of cases.[403] Whilst deletion of this in mice did result in B cell proliferation and the development of CLL like disease, mice also developed $CD5^-$ NHL as well as range of other $CD5^+$ lymphoproliferations with a slow tumour presentation and low penetrance.[404] Other models have therefore aimed to give targeted overexpression of genes more exclusively related to CLL. The T cell leukaemia 1 (Tcl-1) oncogene was originally found to be over expressed in T prolymphocytic leukaemia.[405] Since this discovery, analysis of human tumour-derived B cell lines and primary B cell neoplasia's has revealed a high level of Tcl-1, with Narducci et al finding that Tcl-1 was expressed in B cell malignancies and, in particular, in all 7 cases of CLL investigated.[406]

These observations from human tumour samples led to the development of the Eμ-Tcl-1 mouse model; the entire human Tcl-1 gene was cloned under the control of a murine V_H promoter and the Eμ enhancer to give rise to B cell specific expression of the Tcl-1 gene, as shown in Figure 1.15.[407] The resulting mice spontaneously developed an expansion in $B220^{low}IgM^+CD5^+$ B cells in the peripheral blood, where such cells are rarely found.[407, 408] As well as lymphocytosis, these Tcl-1 Tg mice developed splenomegaly as well as some enlargement of the lymph nodes. Importantly the penetrance of disease in Tcl-1 mice has been found to be 100% and is coupled by features found in the more aggressive, IgV_H un-mutated form of CLL, resulting in a median survival of 11.93 months.[409] The same study went on to demonstrate that Tcl-1 leukaemias respond to the front line CLL therapy fludarabine and express targets for clinical drugs such as Bcl-2. The clinical and molecular relevance of the Eμ-Tcl-1 model has made it suitable as an investigational model for novel CLL therapies and dissection of their mechanisms.

Figure 1.15 ***Cassette used for the production of Eμ-Tcl-1 transgenic mice****.*

The human Tcl-1 gene was cloned under the control of a mouse V_H promoter and Eμ enhancer to give B cell specific expression of the human Tcl-1 gene. The construct also contains the untranslated poly(A) region of the human β-globin gene. Figure adapted from the original description of the model by Bichi (2002).

Whilst the Tcl-1 model, coupled with patient data, indicates that overexpression of the Tcl-1 gene has a major effect on the development of malignant disease, the mechanism by which this occurs is less clear. Initial studies used Tcl-1 transfected cells to demonstrate that the Tcl-1 protein co-precipitated Akt and was able to enhance its kinase activity and nuclear translocation.[410] The activation of Akt is important in cell cycle progression and inhibiting apoptosis. One target of Akt is the proapoptotic protein BAD, upon phosphorylation by Atk its function is supressed.[411] Furthermore, Akt is able to inhibit transcription factors such as FOXO3 which would otherwise promote the transcription of pro-apoptotic genes.[412] With Tcl-1 able to act as a co-activator of Akt, this offers a potential mechanism by which cell survival and proliferation is promoted in the Tcl-1 model.

Further work shows that in the Tcl-1 model there is an upregulation of components of the NF-κB pathway, although whether this effect is direct or via other targets of Tcl-1 is unclear.[413] Compared to normal B cells, CLL cells have been found to have a higher constitutive expression of NF-κB with higher Rel-A DNA binding correlated with increased resistance to apoptosis *in vitro*.[414] This provides an additional mechanism by which disease could arise in the Tcl-1 model and suggests that this mechanism may overlap with that found in CLL.[414] Overall the Tcl-1 model shares a number of characteristics with CLL and provides a model for B cell malignancy where the tumour cells occupy their correct biological niche and exist together with normal B cells.

1.13.3 Immune deficient mice for patient derived xenografts

Whilst the Tcl-1 model provides a murine model that shares features of a human disease, the most appropriate way to investigate therapies for a human disease is to treat the disease itself. This has led to xenograft models where human tumour cells are engrafted into a mouse. However these recipient mice have to be immune compromised to prevent the rejection of the human grafts. The

most commonly used immune compromised background is the severe combined immune deficient (SCID) mouse, which lacks functional T and B cells as a result of a single base pair change in the Prkdc gene.[415] This removes the effector cells of the adaptive immune system and allows for establishment of xenografts. However, SCID mice have high NK cell levels which can result in the lysis of single cell suspensions injected into the periphery.[416] In order to combat this problem, SCID mice have been crossed onto the non-obese diabetic (NOD) background. This results in mice with severely reduced NK cell numbers and function[417] Furthermore, serum from NOD SCID mice does not appear to have any significant haemolytic complement activity.[418] This same study went on to demonstrate that NOD SCID mice have a faster engraftment of human cell lines than SCID mice. Despite this NOD SCID mice still have residual NK cell activity and have a restricted lifespan due to the development of thymic lymphoma. This has led to the development of NSG mice which, on top of the NOD SCID genotype, lack expression of the common cytokine receptor γ-chain. For this reason, NSG have no detectable NK cells or NK cell activity.[419] The improved human cell engraftment in NSG mice is highlighted by experiments where $CD34^+$ cells were isolated from cord blood and allowed to establish for four weeks. After this time approximately 1% of NOD SCID PBMCs were human $CD45^+$ compared to 8% in NSG mice.[419] Since this time and, depending on the cell types used, engraftment rates have improved significantly. One recent study using direct injection of $CD34^+$ cells into the bone marrow reported engraftment as high as 45% in the blood and 75% in the spleen.[420]

The theory behind patient derived xenografts (PDX) is that multiple mice can be engrafted with a tumour sample from a single patient, these can then be subjected to compare the efficacy of multiple treatments against the same tumour.[421] This approach has been used to personalise cancer treatment. For example, transplant of tumours into 'avatar' immune deficient mice allowed for the testing of potential targeted drugs, selected based on whole exome sequencing of the tumour.[422] In one study of patients with various advanced cancers, the treatment response seen in the mouse avatars was replicated in 11 out if the 13 patients investigated.[422] This highlights how immune compromised strains of mice are an important new tool in investigating novel therapies and personalising the treatments received by patients.

The use of PDX models offers several major advantages beyond the fact that the treatment of human disease can be investigated. Firstly for solid tumours, elements of the stroma can be introduced with the malignant cells. Furthermore, injection of peripheral blood or bone marrow allows for the patients immune response to the tumour to be almost completely reconstituted, an important factor when investigating immunotherapy.[423] Whilst it is clear that PDX models are

an incredibly powerful tool for investigating novel cancer therapies against human disease, there has been little consideration of host strains beyond the engraftment of the tumour. The mutations introduced to give rise to immune deficiency are likely to have wider reaching consequences, particularly the NOD genotype which affects a number of genes. These hosts lack cell populations known to be important for mAb effector function, additionally the effect of mutations and lack of endogenous IgG on mAb half-life have not been fully explored. These factors are a vital part of mAb immunotherapy and require consideration in order to fully understand the results obtained from PDX models.

1.14 Hypothesis and aims of thesis

It is well understood that FcγRs are key receptors for a number of mAb functions and are responsible for their efficacy. Previous work has demonstrated that they are vital to the anti-tumour activity of direct targeting mAbs as well as providing important cross-linking required to mediate signally. This thesis aims to investigate this further by using novel *in vitro* and *in vivo* assays. For example, this thesis aims to investigate anti-CD20 therapy in a fully syngeneic mouse model for the first time with dissection as to the mechanism of action for different clinically relevant mAb. Finally, this thesis will investigate differences in the half-life of mAbs in immune compromised mice and determine the mechanisms behind these differences.

As a result this project had the following aims:

1) To Investigate the FcγR cross-linking requirement for the activity of immune stimulatory mAbs.
    a. To generate cell lines expressing each hFcγRs with several different known polymorphisms.
    b. Assess these cells as cross-linking agents in T cell proliferation and cytokine release assays.

2) To investigate the regulation of hCD32b expression in human B cell lines.

3) Develop a murine tumour model for the investigation of clinically relevant anti-hCD20 mAbs.
    a. Use this model to investigate differences in efficacy and mechanism of action between mAbs in isolation and in combination therapies.

4) Investigate the half-life of human IgG1 in immune compromised mice.
    a. Understand the mechanism behind differences in half-life between strains.
    b. Develop strategies for overcoming strain dependent abnormal half-life.

Chapter 2 Materials and Methods

2.1 Mammalian cell culture techniques

The cell lines predominantly used in this project and conditions used to culture them are summarised in Table 2.1. All cells were grown at 37°C in the supplemented media described, cell lines were subcultured every 2-4 days. All cells were grown in a static incubator except HEK 293F and MEXI 293E. Penicillin (P) was used at 100 U/ml and streptomycin (S) at 100µg/ml and combined as penstrep. 2mM L-glutamine (G) and 1mM sodium pyruvate (P) were also added to some cells. All media and supplements were obtained from Life Technologies except FCS (Sigma Aldrich or Lonza) 2-ME (Sigma-Aldrich), CTL-test media (Cellular Technology Limited)

Cell line	**Culture media**	**Supplements**	**% CO_2**	**Additional information**
CHO-K1 Ramos Raji	Roswell Park Memorial Institute (RPMI) 1640	10% FCS GP PS	5%	N/A
Bone marrow derived macrophages (BMDMs)	RPMI 1640	10% FCS GP PS 20% L929 media	5%	6-well plates
HEK 293F	Freestyle 293 expression media	None	8%	Orbital shaking incubator (200rpm)
Human peripheral blood mononuclear cells (PBMCs)	Cellular Technology Limited (CTL) - Test media	GP PS	5%	N/A
Tcl1 hCD20 splenocytes (Eµ-Tcl1 media)	RMPI 1640	10% FCS GP PS 55 µM 2-MercaptoEthanol (2-ME) 0.2mM asparagine	5%	NA
MEXI 293E	MEXI-CM	GP PS	8%	MEXI-TM media for transfection

Table 2.1 ***Culture conditions for mammalian cells used in this project****.*
Base media used and any supplements added are listed. BMDMs were cultured in the presence of media conditioned by the culturing of L929 cells which secrete M-CSF into the media. All cells used were grown in suspension except CHO-K1 and BMDMs which were adhearent All cell culture flasks and plates were obtained from Corning

Cells were incubated in a New Brunswick Galaxy 170 R incubator or an Infors HT shaking orbital shaking incubator. 293F, Ramos and Raji cells were subcultured every 3-4 days to maintain a density of 0.5-2.5 x10^6cells/ml. CHO-K1 cells were subcultured every 2-4 days by removing adherent cells with a cell scraper (Corning) and maintaining a confluency of 20-90%. All cells were grown in suspension with the exception of CHO-K1 and BMDMs which were adherent.

2.1.1 Determining cell viability

To determine viability, cells were stained with either propidium iodide (PI; Sigma-Aldrich) or PI plus annexin V-FITC (in-house). For PI staining alone, 2 drops of 10µg/ml PI in PBS was added to 200µl cell suspension and analysed by flow cytometry. Viable cells were those negative for PI staining. For annexin V PI staining, 100µl cell suspension was stained for 15 minutes with 2x annexin V-FITC PI (160ng/µl annexin V-FITC, 2.6µg/ml PI in 10mM HEPES pH7.4, 140mM NaCl, 2.5mM$CaCl_2$; all Fisher Scientific) before being analysed by flow cytometry. Viable cells were those negative for both PI and annexin V.

2.1.2 Determining cell concentration

Concentration of mammalian cells in solution was determined using a Coulter Counter z1 particle counter (Beckman Coulter). 20µl cell suspension was diluted in 10ml isoton II diluent (Beckman Coulter). For blood samples 2-3 drops Zap-OGLOBIN II lytic reagent (Beckman Coulter) was added to lyse red blood cells. The concentration of cells in the sample was then determined using the particle counter.

2.1.3 Transient transfection of HEK293F cells for surface expression

The day before transfection the cell concentration was determined and the cells diluted to 0.7x10^6 cells/ml and returned to the incubator. The following day, transfections were performed with either 10ml cell suspension in 125ml Erlenmeyer flasks or 3ml in 6-well plates. For flasks, 20µl 293fectin reagent was added to 330µl OtiMEM media (Both life technologies). 10µg plasmid DNA was added to a separate 330µl aliquot of OptiMEM and incubated at room temperature for 5

minutes. For plate transfections 6.6µl 293fectin, 3µg plasmid and 100µl optiMEM were used. The diluted DNA was added to the diluted 293fectin and incubated at room temperature for 20-30 minutes before being added dropwise to the HEK 293F cells and returned to the incubator. Cells were screened for protein expression 48 hours after transfection by flow cytometry.

2.1.4 Transfection of Mexi-293E cells for secreted protein

Mexi-293E cells were harvested by centrifugation at 200g for 10 minutes and were resuspended in MEXI-TM media at 1.6 $x10^6$ cells/ml with 100ml used per transfection. Cell suspension was added to a 500ml Erlenmeyer flask and 100µg plasmid DNA added. Cells were incubated at 37°C +8% CO_2 in a shaking incubator for 10 minutes. 450µl 1mg/ml linear polyethylenimine (PEI) was added dropwise and the cells returned to the incubator for 4 hours. 100ml MEXI-CM media was added to give a concentration of 0.75 $x10^6$ cells/ml. 24 hours after transfection 1.5ml 0.5M valporic acid (Sigma-Aldrich) was added and the transfections incubated for 6 days or until the viability dropped below 75%, as determined by PI staining. Supernatant was harvested by centrifuging at 1800g for 10 minutes before filtering supernatant through a 0.2µm vacuum filter unit.

2.1.5 Stable transfection of CHO-K1 cells

The day before transfection CHO-K1 cells were harvested by removing the media and adding 10ml Trypsin Ethylenediaminetetraacetic acid (TE; Lonza) and incubated at 37°C for 10 minutes. Detached cells were aspirated and washed once in complete RPMI before being plated in a 6-well plate at $3x10^5$ cells/ml in 2ml complete RPMI per well and incubated overnight at 37°C with 5% CO_2. On the day of transfection cells were at a confluency of 50-60%. 4µg plasmid DNA was added to 500µl unsupplemented RPMI media . 30µl GenePORTER reagent (Gelantis) was added to a separate 500µl aliquot of RPMI. The diluted DNA was added to the diluted GenePORTER reagent and incubated at room temperature for 20 minutes. The media was removed from the plated CHO-K1 cells and 1ml transfection mixture was added to each well before returning to the incubator for 3-5 hours. 1ml complete RPMI plus 100µl FCS was then added to each well of the 6-well plate and the cells incubated for 48-72 hours before selection.

2.1.6 Selection of stably transfected CHO-K1 cells

Transfected CHO-K1 cells were removed by scraping. Each well of transfection was resuspended in 20ml complete RPMI with appropriate selection antibiotic as shown in Table 2.2. Geneticin (Life Technologies) was used at a final concentration of 1mg/ml and puromycin (Fisher Scientific) was used at a final concentration of 10µg/ml. 200µl cell suspension was added per well to a 96-well flat bottom plate and incubated for 10-14 days until growing colonies were visible. Once colonies were visible, surface expression of the transfected protein was assessed by flow cytometry and the positive wells expanded into larger plates and eventually T75 flasks.

Plasmid	**Mammalian selection antibiotic**	**Receptors cloned**
pcDNA3 (Life Technologies)	Geneticin	CD16a V and F alleles CD32b1 I and T alleles CD32b2 I and T alleles
pIRES (Clontech)	Geneticin	γ-chain
pCI-puro (Promega/In-house)	Puromycin	CD32a R and H allele γ-chain CD64

Table 2.2 **Plasmids used for stable transfections into 293F cells.**
The antibiotic resistance of each plasmid used for stable selection is listed along with the receptors cloned into each vector. pCI-puro is a modified pCI-neo vector which the neomycin resistance cassette replaced with a puromycin resistance cassette(generated in-house).

2.1.7 Fluorescence activated cell sorting (FACS) of stable transfections

Cells to be sorted were harvested using PBS + 2mM EDTA disodium salt (Fisher Scientific) and washed once in complete RMPI. Cells were resuspended at $1x10^7$ cells/ml and transferred to a 12x75mm polystyrene FACS tube (Becton Dickinson). Cells were stained with appropriate FcγR specific Fluorescein isothiocyanate (FITC) labelled $F(ab')_2$ at a final concentration of 10µg/ml and incubated at 4°C for 30 minutes. Stained cells were then washed twice in 3ml complete RPMI before being resuspended at $5x10^6$ cells/ml. Populations with required receptor expression level were sorted using a FACS Aria using 2-way sorting, sorted cells were collected into a FACS tube

containing 1ml complete RPMI. After sorting, cells were washed in complete RPMI before being cultured in 200µl in a 96 well plate at 37°C with 5% CO_2.

2.1.8 Cryopreservation of transfected CHO-K1 cells

Transfected CHO-K1 cells were harvested using PBS + 2mM EDTA and were washed once in 15ml complete RPMI. The cell pellet was resuspended in 90% complete RPMI + 10% DMSO (Sigma-Aldrich) at approximately $2x10^6$ cells/ml and transferred to 1.8ml cryovials (Thermo Scientific) with 1ml per vial. Samples were stored at -80°C for 2-5 days before being transferred to vapour phase nitrogen storage.

2.1.9 Generation of mouse bone marrow derived macrophages (BMDMs)

All bones of the hind legs of a mouse were dissected and flushed through with sterile, complete RPMI to remove the bone marrow. Bone marrow was pipetted up and down to break up clumps and centrifuged at 450g for 5 minutes. Cells were counted and adjusted to a concentration of $1x10^6$ cells/ml in complete RPMI. 4 ml per well was added to a 6 well plate with the addition of 1ml filtered L929 conditioned media, containing M-CSF, to stimulate macrophage differentiation. The media was replaced every 3 days with the differentiated BMDMs used of days 7-10.

2.2 Protein techniques

2.2.1 Determining protein concentration

Protein concentration was determined using a NanoDrop spectrophotometer (Thermo Scientific) measuring absorbance at 280nm. The NanoDrop was blanked with appropriate buffer before 2µl sample was added to the nanodrop stage and the absorbance recorded. The concentration of the sample was calculated as follows:

$$Concentration = \frac{absorbance}{Extinction\ coefficient\ x\ path\ length}$$

The path length was 1cm and the extinction coefficient used was 1.45 for human IgG or 1.35 for mouse IgG, for all other proteins the extinction coefficient was calculated from the protein sequence using the ExPASy ProtParam tool (http://web.expasy.org/protparam/).

2.2.2 Concentration of protein

Protein samples were concentrated using Amicon Ultra 15ml or 4ml centrifugal filters (EMD Millipore). For mAbs concentrators with a 10kDa molecular weight cut off (EMD Millipore) were used. Samples were added and centrifuged at 3200g until the volume was sufficiently reduced to give the appropriate concentration of protein.

2.2.3 Heat aggregation of IgG

IgG to be aggregated was dialysed into PBS using a slide-a-lyser with a 10kDa molecular weight cut off (Thermo Scientific). IgG was heated to 64°C for 30 minutes. A 20µl sample was analysed by high performance liquid chromatography (HPLC) using a Zorbax GF-250 column (Agilent). To purify the aggregated and monomeric fractions the sample was run through a superdex S200 column with a flow rate of 9ml and hour and fractions taken at 15 minute intervals. Fractions corresponding to monomeric or aggregated IgG were identified from the UV trace with aggregated fractions having a shorter column retention time. Appropriate fractions were pooled and concentrated before being analysed by HPLC and dialysed into PBS for storage at 4°C.

2.2.4 Purification of histidine-tagged proteins

Supernatant containing histidine-tagged proteins was adjusted to have a final concentration of 10mM Imidazole by the addition of 500mM imidazole buffer (20mM sodium phosphate, 0.5M NaCl, 500mM Imidazole pH 7.4; all Fisher Scientific). The sample was loaded onto a 1ml HisTrap column (GE Life Sciences) at a rate of 2ml/minute using an Akta Prime system (GE Life Sciences). The column was washed with 20 column volumes of 20mM Imidazole buffer. The bound protein was eluted with 250mM Imidazole and collected into 0.5ml fractions.

2.2.5 Sodium dodecyl sulphate polyacrylamide gel electrophoresis (SDS-PAGE)

Protein samples were added to 4x Laemmli sample buffer (200mM Tris HCl (pH6.8), 400mM 2-ME, 8% SDS, 0.4% brilliant blue, 40% Glycerol; all Sigma-Aldrich) and heated to 95°C for 5 minutes. Samples were loaded into a 10 well 10% Novex NuPage gel (Life Technologies) in MOPS buffer (5mM MOPS, 70mM SDS, 5mM Tris-HCl, 1mM EDTA). The gel was run at 100v for 30 minutes before being run at 120v for approximately 1 hour. The gel was stained with staining buffer (10% glacial acetic acid, 20% propan-2-ol (both VWR) 0.05% (w/v) Brilliant Blue) for approximately 30 minutes on a shaking platform. The gel was transferred to destain (5% methanol, 7% glacial acetic acid, 4.4L water) and returned to the shaking platform. Once the residual staining was cleared the gel was imaged.

2.2.6 Deglycosylation of proteins

To remove N-linked glycans 12µl protein in PBS (10-20µg) was added to 1µl 5% SDS and 1µl 1M dithiothreitol (DTT) and heated to 95°C for 5 minutes before being cooled at room temperature. 2µl PBS, 2µl 10% NP-40 (Calbiochem) and 2µl (1000 units) PNGase F (Promega) were added and incubated at 37° for 2 hours before being analysed by SDS-PAGE to confirm the removal of sugars.

2.3 Extracellular flow cytometry

For direct labelling of surface proteins $1x10^5$ cells in 100µl culture media were added to a FACS tube. In-house labelled antibodies and $F(ab')_2$ fragments were used at a final concentration of 10µg/ml. Commercial antibodies were used at the recommended concentration. Cells were incubated with fluorescently labelled antibodies at 4°C for 30 minutes or room temperature for 15 minutes in the dark before being washed twice with 1-3ml FACS wash (PBS + 1%BSA (Europa Bioproducts) + 0.01%+ sodium azide (Sigma-Aldrich)). Samples were analysed using a FACScan, FACS Calibur or FACS Canto II (Becton Dickinson). Flow cytometry data analysis was performed using FCS express software (DE Novo software). Fluorescently labelled antibodies used for flow cytometry are listed in Table 2.3.

Antigen	Clone	Isotype	Fluorophore	Supplier
Human CD4	RPA-T4	Mouse IgG1	Pacific Blue	Biolegend
Human CD8	RPA-T8	Mouse IgG1	APC	Biolegend
Human CD16	3G8	$F(ab')_2$ mIgG1	FITC	In-house
Human CD32a/b	AT10	$F(ab')_2$ mIgG1	FITC	In-house
Human CD32b	6G08	Human IgG1	APC or FITC	Bioinvent
Human CD64	10.1	$F(ab')_2$ mIgG1	FITC	In-House
Human CD20	Rituximab	Human Chimeric IgG1	FITC	In-House
Human/mouse B220	RA3-6B2	Rat IgG2a	PerCP or APC	Biolegend or eBioscience
Human IgG	SB2H2	Mouse IgG1	FITC	In-House
Human IgG	Polyclonal	Goat	PE	Jackson
Mouse CD16	AT154-2	$F(ab')_2$ rIgG2b	FITC	In-house
Mouse CD5	53-7.3	Rat IgG2a	FITC or APC	Biolegend
Mouse CD19	1D3	Rat IgG2a	PE	In-house
Mouse CD32	AT130-2	$F(ab')_2$ mIgG2a	FITC	In-house
Mouse CD64	AT152-9	$F(ab')_2$ rIgG2a	FITC	In-house
Mouse FcRIV	AT137	$F(ab')_2$ rIgG2a	FITC	In-house
Mouse/human CD11b	M1/70	Rat IgG2b	Pacific Blue	Biolegend
Mouse CD49b	DX5	Rat IgM	APC	BIolegend
Mouse Ly-6C	HK1.4	Rat IgG2c	PerCP/Cy5.5	Biolegend
Mouse Ly-6G	1A8	Rat IgG2a	APC/Cy7	Biolegend
Mouse CD11c	N418	Armenian Hamster IgG	PE/Cy7	Biolegend
Mouse NK1.1	PK136	Mouse IgG2a	Alexa Fluor 647	Biolegend

Table 2.3 **Antibodies used during extracellular flow cytometry.**
mAbs are listed with their clone name and conjugated fluorophore. For $F(ab')_2$ the isotype of the parental antibody is listed (m=mouse; r=rat). In-house antibodies and $F(ab')_2$ were produced and labelled in-house with the exception of Rituximab which was obtained from Roche and labelled in-house.

2.4 Molecular biology techniques

2.4.1 Production of cDNA

mRNA was extracted from appropriate cells using the Illustra quick prep mRNA extraction kit (GE Healthcare) according to the manufacturers instructions. Briefly, cells (approximately $5x10^6$) were lysed and the mRNA bound to the supplied oligo(dT)-cellulose followed by high and low salt washes to remove impurities. mRNA was then eluted. mRNA was precipitated by the addition of

40µl 2.5M potassium acetate, 10µl glycogen and 1ml 100% ethanol and incubated at -20°C for 30 minutes before being centrifuged at 18,000g for 5 minutes. The supernatant was discarded and the pellet dissolved in 8µl RNAse free water.

cDNA production was performed using the superscript III RT PCR kit (Invitrogen). The precipitated mRNA was added to 1µl random hexamers and 1µl dNTPs and incubated at 65°C for 5 minutes. The following were then added: 2µl 10x RT buffer, 4µl 25mM $MgCl_2$, 2µl 0.1M DTT, 1µl RNase OUT, 1µl (200 units) Superscript III RT. Synthesis used the following program: 25°C 10 minutes, 50°C 50 minutes, 85°C 5 minutes before 1µl RNase H was added and incubated at 37°C for 20 minutes. The cDNA was stored at -20°C for future use.

2.4.2 Genomic DNA extraction and purification

Appropriate cells (approximately $5x10^6$) were harvested and washed twice in 10ml PBS then resuspended in 200µl PBS. The genomic DNA was extracted using the DNeasy DNA isolation kit (Qiagen) according to the manufacturer's instructions. Briefly, the cells were lysed and the DNA bound to an ion exchange column before being washed to remove impurities. The purified DNA was eluted in a final volume of 400µl, quantified using a nanodrop spectrophotometer and stored at -20°C.

2.4.3 Bacterial transformation

Plasmid DNA was added to chemically competent *Escherichia coli* (*E. coli*) (strain and DNA:cell ratio dependent on strain and application) and incubated on ice for 30 minutes in a 1.5ml centrifuge tube (StarLab). Cells were then heat shocked at 42°C for 30-45 seconds then returned to ice for 2 minutes. 0.5ml Super Optimal broth with Catabolite repression (SOC; Life Technologies) was added and incubated at 37°C for 1 hour with shaking. Transformations were spread on a Lysogeny Broth (LB) agar plate supplemented with the appropriate antibiotic (See Table 2.4) and incubated overnight at 37°C.

Plasmid	Bacterial antibiotic resistance
pcDNA3/3.1	Ampicillin (100µg/ml)
pCI-Puro	Ampicillin (100µg/ml)
pCR Blunt II-TOPO	Kanamycin (50µg/ml)
pIRES	Ampicillin (100µg/ml)
pDSG-IBA	Ampicillin (100µg/ml)

Table 2.4 **Plasmids used during cloning**.
The antibiotic for bacterial selection, and concentration required are included.

2.4.4 DNA gel electrophoresis and gel extraction

Unless stated otherwise 0.7% agarose Tris-acetate-EDTA (TAE) gels were prepared with 0.7g UltraPure agarose (Life Technologies) dissolved in 100ml 1x TAE buffer (40mM Tris (Sigma-Aldrich), 20mM glacial acetic acid, 1mM EDTA (VWR)). 5µl GelRed Nucleic acid stain (Biotium) was used per 100 ml to visualise DNA. 6x Blue/Orange loading dye (Promega) was added to samples where appropriate. 5µl O'generuler 1kb and/or 100bp ladder was loaded in the gel along with the sample and run at 120-150V for 40-60 minutes in a kuroGEL tank (Jencons) containing 1x TAE running buffer. Gels were imaged under UV light using a Molecular Imager Gel Doc XR imaging system (Biorad).

For downstream applications DNA bands were cut from the gel and the DNA extracted using a QiaQuick gel extraction kit (Qiagen) according to the manufacturer's instructions with the purified DNA stored at -20°C.

2.4.5 Polymerase chain reaction (PCR)

The general PCR protocol for amplification from genomic DNA, cDNA or plasmid DNA is described below. Where alternative protocols were used these have been described (see DNA sequencing below and results figure legends). Reactions contained the following: 1µl cDNA or plasmid DNA (~100ng) or 5µl genomic DNA (~500ng), 2.5µl 10x pfu buffer, 0.5µl dNTPs, 1µl (2 units) pfu polymerase (all promega), 1µl gene specific forward primer, 1µl reverse primer (Life Technologies) with reactions made up to 25µl with distilled water. The PCR program used is detailed in Table 2.5

.

Step	Temperature	Time
1	95°C	5 minutes
2	95°C	30 seconds
3	55-65°C	1 minute
4	72°	1 minute /kb
Return to step 2 25-35x		
5	72°C	10 minutes

Table 2.5 ***Conditions used for PCR reactions using pfu polymerase****.*
Reactions were set up and PCR run using thr program above. The annealing temperature and the number of cycles performed were dependedent on the specific PCR reaction

Reactions were performed in a PTC-200 thermal cycler (MJ research). For Overlap PCR individual fragments were produced as detailed above and agarose gel purified. 3-5µl of each fraction was used per overlap reaction with dNTPs, pfu buffer and pfu polymerase added as before. 15 cycles of the PCR program were performed before adding: additional forward and reverse primer, additional pfu buffer, dNTPs, pfu enzyme and water to bring the total volume to 50µl before a further 20 cycles of PCR were performed and the reactions run on an agarose gel. All primers used for PCR reactions are listed in Appendix A.

2.4.6 “Blunt end” ligation

PCR products were ligated into pCR BluntII TOPO plasmid (Life Technologies) according to the manufacturer’s instructions. Briefly, 2µl PCR product (20-50ng), 0.5µl pCR BluntII TOPO vector and 1µl salt solution were incubated for 15 minutes at room temperature then transformed into 30µl chemically competent TOP10 *E. coli*.

2.4.7 DNA restriction digests

Reactions were performed using the appropriate 10x restriction buffer (Promega) for the enzyme(s) to be used. 1µl (10-20 units) restriction enzyme(s) (Promega) and 2-3µl plasmid DNA were added to the buffer and water added to bring the final volume to 10µl for digests with a single enzyme and 20µl for double digests. Reactions were incubated at 37°C for 1-6 hours, depending on enzymatic activity and buffer compatibility, in a thermal cycler or water bath.

2.4.8 “Sticky end” ligation

3µl 10x T4 ligase buffer and 3µl (3-9 units) T4 ligase (Both Promega) were added to 12µl purified DNA insert, 3µl digested plasmid, 9µl water and incubated overnight at 4°C. The next day the reaction was transformed into 100µl JM109 cells diluted in 200µl 0.1M $CaCl_2$.

2.4.9 Plasmid DNA purification.

Single colonies of plasmid transformed bacteria were picked and placed into 10ml LB media with appropriate selection antibiotic and incubated for 7-16 hours at 37°C with shaking. For minipreps, bacteria were pelleted by centrifugation at 3200g for 10 minutes and the plasmid DNA extracted using a Miniprep plasmid purification kit (Qiagen) according to the manufacturer’s instructions. Briefly, bacteria were lysed and the protein precipitated. DNA was bound to an ion exchange column, then washed to remove contaminants and the DNA eluted from the column. For Maxipreps, the 10ml culture was added to 100ml LB with selection antibiotic and incubated for 20 hours at 37°C. Cells were pelleted by centrifugation at 3200g for 20 minutes. The DNA was extracted using a HiSpeed Plasmid Maxi kit (Qiagen) using similar principles to the miniprep kit. DNA yield was quantified using a nanodrop spectrophotometer and the A_{260}/A_{280} ratio determined.

2.4.10 Site directed mutagenesis

The QuickChange Lightning site-directed mutagenesis kit (Agilent) was used according to the manufacturer’s instructions. Briefly reactions contained: 5µl 10x reaction buffer, 10-100ng plasmid template, 2.5µl primer, 1µl dNTP mix, 1.5µl Quick solution, 1µl Quickchange lightning enzyme and water up to a total volume of 50µl. The PCR program used was as detailed in Table 2.6

Step	Temperature	Time
1	95°C	2 minutes
2	95°C	20 seconds
3	60°C	10 seconds
4	68°	30 sec /kb
Return to step 2 18x		
5	68°C	5 minutes

Table 2.6 **Reaction conditions for site directed mutagenesis.**
All reactions were performed in a thermal cycler with the extension time in step 4 dependent on the size of the plasmid template rounded up to the nearest Kb

Following the reaction, template DNA was digested by the addition of 2µl DpnI and incubated at 37°C for 30 minutes. 2µl of the reaction was transformed into 30µl XL10 Gold chemically competent *E. coli* with the addition of 2-ME (both Agilent).

2.4.11 DNA sequencing (in-house)

Reactions for Sanger sequencing contained: 2µl plasmid DNA (150-300ng), 2µl 10x sequencing buffer, 2µl Big-dye terminator v3.1 mix (both Applied Biosystems), 1µl 1µM sequencing primer and 3µl water. The conditions for the reaction are detailed in Table 2.7.

Step	Temperature	Time
1	96°C	10 seconds
2	50°C	5 seconds
3	60°C	4 minutes
Return to step 1 24x		

Table 2.7 **Reaction conditions for in-house performed Sanger sequencing.**
Reactions were performed in a thermocycler before products were precipitated and analysed by capillary electrophoresis

Reactions were precipitated by the addition of 25µl 100% ethanol (Hayman) and 1µl 3M NaAc (Sigma-Aldrich) and incubated on ice for 10 minutes. Reactions were centrifuged at 14500g in a microcentrifuge at 4°C for 30 minutes. The supernatant was removed and 125µl 70% ethanol was added to the pellet before centrifuging at 14500g for 5 minutes, supernatant was discarded and the pellet air dried for 10 minutes, then resuspended in 10µl formamide. Sequencing reactions

were evaluated by capillary electrophoresis with the data analysed using Lasergene SeqMan software (DNASTAR).

2.4.12 DNA sequencing (out-sourced)

For DNA to be sequenced externally the plasmid DNA was diluted to 100ng/ml in water with 5µl sent per reaction to Source Bioscience. Gene specific primers diluted to 3.2pM in water were also sent with common plasmid primers supplied by Source Bioscience. Sequencing data was analysed as before.

2.4.13 qPCR

qPCR reactions for CD32b contained: contained 10µl 2x buffer, 1.1µl 5µM 6-fluorescein amidite (FAM) probe, 2µl 10µM forward primer, 2µl 10µM reverse primer, 2µl cDNA, 2.9µl water. Control reactions contained 10µl 2x buffer, 1µl 20x assay (HMBS Hs00609296_g1 or HPRT1 Hs02800695_m1), 2µl cDNA and 7µl water. Probes, buffers and control gene reactions were obtained from Life Technologies and gene specific primers from Eurogenetec. All reactions were carried out in 384 well plates using a LightCycler 480 (Roche). Reaction conditions were 95°C for 10 minutes followed by 40 cycles of 95°C 15 seconds, 60°C 1 minute then a final extension of 72°C for 5 minutes.

2.5 *In vivo* experiments

Animals used throughout these experiments were maintained in conventional barrier facilities except immune compromised mice which were kept in individually ventilated cages (IVC). All mice expressing human transgenes were on a C57BL/6 background unless stated otherwise. All experiments were conducted under Home Office project licence PPL30/2964, animals had constant access to food and water with a 12 hour light/dark cycle. A personal license (I5DO82827) was obtained and used in carrying out licenced procedures following appropriate training.

2.5.1 Eμ-Tcl-1 tumour splenocyte harvesting and preservation

Spleens from mice bearing Eμ-Tcl1 tumours were harvested and a single cell suspension obtained by passing them through a 100μm cell strainer (Becton Dickinson). Cell number was determined using a coulter counter and cells resuspended at a minimum of $1x10^8$ cells/ml in FCS +10% DMSO. Cell suspension was divided into 1ml aliquots in cryovials and stored at -80°C for 1-5 days before being transferred to vapour phase nitrogen storage.

2.5.2 Passage of Eμ-Tcl-1 tumours

Frozen splenocytes were placed in a water bath at 37°C until thawed before being transferred to a universal tube containing 20ml complete RPMI media. Cells were centrifuged at 450g for 5 minutes before being resuspended at $5x10^6$ cells/ml in Eμ-Tcl1 media and rested at 37°C + 5% CO_2 for 1 hour. 2 ml cells suspension per mouse was centrifuged at 450g for 5 minutes and resuspended in 0.5ml sterile PBS. Mice were injected with the cell suspension intraperitoneally (i.p.) and monitored for tumour cells in the peripheral blood every 7-14 days.

2.5.3 Eμ-Tcl-1 tumour screening

Mice receiving Eμ-Tcl-1 tumours were bled every 7-14 days with approximately 30μl tail blood taken onto 10μl heparin sodium solution (Wockardt). Blood was then assessed for the white blood cell (WBC) count and immunophenotype by flow cytometry. WBC was measured by diluting 10μl heparinised blood in 40μl PBS (Severn Biotech). 20μl diluted blood was added to 10ml Coulter Isoton III diluent (Beckman Coulter) before adding 2-3 drops of ZAP-OGLOBIN II red blood cell lytic reagent (Beckman Coulter). WBC count was determined using a Coulter Z1 particle counter.

Flow cytometry was performed with 10μl heparinised peripheral blood added to a FACS tube and stained with 0.5μg FITC anti-mouse CD5 and 0.1μg PerCP/APC anti-mouse B220 or PE anti-mouse CD19. The total volume was made up to 100μl with FACS wash buffer and incubated at 4°C for 30 minutes. 1ml red blood cell lysis buffer (diluted 1 in 10; AbD Serotec) was added to each sample. Samples were centrifuged at 450g for 5 minutes and the supernatant discarded before being washed in 3ml FACS wash buffer. Finally cells were analysed using a FACS Calibur flow cytometer.

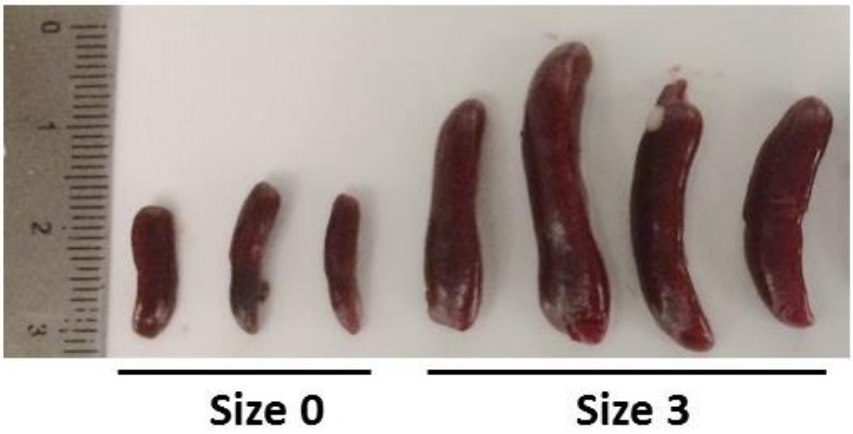

Figure 2.1 ***Representative spleen sizes for mice in Eμ-Tcl-1 experiments****.*

Wild type spleens are shown (size 0) following dissection from healthy, age matched controls. Spleens from mice bearing terminal Tcl-1 tumours are shown, determined to be size 3 by palpation.

Tumours in conventional mice were deemed terminal when 2 of the following criteria were met: greater than 80% peripheral tumour lymphocytes, WBC count above 25 $x10^6$ cells/ml or spleen size independently determined as 4 out of 5 on an arbitrary scale. Immune compromised mice were terminal when the white blood cell count exceeded $20x10^6$ cells/ml and spleen reached size 3, which is illustrated in Figure 2.1.

2.5.4 Administration of therapeutic agents

Antibodies for *in vivo* administration were dialysed into PBS and sterile filtered before being diluted to an appropriate concentration in sterile PBS. 200μl diluted antibody was either administered i.p. or i.v into a tail vein. Agents requiring oral dosing were resuspended at 1mg/ml in appropriate vehicle and administered by oral gavage using a dose dependent on the weight of the animal.

2.5.5 Collection of serum and plasma

Serum was collected by tail tipping with approximately 40μl blood taken into a 0.5ml microfuge tube (Starlab) and allowed to clot overnight at 4°C. Clotted blood was then centrifuged at 5000g for 5 minutes in a bench top centrifuge, the serum was removed and stored at -20°C. For plasma collection 40μl blood was taken onto 10μl sodium heparin and centrifuged at 2200g for 5 minutes in a bench top centrifuge. Plasma was removed and stored at -20°C.

2.5.6 Bone marrow chimera generation

1 week prior to irradiation mice were placed on acid water (tap water, pH2.5, autoclaved). On day -1 mice were sedated with 100µl hypnorm (VetPharma) diluted 1 in 10 in sterile PBS and injected i.p. Mice were irradiated with a dose of 1.5Gy using a Gulmay X-ray generator, before being wrapped in cotton wool after irradiation to keep warm. On day 0 mice were irradiated again as before. Bone marrow was prepared from donor mice by dissecting the bones of the hind legs and syringing out the bone marrow. The bone marrow was passed through a 70µM cell strainer and resuspended at 1-2.5x10^7 cells/ml in sterile PBS. 200µl bone marrow suspension was injected i.v. into recipient mice and allowed to reconstitute for 56-84 days. 14 days after irradiation mice were taken off acid water. Reconstitution was assessed by flow cytometry of peripheral blood.

2.6 Enzyme linked immunosorbent assay (ELISA)

96 well Nunc MaxiSorp ELISA plates (Thermo Scientific) were coated with specific antibody (Sigma-Aldrich; see section 2.6.1 for details) diluted in coating buffer (Na_2CO_3 1.59g/L, $NaHCO_3$ 2.93g/L; Fisher Scientific). Plates were incubated at 37°C for 1 hour then incubated overnight at 4°C. Coating solution was discarded and 150µl PBS +1% BSA added per well then incubated at 37°C for 1 hour. Plates were washed 3 times with PBS+ 0.05% Tween20 (Sigma-Aldrich) using a Skanwasher 300 (Skatron). Serum or plasma samples were added to the plate in 100µl/well with an initial dilution of 1 in 100 followed by 1 in 2 serial dilutions. Additionally relevant standards were also added to the plate. Samples were incubated for 90 minutes at 37°C. Plates were washed 5 times before 100µl Horseradish peroxidase (HRP) conjugated $F(ab')_2$ specific antibodies (Jackson Immunoresearch; see section 2.6.1 for details) diluted in PBS+ 1% BSA. After incubating for 90 minutes at 37°C for 90 minutes plates were washed twice and 100µl substrate added (*o*-Phenylenediamine dihydrochloride tablet (Sigma-Aldrich) dissolved in 24.7 ml citrate (stock:19.2g/L; BDH), 25.3ml Na_2HPO_4 (stock; 28.4g/L; Fisher Scientific), 50 ml dH_2O). Once sufficient colour change was achieved 5 0µl 2.5M H_2SO_4 (VWR) was added per well. Absorbance was measured at 450nm on an Epoch microplate reader (Biotek). Analysis was performed in Excel with the linear range of the standard curve plotted and linear regression used to calculate the unknown values.

2.6.1 ELISA for human and mouse IgG

ELISA for human IgG were performed as described above using the following reagents and dilutions. The coating antibody was a goat anti-human IgG, Fc specific antibody (Sigma-Aldrich) used at a final concentration of 5μg/ml. The detection antibody was a Horseradish peroxidase conjugated $F(ab')_2$ goat anti-human (Fc specific) (Jackson immunoresearch) diluted 1 in 10000.

ELISA for mouse IgG were performed as above with the following changes. The coating antibody used was a Rabbit anti-mouse IgG diluted 1 in 2000 in coating buffer. Due to the increased concentration, plasma samples were diluted 1 in 200 whilst the concentrations of the standards (mIgG1 and mIgG2a) remained the same. An HRP conjugated Rabbit anti-mouse IgG was used as the detection antibody at a final concentration of 10μg/ml. All results were analysed as before.

2.7 Peripheral blood mononuclear cell (PBMC) assays

2.7.1 Isolation of human PBMCs

Human PBMCs were isolated from either leukocyte cones or whole blood. Leukocyte cones were obtained from the National Blood Service and whole blood from healthy volunteers. Blood samples were diluted 1 in 2 with PBS +2mM EDTA and 25ml diluted blood was layered onto 15ml room temperature lymphoprep (Axis Shield) in a 50ml falcon tube. Tubes were centrifuged at 800g for 20 minutes, after which the PBMC layer at the interface was removed with a Pasteur pipette and washed twice in a total volume of 40ml PBS +2mM EDTA by centrifugation at 400g for 10 minutes. For cryopreservation PBMCs were resuspended at $1x10^8$ cells/ml in PBMC freeze media (40% complete CTL, 50% FCS or human AB serum, 10% DMSO).

2.7.2 Carboxyfluorescein succinimidyl ester (CFSE) labelling of cells

Cells for CFSE labelling were resuspended at $1x10^7$ cells/ml in serum free RPMI in a 50ml falcon tube. CFSE (Sigma-Aldrich) was pipetted onto the inside wall of the tube to give a final concentration of 2pM CFSE. The tube was rapidly mixed and incubated at room temperature in

the dark for 10 minutes. Complete RPMI was added to a to a total volume of 40ml and centrifuged at 450g for 10 minutes before being washed again and suspended in appropriate growth media.

2.7.3 PBMC proliferation assay

CFSE labelled PBMCs were cultured at $1x10^7$ cells/ml in 1.5ml complete CTL media per well in a 24 well plate for 3 days. Cells were harvested by pipetting and washed once in 40ml complete CTL media and resuspended at $1x10^6$ cells/ml. 100µl cells suspension was added per well to a U bottom 96 well plate with 50µl monoclonal antibody (at 3x final concentration in complete CTL media) and incubated for 4 days at 37°C +5% CO_2. After 48 hours 50µl culture supernatant was removed and stored at -80°C for cytokine analysis.

The stimulation antibodies used in proliferation assays and their final concentration are listed in Table 2.8.

Antibody	**Target**	**isotype**	**Source**	**Final concentration (µg/ml)**
Avastin (bevacizumab)	VEGF-A	Human IgG1	Roche	15
OKT3	CD3	Mouse IgG2a	In-house	0.1
UCHT1	CD3	Mouse IgG1	eBioscience	15
TGN1412	CD28	Human IgG4	In-house	1
Ancell 28.1	CD28	Mouse IgG1	Ancell	15
Campath-1H (alemtuzumab)	CD52	Human IgG1		15
GA101 (obinutuzumab)	CD20	Human IgG1	Roche	15
MabThera (rituximab)	CD20	Human IgG1	Roche	15
Erbitux (cetuximab)	EGFR	Human IgG1	Merck	15

Table 2.8 ***Antibodies used for stimulation in T cell proliferation and cytokine release assays.***
mAbs are listed with their isotype and human target. The final concentration used in the assays is listed, antibodies were made to 3x this concentration in complete CTL media to give the final concentration when added to the labelled PBMCs

2.7.4 CHO based T cell proliferation assays

CFSE labelled human PBMCs were centrifuged at 300g for 10 minutes and resuspended in 40µl PBS +0.5% BSA +2mM EDTA per 10^7 cells. T cell isolation was performed by negative selection using a pan T cell isolation kit, human (Miltenyi Biotech) according to the manufacturers protocol. Purified cells were resuspended at $1x10^6$ cells/ml in complete CTL media. FcγR transfected CHO-K1 cells were harvested using PBS +2mM EDTA then washed once in complete CTL media and resuspended at $2 x10^6$ cells/ml. 50µl cell suspension, 50µl purified T cells and 50µl diluted antibody was added to each well of a 96 well plate and incubated at 37°C +5% CO_2 for 4 days. After 48 hours, 50µl of culture supernatant was removed and stored at -80°C for cytokine analysis.

2.8 Cytokine measurement

Cytokine concentrations in assay supernatants were determined by Luminex and Meso Scale Discovery (MSD) assays. Culture supernatants were diluted in complete CTL media using the dilutions in Table 2.9 to ensure concentrations were within the detectable ranges of the assays.

Sample	Dilution
OKT3 stimulated	1 in 10
TGN1412 stimulated	1 in 10
CHO samples MSD	1 in 100
CHO samples Luminex	1 in 50
All other samples	1 in 3

Table 2.9 ***Dilution factors used for cytokine release***
Assay supernatant samples were collected from T cell and CHO based T cell proliferation assays. Samples were diluted in complete CTL media to ensure concentrations were within the standard curves of Luminex and MSD assays.

The MSD assays used were 10-plex and the Luminex was an 18-plex, the analytes measured in each assay are indicated in Table 2.10.

Analyte	MSD	Luminex
GM-CSF		X
IFN-γ	X	X
IL-10	X	X
IL-13	X	X
IL-17a		X
IL-1b	X	X
IL-2	X	X
IL-4	X	X
IL-5		X
IL-6	X	X
IL-7		X
IL-8	X	X
IP-10		X
MCP-1		X
MIP1-a		X
MIP1-b		X
TNF-α	X	X
IL-12p70	X	X

Table 2.10 ***Analytes investigated in MSD and Luminex assays****.*
Cytokine concentrations in proliferation assays were measured by MSD and Luminex. Those cytokines analysed in each format are indicated by a cross. 17 analytes were measured by Luminex and 10 by MSD

2.8.1 MSD

MSD analysis used a Proinflammatory Panel 1 (human) V-PLEX kit (Meso Scale Discovery). The supplied calibrator was resuspended in 250µl diluent 2 and 1 in 4 serial dilutions performed. 50µl diluted sample (see Table 2.9) or calibrator was added per well of the MSD plate and incubated at room temperature with shaking for 2 hours. The MSD plate was washed 3 times with 150µl/well PBS +0.05% Tween-20. 25µl detection antibody mix (60µl each antibody made up to 3ml with diluent 3) was added per well and the plate incubated with shaking for 2 hours at room temperature. The plate was washed 3 times and 150µl 2x read buffer added per well before being read on an MSD SECTOR S 600 instrument. Data was analysed in MSD discovery workbench software using lot specific calibrator concentrations.

2.8.2 Luminex

Luminex was performed using a custom Milliplex HCYTOMAG-60K human cytokine magnetic panel (Millipore) Vials of detection beads were sonicated for 30 seconds then vortexed for 1 minute. 60µl of each detection bead was mixed and the total volume made up to 3ml with bead diluent. The cytokine standard was prepared according to the supplied protocol to make 6 standards. 200µl wash buffer was added to each well of the assay plate and incubated at room temperature with shaking for 10 minutes. Buffer was removed and 25µl diluted sample, standard or control was added with 25µl mixed beads and 25µl matrix solution (CTL media for standards and controls, assay buffer for samples). The plate was incubated overnight in the dark with shaking at 4°C before being washed twice using the protocol in Table 2.11 and 25µl detection antibody cocktail added per well. After 1 hour at room temperature with shaking, 25µl Streptavadin-PE was added per well and the plate incubated for 20 minutes. Finally, the plate was washed twice and the beads resuspended in 150µl sheath fluid before being run on a Luminex100 instrument using xPONENT software (Luminex Corporation).

Step	**Time**	**Comments**
Rest plate on magnet	60 seconds	Allows magnetic beads to settle
Remove well contents	N/A	Invert plate whilst attached to magnet
Add 200µl wash buffer	N/A	N/A
Resuspend beads	30 seconds	On plate shaker

Table 2.11 ***Plate washing steps used during Luminex assays.***
The described wash protocol was carried out twice for most steps during the Luminex assay. It is important to ensure the beads remain in the plate when discarding the wash buffer by keeping the magnet on the plate.

2.9 Internalisation/quenching assays

AlexaFluor 488 labelled antibodies were added to the cells (200µl) at a final concentration of 5µg/ml and the plate returned to the incubator. The antibodies used for this assay were: BHH2 mIgG2a, Herceptin hIgG1 (Genentech), SB2H2 mIgG1 and BHH2 hIgG2, unless stated otherwise all were produced in-house, with all AlexaFluor 488 labelling performed in-house. At the end of the assay, media was removed and 200µl ice cold PBS added per well. Adherent cells were harvested by scraping and 100µl cell suspension added to each of 2 FACS tubes. To one tube 2.5µl anti-Alexafluor488 antibody (Life Technologies) was added and the tubes incubated in the fridge for 30 minutes. All samples were washed in FACS wash before analysis on a FACS Calibur.

Fluorescence from unquenched sample represents the total antibody bound to the cell surface and internalised whereas the fluorescence from quenched samples only represents that from internalised antibody. The ratio of the quenched to unquenched MFI represents the proportion of total bound antibody which has been internalised.

2.10 Bead phagocytosis assay

To fluorescently label beads for use in phagocytosis assays, 400µl of 1mg/ml BSA or BSA-Alexa Fluor 488 in 50mM sodium citrate (pH 4.2) was added to 200µl 3µm latex beads (Polysciences inc.). This was incubated for 1 hour at 4°C with end over end agitation. Beads were washed 3 times in sterile PBS with centrifugation at 14500g between washes. Beads were resuspended in a final volume of 400µl PBS.

BMDMs were harvested from a 6 well plate using PBS +2mM EDTA and gentle scraping before diluting to 2.5 $x10^6$ cells/ml. 200µl cell suspension was added per well to a 96 well plate in complete RPMI +20% L929 and incubated overnight. 3µm BSA coated or Alexafluor488-BSA coated latex beads (Life Technologies) were diluted to an appropriate final concentration (1µl stock contains 13 beads per macrophage when plated at $5x10^4$/well. Beads were added to the BMDMs and incubated at 37°C for 1 hour. Media was discarded and wells washed with 200µl PBS. 200µl PBS was added per well and phagocytosis assessed by microscopy or by scraping cells and analysing them by flow cytometry.

Chapter 3 Generation and characterisation of FcγR transfected CHO-K1 cells to investigate the role of individual FcγRs in inducing cytokine release following TGN1412 stimulation.

3.1 Chapter introduction

As described in the introduction, the anti-CD28 antibody TGN1412 resulted in severe cytokine release syndrome following infusion in a first in man trial.[157] This toxicity had not been predicted by *in vitro* or *in vivo* studies leading up to the trial.[156] Following on from this trial, there has been an effort to develop assays which can predict the toxicity of immunomodulatory antibodies such as TGN1412. These assays found that, in order to stimulate cytokine release, TGN1412 required cross-linking; either through immobilisation of the assay on plastic or through the addition of a secondary cross-linking antibody.[158, 159] The methods of cross-linking employed in these previous assays are not biologically relevant factors that could have occurred in the TGN1412 trial. Previous work had identified high density PBMC preculture as being able to induce cytokine release following TGN1412 without the need for additional cross-linking agents.[160] This preculture was subsequently suggested to result in the upregulation of CD32b, providing a mechanism for TGN1412 induced toxicity which could occur *in vivo*.[161]

The aim of this chapter was to further investigate and dissect the FcγR cross-linking requirement for the anti-CD28 mAb TGN1412 and to develop an assay that can predict toxicity using biologically relevant cross-linking. As has been described in the introduction, there are 6 FcγRs in humans, all capable of binding to IgG. As discussed, these receptors are known to be important for many biological functions, including those of immunomodulatory antibodies. However, investigating these functions is made challenging by the presence of multiple receptors on effector cells, making it difficult to elucidate the importance of each receptor. Furthermore, the complexity is increased by the presence of polymorphisms in the receptors which makes comparisons between human samples difficult. For example, CD32a is a low affinity receptor which can either have a histidine or arginine residue at position 131.[354] The H131 allele of CD32a is the only human FcγR capable of binding efficiently to IgG2, as well having a 1.5 fold higher affinity for IgG1 than R131.[290] CD16a is another low affinity FcγR with a polymorphism at amino acid position 158, leading to altered affinity for IgG; V158 having a higher affinity for human IgG1 and IgG3 than F158.[372] CD32b is the only inhibitory FcγR in humans and has a defined polymorphism at position 232. This substitution

is in the membrane spanning region of the receptor and does not affect the binding to IgG, however T232 has a decreased ability to associate with lipid rafts.[359] Lipid rafts are areas of membrane insoluble in Triton X-100, which allow signalling molecules to become clustered to increase the efficiency of signalling. This is evidenced by studies demonstrating that the T232 allele of CD32b led to reduced inhibition of BCR signalling compared to the I allele.[359] Reduced clustering of CD32b as a result of the T232 allele could impair clustering of mAb via the receptor.

Therefore, to reduce the complexity of the variation inherent on immune cells, stably transfected cell lines were generated, which allowed for a single FcγR to be studied in isolation with a uniform expression level that was reproducible between assays.

3.2 Generation of human FcγR plasmids

In order to generate transfected cells expressing FcγRs, plasmids were generated containing the FcγR gene under the control of a constitutive promoter. Additionally the FcR γ-chain was cloned as co-expression is required with CD16a and CD64 in order to give expression at the cell surface. All polymorphic variants of human FcγRs were generated. The production of each plasmid is detailed below, following generation all plasmids were transformed into JM109 *E. coli,* cultured and maxi preps performed. The maps for all plasmids used are presented in Appendix B.

3.2.1 CD32a

The human CD32a gene was previously cloned into the pCI-puro vector by Dr Claude Chan. As the gene has two major polymorphic variants, it was important to determine which allele had been previously cloned. Therefore, the plasmid was sequenced in-house using the T7 and T3 primers. The sequencing trace is shown in Figure 3.1a; this demonstrates that the original construct would encode for a histidine at position 131. Site directed mutagenesis was carried out to introduce a single base pair change to give an arginine at position 131. The general principles for site directed mutagenesis reactions is shown in Figure 3.2, with the primer designed to contain the point mutation flanked by sequence complementary to CD32a DNA. Following mutagenesis, the parental DNA was digested with DpnI, an enzyme which specifically digests methylated DNA. The product of the mutagenesis reactions was transformed into XL10 gold *E. coli* and mutagenesis

confirmed by DNA sequencing. Figure 3.1b shows the sequencing trace of CD32a following mutagenesis, indicating that the mutagenesis was successful with an arginine now coded at position 131.

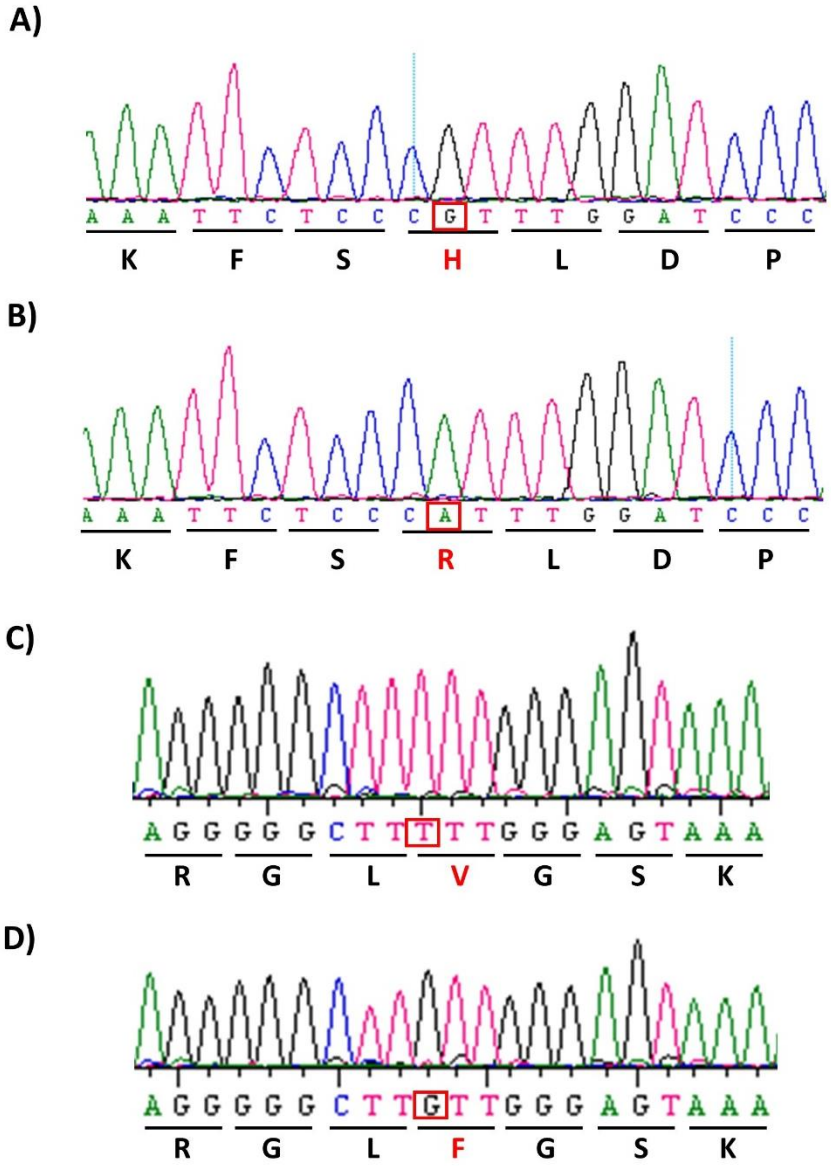

Figure 3.1 ***Identifying polymorphic variants of hCD32a and CD16a.***
The hCD32a gene in the pCI-puro vector was sequenced using Sanger sequencing with the results analysed using Lasergene SeqMan Pro software and the chromatograms shown. A) The previously made CD32a construct was shown to be the H131 allele as identified by the highlighted 'G' base. B) Following site directed mutagenesis, the R131 allele was generated with the changed base highlighted. C) Sequencing also confirmed that the original CD16a construct was the V158 allele. D) Following site directed mutagenesis, sequencing confirmed that the CD16a F158 allele had been generated.

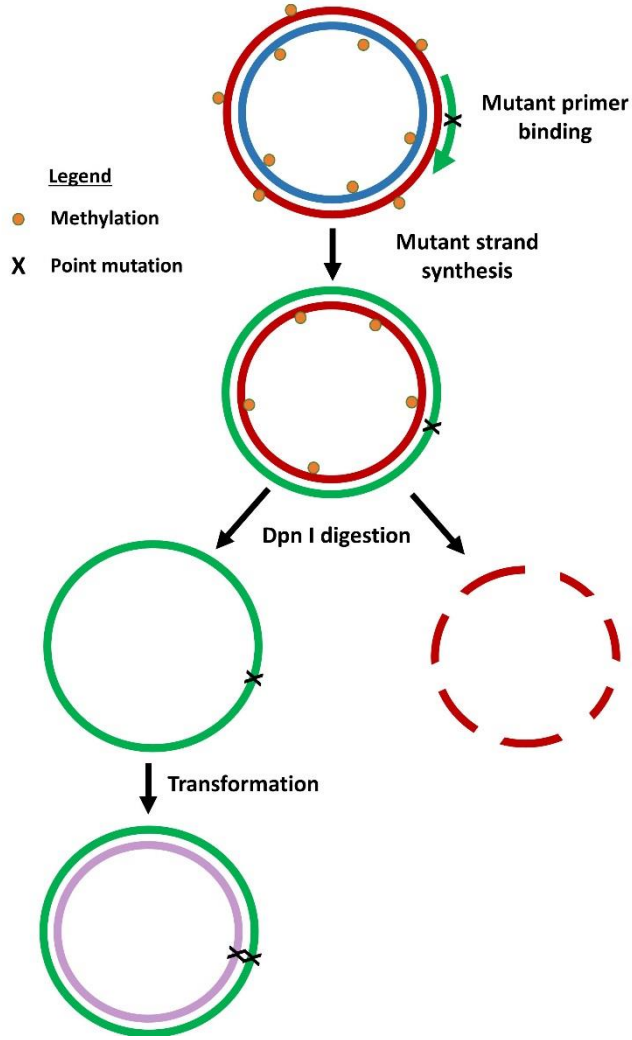

Figure 3.2 ***Schematic of site directed mutagenesis reactions***

A PCR primer was designed with mismatched base(s) and gene specific flanking sequence. PCR was performed to generate the mutant strand using the Quickchange lightning site-directed mutagenesis kit. DpnI digestion was performed to digest the parental, methylated DNA. The remaining mutant strands were transformed into chemically competant XL10 gold E. coli in which the double stranded plasmid was produced and amplified.

3.2.2 CD16a

A plasmid construct containing the human CD16a gene in the pcDNA3 vector was previously cloned by Dr Claude Chan. Prior sequencing, as presented in Figure 3.1c demonstrated that this construct contained the high affinity V158 allele. In order to generate the low affinity F158 allele, site directed mutagenesis was again performed using a gene specific primer, after which the presence of F158 was confirmed by DNA sequencing as shown in Figure 3.1d.

3.2.3 CD32b1, CD32b2 and CD64

Plasmid constructs for all allelic variants of CD32b (CD32b1 and CD32b2, I232 and T323) as well as CD64 had been previously cloned by Dr Claude Chan. These plasmids were sequenced using plasmid primers to confirm that the sequences were as expected (data not shown)

3.2.4 Human γ-chain

The human γ-chain is required for functional activity of CD64 and CD16a as it contains the ITAM motifs required for signalling. Additionally, the γ-chain required for transport of these receptors to the cell surface. Therefore, to generate transfected cell lines, CD16a and CD64 were co-transfected with the γ-chain in order to obtain surface expression of the functional receptor. The human γ-chain was previously cloned by Claude Chan into the pCI-puro vector. However, here the gene was subcloned into pCI-puro in order to give an alternative mammalian antibiotic selection for co-transfection alongside the FcγR constructs.

Accordingly, the human γ-chain in pCI-neo, and the pCI-puro vector were sequentially digested with NheI and NotI before being separated on a 0.7% agarose gel. The γ-chain and cut vector were extracted from the gel and sticky-end ligated using T4 ligase. The ligation products were transformed into JM109 chemically competent *E. coli*; several colonies were picked and minipreps performed to isolate plasmid DNA. Subsequently, digests were performed on purified plasmids using NotI and NheI to confirm the correct ligation. These digests were run on an agarose gel shown in Figure 3.3, with a band at 5.5kb corresponding to the cut plasmid. The bands at 350bp corresponded to the human γ-chain, showing that in colonies 2 and 3, the γ-chain had been successfully ligated into pCI-puro whereas colony 1 only contained the empty vector.

Once all plasmids were produced, maxi preps were performed to amplify the plasmids and, additionally, all plasmids were re-sequenced to confirm their integrity.

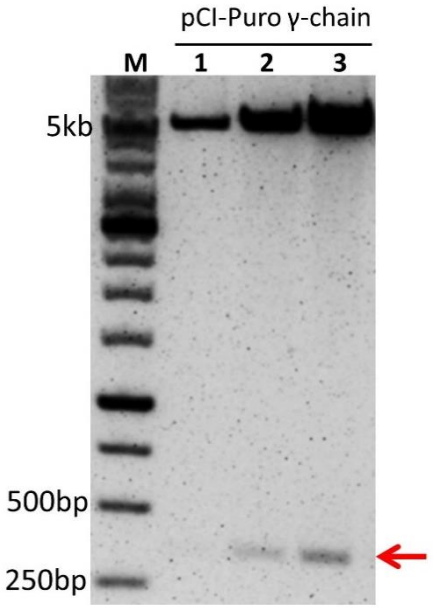

Figure 3.3 ***Cloning of human γ-chain into pCI-puro****.*
Following ligation of the DNA for the human γ-chain into pCI-puro digests were performed with NheI and NotI to confirm presence of the inserted gene. Reactions were run on a 0.7% agarose gel at a constant 120v and visualised under UV light. The band at 5.5kb corresponds to pCI-puro. Colonies 2 and 3 have a band at 350bp, indicated by the red arrow, corresponding to human γ-chain showing that it was successfully ligated into pCI-puro.

3.3 Transient expression of FcγRs in 293F cells

The HEK 293F transient expression system was first used to confirm that FcγR containing plasmids were able to result in cell surface receptor expression. Transfections were performed using 293 fectin and the expression analysed 24 hours after transfection by staining using a receptor-specific FITC labelled $F(ab')_2$. An irrelevant FITC labelled $F(ab')_2$ was used as a control with analysis performed by flow cytometry. For CD16a and CD64, the human γ-chain was co-transfected with the receptor-specific plasmids in order to give expression at the cell surface; the receptor to γ-chain DNA ratio was maintained at 2:1. Viable cells were gated based on forward (FSC) and side (SSC) scatter profiles as can be seen in Figure 3.4a. Surface receptor expression was assessed by fluorescence. The expression of each receptor is presented in Figure 3.4b, demonstrating that all alleles of the FcγRs investigated could be expressed in 293F cells. The expression pattern was similar for all of the receptor variants investigated. These transient expression experiments demonstrated that the plasmids produced were capable of giving surface receptor expression and that all polymorphic variants could be detected using specific $F(ab')_2$.

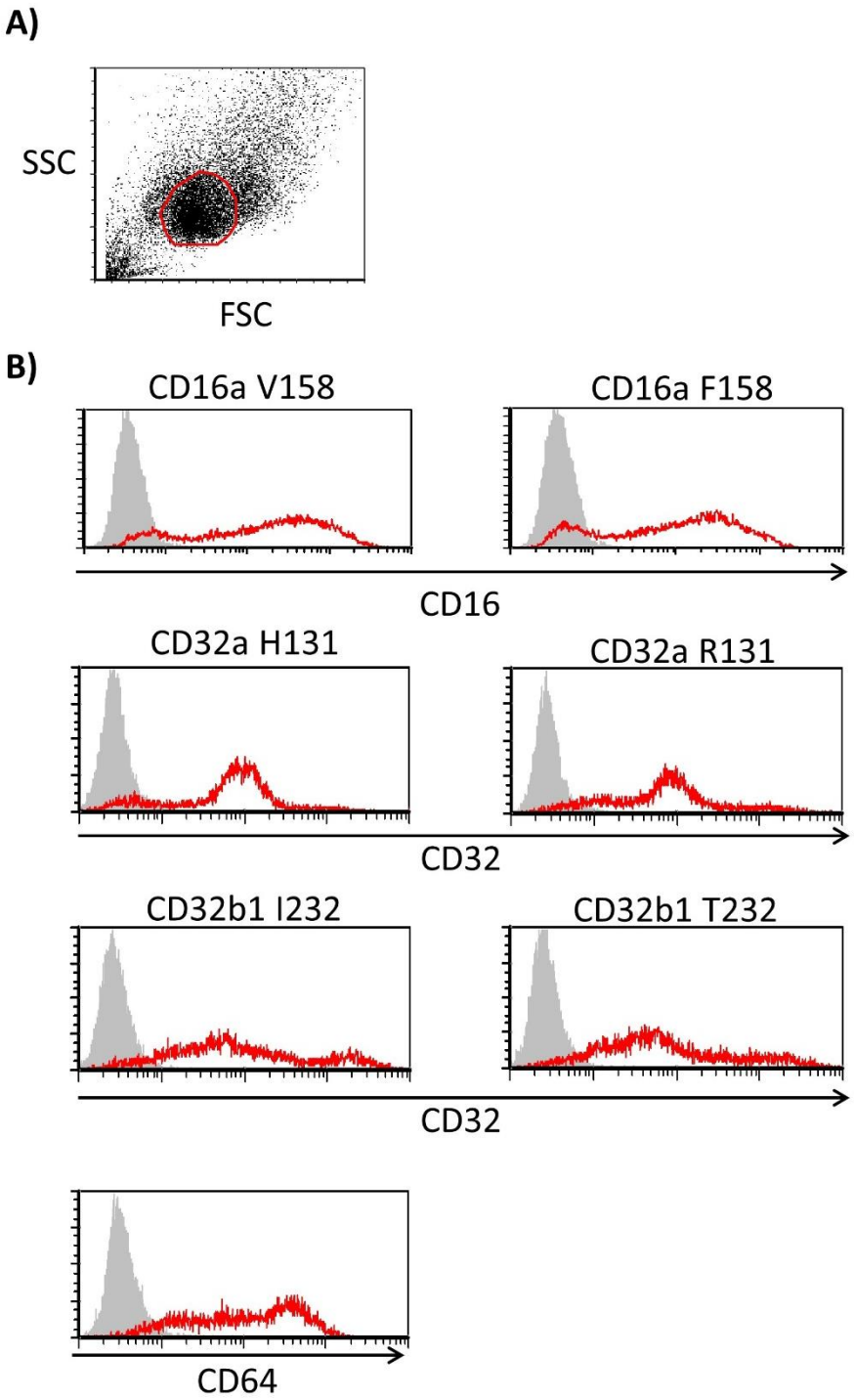

Figure 3.4 ***Transient expression profiles for the expression of human FcγRs in 293F cells***.

293F cells were co-transfected with CD16a (V or F allele), CD32a (H or R allele), CD32b1 (I or T allele) or CD64. CD16a and CD64 were co-transfected with the human γ-chain (2:1 ratio, 10µg total DNA). 48 hours after transfection expression was assessed by staining cells with receptor specific F(ab')$_2$ FITC (CD16a: 3G8, CD32a or b: AT10, CD64: 10.1) or irrelevant control. A) Forward and side scatter was used to gate on viable cells. B) Flow cytometry on gated cells to assess receptor expression. Staining with receptor specific F(ab')$_2$ is shown in red with the irrelevant control in grey.

3.3.1 Use of mAbs to discriminate between the polymorphic variants of CD16a

The V158F polymorphism in CD16a is most widely distinguished through DNA sequencing due to the single neucleotide change responsible. However, this can be a challenging process due to copy number variation, which commonly occurs in the FcγR locus (Dr Chantal Hargreaves; personal communication). Genotyping is further complicated by the genetic similarity that exists between CD16a and CD16b, making it difficult to distinguish between the 2 receptors by conventional PCR.[424] However, there have been reports that the antibody MEM-154 is able to distinguish between the polymorphic variants by preferentially binding to the V158 allele.[425] This previous assay made use of differences in fluorescence between 3G8 and MEM-154 staining to phenotype patient samples. To investigate if the mAb could be utilised to both phenotype and infer the copy number of CD16a, 293F cells were transiently transfected with the human γ-chain as well as the V or F alleles of CD16a. The V and F alleles of CD16a were transfected in differing proportions in an attempt to replicate copy number variation. Transfected cells were stained with FITC labelled MEM-154, either alone or with competition from unlabelled 3G8; an anti-CD16 antibody with minimal binding preference to either polymorphic variant.[372]

Figure 3.5a demonstrates the typical transfection efficiency obtained for the transfection of 293F cells with CD16a V158, F158 or both alleles; in all cases CD16a was co-transfected with the human γ-chain. The efficiencies were similar for all transfections as determined by staining with 3G8 $F(ab')_2$. Transfected 293F cells were stained with FITC labelled MEM-154, either alone or with competition from unlabelled 3G8. Figure 3.5b shows the percentage of MEM-154 positive cells, normalised to MEM-154 alone on CD16a VV transfected cells. These results indicate that with MEM-154 alone, there was a significantly lower percentage of positive cells in the FF transfection, suggesting that this phenotype could be easily distinguished from cells expressing the V158 allele. When competition was added from 3G8, the VV transfected cells had a significantly higher percentage positive compared to the other phenotypes investigated, allowing cells with this phenotype to be readily identified. When analysing the mean fluorescence intensity (MFI) in Figure 3.5c, the staining with MEM-154 appears to be approximately dose dependent with regards to the V allele of CD16a, with the exception of the VF transfection. When competition was added from 3G8, the MFI was higher for the VV transfection that for any of the other phenotypes.

In this assay, it was possible to distinguish between the 3 main polymorphic variants of CD16a (VV, VF, FF) with Figure 3.5b summarising the percentage MEM-154 positive data between the main variants. Despite this, the copy number variants could not be clearly distinguished in this assay regardless of a trend towards the MFI being dose dependent on the presence of the V158 allele.

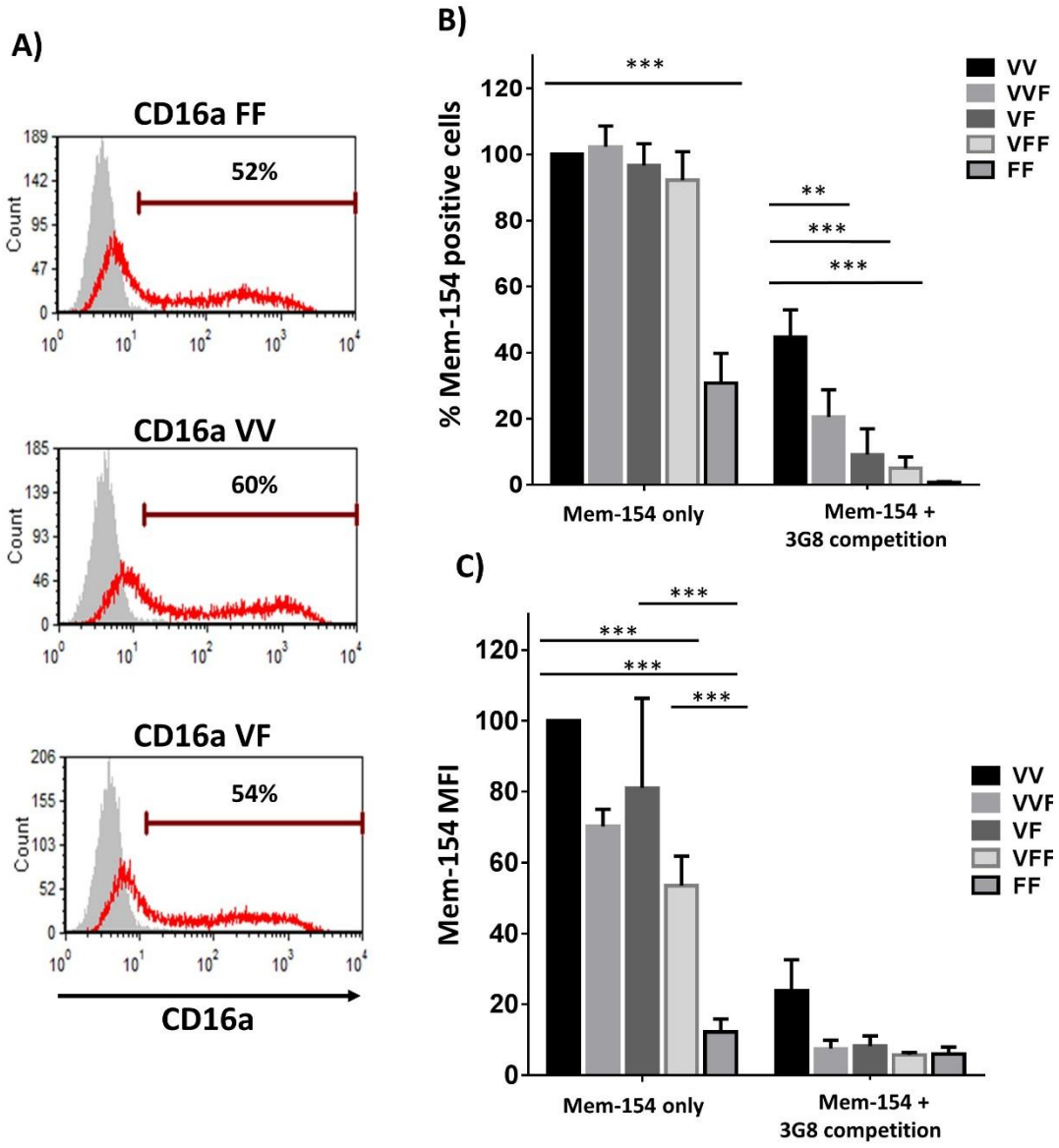

Figure 3.5 ***Flow cytometry to distinguish polymorphic variants of CD16a***.
*$1x10^7$ 293F cells were transfected with the V and/or F alleles of CD16a as well as the human γ-chain. The total DNA transfected was 10μg with γ-chain kept at a constant 3.3μg. A) representative transfection levels determined by flow cytometry 24 hours after transfection using 3G8 $F(ab')_2$ FITC in red and irrelevant control in grey. B) Transfected cells were incubated with MEM-154 FITC and the % positive shown with MEM-154 alone or with competition from 10μg/ml 3G8 as determined by flow cytometry. Results are normalised to MEM-154 staining on VV transfection. FF cells gave reduced staining with MEM-154 alone compared to other phenotypes. With competition VV could be distinguished from all other genotypes. C) The MFI of the same experiment normalised to MEM-154 staining on V allele transfected cells. VV and FF can be distinguished from each other as well as VF from VF. Results from 3 independent experiments. Bars show mean +SD, one-way ANOVA with multiple comparisons. (**p<0.01; ***p<0.001).*

3.4 Generation of CHO-K1 cell lines stably expressing FcγRs

Transient transfections were useful for confirming the functionality of plasmid constructs, however a range of expression was observed which dropped after 48 hours. For reproducible cell based assays, uniform and consistent FcγR expression was required. To achieve this, CHO-K1 cells were stably transfected with the various polymorphic variants of human FcγRs. CD64 and CD16a were cotransfected with the human FcR γ-chain to ensure surface expression. Transfections were performed using the geneporter reagent, after which cells were incubated with appropriate antibiotic selection for the plasmid used (1mg/ml Geneticin or 10µg/ml Puromycin). Transfected cells were cultured in 96 well plates and, after 10-14 days of selection, were screened for FcγR expression by flow cytometry. Wells containing FcγR positive cells were expanded and where necessary sorted on a FACS Aria to obtain a uniform level of expression. Figure 3.6 shows an example of FACS sorting for CD32b1 transfected CHO-K1 cells. Prior to sorting, CD32 positive and negative populations were present. After sorting on a FACS Aria, the collected cells were cultured and re-screened (Figure 3.6 post-sort) indicating that a single population was obtained with a uniform expression of CD32b1. This strategy of FACS sorting was used for all transfections where a range of expression levels was observed; in some cases multiple rounds of FACS sorting was required to obtain uniform receptor expression.

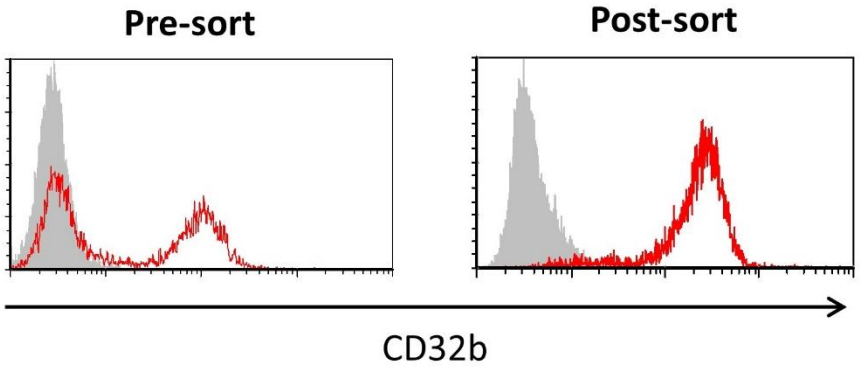

Figure 3.6 ***Expression profiles of FACS sorted CD32b1 transfected CHO-K1 cells****.*
CHO-K1 cells transfected with human CD32b1 T232 allele were stained with AT10 F(ab')$_2$ FITC (red histogram) or irrelevant control (grey). The left panels shows the fluorescence before sorting with a CD32 positive and negative population identified. Stained cells were sorted on a FACS Aria, gated on the live cells that were positive for CD32, a single, CD32 positive population obtained after sorting is shown in the right panel.

After sorting to obtain populations with uniform FcγR expression, all CHO-K1 cells were screened to confirm the expression of FcγR on the cell surface. Figure 3.7 demonstrates that a single peak

was seen for the expression of FcγRs on all stably transfected cell lines, suggesting uniform expression. Cells transfected with CD32b2 T232 demonstrated some non-specific staining with the irrelevant control, which is could be a result of non-specific binding due to the particularly high expression of this receptor.

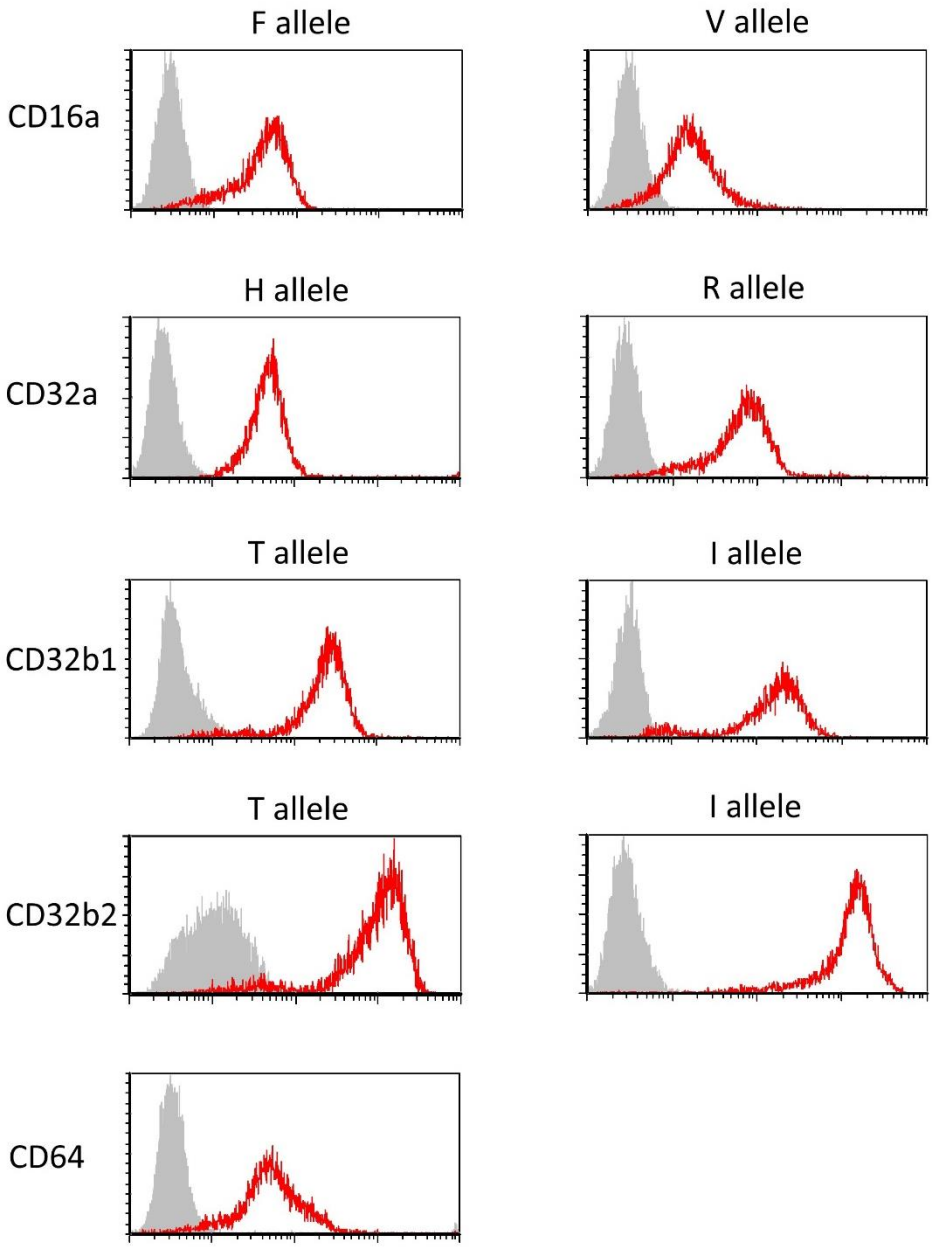

Figure 3.7 ***Expression profiles for CHO-K1 cells stably transfected with FcγRs.***
CHO-K1 cells stably transfected with FcγRs were harvested with PBS +2mM EDTA. 1x10^5 cells were stained with a receptor specific F(ab')$_2$ FITC at 10μg/ml (CD32a/b = AT10; CD16a = 3G8; CD64 = 10.1) represented by the red histogram with irrelevant control in grey. Stained cells were analysed by flow cytometry with results showing a single peak for all cell lines, suggesting a uniform FcγR expression level for all cell lines.

3.4.1 Determining the number of molecules of FcγRs at the cell surface of CHO-K1 transfectants an d PBMCs

In order to calculate relative FcγR expression between cell lines and to allow comparison to physiological receptor expression, Quantibrite beads were used; these contain defined number of PE molecules on the beads, as can be seen in Figure 3.8b. By plotting the number of PE molecules against MFI, it was possible to calculate the number of PE labelled FcγR antibodies bound to the surface of CHO-K1 cells or PBMCs and consequently deduce the number of molecules of a receptor on the cell surface.

Figure 3.8a shows the gating strategy used to identify the cell populations within PBMC samples. The number of molecules of FcγR on the surface of each PBMC population was calculated as shown in Figure 3.8c; as expected $CD19^{+}$ B cells highly expressed CD32b (9576 molecules/cell); all other receptors were expressed at less than 30 molecules/cell on B cells. $CD56^{+}$ NK cells expressed high levels of CD16a with 2 distinct populations; the average for the main population was 19500 CD16a molecule/cell whilst a separate $CD16a^{Hi}$ population expressed the receptor at an average of 57000 molecules/cell, although this was highly variable (range 22000-110000). These $CD16a^{Hi}$ cells were found to be the $CD56^{dim}$ population, which are thought to have a higher cytotoxic activity than $CD56^{bright}$ $CD16a^{lo}$ cells.[426] Unexpectedly, some donors were found to have a higher than expected expression of CD32b on NK cells; in one case expression of 2313 molecules/cell was observed. For two other donors, there was low expression (155 and 223 molecules/cell) whilst for the remaining donor expression was under 20 molecules/cell. In humans there are two major subsets of $CD14^{+}$ monocytes known as classical and non-classical monocytes. Classical monocytes are known to be CD16 negative whilst non-classical monocytes express high levels of CD16a.[427] These populations with distinct levels of CD16a expression were found in this study. There was no difference in the expression of the other FcγRs between the monocytes subsets, all $CD14^{+}$ cells expressed high levels of CD32a and CD64 (7100 and 11,200 molecules/cell) whilst expressing low levels of CD32b. There were two distinct populations of CD16a expression in $CD14^{+}$ cells; one with a low level of CD16a expression (43 molecules/cell) as well as a population with a high level of CD16a expression (14,000 molecules/cell).

Figure 3.8d presents the number of molecules of FcγRs on the surface of transfected CHO-K1 cells, showing that all receptors are highly expressed with expression varying between 48,000 (CD32a H) and 312,000 (CD32b1 I) molecules/cell. When these results were compared to the highest

expressing PBMC populations in Figure 3.8e, it is clear that the CHO-K1 cells have an FcγR expression level that is elevated compared to physiological levels. The only exception is CD16a expression on CHO-K1 cells transfected with V158, where the number of molecules on the cell surface was comparable to CD16a expression on CD16a Hi NK cells. This CD16a Hi population accounts for the majority of CD56+ cells (60-70%). The higher than physiological FcγR expression on CHO-K1 cell lines is an important consideration for later assays where these cell lines were used as feeder cells.

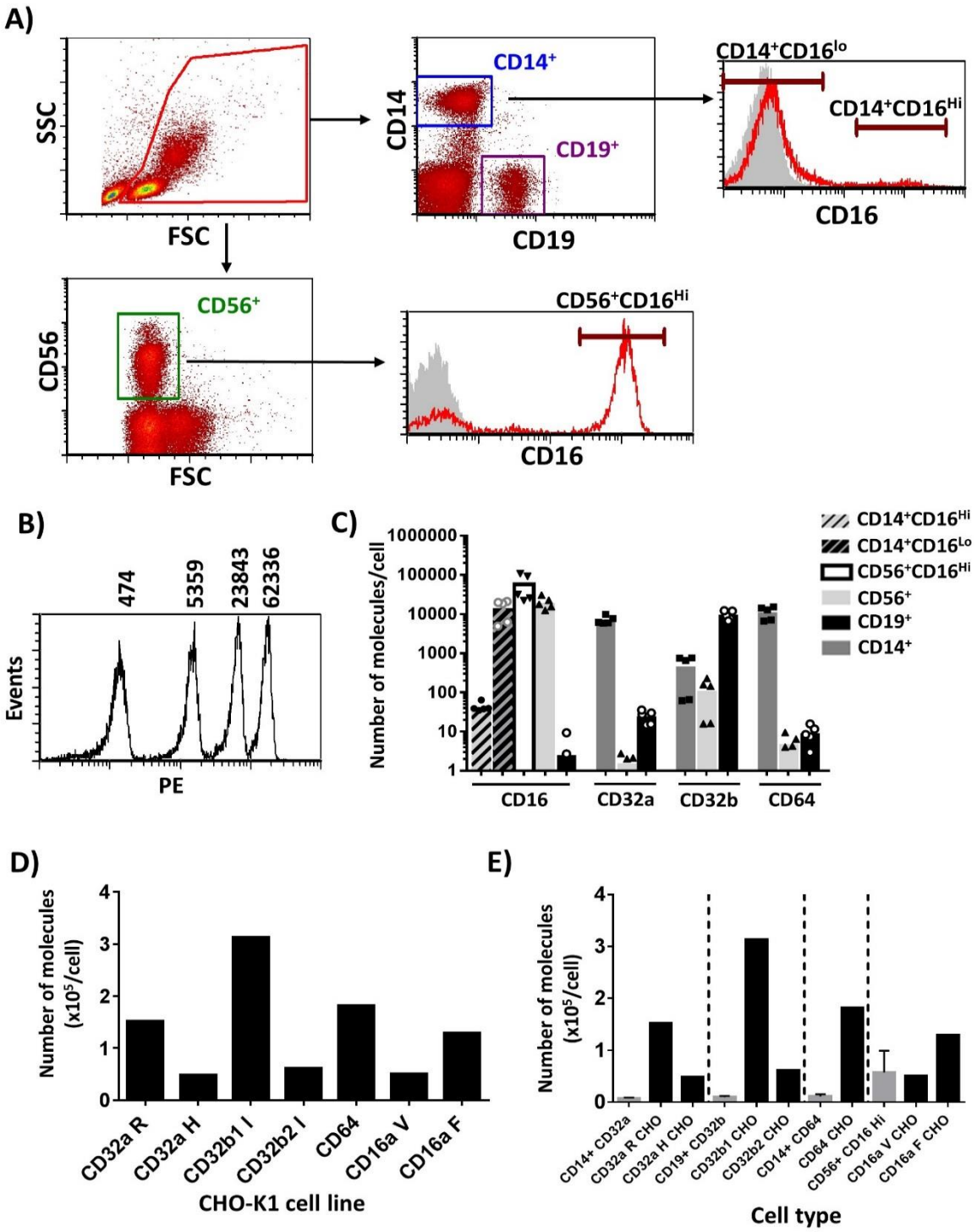

Figure 3.8 ***Quantification of the number of FcγR molecules on trasnfected CHO-K1 cells and PBMCs.***
PBMCs from healthy donors were stained with fluorescently labelled mAb against CD56, CD14 and CD19 as well as F(ab')$_2$ FITC against FcγR or an isotype control. Cells were stained at room temperature and washed twice before analysis by flow cytometry. A) Gating strategy used to identify populations within PBMC samples. B) Quantibrite Beads with defined numbers of PE molecules on their surface were analysed by FACS with the number of PE molecules indicated above the corresponding peak and used to create a standard curve. C) The number of molecules of FcγRs on the surface of PBMC subsets from healthy donors was calculated by staining samples with receptor specific PE labelled mAb points represent individual donors. D) The number of molecules of FcγRs on the surface of stable transfected CHO-K1 cells was calculated by staining with PE labelled mAbs. E) Comparison of number of FcγR molecules on transfected CHO-k1 cells and highest expressing PBMC population. Transfected CHO-K1 cells had a higher number of FcγR on their surface compared to PBMC subsets with the exception of CD16a where expression was similar on CD56+CD16 hi PBMCs and on CD16a V CHO-K1 cells. Bars show mean +SD for PBMC samples.

3.4.2 Binding of aggregated IgG to FcγR transfected CHO-K1 cells

Whilst transfected CHO-K1 cell lines have been demonstrated to express FcγRs through use of receptor specific antibodies, their biological function is to recognise the Fc region of antibodies. Therefore, the ability of the receptors to bind monomeric and aggregated pooled human IgG was investigated. CHO-K1 cells stably expressing FcγRs were stained with receptor specific FITC labelled $F(ab')_2$ to confirm receptor expression. A separate sample of transfected cells was incubated with A488 labelled pooled monomeric human IgG, or heat aggregated human IgG. Following washing, the cells were analysed by flow cytometry to investigate IgG binding.

The results in Figure 3.9 suggest that all cell lines investigated were able to bind to monomeric and aggregated human IgG. For CD16a F158, the binding was low for both monomeric (red histogram) and aggregated IgG (blue histogram). CD32a and CD32b transfected cells appeared to have low binding to monomeric IgG but with aggregated IgG there was a high level of fluorescence, suggesting a higher capacity to bind aggregated rather than monomeric IgG. The CD64 transfected CHO-K1 cell line was the only one that gave a high level of fluorescence with monomeric IgG, implying that this was the only receptor able to efficiently engage IgG in its monomeric form as expected.[290] CD64 transfected CHO-K1 cells were also able to efficiently bind to aggregated human IgG1 although apparently to a lower level than monomeric IgG. Experiments investigating the binding of monomeric and aggregated IgG were performed using the other FcγR polymorphic variants (CD32b1 T232, CD16a V158, CD32a H131) however no major differences were seen in binding by flow cytometry.

Having established cell lines expressing high levels of individual FcγRs, these were subsequenctly investigated in terms of their capacity to mimic different FcγR expressing immune cells in assays with immunostimulatory mAb such as TGN1412.

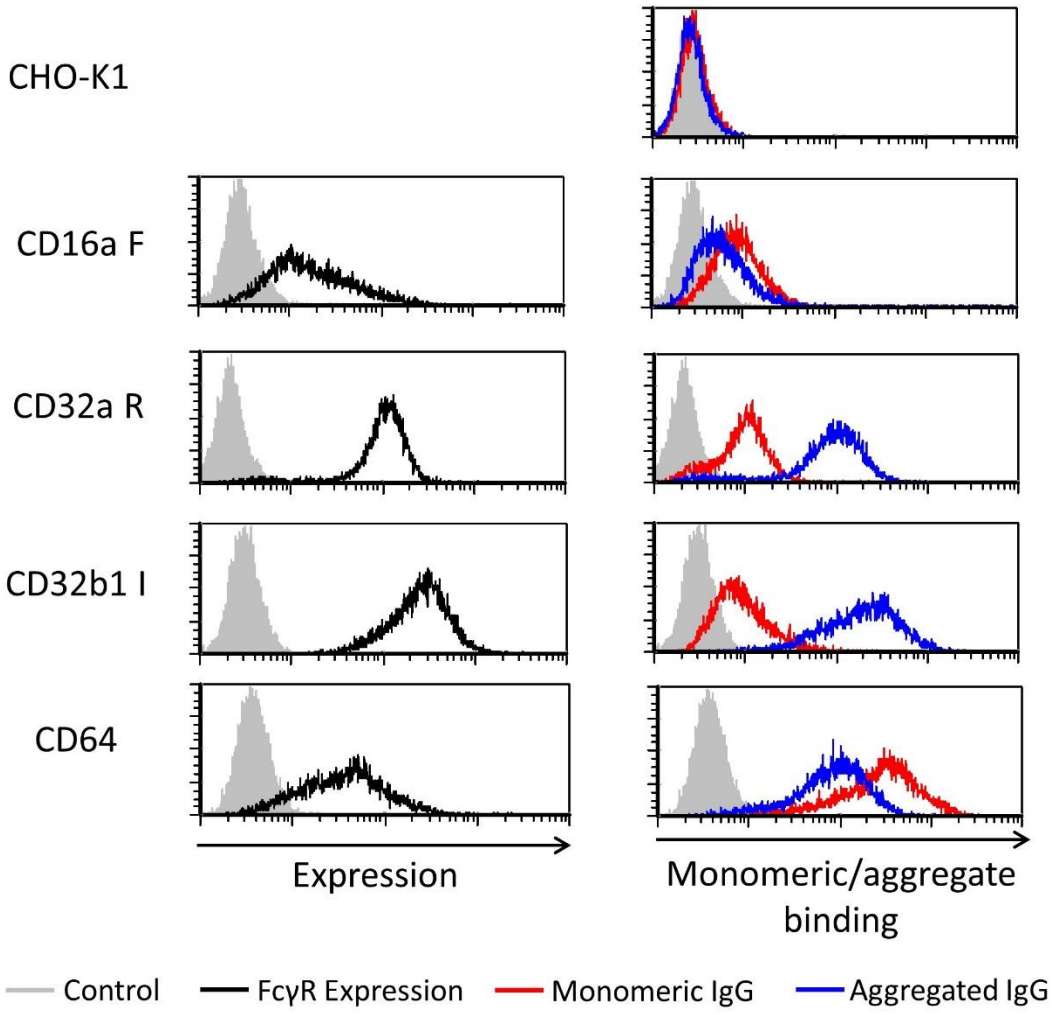

Figure 3.9 ***Binding of monomeric and aggregated human IgG to FcγR transfected CHO-K1 cells****.*
In the left panel FcγR transfected CHO-K1 cells were stained with a receptor specific FITC labelled F(ab')$_2$ (black histogram) or irrelevant control (grey) to confirm expression. In the right panel cells were incubated with an irrelevant FITC labelled F(ab')$_2$ (grey); A488 labelled monomeric, pooled human IgG (Red) or heat aggregated, A488 labelled, pooled human IgG (Blue). Binding was analysed by flow cytometry. CD16a bound monomeric and aggregated IgG at a low level whilst CD32a and CD32b bound monomeric IgG to a low level but higher fluorescence was seen with aggregated IgG. Only CD64 transfected CHO-K1 cells showed high binding to monomeric IgG.

3.5 Requirement of FcγRs for T cell stimulatory antibodies

Prior to the establishment of the FcγR-expressing CHO-K1 transfectants, Dr Ruth French and Dr Kam Hussain had previously developed an assay for the *in vitro* analysis of T cell proliferation and cytokine release following T cell targeting antibodies. Previously, PBMCs cultured at a low density of 1x10^6 cells/ml, or purified T cells, were found not to result in any T cell proliferation when stimulated with TGN1412. In both cases, analysis of culture supernatants revealed that there was

no significant increase in inflammatory cytokine levels following TGN1412 stimulation). However, when the PBMCs were precultured at high density ($1x10^7$ cells/ml) for 48 hours prior to stimulation, TGN1412 was able to result in T cell proliferation at a similar level to that induced by anti-CD3 antibodies.[161] This assay was previously developed in Southampton, with the aim to replicate the experiments at Huntingdon Life Sciences (HLS, now called Envigo) before extending the experiments to investigate individual FcγR requirement using transfected CHO-K1 cell lines. In all experiments the Ancell anti-CD28 mAb (28.1) was used as a positive control as, unlike TGN1412, it is known not to require cross-linking to induce T cell proliferation as well as binding to a different CD28 epitope.[428]

3.5.1 PBMC proliferation assays

To measure the proliferation of T cells following stimulation, PBMCs from healthy donors were labelled with CFSE and incubated at high density ($1x10^7$ cells/ml) for 48 hours. They were then incubated for 4 days in the presence of stimulatory mAbs before the proliferation was measured by flow cytometry. Figure 3.10a presents the gating strategy used during analysis; live lymphocytes were gated based on forward and side scatter before $CD4^+$ and $CD8^+$ populations were identified using antigen specific mAbs. The proliferation of each cell population was determined by CFSE dilution with example plots shown in Figure 3.10b. Here it can be seen that when cells were unstimulated, a single peak was observed for CFSE fluorescence. However, when cells were stimulated with the Ancell anti-CD28 super-agonist antibody (clone 28.1), the CFSE fluorescence was diluted. For each division a cell undergoes, the CFSE fluorescence is approximately halved, allowing the proportion of cells that have undergone division to be determined.

Following PBMC proliferation assays, individual wells were observed under a microscope to look for clustering of cells. As can be seen in Figure 3.11a, the control mAb Avastin did not result in the formation of any significant cell clusters. However, when PBMCs were stimulated with OKT3, distinct clusters of cells were formed in the bottom of the well. The degree of this clustering was approximately proportional to the amount of proliferation that had occurred. For each PBMC donor the proliferation assay was performed in triplicate, with the averages of these triplicates for a single donor shown by the points in Figure 3.11b. The PBMC donors came from 2 sources; CRA donor PBMCs were isolated from leukocytoke cones obtained from the National Blood Service

in Southampton; and HLS donor PBMCs were isolated from fresh whole blood from healthy donors at Huntingdon Life Sciences. In both cases, PBMCs were frozen before use in assays.

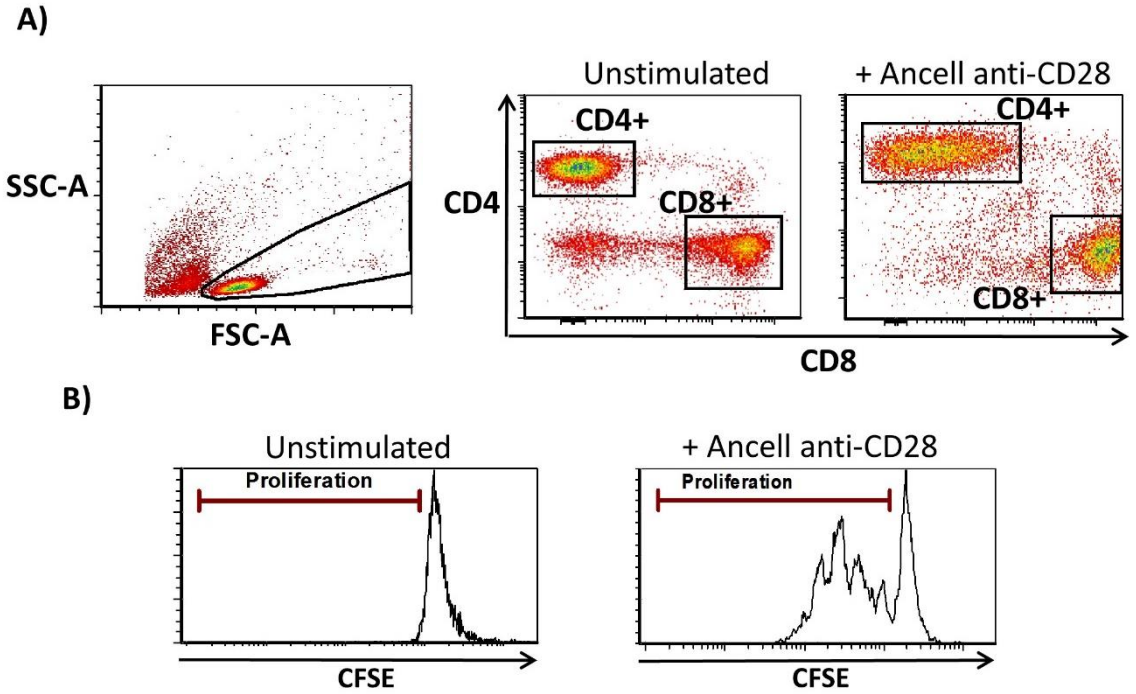

Figure 3.10 ***Gating for T cell proliferation following mAb stimulation***
CFSE labelled PBMCs from healthy donors were incubated at high density (1x10^{7}cells/ml) for 48 hours before being incubated with T cell targeting mAbs for 4 days and proliferation analysed by flow cytometry. A) Live lymphocytes were gated based on forward and side scatter before CD8$^+$ and CD4$^+$ populations were identified using antigen specific fluorescently labelled antibodies. Examples show unstimulated cells and those stimulated with Ancell anti-CD28 (28.1) B) Within each population, T cell proliferation was measured by the dilution of CFSE, plots here show CD8$^+$ cells. Unstimulated cells gave a single peak with uniform CFSE fluorescence indicating no proliferation. When stimulated division was induced with each division halving the CFSE fluorescence allowing the percentage of a population that had divided to be determined.

It is clear from the results in Figure 3.11b that there was a high level of variability between individual PBMC donors. These assays were previously developed in Southampton, with the aim of transferring the assays to HLS using HLS PBMC donors; however, there appeared to be variation between the 2 sources of PBMCs, particularly when focussing on TGN1412 stimulation. The average CD4$^+$ proliferation with TGN1412 by CRA donors was 41.2% (1.59% for Avastin) compared to 14.4% (5.16% for Avastin) with HLS donors. With CRA donors all T cell targeting antibodies (except UCHT1 on CD4$^+$) resulted in a significant increase in proliferation compared to Avastin. When investigating the assays with HLS donors, only UCHT1 (CD4$^+$ and CD8$^+$), Ancell (CD4$^+$ and CD8$^+$) and OKT3 (CD8$^+$ only) induced a significant increase in proliferation ($p<0.01$). With TGN1412 stimulation there was a significant increase in proliferation compared to Avastin in CD4$^+$ cells from CRA donors. There was a trend towards TGN1412 induced proliferation in CD8$^+$ cells from CRA samples and CD4$^+$ cells from HLS samples however, in both cases this did not reach significance.

Despite this variation, the trends were similar between donors regardless of PBMC source. One such trend was the differential proliferation of $CD4^+$ and $CD8^+$ populations; there was a trend towards the anti-CD28 antibodies (Ancell and TGN1412) inducing increased proliferation in $CD4^+$ cells compared to $CD8^+$. The opposite trend was observed when PBMCs were stimulated with anti-CD3 antibodies (UCHT1 an OKT3). This experiment also included a number of non-T cell targeting antibodies (Avastin, Campath, GA101 and cetuximab) none of which resulted in any significant T cell proliferation. Overall, these experiments demonstrate that, despite a high level of inter-donor variation, this assay format could be used to robustly measure T cell proliferation in response to antibody stimulation, most significantly with TGN1412. Importantly, the trends previously observed between mAbs in Southampton could be reproduced when the assays were performed at HLS.

In these assays the PBMCs were precultured as this was previously found to be necessary in order to induce TGN1412 mediated proliferation.[160] Additionally, CD32b was identified as being upregulated following high density preculture of PBMCs.[161] Therefore the number of molecules of CD32b at the cell surface of monocytes following high density preculture was determined using quantibrite beads. Figure 3.12 indicates that there were very few CD32b molecules at the surface of $CD14^+$ fresh monocytes. However, following 48 hours at high density, there was a 148-fold increase in the number of molecules of CD32b at the cell surface. This result suggests that there may be a role for CD32b in facilitating TGN1412 induced T cell proliferation. The expression of CD32b on monocytes was compared to that on CD32b transfected CHO-K1 cells. High density monocytes were found to have a comparable number of CD32b molecules on their surface to CD32b2 (I232) transfected CHO-K1 cells whilst CD32b1 (I232) transfected cells had approximately 4 times more CD32b at the cell surface.

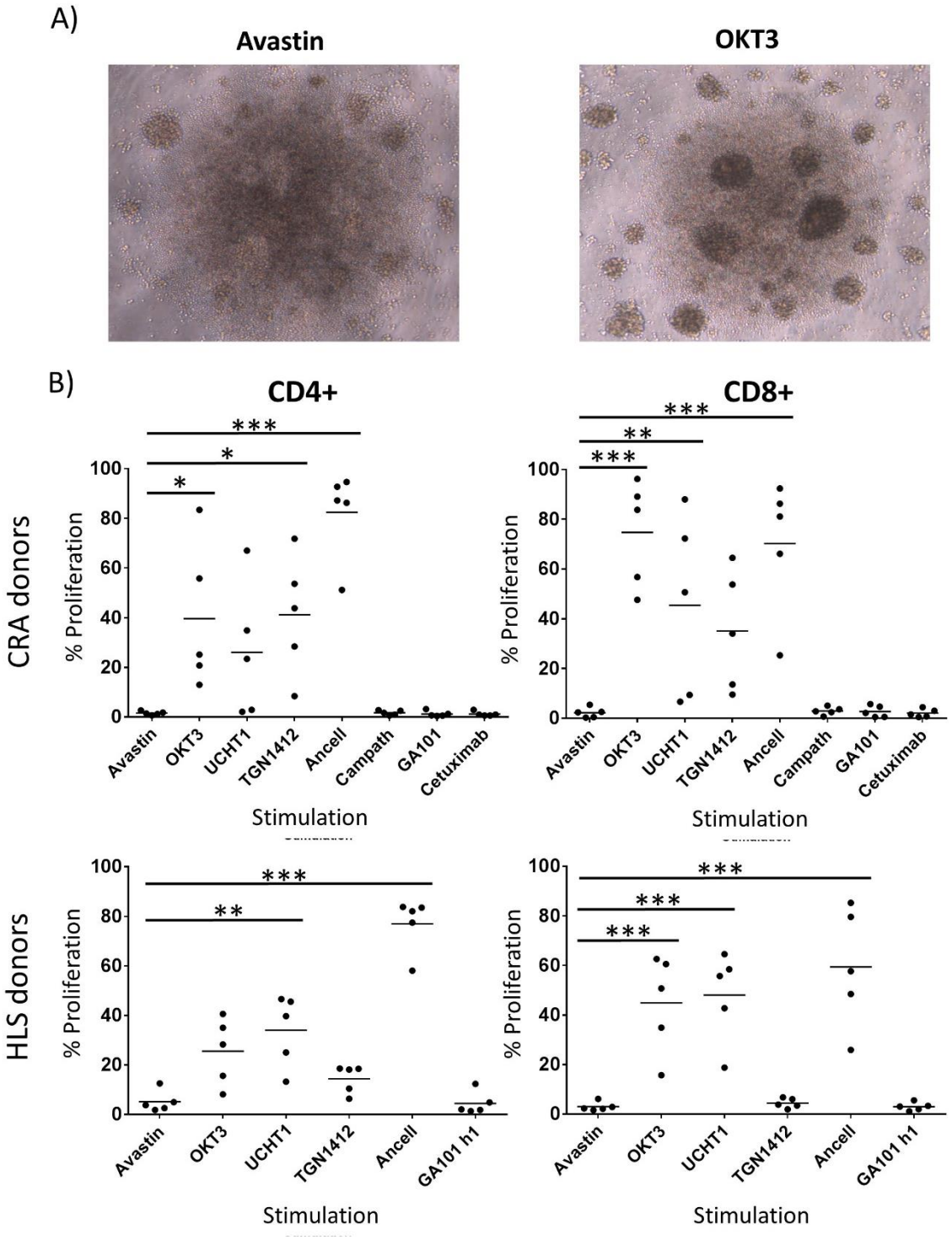

Figure 3.11 ***PBMC based T cell proliferation assay.***
*CFSE labelled Human PBMCs were precultured at 1x10^{7}cells/ml for 48 hours before being cultured for 4 days with mAb stimulation. A) Distinct clusters of cells formed when cells were stimulated with T cell targeting antibodies such as OKT3 compared to unstimulated cells. B) Following culture cells were stained with anti-CD4 and anti-CD8 mAbs and proliferation assessed by CFSE dilution in each population. Points represent averages of triplicates for individual donors sourced in Southampton (CRA donors) or Huntingdon life sciences (HLS donor). T cell targeting antibodies were able to induce T cell proliferation although this was variable between donors and between the source of the PBMCs. In particular TGN1412 induced greater proliferation with CRA donors than with PBMCs from HLS donors. 2-way ANOVA with multiple comparisons (*P<0.05; **P<0.01; ***P<0.001).*

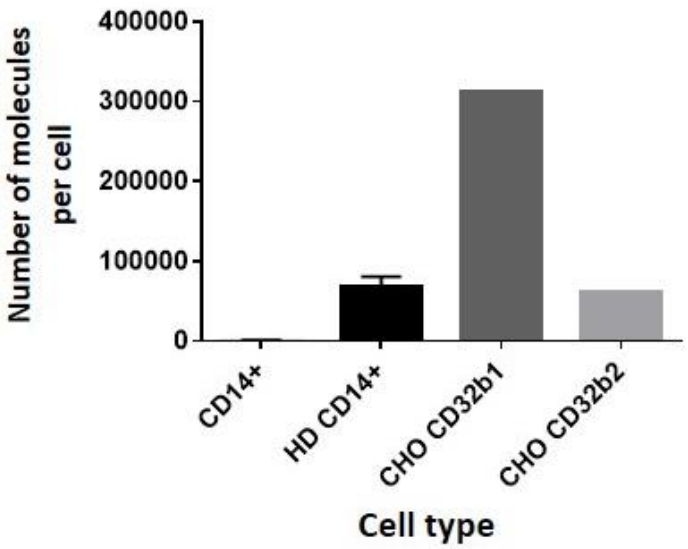

Figure 3.12 ***Quantibrite analysis of CD32b expression in monocytes and CHO-K1 transfectants.*** *Monocytes were isolated from healthy donor PBMCs. The number of molecules of CD32b on the cell surface was calculated using a PE labelled anti-CD32b mAb and quantibrite beads. Results were calculated for fresh monocytes (CD14+) or following 48 hours of high density (1x10^7/ml) preculture (HD CD14+) n=2; mean=SD. Additionally analysis was performed for CD32b1 and CD32b2 transfected CHO-K1 cells.*

3.5.2 CHO-K1 based T cell proliferation assays

Previous experiments had shown that purified T cells do not proliferate when stimulated with TGN1412, despite PBMCs from the same donor resulting in proliferation following high density preculture.[161] Initial experiments identified TGN1412 cross-linking as being necessary for replicating *in vitro* toxicity. However, this was achieved through immobilising TGN1412 by air drying onto plastic wells, or with an immobilised anti-human Fc mAb.[159] This does not provide a biologically relevant mechanism for TGN1412 cross-linking. PBMC proliferation assays suggest that the non-T cell populations present in PBMCs can induce T cell proliferation, most likely through antibody cross-linking via FcγRs. In order to investigate the requirement for FcγR cross-linking for mAb activity and to investigate the specific receptors required, CHO-K1 based proliferation assays were performed. T cells were isolated, using magnetic negative selection, from CFSE labelled PBMCs taken from healthy donors. 5x10^4 purified T cells were incubated with T cell targeting mAbs at appropriate concentrations and 1x10^4 CHO-K1 cells or CHO-K1 cells that had been stably transfected to express different human FcγRs. The FcγR alleles used in this assay were CD32b1 I232, CD16a F158 and CD32a R131. These alleles were chosen as they had the most

uniform FcγR expression at the time the assays were performed. For both CD16a and CD32a the lower affinity alleles were used, moreover the F158 allele of CD16a is found at a higher frequency in the general population than V158.[372] Additionally CD32b1 was chosen as phenotyping suggested that the highest level of CD32b expression on PBMCs was on B cells which preferentially express the b1 isoform with the I232 allele found at a higher frequency.[365] The cells were co-cultured for 4 days before proliferation was measured by analysing CFSE dilution in the $CD4^+$ and $CD8^+$ populations.

Figure 3.13 presents the results of the CHO-K1 based assays, performed in duplicate with points representing averages for individual PBMC donors. These results demonstrate that the Ancell 28.1 antibody was the only mAb able to induce significant proliferation regardless of the CHO-K1 cells present in the assay, including untransfected CHO-K1 cells. This suggests that the antibody does not require cross-linking via FcγRs to induce T cell proliferation. OKT3 was only able to induce significant proliferation, compared to Avastin, when CD64 transfected cells were present and even then only $CD8^+$ cells were seen to proliferate. Additionally, these results imply that OKT3 requires cross-linking via the high affinity receptor CD64 in order to induce T cell proliferation.

TGN1412 did not induce any significant proliferation when co-cultured with untransfected CHO-K1 cells, further suggesting that this mAb requires cross-linking to induce proliferation. TGN1412 was able to induce significantly higher T cell proliferation than Avastin when CHO-K1 expressing CD32b or CD32a were present. Additionally, there was a trend towards increased proliferation with CD64 transfected CHO-K1 cells, however, this did not reach significance. With CD32a and CD32b transfected cells there was significant TGN1412 induced proliferation in both $CD4^+$ and $CD8^+$, strongly suggesting that TGN1412 can achieve effective cross-linking from these receptors to elicit proliferation and that this cross-linking may be responsible for *in vivo* toxicity.

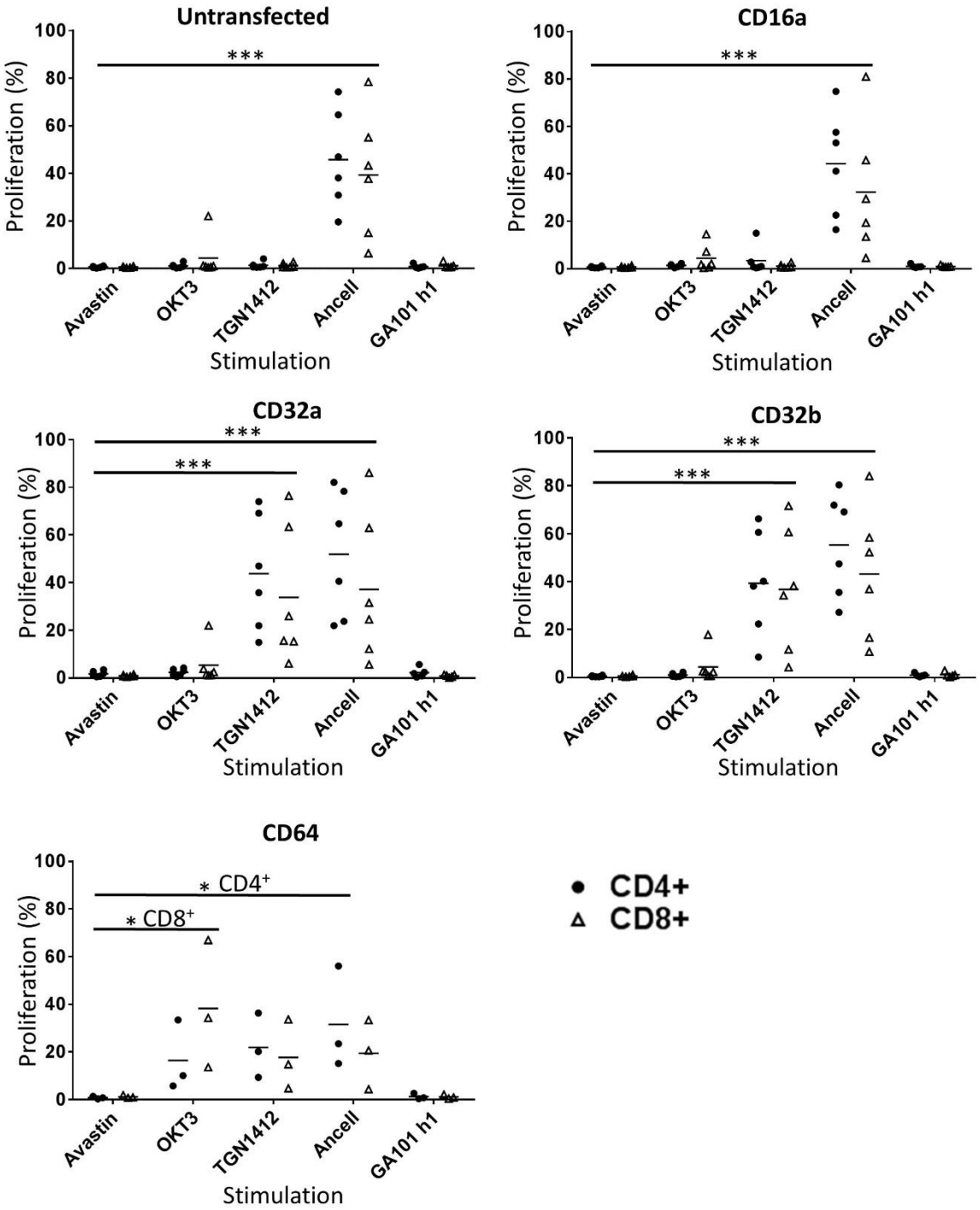

Figure 3.13 ***CHO-K1 based T cell proliferation assays.***
*Frozen PBMCs were thawed and labelled with CFSE before T cells were isolated using a MACs pan-T cell isolation kit. $5x10^4$ T cells and $1x10^4$ CHO-K1 (untransfected or FcγR transfected) were co-cultured with mAbs in a total volume of 150µl. The proliferation of the $CD4^+$ and $CD8^+$ populations was determined by CFSE dilution measured using flow cytometry. Ancell 28.1 gave significant proliferation regardless of the CHO cells present. TGN1412 only gave significant proliferation with CD32b and CD32a transfected CHO-K1, there was a trend towards increased proliferation with CD64 cells however this did not reach significance. Points sow the average of duplicates for individual donors (n = 3-6). 2-way ANOVA with multiple comparisons (***p<0.001; *p<0.05), statistics refers to $CD4^+$ and $CD8^+$ unless stated otherwise.*

3.6 Analysis of cytokines produced by T cell proliferation assays

One of the main clinical complications arising from TGN1412 when it was used in humans was the induction of a rapid and unregulated cytokine storm.[157] To ascertain if this occurred in the *in vitro* assays performed here, supernatant samples were taken from the PBMC and CHO-K1 based proliferation assays. Concentrations of inflammatory cytokines in the supernatants were measured by MSD or Luminex technology. Samples were run in both assay formats in order to investigate the variability between the platforms which has been previously observed.[429] Cytokine analysis was performed on supernatant samples from PBMC assays using 4 donors; the proliferation obtained for each donor in these assays is presented in Table 3.1.

PBMC Donor		**OKT3 induced Proliferation (%)**	**TGN1412 induced Proliferation (%)**
CRA53	$CD4^+$	7.3	67.9
	$CD8^+$	24.3	41.1
CRA57	$CD4^+$	7.7	45.7
	$CD8^+$	24.5	27.2
CRA108	$CD4^+$	20.1	38.3
	$CD8^+$	47.3	18.1
CRA157	$CD4^+$	5.9	33.0
	$CD8^+$	15.2	12.5

Table 3.1 ***Results of PBMC proliferation assays performed on samples used for cytokine analysis.***
Proliferation in the CD4+ and CD8+ populations was measured by CFSE dilution following stimulation with OKT3 or TGN1412 in PBMC proliferation assays. The most relevant cell populations are highlighted (CD4+ for OKT3 and CD8+ for TGN1412) with results the averages of 3-4 independent experiments, each performed in triplicate by Dr Kam Hussain. Supernatants from these samples were used in cytokine analysis by MSD and Luminex.

3.6.1 Comparison of cytokine levels between MSD and Luminex assays

Cytokine levels obtained from PBMC assays were analysed using both the MSD and Luminex platforms to determine the cytokine concentration. There was a high degree of variability between the assay formats which is highlighted in Figure 3.14. Shown are representative plots for a cytokine found at a high concentration (TNF-α) and one found at a low concentration (IL-2). When looking at the concentrations of IL-2 in Figure 3.14a, MSD gave a consistently higher concentration of analyte than Luminex. For TGN1412 stimulated CRA53 PBMCs, the concentration of IL-2 was eight times higher with MSD compared to Luminex. For a number of samples, the concentration was below the detectable limit for Luminex and has therefore been given the value 0. However, both Luminex and MSD suggest that, with TGN1412 stimulation, IL-2 levels were highest with PBMCs from CRA157 and lowest from CRA57, suggesting that whilst absolute values vary between the different platforms, they both identify the same trends between donors.

When the concentrations of TNF-α were measured (Figure 3.14) in the same assay, the Luminex platform suggested higher absolute concentrations of analyte compared to MSD. Despite this discrepancy, the hierarchy of concentrations between donors was maintained between MSD and Luminex. The results seen here with IL-2 and TNF-α are representative of the other analytes assessed on both platforms; MSD tended to give record higher concentrations for analytes present at low concentrations, whilst Luminex tended to give higher readings for cytokines present at a high concentration (full data not shown). Given that the trends were maintained between donors, from this point onwards results will only be presented for Luminex, given the larger number of analytes examined using this platform.

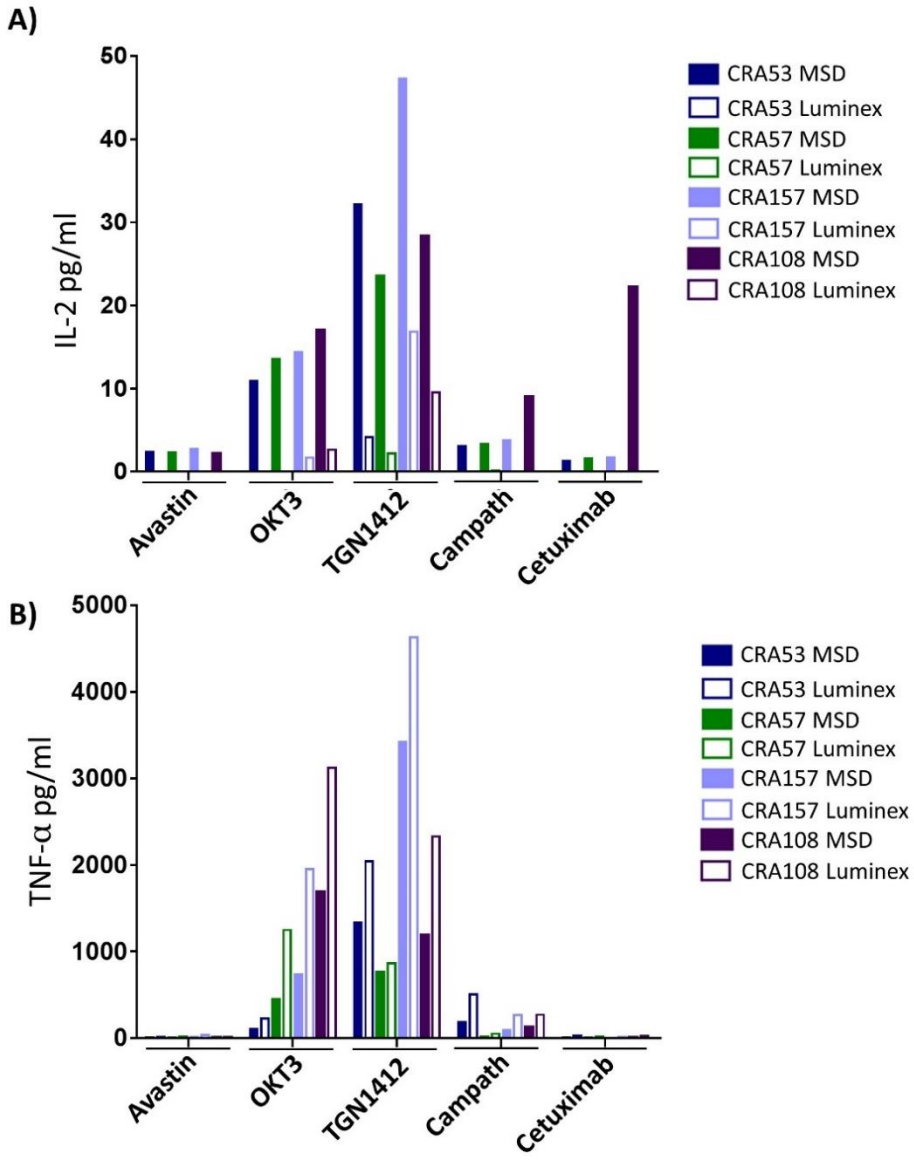

Figure 3.14 ***Comparison of TNF-α and IL-2 concentrations determined by MSD and Luminex.***

A PBMC proliferation assay was carried out on cells isolated form 3 donors. Following high density (1x10^{7}cells/ml) preculture, PBMCs were stimulated with antibodies for 48 before the concentrations of IL-2 (a) and TNF-α (b) were analysed by MSD and Luminex. A) IL-2 levels following TGN1412 stimulation were consistently higher when analysed by MSD compared to Luminex. B) The opposite trend was seen for TNF-α where Luminex gave higher readings. In both cases, whilst absolute values varied, the 2 platforms gave the same trends between donors.

3.6.2 Cytokine release from T cell proliferation assays

A Luminex assay was performed to analyse the cytokines secreted during PBMC and CHO-K1 based T cell proliferation assays. Full results for the cytokines where levels were quantifiable are presented in Figure 3.15. As is to be expected, the control, non-T cell targeting antibodies Avastin and rituximab did not induce any significant levels of any of the cytokines investigated. Following stimulation with TGN1412 a wide range of cytokines were detectable in the culture supernatant.

IFN-γ levels were in excess of 500pg/ml for all PBMC donors with donor CRA53 producing levels over 25ng/ml. Additionally, TGN1412 was able to consistently induce secretion of TNF-α, IL-6, IL-8, MCP-1 and MIP-1a/b, suggesting that the induction of proliferation also results in the secretion of cytokines. There were no obvious trends between the different PBMC donors investigated; for example, CRA57 produced the lowest concentrations of a number of analytes (including TNF-α and IFN-γ) following TGN1412 stimulation, yet produced the highest levels of MCP-1. Furthermore, this did not appear to correlate to the proliferation data where CRA57 had the second highest level of T cell proliferation following TGN1412 stimulation.

OKT3 stimulation also resulted in detectable levels of the majority of cytokines investigated, however in general these levels were lower than those resulting from TGN1412 stimulation. Following stimulation with OKT3, CRA108 tended to result in the highest levels of most cytokines, most notably MIP1-a/b, TNF-α and GM-CSF; this correlates with this donor giving the highest proliferation following OKT3 stimulation. Interestingly, the anti-CD52 antibody Campath-1H did not induce any significant T cell proliferation. However, following stimulation, the supernatant contained detectable levels of IL-1b, IL-6, IP-10, MCP-1 and MIP1a/b. Not all of these cytokines were detected with all PBMC donors, suggesting that there may be donor-specific factors involved in the response to Campath-1H stimulation.

In addition to samples from the PBMC assays, supernatants from a single donor used in the CHO-K1 based assay were also run on the Luminex platform. Samples from assays with untransfected CHO-K1 cells and with CD32b transfected cells were analysed following stimulation with TGN1412 or a human IgG4 isotype control. These results, represented by the open bars in Figure 3.15 suggest that TGN1412 cross-linking by CD32b was required in order to induce cytokine release following stimulation. The concentrations of GM-CSF (1060 pg/ml), IL-4 (86 pg/ml) and IL-5 (452 pg/ml) in the supernatant of CD32b CHO following TGN1412 stimulation were higher than for any of the donors used in the PBMC proliferation assays. TNF-α (1700 pg/ml), IFN-γ (1720 pg/ml) and IL-10 (200 pg/ml) were all secreted following TGN1412 stimulation with CD32b cross-linking. There were a number of cytokines that were consistently identified in PBMC assay samples but were not detected in samples form the CHO-K1 assay, these include: IL-6, IL-8, IP-10, MCP-1 and MIP1α/β. When taken together, these results demonstrate that following stimulation with a number of antibodies, including TGN1412, high cytokine concentrations could be measured in culture supernatants. Additionally, purified T cells could be induced to secrete various cytokines provided TGN1412 was cross-linked by CD32b expressing CHO-K1 cells.

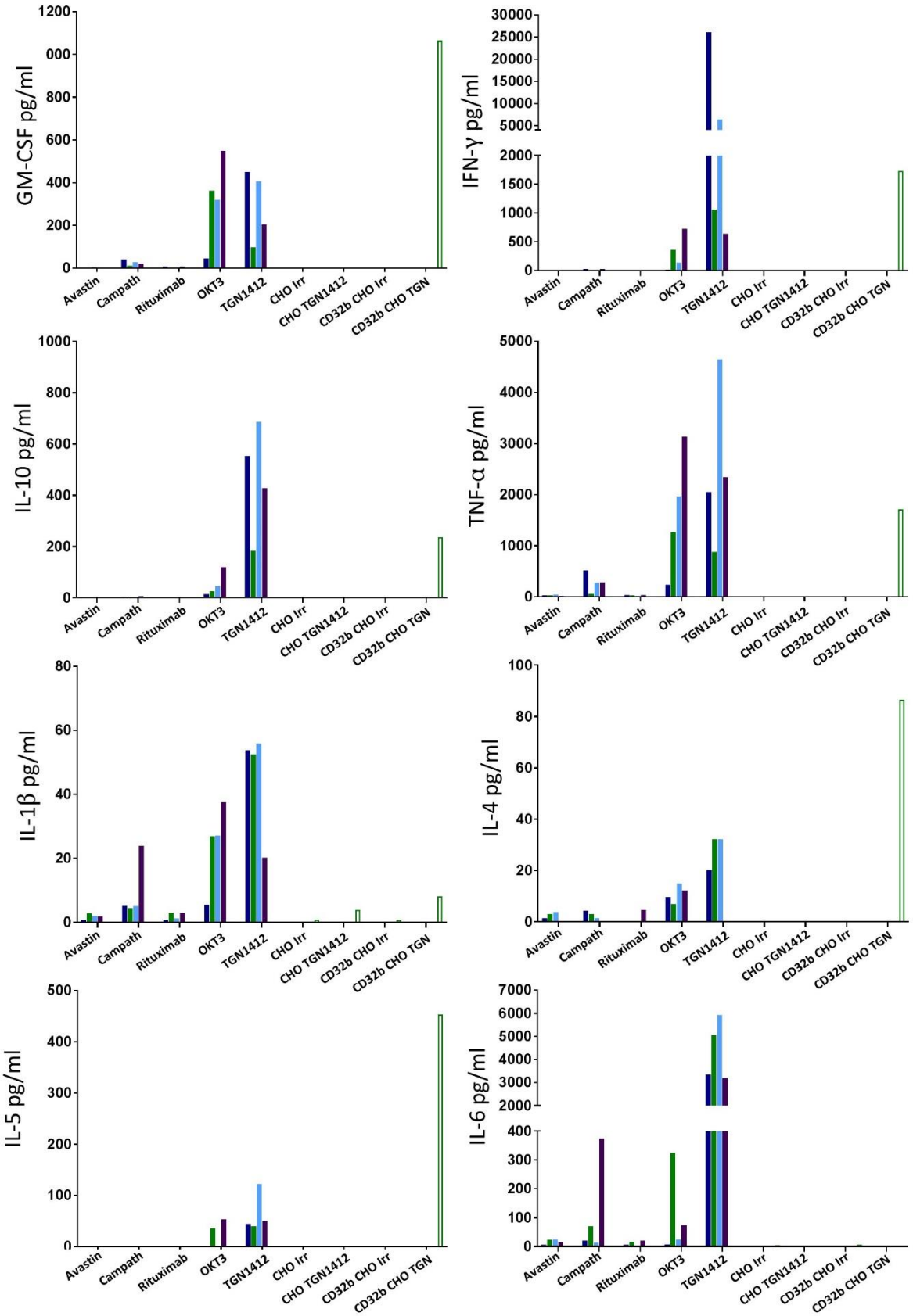
GM-CSF pg/ml
IFN-γ pg/ml
IL-10 pg/ml
TNF-α pg/ml
IL-1β pg/ml
IL-4 pg/ml
IL-5 pg/ml
IL-6 pg/ml
Avastin
Campath
Rituximab
OKT3
TGN1412
CHO Irr
CHO TGN1412
CD32b CHO Irr
CD32b CHO TGN

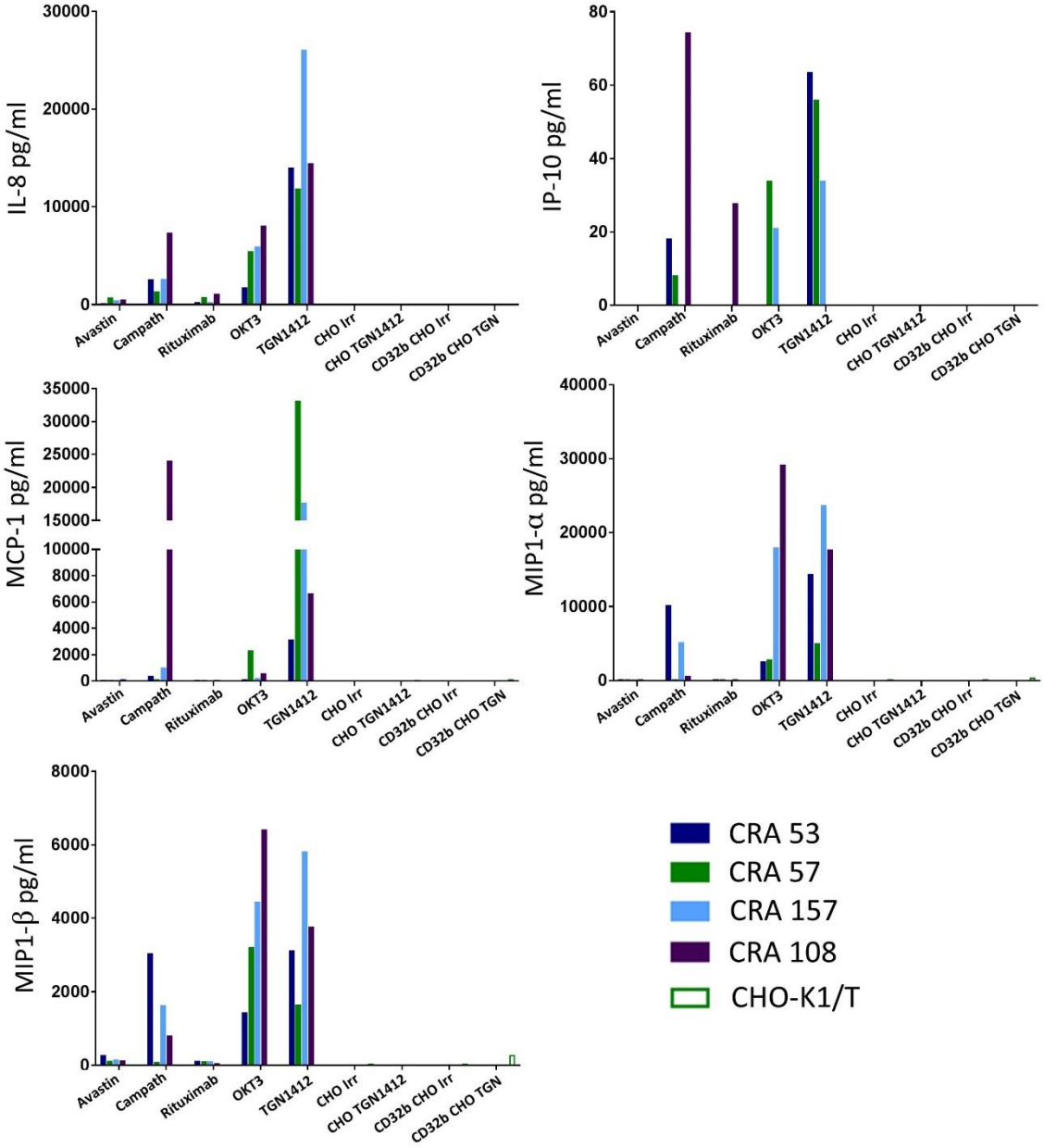

Figure 3.15 ***Cytokine concentrations in supernatants from proliferation assays***.

Proliferation assays were carried out using PBMCs from donors CRA53, 57, 157 and 108. 48 hours after antibody stimulation, 50µl supernatant was removed and stored at -80°C before the concentrations of cytokines measured by Luminex. Results indicate that, for most analytes, TGN1412 was able to induce the secretion of the highest concentrations of cytokines whilst OKT3 was also able to induce high levels of a number of cytokines. Additionally supernatant samples were analysed from a CHO-K1 based proliferation assay (open green bars) using CHO-K1 cell that were either untransfected or transfected with hCD32b. Only when hCD32 CHO-K1 cells were present, and cells were stimulated with TGN1412 were any measurable cytokines detected.

3.7 Chapter discussion

In this chapter, plasmids were produced for the major polymorphic variants of human FcγRs. Initial experiments using transient transfections indicated that receptors could be expressed and recognised by receptor specific antibodies. Transiently transfected cell lines were used in a flow cytometry assay to distinguish between the polymorphic variants of CD16a. This assay was based on previous observations that the antibody MEM-154 has a higher affinity for the V allele of CD16a than the F allele.[425] In the adapted assay used here, results were consistent with those previously seen, with MEM-154 preferentially binding to the V allele. In the previous study, NK cells from F158 homozygous donors were only 4.5% positive when stained with MEM-154; here this was 30.8% when using 293F transfectants. The main reason for this discrepancy is likely to be the high expression level of CD16a obtained in the transient transfections; those cells with the highest receptor expression are likely to be those that MEM-154 stains. Nonetheless, CD16a F158 transfected cells have a significant reduction in MEM-154 positive cells compared to other phenotypes, allowing them to be easily distinguished. The previous study used fluorescently labelled 3G8 whereas here, unlabelled 3G8 was used to provide competition for MEM-154 binding; this competition augmented the ability of MEM-154 to distinguish V158 cells from VF heterozygous cells. Finally, the results here suggest that, with further refinement, this assay may be able to distinguish between copy number variations in CD16a. However, these results are based on an *in vitro* overexpression system and transferring this to human samples could be challenging as the assay requires comparative analysis between the 3 major phenotypes.

Using the plasmid constructs, CHO-K1 cells were generated which stably expressed polymorphic variants of hFcγRs. One of the challenges encountered during this was the tendency for receptor expression levels to drift over time. This was most apparent for CD16a and CD64 transfected CHO-K1 cells, suggesting that this phenomenon may arise as a result of co-transfection of 2 plasmids.

The expression of FcγRs on stably transfected CHO-K1 cells was compared to that observed on PBMCs obtained from healthy donors; these data revealed that receptor expression on CHO-K1 cells was higher than that physiologically observed. Additionally, these data highlighted the variability in FcγR expression level between PBMC donors. Two distinct expression levels of CD16a were observed on $CD56^{+}$ cells. These correspond to the $CD56^{dim}$ (expressing high CD16a) and $CD56^{bright}$ populations (expressing low CD16a).[430] $CD56^{bright}$ NK cells have been shown to secrete large amounts of cytokine following monocyte activation, whilst $CD56^{dim}$ cells are thought to have

a higher cytotoxic activity, indicating that these two subsets are functionally distinct.[426] Furthermore, the data in this chapter indicates that even within the CD16a^{Hi} population, expression is variable between donors, with the number of molecules ranging between 12200 and 30200 for different donors. This could be natural variation that occurs, however it has also been described that activation of NK cells results in a downregulation of CD16a.[431] This suggests that the variability in expression could be related to the NK cell activation of the donors. For some donors there appeared to be a low level of CD32b expression on NK cells, with a highest level of 2313 molecules per cell for 1 donor. Whilst this may be an artefact, it is also possible that this represents expression of CD32c. This receptor is identical to CD32b extracellularly, however the majority of individuals carry a CD32c haplotype containing an upstream stop codon, preventing receptor expression.[313] In one study of 146 individuals, only 20% contained one or more open reading frame for CD32c, although expression was not confirmed at the protein level.[312] It is therefore possible that the anti-CD32b mAb used here is detecting expression of CD32c on the NK cells of some individuals here.

It was suggested by data in this chapter that CD64 was the only receptor able to efficiently bind to monomeric pooled IgG. This is consistent with previous work; SPR found CD64 to have a K_A of 650 x10^5M^{-1} for human IgG1, 12.5 fold higher than the affinity of the next highest affinity receptor, CD32a.[290] As expected, CD32a and CD32b were able to bind to aggregated pooled IgG more efficiently than monomeric. It is likely that this differential binding of monomeric and aggregated IgG reflects the biological functions of the receptors. The low affinity receptors CD32a and CD32b function to induce or regulate an immune response, therefore it is important that they respond to immune complex rather than monomeric circulating IgG, which would result in signalling in the absence of antigen.

Whilst the biological function of CD64 (particularly with regards to the biological significance of monomeric IgG binding) remains unclear, the structural basis for its high affinity has been investigated. Most notably, this revealed a hydrophobic pocket on the surface of CD64 where Leu235 of IgG1 Fc was able to bind efficiently.[293] Further structural evidence suggested that CD64 may be more efficiently able to bind glycans on IgG1 compared to the low affinity receptors.[294] Interestingly, CD16a appeared to have very low binding to both monomeric and aggregated IgG with a slight preference for monomeric IgG. This is surprising given that, akin to CD32a and CD32b, CD16a is known to have a low affinity for monomeric IgG; it has been previously shown to be only able to bind IgG3 as a monomer yet has a high affinity for complexed IgG1.[290] One possible explanation is that one subtype of IgG is preferentially aggregating. In the same study, aggregated

IgG of specific isotypes was generated with receptors showing preferential binding to certain isotypes, this could explain the binding patterns for aggregated IgG observed in the work performed here. This, coupled with the relatively high concentrations of aggregated IgG used here may explain why no major differences were observed between polymorphic variants of FcγRs. Previous experiments using low concentrations of aggregated IgG of defined isotype was able to identify differences in binding between the variants.[290]

PBMC proliferation assays were performed in this chapter to analyse the effect of a range of immunostimulatory antibodies. One observation from these assays was that activated, proliferating T cells form distinct multi-cell clusters in the plates. Clustering of T cells has been previously shown to induce an intracellular signalling cascade that results in reduced Cbl-b mediated inhibition of PI3K, resulting in activation of Rho and NFκB.[432] This process may enhance the proliferation of T cells following cross-linking in addition to the intrinsic signalling resulting from CD28 or CD3 stimulation.

It has been previously shown that the anti-CD3 antibodies OKT3 and UCHT1 require cross-linking by other non-CD3 positive cell populations as they do not induce proliferation when isolated T cells are stimulated.[161] The same work identified that, as well as additional cell populations, PBMCs require high density preculture before TGN1412 stimulation in order to induce significant proliferation. It is apparent from the work in this chapter that there is significant variation in proliferation between PBMC donors; this is an area that requires further investigation. One possible explanation for the variability is that antibody target expression may vary between donors, affecting proliferation. However, when looking at individual donors, those that showed low response to TGN1412 also responded poorly to anti-CD3 antibodies. It therefore seems likely that response is dependent on some inherent property (e.g. cell health or immune activation status) of the donor samples.

The results presented in this chapter indicate that when assays were performed using CRA PBMC donors at HLS, results obtained were similar to those obtained from the same donors when assays were performed in Southampton. This is summarised in Table 3.2 where the $CD8^+$ proliferation for 2 donors is shown, suggesting that with the same PBMC donors, results are repeatable between location. However, when the same set of assays were performed using PBMC donors from HLS, proliferation achieved with TGN1412 and OKT3 stimulation was lower than was seen with CRA donors. One possible explanation for this is the method of PBMC preservation; CRA samples were frozen in the presence of human AB serum, whereas HLS samples were frozen in

FCS. The use of human AB serum has been found to lead to improved cell viability and proliferation after thawing (Dr K. Hussain, personal communication). Moreover, HLS PBMCs were isolated from whole blood, whereas CRA PBMCs were purified from National Blood Service leukocyte cones. These sources have different relative proportions of cell subsets; PBMCs from whole blood contains 50-80% neutrophils whereas they constitute less than 5% of leukocyte cone PBMCs (Dr K. Hussain, personal communication). Whilst neutrophils should be removed by the lymphoprep step there may be some carry-over, as well as other differences in the cell populations present. Overall, this assay format is repeatable across different labs and is capable of inducing T cell proliferation following TGN1412 stimulation.

Antibody	**CRA160 $CD8^+$ proliferation (%)**		**CRA161 $CD8^+$ proliferation**	
	Southampton	HLS	Southampton	HLS
OKT3	50.7	47.6	96.4	96.2
UCHT1	9.2	6.7	90.1	88.0
TGN1412	10.0	13.6	66.4	64.5
Ancell 28.1	85.1	81.1	92.3	91.4

Table 3.2 ***Comparison of proliferation assays performed in Southampton and at HLS****.*
Proliferation assays were performed at HLS and in Southampton using PBMCs from the same donor and stimulated with the various antibodies. Results indicate that proliferation of the $CD8^+$ (as determined by CFSE dilution) was similar for the same conditions regardless of whether the assay was performed at HLS or in Southampton.

A number of assays have been previously developed for replicating the *in vitro* toxicity seen following TGN1412 stimulation; these highlighted the need for cross-linking of TGN1412. However, they achieve it either through immobilisation of antibody on a plastic surface or through the use of a secondary anti-IgG cross-linking antibody.[158, 159] Whilst these assays highlight the importance of cross-linking, it is not provided in a biologically relevant manner. The assays used in this chapter build on the work of Romer where high density preculture was found to facilitate cytokine release by soluble TGN1412.[160] This previous study suggested that preculture increased the tonic activation of T cells. However, work in this chapter suggests that upregulation of CD32b following high density culture is responsible for TGN1412 induced proliferation. This is corroborated by the CHO-K1 assay where high density preculture was not performed yet proliferation was still achievable when isolated T cells were incubated with CD32b-expressing CHO-K1 cells. It has been found that CD32b is upregulated on human monocytes in response to high density preculture.[161,

[433] In this chapter, this upregulation resulted in a mean of 128,000 molecules of CD32b on the cell surface, this was still 2.4 fold lower than the expression of CD32b1 on CHO-K1 cells used for proliferation assays. This suggests that the cross-linking provided by transfected CHO-K1 cells is likely to be greater than that achieved *in vivo* or through using *ex vivo* samples in other assay formats.

One of the main aims of this study was to investigate the FcγR cross-linking requirement for T cell stimulating antibodies; this was investigated using CHO-K1 cells that had been stably transfected with a single FcγR. An additional advantage of this system is that the polymorphic variant of CD16a and CD32a can be controlled, which is not possible in the PBMC assay without donor genotyping. TGN1412 was able to induce proliferation when cross-linked by CD32a, CD32b or CD64. The requirement for CD32b cross-linking has been previously investigated, where it was found that using a CD32b blocking antibody in a PBMC assay significantly reduced T cell proliferation following TGN1412 stimulation.[161] This adds to further work demonstrating that interactions between Fc and CD32b are important for the activity of agonistic mAbs targeting costimulatory molecules such as CD40.[434] Furthermore, the results presented here demonstrate that cross-linking by CD32a is also able to induce proliferation following TGN1412 stimulation. This result is unsurprising, given that CD32a and CD32b have 94.5% protein sequence identity for their extracellular domains (alignment of Uniprot accessions P12318 and P31994 using ClustalW2[435]).[307] CD32a contains a motif that allows the receptor to form a dimer at the cell surface; it is possible that this may enhance the ability of the receptor to cross-link TGN1412.[302] Given the sequence similarity, it is likely for the same phenomenon to occur with CD32b, although this has not been formally demonstrated.[302] CD16a expressing CHO-K1 cells were unable to facilitate TGN1412 induced proliferation, despite the receptor having a similar affinity for IgG4 as CD32a and CD32b, as measured by biacore.[290] Additionally, the expression of CD16a on the CHO-K1 cells was similar to that of CD32a; this suggests that CD32a and CD32b have an enhanced innate ability to cross-link TGN1412, possibly as a result of their dimerization motifs. TGN1412 stimulation in the presence of CD64 transfected cells also resulted in proliferation, which is likely to occur as a result of the high affinity of CD64 for IgG4.[290]

The anti-CD3 mAb OKT3 was only able to induce significant proliferation in the CHO-K1 based experiments in the presence of CD64 transfected CHO-K1 cells. In order to induce proliferation, anti-CD3 mAbs typically require co-stimulation, for example through CD28.[436] This would normally be provided from other cell populations not present in the CHO-K1 based assays. However, the anti-CD3 OKT3 has been previously shown to induce T cell proliferation following cross-linking,

either through immobilisation on plastic, or via FcγRs on monocytes in order to induce proliferation.[437, 438] This is consistent with the observations in this study and others, suggesting that mouse IgG2a (such as OKT3) can bind to CD64. Cross-linking via this receptor was demonstrated to be required for OKT3 activity.[439] Furthermore, UCHT1 is a mouse IgG1, an isotype known only to bind to the R allele of CD32a. In the PBMC proliferation assay, 2 donors did not give proliferation in response to UCHT1; it is therefore likely that these donors were homozygous for H131.

The Ancell 28.1 antibody was able to induce proliferation without any FcγR cross-linking as well as in purified T cells or PBMC assays without high density preculture. This is consistent with previous experiments identifying 28.1 as a superagonist, capable of inducing T cell proliferation without any T cell receptor (TCR) stimulation.[428] The same study also demonstrated that TGN1412 could induce the proliferation of purified T cells only when cross-linked, although this was achieved using an anti-human IgG4 cross-linking antibody. Whilst this identifies the need for cross-linking, it does not provide a biologically relevant method of cross-linking that can explain the *in vivo* toxicity. In this chapter, cross-linking was provided by FcγRs. Whilst these are overexpressed on CHO-K1 cells, these results indicate a more biologically relevant mechanism by which TGN1412 could be cross-linked to result in *in vivo* toxicity.

Very little cytokine release was observed with the non-T cell targeting antibodies rituximab and Avastin, suggesting that cytokine release is correlated with T cell activation. In contrast, Campath induced detectable levels of several cytokines; whilst this mAb was developed for use in B cell malignancies, its target, CD52, is also expressed on T cells and NK cells. Cytokine release has been reported *in vivo* following Campath infusion, however the cytokines reported previously were TNF-α, IFN-γ, and IL-6.[440] In the present study, Campath induced secretion of TNF-α and IL-6, however levels were lower than given by TGN1412 and not detected with all donors. The primary cytokines detected following Campath stimulation were IL1-b, IL-6, IL-8 and MIP1α/β. Early studies identified that cytokine release following Campath stimulation was dependent on CD16a engagement with cytokines secreted from NK cells. [440] Whilst a later study confirmed the importance of NK cells, the depletion of neutrophils significantly reduced cytokine secretion following Campath stimulation.[441] This could explain the low levels of cytokines observed in this chapter following Campath stimulation, as all assays performed with Campath used PBMCs isolated using lymphoprep, which should exclude the majority of neutrophils. Although the cytokines detected in this study differ from those seen previously, they emphasise the proinflammatory response obtained with Campath stimulation.

The cytokines released in response to TGN1412 in this chapter include those reported as being found at high concentrations in the blood of volunteers during the TGN1412 trial. This includes TNF-α, IFN-γ, IL-4, IL-6, IL-8 and IL-1b.[157] This suggests that the assay format used here is appropriate for re-capitulating the adverse events seen *in vivo* following TGN1412 stimulation. There does not appear to be a clear correlation between the concentrations of cytokines and the observed T cell proliferation. For example, the highest concentration of the proinflammatory cytokine TNF-α following TGN1412 stimulation was achieved with PBMCs from CRA157, the donor that resulted in the lowest proliferation. For IFN-γ the donor that gave the highest TGN1412 induced proliferation (CRA53) did give the highest concentrations of cytokine, however the next highest levels were given by the donor with the lowest proliferation, CRA157. One caveat to this is the small number of samples investigated here, especially when considering the large variation between donors, making it difficult to identify or exclude correlations between proliferation and cytokine release. When using a larger number of donor samples, a correlation was observed between percentage proliferation and the release of cytokines including IL-2, TNF-α and IFN-γ (Dr Kam Hussain, personal communication). One complicating factor is that the supernatant samples were collected at a different time to the assessment of proliferation; carrying out both analyses at the same time point may result in a clearer correlation. Overall, the data presented here implies that the release of cytokine may be an all-or-nothing response, with cytokine released when proliferation occurs, regardless of the magnitude of proliferation. The concentrations of cytokines produced may not be determined by the magnitude of proliferation but by donor specific factors unrelated to their proliferative capacity.

The CHO-K1 proliferation assays also show that there was cytokine release following TGN1412 stimulation with CD32b transfected cells. There were a number of cytokines found in PBMC assay supernatants that were not seen in the CHO-K1 assay, such as IL-6. It is likely that these cytokines are secreted by cell populations present in the PBMC cultures but not in the CHO-K1 assays suggesting they are secreted by non-T cells. IL-6 can be produced by T cells, however its absence from the CHO-K1 cultures suggests that in the PBMC assay, it may be secreted by other cell populations such as monocytes, where it has been shown to be secreted in response to TNF-α stimulation.[442] It is important to consider that for the CHO-K1 assay, cytokine analysis was performed using PBMCs from a single donor; given the variability seen between donors it will be important to repeat this analysis with additional donors.

Overall, in this chapter CHO-K1 cells were generated that expressed polymorphic variants of human FcγRs; these were subsequently characterised and demonstrated binding to monomeric

and aggregated IgG. This assay allowed for T cell proliferation and cytokine release to be analysed in a way that provided more biologically relevant cross-linking than antibody immobilisation. It remains to be seen how these assays could predict the toxicity of a novel reagent, prior to *in vivo* investigation. Transfected cells could be used to provide antibody cross-linking which could recapitulate the toxicity of TGN1412 observed *in vivo.* This highlights the importance of FcγRs in the activity of immunostimulatory mAbs and emphasises the need to understand the effect of FcγR mediated cross-linking on new mAbs. These mAbs do not normally rely on effector cell activity for their function, a role requiring FcγR engagement. The results shown here add weight to FcγRs having a more complex function than acting as mediators of immune effector cell function.

Chapter 4 Investigating the lack of CD32b expression in Ramos cells

4.1 Chapter introduction

CD32b, as has been described in the introduction, is the only inhibitory FcγR present in humans. Additionally, it is the only FcγR expressed by B cells where its function is thought to be to modulate the signalling mediated by the BCR; this feedback loop provides an important checkpoint to restrict excessive antibody production and reduce the risk of autoimmunity.[322] CD32b is also expressed on macrophages and monocytes, alongside activatory receptors, where it is thought to provide a threshold for cell activation. There are two isoforms of CD32b in humans; CD32b1 is the major isoform expressed on B cells and contains a 19 amino acid insertion in its cytoplasmic domain, not found in CD32b2.[443] Whilst the two isoforms do not differ in their ability to bind to IgG, the insertion in CD32b1 prevents localisation into clathrin coated pits and thus efficient IC endocytosis.[308]

Ramos and Raji cells are widely used B cell lines, derived from Burkitt's lymphoma patients.[444, 445] These cells have been used extensively to study immunotherapy *in vitro*, particularly as target cells for ADCC, CDC and ADCP assays.[185, 265, 446] They represent a convenient alternative to using primary *ex vivo* samples, reducing the inter donor variation that comes with them. One major difference between Ramos and Raji cell lines is their expression of CD32b. Unlike most B cells, Ramos cells do not express of CD32b, whereas Raji cells maintain expression.[210] In this chapter, the lack of CD32b expression at the cell surface was before investigating the potential basis for this.

Expression of CD32b is thought to be an important factor in the response to immunotherapy. Patients who had a higher level of CD32b expression were found to respond less well to therapy with the anti-CD20 mAb rituximab.[255] It is believed that this reduced response is a result of mAb internalisation though binding to CD32b.[253, 254] Investigating why the Ramos cell line lacks expression CD32b may give a mechanistic insight into how some patients respond better to anti-CD20 immunotherapy through reduced expression of CD32b. Furthermore, as described in the previous chapter, CD32b cross-linking can be required for the activity of immunomodulatory mAbs. With B cells thought to provide the highest *in vivo* expression level of CD32b, understanding the causes of reduced expression could be important with regard to immune modulatory mAb activity.[161] Therefore, the aim of this chapter was to understand the mechanism by which Ramos

cells fail to express CD32b. Whether this lack of CD32b expression was due to defects at the transcriptional or translational level was investigated before determining if CD32b expression could be restored using small molecule inhibitors.

4.2 Confirmation of CD32 expression on Ramos and Raji cells by flow cytometry

Initially, Ramos cells were screened in order to confirm their lack of CD32b expression at the cell surface. Ramos and Raji cell suspensions were stained with AT10 (anti-CD32) $F(ab')_2$ FITC or an irrelevant control for 15 minutes at room temperature before being washed twice with FACS wash. Samples were then analysed by flow cytometry, as can be seen in Figure 4.1. Viable cells were identified by forward and side scatter and the expression of CD32 was determined. This demonstrated that CD32 could be detected on the surface of Raji cells but that there was no detectable expression on Ramos cells. Whilst this shows that no CD32 was expressed at the surface of Ramos cells, it does not identify whether this was due to a lack of transcription, translation or transport of the receptor to the membrane.

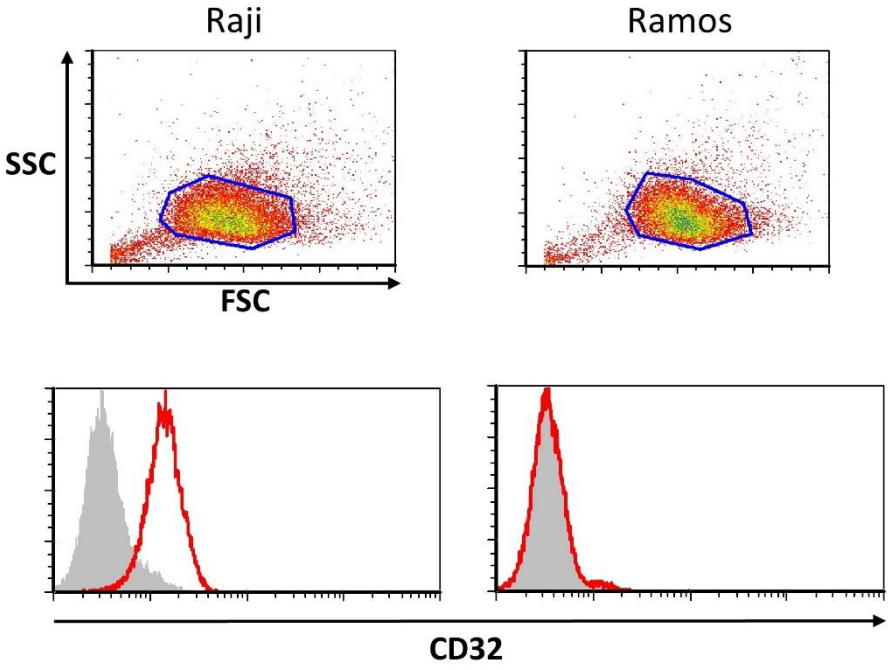

Figure 4.1 ***Expression of CD32 by Raji and Ramos cells.***
100µl Ramos and Raji cell suspension at 1x10⁶ cells/ml were stained with AT10 $F(ab')_2$ FITC (red histogram) or irrelevant control (grey) at a final concentration of 10µg/ml. Viable cells were gated based on forward and side scatter (top panels) before the expression of CD32 was determined (bottom panels). Surface expression of CD32 was detectable on Raji but not Ramos cells.

4.3 The effect of proteasome inhibition on CD32b expression

Having established that there was no detectable expression of CD32 at the cell surface of Ramos cells, experiments were performed to determine the mechanism behind this. One possibility was that CD32b was being translated but was not reaching the cell surface due to being degraded within the cell. In order to investigate this mechanism, Ramos and Raji cells were incubated for 48 hours with the proteasome inhibitor bortezomib. This acts by inhibiting the 26S proteasome, preventing ubiquitin-mediated protein degradation.[447]

Bortezomib is used as a chemotherapy drug and as such has substantial cytotoxicity against a range of cell lines *in vitro.*[448] Therefore, the viability of Ramos and Raji cells following incubation with bortezomib for 48 hours was determined. This was performed by staining with annexin V-FITC and propidium iodide (PI). To determine cell death, debris was first excluded by forward and side scatter before viable cells were identified as being double negative for annexin V and PI (Figure 4.2). As can be seen in Figure 4.2b, cell death increased at bortezomib concentrations above 5nM. When used at 10nM, the majority of cells in the culture were no longer viable. The expression of CD32 was investigated following bortezomib treatment by flow cytometry. Cells were stained with AT10 $F(ab')_2$ FITC or an irrelevant control. Due to the high cell death, samples treated with 10nM bortezomib were not investigated for CD32 expression. Figure 4.2c indicates that bortezomib did not alter the expression of CD32 at any concentration used. Ramos cell continued to be negative for surface CD32 expression whilst for Raji cells there was no accumulation of surface CD32 following bortezomib treatment. This suggests that inhibition of the proteasome is not able to restore surface CD32b expression and thus CD32b degradation is not responsible for the lack of expression in Ramos cells.

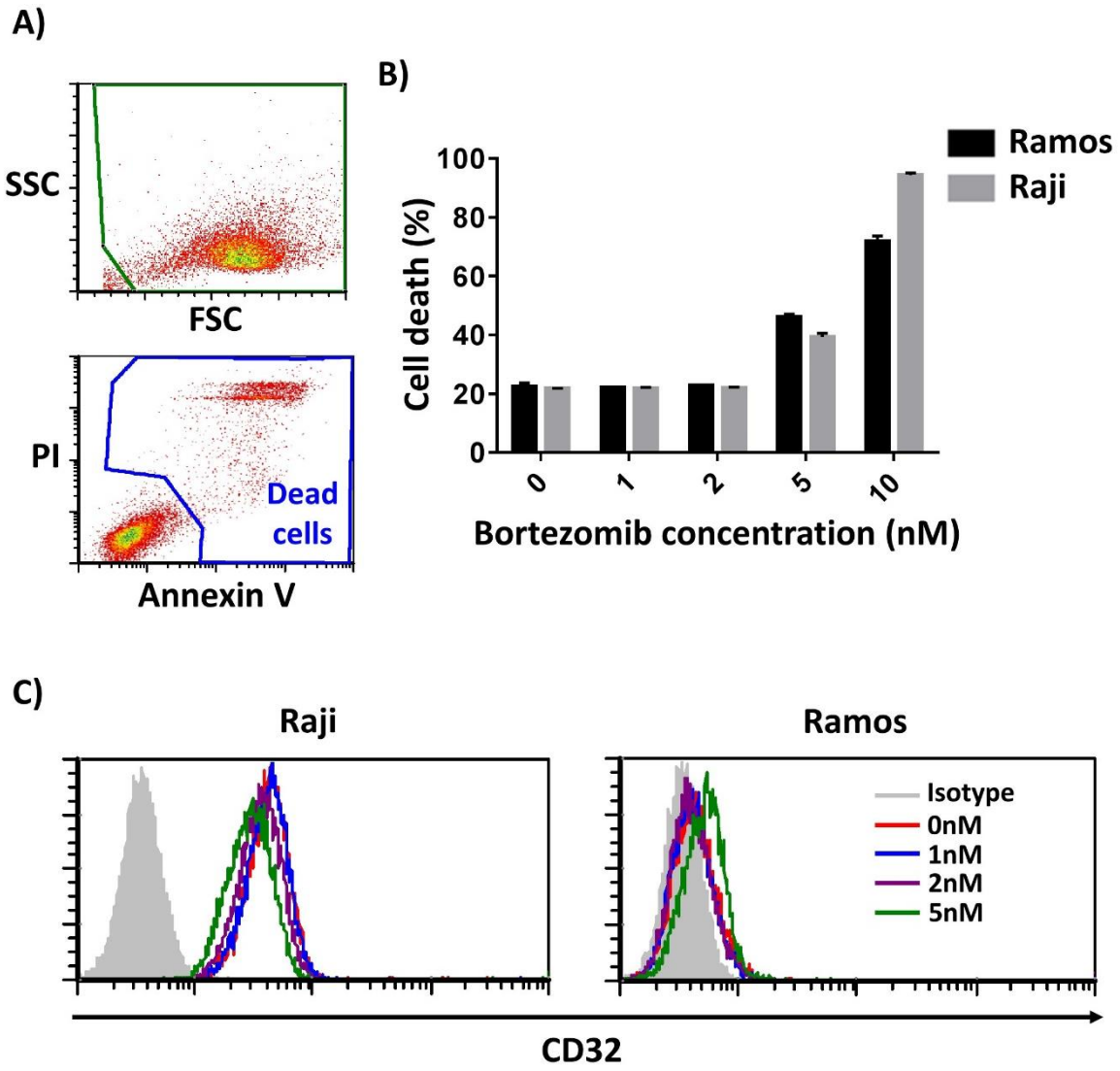

Figure 4.2 ***Effect of proteasome inhibition on CD32 expression in Ramos and Raji cells***
200µl Ramos and Raji cells at 0.5x10^{6}cells/ml were incubated with bortezomib at the indicated final concentrations. A) Cultures were stained for 15 minutes with 2x annexin V-FITC PI (160ng/µl annexin V-FITC, 2.6µg/ml PI in 10mM HEPES pH7.4, 140mM NaCl, 2.5mMCaCl$_2$) before being analysed by flow cytometry. Debris was excluded based on forward (FSC) and side scatter (SSC) before viable cells were identified as being double negative for PI and annexin V. B) The percentage cell death in each culture was determined with bars showing mean +range for duplicates from a single experiment. C) Cultures were stained for CD32 expression using AT10 F(ab')$_2$ FITC (coloured histograms) or irrelevant control (grey) and expression investigated by flow cytometry. The isotype control plotted is from a culture treated with 0nM bortezomib, however the fluorescence did not alter with increased drug concentration. Results show that addition of bortezomib did not alter the expression level of CD32 on either cell line.

4.4 Semi quantitative PCR for CD32b

With CD32 protein not detectable at the surface of Ramos cells, it was investigated whether mRNA for CD32b was present. mRNA was extracted from Ramos and Raji cells with an mRNA extraction kit using oligo (dT) beads. cDNA was generated by reverse transcription from mRNA using the

Superscript II reverse transcription kit. Semi quantitative PCR was performed using 20, 25 or 30 reaction cycles in order to semi-quantitatively compare the levels of mRNA between Ramos and Raji cells. In addition, PCR was performed for GAPDH to confirm comparable levels of cDNA were used in each reaction. Figure 4.3a shows amplified bands, corresponding to the PCR product using CD32b specific primers. A band was observed in the Ramos samples at the expected molecular weight, suggesting that CD32b mRNA was present in the sample. However, the bands seen in the Raji sample, particularly at 25 and 30 cycles were far more intense, suggesting that Raji cells have a greater amount of CD32b mRNA. Importantly, Figure 4.3b shows that comparable bands were seen in Ramos and Raji samples when using GAPDH specific primers. This indicates that equivalent amounts of cDNA were present in the Ramos and Raji reactions. This result suggests that the CD32b mRNA was present in Ramos cells. However this result was only semi quantitative and may have given a misleading indication as to the amount of transcripts present as a result of the power of PCR to amplify even very small numbers of template molecules within the large number of cycles performed and the quantity of cDNA used.

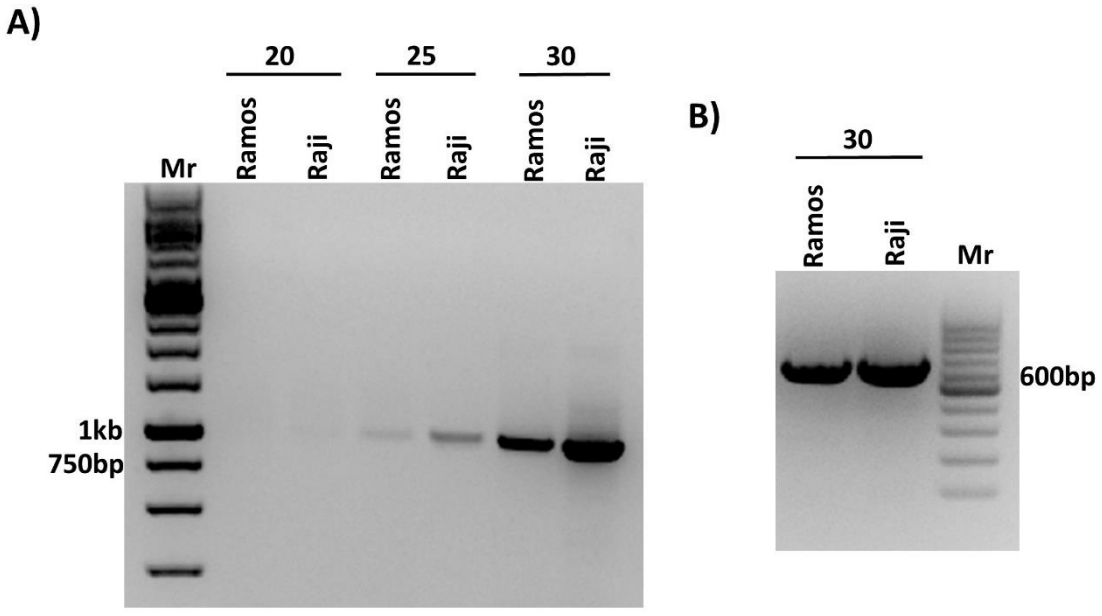

Figure 4.3 ***Semi-quantitative PCR for CD32b in Ramos and Raji cells.***
*mRNA was extracted from Ramos and Raji cells using oligo (dT) beads before being converted to cDNA by reverse transcription using superscript II reverse transcription kit. Reactions contained: 1µl 1in10 diluted cDNA, 2.5µl pfu buffer, 1µl forward primer, 1*µl reverse primer, 0.5µl dNTPs, 1µl pfu polymerase, 18µl water. *A) PCR was performed using CD32b specific primers and cDNA from Ramos and Raji cells. 20, 25 or 30 cycles of PCR was performed. B) PCR was also performed using GAPDH specific primers as a loading control with 30 reaction cycles performed. All reactions were run on 0.7% agarose gels with gel red DNA dye before being visualised under UV light.*

4.5 qPCR for CD32b1 and CD32b2 in Ramos and Raji cells

With results suggesting that CD32b mRNA was present at the mRNA level in Ramos cells, qPCR was performed in order to confirm this result. Furthermore, the qPCR was performed using primers specific for CD32b1 and CD32b2 in order to determine which isoform was present in each cell type. Reactions were performed in 384 well plates with reactions for the HPRT1 and HMBS genes also performed as reference samples. These reference genes has been previously found to amplify under the same reaction conditions as CD32b (Dr Chantal Hargreaves, personal communication). Sample cDNA was used in the reactions at 10ng/µl as determined by nanodrop. The HMBS control gene came up too late to plot a standard curve, however the results for the HPRT1 gene are shown in Figure 4.4. It can be seen in Figure 4.4a that the curves for triplicates were tight, suggesting that the results were consistent. This allowed a standard curve to be plotted for cycles against log concentration as can be seen in Figure 4.4b. The crossing point (Cp) was determined as the cycle where the fluorescence rose significantly above baseline; the Cp results are summarised in Table 4.1. These results allowed a standard curve to be plotted, the equation of which was used to normalise the Ramos results. The standard curve suggested that the concentration of Ramos DNA used in the reactions was 6.31ng/µl, this was therefore the assumed concentration of Ramos cDNA used in subsequent CD32b specific reactions.

	HPRT1 Cp		**CD32b1 Cp**		**CD32b2 Cp**	
Concentration (ng/µl)	**Raji**	**Ramos**	**Raji**	**Ramos**	**Raji**	**Ramos**
472	23.23		26.28		29.91	
236	24.66		27.83		31.24	
118	26.28		29.66		32.65	
29.5	28.43		31.91		35.00	
7.38	29.87		32.81		N/A	
6.31		30.29		N/A		N/A
1.84	31.85		35.00		N/A	
0.46	34.25		N/A		N/a	

Table 4.1 ***Results of qPCR on Ramos and Raji cell cDNA.***
Results of qPCR on Ramos and Raji cell cDNA. Following qPCR the crossing point (Cp) values were determined for the reference gene (HPRT1) and the test genes CD32b1 and CD32b2. N/A indicates that the Cp was reached after 35 cycles and therefore no value was determined

qPCR reactions were performed to probe for the presence of CD32b1 and CD32b2 in cDNA samples form Ramos and Raji cells. Figure 4.5 shows that, once again, the triplicates were similar for Raji standards, suggesting that the results were consistent and reproducible. It is clear from the curves that CD32b2 fluorescence comes up at later cycles than for CD32b1, suggesting that the CD32b2 cDNA is less prevalent than CD32b1. It can also be seen that the curves corresponding to Ramos cell cDNA samples come up far later than those for Raji. The Cp values obtained for these curves are presented in Table 4.1. These results indicate that CD32b1 was not detectable in the cDNA from Ramos cells as the curve did not go above baseline until after 35 cycles, the threshold for detection. In contrast CD32b1 was detectable in Raji cell cDNA down to a concentration of 1.84ng/µl. CD32b2 cDNA was only detectable up to 29.5ng/µl in Raji cells but was not detectable in Ramos cDNA. This suggests that in Raji cells CD32b1 is the most prevalent isoform of CD32b, at least at the mRNA level; being approximately 15 times more prevalent than the b2 isoform. Overall there appeared to be negligible cDNA for either isoform of CD32b in samples from Ramos cell lysates, suggesting that the lack of expression may be due to a deficiency in transcription of the gene.

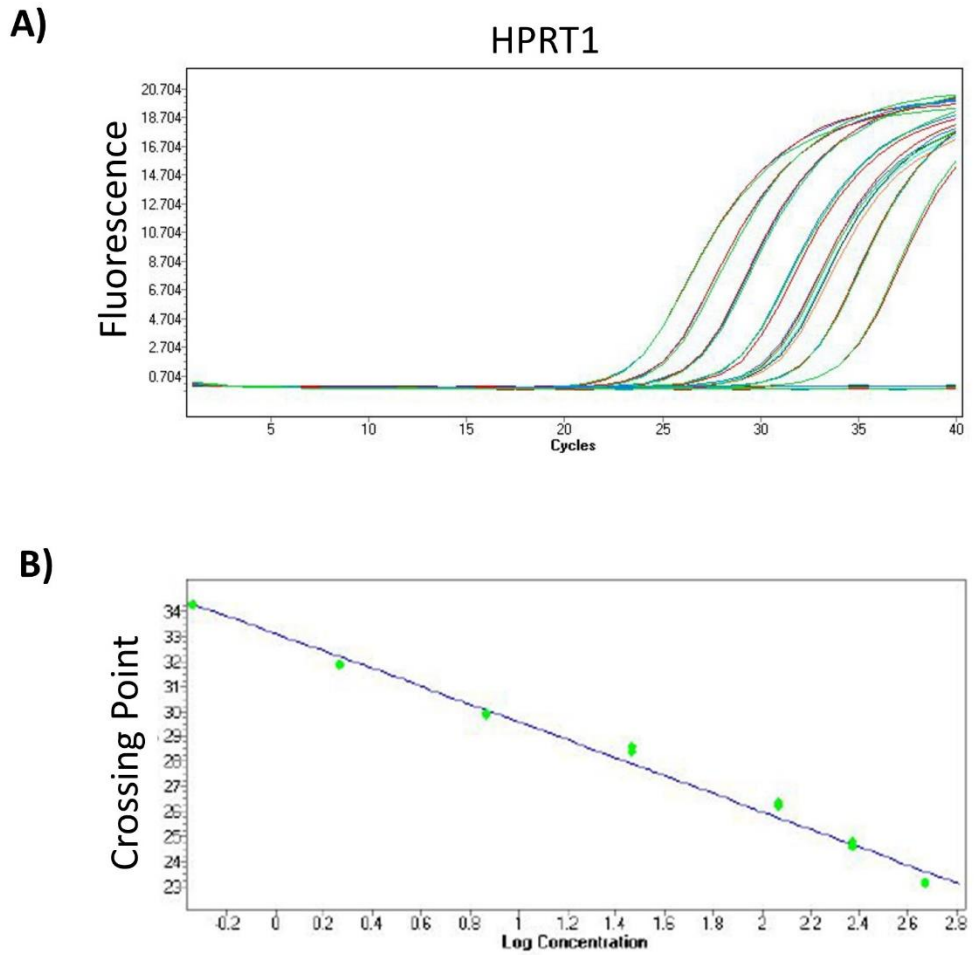

Figure 4.4 ***qPCR for the HPRT1 gene in Ramos and Raji cells.***
Reactions contained 10µl 2x buffer, 1µl 20x HPRT1 assay, 2µl cDNA, 7µl water and qPCR performed. Raji cDNA was used at 472, 236, 118, 29.5, 7.38, 1.85 and 0.46 ng/µl A) fluorescence curves for HPRT1 reaction samples. B) Standard curve generated from Raji cells samples, this curve was used to normalise the results for later reactions and suggested that the concentration of Ramos DNA used was 6.31ng/µl.

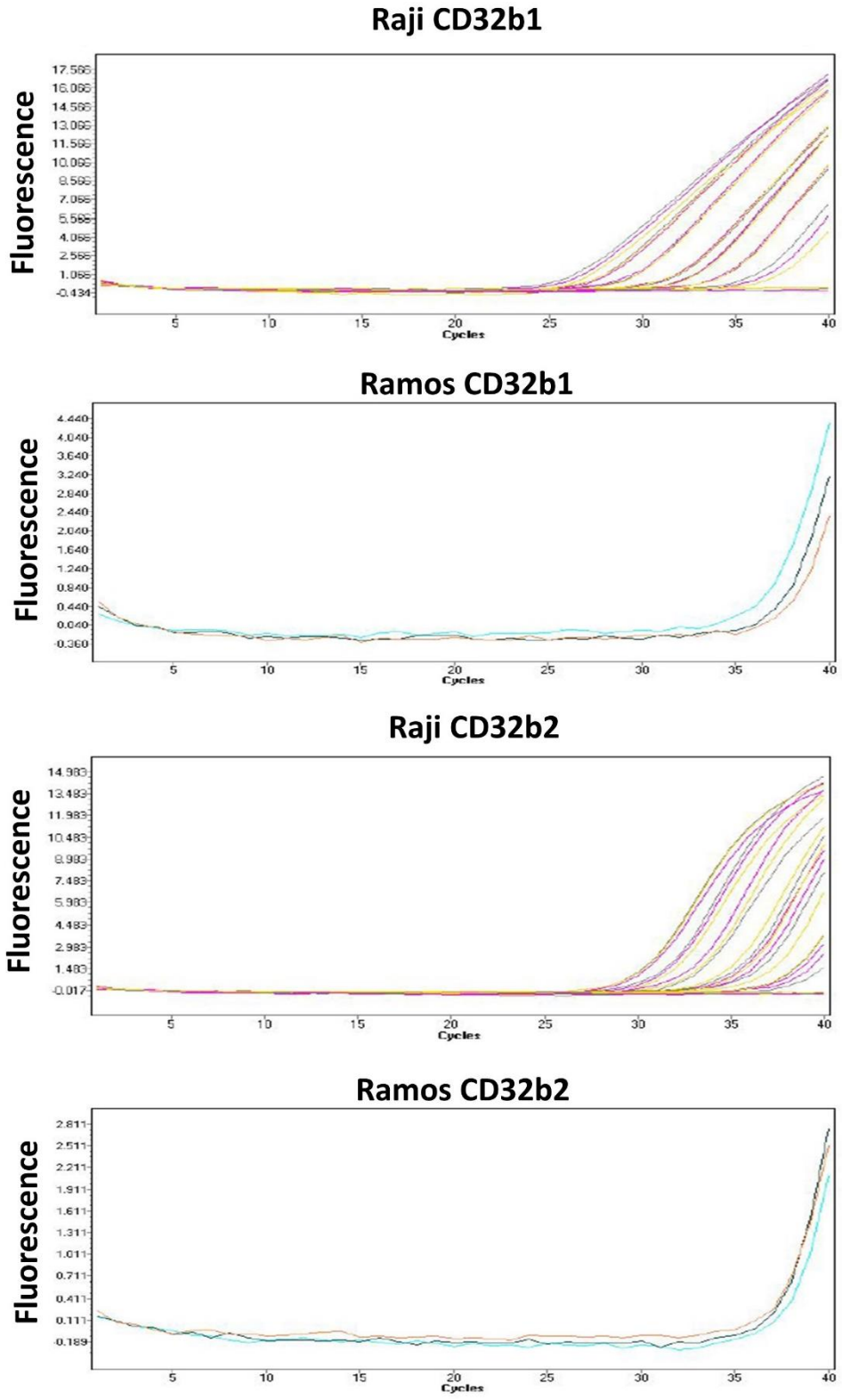

Figure 4.5 ***qPCR for CD32b1 and CD32b2 using cDNA from Ramos and Raji cells.***

Reactions contained 10µl 2x buffer, 1.1µl 5µM probe, 2µl 10µM forward primer, 2µl 10µM reverse primer, 2µl cDNA, 2.9µl water. Raji cDNA was used at 472, 236, 118, 29.5, 7.38, 1.85 and 0.46 ng/µl with Ramos cell cDNA normalised to a concentration of 6.31ng/µl from the HPRT1 standard curve. PCR reactions were performed in a light cycler using primers specific for either CD32b1 or CD32b2. Curves corresponding to Ramos samples are indicated, showing that these curves came up after 35 cycles of PCR, beyond the limit of detection.

4.6 Isolation and sequencing of CD32b in Ramos cells

Having established that CD32b was not expressed at the cell surface and that there was only negligible CD32b mRNA in Ramos cells, the gene was isolated and sequenced to determine if there were any mutations in CD32b in Ramos cells. PCR was performed on cDNA from Ramos and Raji cells using CD32b specific primers. Following amplification (35 cycles), PCR products were separated on a 0.7% agarose gel (Figure 4.6). This demonstrated that, as in the semi-quantitative PCR, bands were present corresponding to the CD32b gene when using cDNA from both cell types; albeit with more product in the Raji sample. The bands were excised from the gel and blunt end ligated into the pCR-BluntII TOPO vector before being sequenced externally using the M13 forward and reverse primers. Sequencing showed that the CD32b gene isolated from Raji cells matched the canonical sequence for the gene (NCBI accession: NM_004001; data not shown). The sequence of CD32b isolated from Ramos cells only identified one heterozygous variant from the canonical gene sequence. As shown in Figure 4.6, this was a synonymous mutation, not altering the amino acid sequence. These results suggest that there were no differences within the transcribed CD32b gene in Ramos cells which were likely to prevent the production of protein.

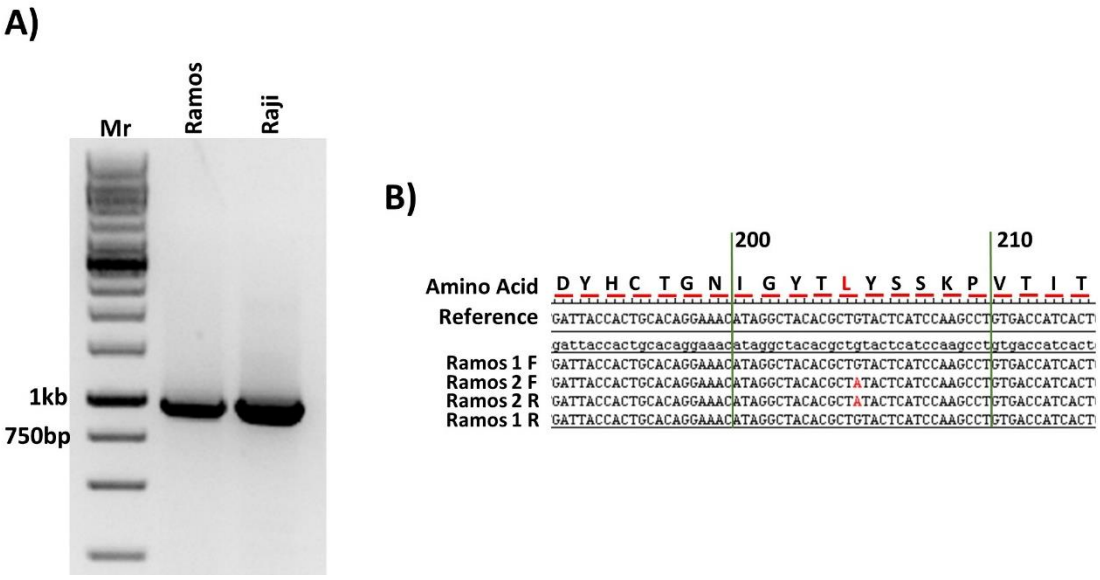

Figure 4.6 ***Isolation and sequencing of CD32b gene in Ramos and Raji cells.***
PCR was performed using CD32b specific primers, on cDNA generated from Ramos and Raji cells. Reactions contained: 1µl cDNA, 2.5µl pfu buffer, µl forward primer, 1µl reverse primer, 0.5µl dNTPs, 1µl pfu polymerase, 18µl water. A) After 35 cycles of PCR reactions were run on a 0.7% agarose gel with bands seen at the expected molecular weight for both cell lines. The bands were excised from the gel and the DNA extracted before being blunt-end ligated into the pCR-BluntII TOPO vector. Ligation products were transformed into JM109 E. coli, colonies picked and minipreps performed to isolate plasmid DNA. B) Plasmids were sequenced using M13 forward and reverse primers with Ramos cells found to be homozygous at 1 position (red) different to the canonical sequence, however this was a synonymous mutation. Numbers indicate the amino acid position based on numbering from the Uniprot consensus sequence (P31994).

4.7 Sequencing of the CD32b promoter in Ramos cells

Results suggested that the CD32b gene could be amplified from Ramos cell cDNA, however the number of transcripts in the cells was negligible and far lower than that in Raji cells. Therefore, the upstream promoter region for CD32b was sequenced in Ramos and Raji cells. Specific primers were used to amplify 1.2kb upstream from the translation start site of the CD32b gene. Following PCR, the reactions were analysed on a 0.7% agarose gel, as can be seen in Figure 4.7a. A single band was seen at approximately 1.2kb which was excised from the gel and the DNA extracted. Following blunt-end ligation, transformation and amplification of plasmid DNA, the CD32b promoter was sequenced.

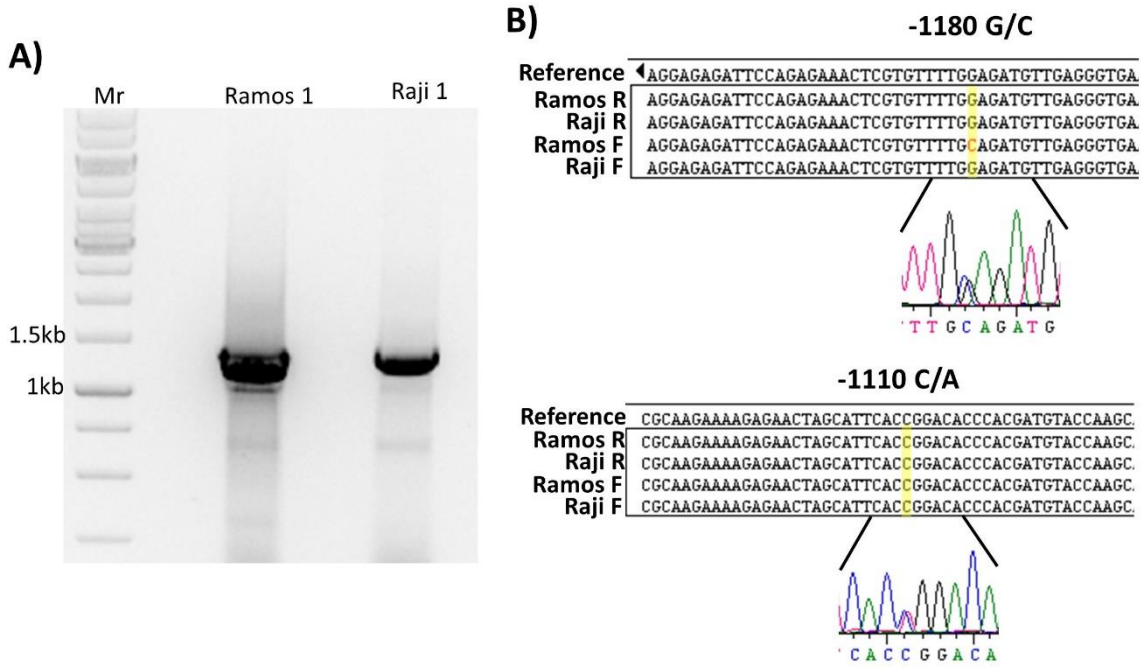

Figure 4.7 ***Sequencing of the CD32b promoter in Ramos and Raji cells.***
1.2kb upstream of the CD32b promoter was amplified from Ramos and Raji cell genomic DNA. A) PCR was performed using specific primers with the resulting reactions run on a 0.7% agarose gel, with bands seen at the expected weight of approximately 1.2kb.These bands were cut from the gel and the DNA extracted before being blunt-end ligated into the pCR-BluntII TOPO vector and transformed into JM109 cells. Colonies were picked and cultured before plasmid DNA was extracted and purified using a miniprep kit. B) Plasmids containing the Ramos and Raji CD32b promoter were sequenced externally using M13 forward and reverse primers. Sequencing showed that the Raji cell promoter did not alter from the reference sequence. The Ramos CD32b promoter varied at 2 sites as indicated, 1180 and 1110bp upstream of the transcription start site. Ramos cells were heterozygous at these positions as indicated by the sequencing traces.

The results of the sequencing demonstrated that the sequence of the CD32b promoter in Raji cells did not differ from the reference sequence. In contrast, the promoter from Ramos cell DNA varied at two sites; 1110 and 1180bp upstream from the transcription initiation site. As can be seen from the sequencing traces in Figure 4.7b, Ramos cells were heterozygous for the two polymorphisms.

In the case of the -1110 polymorphism, all reads were called as having a cysteine at this position however, looking at the trace clearly identifies the heterozygosity. The location of these sequence differences a large distance upstream of the transcription initiation, coupled with the fact that they are heterozygous is unlikely to account for the complete lack of CD32b expression in Ramos cells.

4.8 Effect of methylation inhibition on CD32b expression

With results suggesting that Ramos cells did not express CD32b due to a low level of transcription, despite no significant alterations in promoter sequence, the effect of epigenetic changes was investigated. DZNep (3-deazaneplanocin) is an inhibitor of the enhancer of zeste homology 2 (EZH2) regulator which normally acts as a histone lysine methyltransferase to silence expression of target genes.[379, 449] In contrast, azacitidine is able to inhibit the methylation of DNA; and therefore functions to reverse gene silencing induced by hypermethylation of DNA. [450, 451]

Ramos and Raji cells were incubated in the presence of azacitidine or DZNep for 48 hours. Both drugs are known to have potent cytotoxic activity, particularly at high concentrations. Therefore, the viability of samples following culture was determined using PI staining. Figure 4.8a demonstrates that, following incubation with DZNep, there was no major change in viability for either cell line. Following treatment with azacitidine, there was no reduction in the viability of Raji cells, however Ramos cell viability was reduced, particularly with 20µM azacitidine.

Following incubation with azacitidine or DZNep, the expression of CD32 on live cells was investigated by flow cytometry. Results in Figure 4.8b indicate that for Raji cells, expression of CD32 was maintained at similar levels following culture with either drug. Additionally, there was no expression of CD32 on Ramos cells after treatments with either DZNep or azacitidine. This suggests that DNA or histone methylation is not responsible for the lack of CD32 expression on Ramos cells whilst having no effect on CD32 expression on Raji cells.

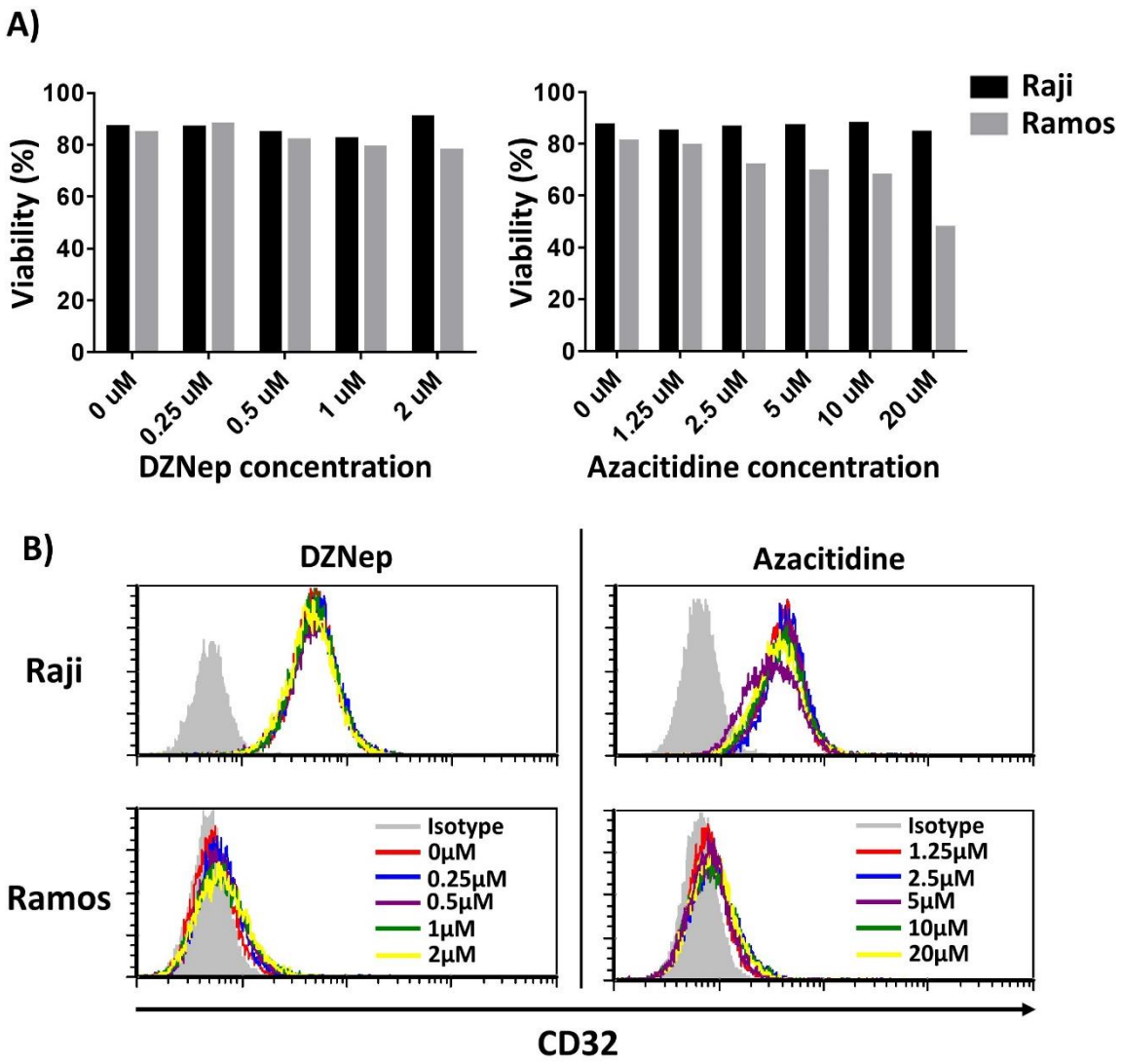

Figure 4.8 ***The Effect of epigenetic inhibitors on CD32 expression on Ramos and Raji cells.***
200µl Ramos or Raji cells at 0.5x10^6 cells/ml were cultured in the presence of DZNep or azacitidine at the indicated concentrations for 48 hours. A) Following incubation cell viability was determined by PI staining with analysis by flow cytometry. B) Cell suspension was stained for CD32 expression using AT10-F(ab')$_2$ FITC (coloured histograms) or an isotype control (grey) for 15 minutes at room temperature before being washed with FACS wash and analysed by flow cytometry. Viable cells were gated and CD32 expression analysed. The control shown was for 0µM drug however fluorescence did not change ant increasing drug concentration. Neither drug altered the expression level of CD32 on Raji cells whilst no expression was seen on Ramos cells following treatment with either drug.

4.9 Chapter discussion

In this chapter, the lack of expression of CD32b in Ramos cells was investigated. This is unusual as CD32b is normally highly expressed on the surface of B cells. [218] To begin with, the lack of CD32b expression was first confirmed; Raji cells were used as positive control throughout this chapter as

they are also a B cell line derived from a patient with Burkitt's lymphoma. One possible explanation for the lack of expression on Ramos cells was that CD32b was being rapidly broken down and turned-over by the proteasome following translation, preventing the protein from being expressed at the cell surface. Through its binding to the 26S proteasome, bortezomib is able to prevent ubiquitin mediated protein degradation which, as shown in this chapter, can result in apoptosis.[452] However, proteasome inhibition did not restore CD32b expression, suggesting that degradation was not the mechanism for lack of surface expression. Importantly, this does not exclude lysosome mediated protein degradation as a mechanism for lack of surface CD32b expression, and this could therefore be further investigated.[453]

With no detectable expression of CD32b at the protein level, it was investigated if the CD32b gene in Ramos cells contained mutations which could prevent protein translation or result in protein misfolding and instability. This phenomena occurs in the closely related CD32c gene where 80% of individuals are homozygous for a variant of the gene containing a premature stop codon.[313] Moreover this stop codon is co-inherited with a polymorphism that insets a proline residue, with demonstrations that this residue is able to disrupt the protein sufficiently to prevent expression (unpublished observations; data not shown). Alternatively, one simple possibility was the presence of a stop mutation within the gene which would prevent translation. However, sequencing of CD32b from cDNA did not identify any significant variation from the reference sequence. Importantly, the signal peptide sequence was as expected, meaning that a lack of transport to the cell membrane was unlikely to be responsible for the lack of surface protein expression. Taken together, these results suggested that the lack of CD32b expression in Ramos cells was not due to defective translation. Therefore, the role of transcription was investigated.

Initially, semi-quantitative PCR showed that the CD32b gene was being transcribed and could be specifically amplified from Ramos derived cDNA, albeit at a lower level than Raji cells. However, these reactions used a large quantity of cDNA and therefore transcripts at a low level may be "over-amplified" giving a false impression of prevalence. Moreover, it is difficult to compare quantities in this manner, thus qPCR was used to allow more comparative analysis between Ramos and Raji cells. The results of qPCR suggested that CD32b1 was more highly expressed in Raji cells than CD32b2 with the latter only detectable at higher cDNA concentrations. This is consistent with results showing that the b1 isoform is the abundant form in B cells, despite a low level of CD32b2 being observed.[443] There did not appear to be any detectable CD32b of either isoform in Ramos samples. This is consistent with the flow cytometry data and suggests that the lack of CD32b expression in Ramos cells results from a lack of transcription rather than translation. One

drawback of this experiment was that the amount of Ramos cDNA used in the reactions was low and perhaps using an increased concentration might allow detection of the CD32b transcript. Despite this, it is clear from the comparison with Raji cells that CD32b transcript was negligible in Ramos cells.

It has been reported that polymorphisms exist within the promoter of CD32b that result in significantly reduced expression.[454] A single base pair polymorphism, 343bp upstream of transcription start, has been found to reduce binding of the AP1 transcription complex.[454] Given this, sequencing of 1.2kb upstream from the transcription start site was performed as this sequence was described to contain the promoter elements for CD32b.[455] Sequencing identified two sites in Ramos cells at -1110 and -1180 where the Ramos CD32b sequence cells differed to the reference sequence and that for Raji cells. However, at this site Ramos cells were heterozygous for the polymorphism. It is not possible from the data presented here to determine if both polymorphisms occur on the same strand of DNA. The polymorphism found here at -1180 has not been previously annotated, however the variant at position -1110 has been assigned the identifier rs150554613 and has been identified as a binding site for the transcriptional regulator CTCF (1000 genomes project, rs150554613). CTCF is thought to be important in regulating chromatin structure and may additionally act as an insulator element between enhancers and transcription factors.[456] With additional evidence suggesting that CTCF may facilitate the formation of chromatin loops, this could insulate genes within the loop from neighbouring housekeeping genes.[457, 458] Importantly, both of these proposed functions result in the repression of transcription; therefore disruption of the CTCF binding site would seem unlikely to be responsible for the lack of CD32b expression in Ramos cells. Additionally, previous work has identified the 5' site of the minimal promoter required for CD32b expression lies between nucleotides -154 and +21.[455] This makes it unlikely that the mutations identified at such distal sites (-1110 and -1180) have a major effect on CD32b expression, especially as Ramos cells are heterozygous for the mutation. However to formally demonstrate this, the wild type and alternate CD32b promoter could be further investigated by generating plasmids with a reporter gene (for example, luciferase) to determine if this resulted in different expression of the reporter gene.

Methylation of DNA is a major epigenetic factor that is able to regulate gene transcription. This is a dynamic process where the addition of methyl groups to the C5 position of CpG dinucleotides is able to repress transcription.[75] Following uptake into cells, azacitidine can become incorporated in DNA and RNA where it forms covalent bonds with methyltransferases, the family of enzymes responsible for DNA methylation.[459, 460] In doing so, azacitidine is able to inhibit DNA methylation

and reduce this transcriptional repression. One consequence of this inhibition is that it results in apoptosis of cells, something which was observed in this chapter.[461] However, treatment with azacitidine did not result in CD32b expression in Ramos cells, suggesting that DNA methylation was not responsible for the lack of CD32b expression in Ramos cells. DZNep is able to indirectly inhibit histone methylation and, as such, activates a different set of genes to azacitidine.[462] However, DZNep treatment was not able to induce expression of CD32b in Ramos cells, suggesting that expression was not being prevented by histone methylation.

Whilst this study has investigated whether DNA or histone methylation could be responsible for the lack of CD32b expression in Ramos cells, it has not investigated epigenetic changes through chromatin remodelling.[463] This offers another potential mechanism by which transcription of CD32b could be downregulated. Histone acetylation is associated with activation of transcription; histone acetytransferases transfer acetyl groups to the internal lysine residues and this changes the charge hydrophobicity of the complex.[464] In doing so, the structure opens up, allowing the binding of transcription factors.[465] Determining chromatin structure at the CD32b locus could offer further insight into the lack of CD32b expression by Ramos cells. Alternatively, histone deacetlyase inhibitors could be used to investigate whether these are able to restore CD32b expression in Ramos cells.

Another possible reason for loss of CD32b expression in Ramos cells is gene translocation. Such an occurrence has been reported in a patient with ALL, where the CD32 locus was translocated from chromosome 1 to chromosome 2, therefore coming under the control of alternative regulatory elements. [466] Additionally, translocations of CD32b have also been reported in follicular lymphoma cells. [467] In both cases, these translocations resulted in deregulation of the CD32b gene. This latter study reported that the translocation resulted in the over expression of the B2 isoform of CD32 in tumour cells; the isoform normally restricted to myeloid cells. Whilst previous studies describe an overexpression of CD32b as a result of translocation, alternative translocation could result in reduced transcription. Although this would need to be further investigated, it offers a possible explanation for the lack of CD32b expression in Ramos cells which remains to be explored. On the other hand, lack of expression may result from aberrant expression of a transcriptional regulator, for example over expression of a repressor or lack of a transcriptional driver. Both these factors would reduce the expression of CD32b without any observed changes in the gene or promoter sequence. Furthermore, CD32b expression may be regulated by micro RNA (miRNA) which are differentially expressed between Ramos and Raji cells. miRNA are approximately 22 bases in length and bind to the 3' untranslated region (UTR) of an mRNA transcript to reduced gene

expression.[468] To investigate this further, the 3' UTR of CD32b in both cell lines should be investigated, miRNA binding prediction software could subsequently be used along with miRNA expression profile data to determine if this mechanism of regulation is responsible for the lack of CD32b expression in Ramos cells. Finally, the structure of the CD32b mRNA itself may be important in regulating the expression of CD32b. mRNA is capable of forming secondary structures where base pairing occurs within an mRNA molecule.[469] This can slow the progress of ribosomes during transcription, resulting in reduced protein expression.[470]

Ramos cells are a Burkitt's lymphoma cell line; it would therefore be interesting to investigate the expression of CD32b in primary samples to determine whether the lack of expression occurs regularly in patients. This could be used to identify patients who may respond better to rituximab therapy. Furthermore, gaining an understanding of the mechanism by which CD32b is downregulated in Ramos cells could provide an insight into novel ways of overcoming CD32b mediated resistance to rituximab therapy. It has been shown in the previous chapter that CD32b is able to cross-link the immune stimulatory mAb TGN1412, a pre-requisite for its function. Moreover, previous studies by White et al have revealed that CD32b cross-linking is required for the activity of an anti-CD40 mAb.[434] Combined these results highlight the importance of CD32b expression for the activity of agonistic mAb. Therefore understanding reduced expression of CD32b *in vivo* could lead to ways to boost expression and enhance the cross-linking required for immune stimulatory mAb activity.

Overall, this chapter has confirmed previous results that Ramos cells do not express CD32b at the protein level. Furthermore, these experiments demonstrate that this lack of expression is due to the negligible CD32b transcription in Ramos cells. So far, however, no mechanism has been identified for the transcriptional defect. Promoter sequencing did not identify any significant variation in Ramos cells; additionally, the use of methylation inhibitors failed to restore CD32b expression. Further investigation is required to deduce this mechanism and to infer any clinical relevance for this.

Chapter 5 Use of the Eμ-Tcl1 hCD20 mouse model to investigate anti-hCD20 antibody therapy and FcγR requirements *in vivo*

5.1 Chapter introduction

The first mAb approved by the FDA for use in cancer was the anti-hCD20 mAb rituximab in 1997.[471] Since then, several more mAbs targeting CD20 have been approved for use, with more still under clinical and pre-clinical investigation, these are summarised in Table 5.1. As has been described, these mAbs have been proposed to differ in their mechanisms of action and in their efficacy. The most notable of these more recent anti-hCD20 mAbs is obinutuzumab (GA101, OBZ); this has been modified from its parental mAb by being produced in a cell line which overexpresses β-1,4-N-acetyl-glucosaminyltransferase III and Golgi α-mannosidase II. This is thought to be responsible for the mAb having a higher affinity for FcγRs due to being enriched for bisected non-fucosylated oligosaccharides.[185] Additionally, obinutuzumab has been found to be a type II anti-CD20; the differences between type I mAbs such as rituximab and type II have been fully discussed earlier. Briefly, type I mAbs are able to cause CD20 redistribution into lipid rafts and result in efficient CDC whereas type II mAbs do not. In contrast, type II mAbs are able to induce more efficient direct cell killing, offering a potential additional mechanism for their action.[178, 179] The relative *in vivo* contributions of the various effector mechanisms by which anti-hCD20 mAbs can act is still a matter of debate.[128]

Anti-CD20 mAb have become a key component of the treatment for B cell malignancies, typically in combination with chemotherapy. More recently, work has suggested that, when combined with chlorambucil, obinutuzumab resulted in a longer progression free survival in CLL patients, compared to rituximab-chlorambucil.[263] This has been proposed to be due to obinutuzumab inducing a lower level of CD20 internalisation; one of the main mechanisms by which rituximab resistance has been thought to arise.[254] Increasingly, anti-CD20 mAbs are being used in combination with small molecules with the aim of improving efficacy further. One example is the PI3Kδ inhibitor idelalisib, or the closely related molecule GS9820, which has improved pharmacokinetics in mice (Stacey Tannheimer, Gillead Sciences inc; personal communication). Idelalisib has been approved by the FDA in for use in combination with rituximab in relapsed CLL and NHL patients.[472]

Name	Trade Name	Source	Comments
Ibritumomab	Zevalin	Mouse	Used as radioimmunotherapy. FDA Approved for NHL in 2002[473]
Obinutuzumab	Gazyva	Humanised	Type II, FDA approved for CLL and FL
Ocaratuzumab	N/A	Humanised	Under phase III development for FL[474]
Ocrelizumab	N/A	Humanised	Under development for use in multiple sclerosis, modified rituximab[475]
Ofatumumab	Arzerra	Human	FDA approved for CLL in 2009
Rituximab	Rituxan/MabThera	Chimeric	FDA approved in 1997
Tositumomab	Bexxar	Mouse	I131 conjugated for radioimmunotherapy, FDA approved for NHL
Veltuzumab	N/A	Humanised	Under development for use in NHL, CLL and ITP[476]

Table 5.1 ***Anti-CD20 mAbs approved by the FDA and under clinical development.***
Summary of data, unless referenced otherwise data is adapted from the reference table produced by Janice Reichart (2015). mAbs without trade names are currently not FDA approved. FDA= Food and drug administration, NHL=Non-Hodgkin lymphoma, CLL=Chronic lymphocytic leukaemia, FL=Follicular lymphoma, ITP Immune thrombocytopenic purpura.

Given the increase in the number of anti-CD20 mAbs being developed, as well as an increase in combination therapies, it has become vital to develop biologically relevant models for understanding the efficacy of mAb therapy, as well as combinations with small molecules. This allows for direct comparison of reagents in a biological system that most accurately reflects the situation in patients. This often involves the use of *in vivo* mouse models in order to provide the components required for all possible mAb effector mechanisms. As has previously been described, Tcl-1 transgenic mice develop spontaneous CLL like disease, characterised by an expansion in $CD5^+$ B cells in the blood and spleen.[477] This occurs due to B cell specific expression of the human Tcl-1 gene under a mouse V_H promoter and Ig_H-Eμ enhancer.[407] A number of experiments have previously shown that Tcl-1 tumours are sensitive to anti-mouse CD20 mAbs (Dr M Carter, personal communication) making this model suitable for the investigation of immunotherapy. However, this Tcl-1 model is of limited use to the investigation of clinically relevant mAbs which target human CD20.

In this chapter, a Tcl-1 hCD20 Tg mouse model was developed and assessed, which was obtained by crossing the Tcl-1 mice onto the hCD20 background (hCD20 Tg). The aim of this chapter was to determine if Tcl-1 hCD20 tumours could be a suitable model for investigating anti-hCD20 immunotherapy. The engraftment of these tumours into hCD20 Tg mice was investigated, to produce a syngeneic mouse model where the target antigen was expressed on both the malignant and normal B cells. Additionally, the clearance of tumour cells by rituximab and obinutuzumab was compared in order to understand differences in efficacy between mAbs. Subsequently, the mechanism of action was investigated by making use of mice lacking in the γ-chain and therefore not expressing activatory FcγRs. The aim of this was to understand whether activatory FcγRs were essential to the anti-tumour activity of the type I mAb rituximab and the type II mAb obinutuzumab.

5.2 Characterisation of spontaneous Tcl-1 hCD20 tumours

Eμ-Tcl-1 hCD20 Tg mice were generated by crossing Tcl-1 mice onto the human CD20 +/- background. These mice developed spontaneous tumours which were positive for hCD20. Mice presented with an accumulation of $CD5^{low}$ $B220^{low}$ lymphocytes in the peripheral blood throughout their life, as detected by flow cytometry (Figure 5.1a). As well as the proportion, the number of tumour cells within the peripheral blood also increased over time. Figure 5.1b demonstrates that at each time point investigated (4 months, 6 months, 8 months, terminal disease), there was a significantly higher number of tumour cells in the periphery compared to the previous time point. This accumulation was consistent between Tcl-1 and Tcl-1 hCD20 mice (data not shown) suggesting that disease progression was not effected by the hCD20 transgene. Whilst there was variation between individuals, disease became terminal in Tcl-1 hCD20 animals when an average of 1.15 $x10^7$ tumour cells/ml blood was reached. Data on the number of tumour cells over time in spontaneous Tcl-1 tumours was obtained from Dr Matt Carter.

Typically, Tcl-1 mice reached terminal disease between 300 and 450 days of age, as can be seen in Figure 5.1c. This also demonstrated that the survival of these mice was effected by the presence of the Tcl-1 gene and not the hCD20 gene, as survival was comparable between Tcl1 and Tcl-1 hCD20 mice. Additionally, both Tcl-1 and Tcl-1 hCD20 mice had significantly reduced survival compared to hCD20 mice (log-rank test $p<0.0001$). As well as peripheral accumulation of tumour cells, Tcl-1 mice presented with splenomegaly as was observed upon dissection of a terminal Tcl-

1 mouse (Figure 5.1d, right panel) compared to an age matched control (Figure 5.1d, left panel). Furthermore, Tcl-1 mice presented with slight lymphadenopathy, which was most apparent in the brachial and inguinal lymph nodes. When spleen weights of Tcl-1 and Tcl-1 hCD20 mice with terminal disease were investigated (Figure 5.1e), they were found to have a significantly higher spleen weight compared to aged matched C57BL/6 or hCD20 controls ($p<0.01$). Moreover, there was no significant difference in spleen weight between Tcl-1 and Tcl-1 hCD20 mice.

Overall, these data demonstrate that Tcl-1 hCD20 mice develop spontaneous disease, which is characterised by an accumulation of $CD5^{low}B220^{low}$ tumour cells in the periphery and spleen. The development of spontaneous tumours was comparable between Tcl-1 and Tcl-1 hCD20 mice, suggesting that the addition of the hCD20 transgene has no effect on tumour progression.

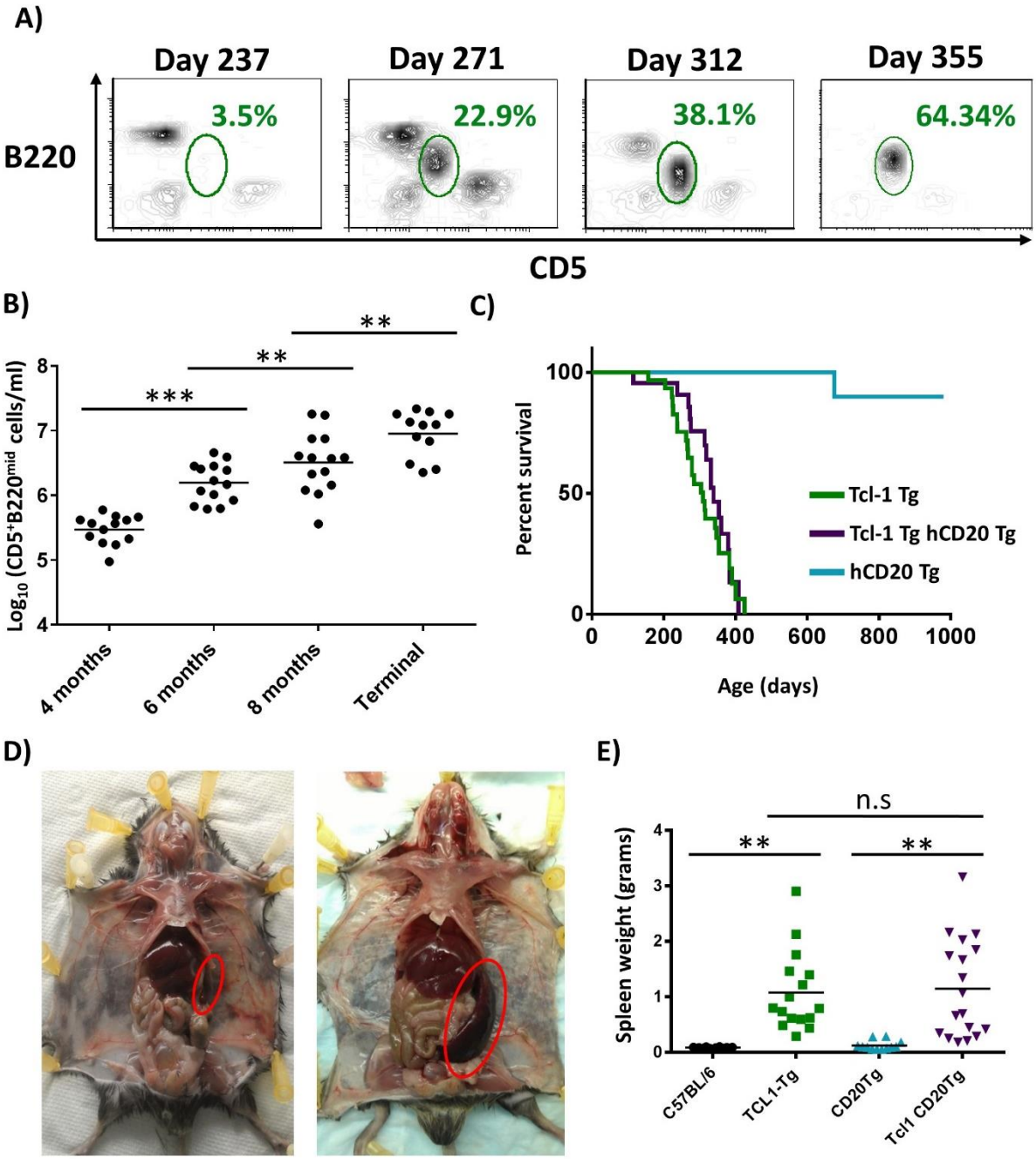

Figure 5.1 ***Characterisation of Tcl-1 hCD20 mice****.*
*A) Peripheral blood was collected from Tcl-1 hCD20 mice and analysed by flow cytometry. Tumour cells could be detected by flow cytometry as being $CD5^{Low}B220^{low}$ with an accumulation over time. B) Tumour cell numbers in the peripheral blood of Tcl-1 hCD20 mice over were determined by flow cytometry and total WBC count. At 2 monthly intervals there was a significant increase in the number of circulating tumour cells with a further increase when disease was terminal (paired t-test ***p<0.001, **p<0.01). C) Survival of hCD20, Tcl-1 and tcl-1 hCD20 mice. Tcl-1 and Tcl-1 hCD20 mice had a significantly shorter survival than matched hCD20 controls (long-rank test p<0.0001). The addition of the hCD20 transgene having no significant effect on survival (Tcl-1 median survival:309 days, Tcl1 hCD20: 339 days; log-rank test p=0.36). D) Dissection of terminal Tcl-1 mouse (right panel) and C57BL/6 aged matched control (left). Tcl-1 mice displayed splenomegaly as well as slight lymphadenopathy. E) The spleens of terminal Tcl-1 or Tcl-1 hCD20 had a significantly increased spleen weight compared to controls (one-way ANOVA **p<0.01). Tcl-1 mice did not have a significantly different terminal spleen weight to Tcl-1 hCD20 mice.*

5.3 Passage of spontaneous tumours

As has been demonstrated, there was considerable variation in the presentation of spontaneous tumours, both in the time taken to present and in physiological factors, such as spleen size and the number of tumour cells in the peripheral blood when disease becomes terminal. These factors prevent spontaneous Tcl-1 hCD20 tumours from being an ideal *in vivo* tumour model to study various forms of immunotherapy unless large numbers of mice are used to reflect the heterogeneity. To overcome the long time factors associated with terminal disease and to ensure mice with uniform disease were treated, splenocytes from mice with spontaneous tumours were passaged into recipient mice where tumours were allowed to establish.

5.3.1 Passage of Tcl-1 hCD20 tumours into C57BL/6 mice

Splenocytes from Tcl-1 hCD20 mice with spontaneous tumours were first passaged into C57BL/6 mice with $1x10^7$ splenocytes injected intraperitoneally (i.p) into recipient mice. These mice were monitored with the number of tumour cells in the peripheral blood determined by flow cytometry and by white blood cell count. Splenocytes from 10 different spontaneous tumours were passaged into recipients sex matched to the original spontaneous tumour. Only three of the ten tumours presented with disease in recipient mice, as determined by an expansion of $CD5^{low}B220^{low}$ cells in the peripheral blood (Figure 5.2a). Tumour cells, as well as normal B cells, were clearly detectable in the blood of one of these recipient mice by flow cytometry (Figure 5.2b). Tumours EU1 and EU2 gave terminal disease within 55 days of injecting splenocytes. In contrast, tumour DN5 was slower in its presentation, with disease not becoming terminal until day 221 after receipt of splenocytes, highlighting the variable growth kinetics between tumours.

It was important to determine whether Tcl-1 hCD20 continued to express hCD20 following passage into C57BL/6 recipients. This was investigated by staining peripheral blood with fluorescently labelled rituximab. Figure 5.2c presents the staining for hCD20 on normal circulating B cells ($B220^+CD5^-$; grey histogram) and Tcl-1 hCD20 tumour cells ($B220^{low}CD5^{low}$; red histogram) in the recipient mice where peripheral tumour cell were observed. This demonstrates that, as expected, the normal circulating B cells did not express hCD20. However, there did not appear to be any expression of hCD20 on the tumour cells, with the exception of tumour EU1 where there was a

small proportion of tumour cells with some expression of hCD20. Overall, the low rate of tumour passage, coupled with the lack of hCD20 expression, prevented Tcl-1 hCD20 passage into C57BL/6 from being a suitable model for investigating anti-CD20 immunotherapy.

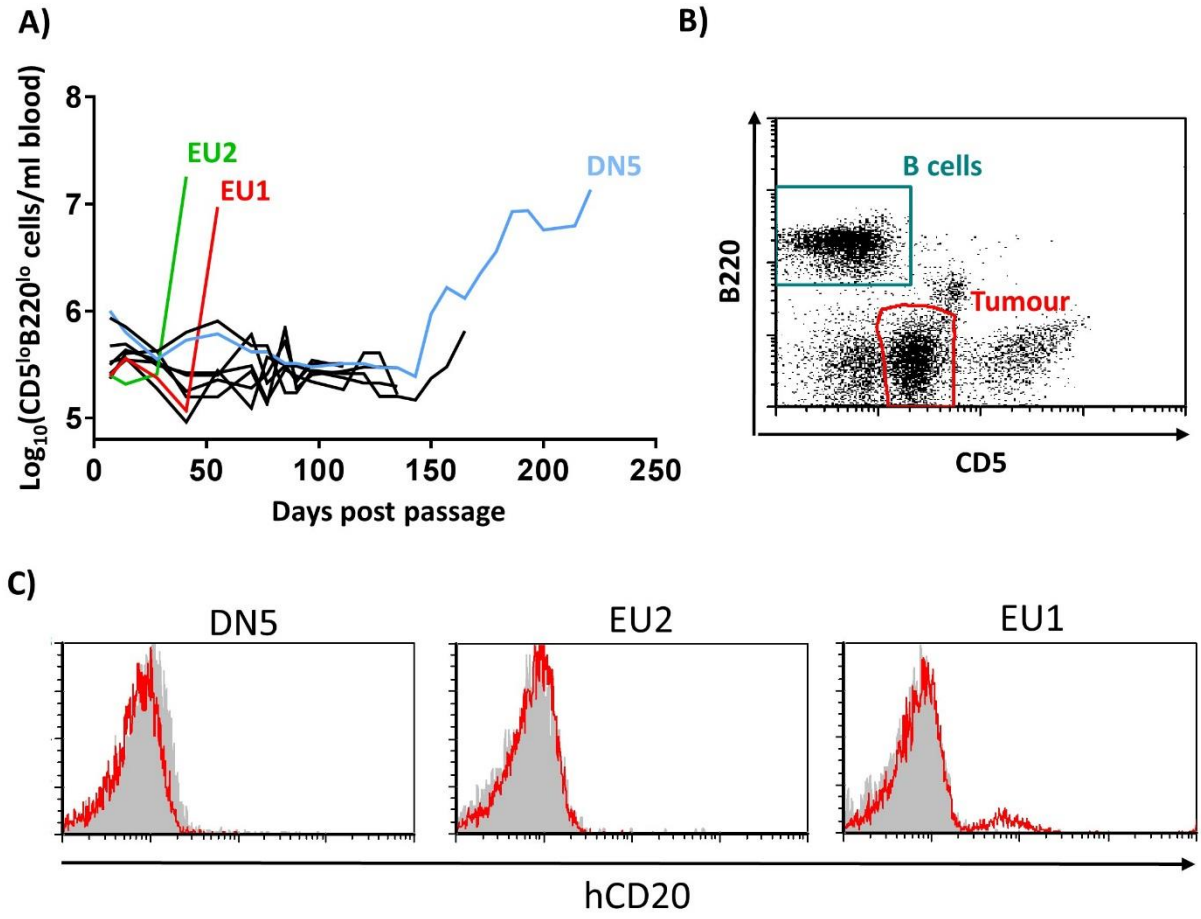

Figure 5.2 ***Passage of Tcl-1 hCD20 splenocytes into C57BL/6 recipients****.*
Frozen Splenocytes from mice with spontaneous Tcl-1 hCD20 tumours were thawed and 1x10^7 cells injected i.p. into C57BL/6 mice. The number of tumour cells (CD5^{lo}B220^{lo}) in the peripheral blood was determined by flow cytometry and WBC count. A) Out of the 10 tumours passaged, only 3 (DN5, EU1, EU2) developed established disease with an expansion in tumour cells in the circulation. B) Staining for B220 and CD5 allowed tumour cells and normal B cells to be identified in the blood by flow cytometry. C) Expression of hCD20 was determined by staining with fluorescently labelled rituximab. Normal C57BL/6, recipient B cells (grey histogram) were negative for rituximab staining as expected. Tumour cells (red histogram) were also negative for rituximab staining except for a small population in the mouse passaged with tumour EU1.

5.3.2 Passage of Tcl-1 hCD20 tumours into hCD20 +/- mice

With the aim of overcoming the poor tumour passage and the loss of hCD20 expression, Tcl-1 hCD20 tumours were passaged into human CD20 +/- (hCD20) mice. As before, 1x10^7 splenocytes were injected i.p. into recipient mice and the circulating tumour cells were detected by flow cytometry, as well as performing total WBC counts. Figure 5.3a shows representative staining of

peripheral blood for B220 and CD5, identifying the $CD5^{lo}B220^{lo}$ tumour population. The expression of hCD20 on the tumour cells in the peripheral blood was detected by staining with fluorescently labelled rituximab. Figure 5.3b suggests that hCD20 is expressed on circulating Tcl-1 cells in recipient mice (red histogram) compared to an isotype control (grey). In total, 14 spontaneous tumours were passaged, 13 of which gave detectable tumour in the peripheral blood; in all these cases hCD20 was expressed on tumour cells (data shown for representative example).

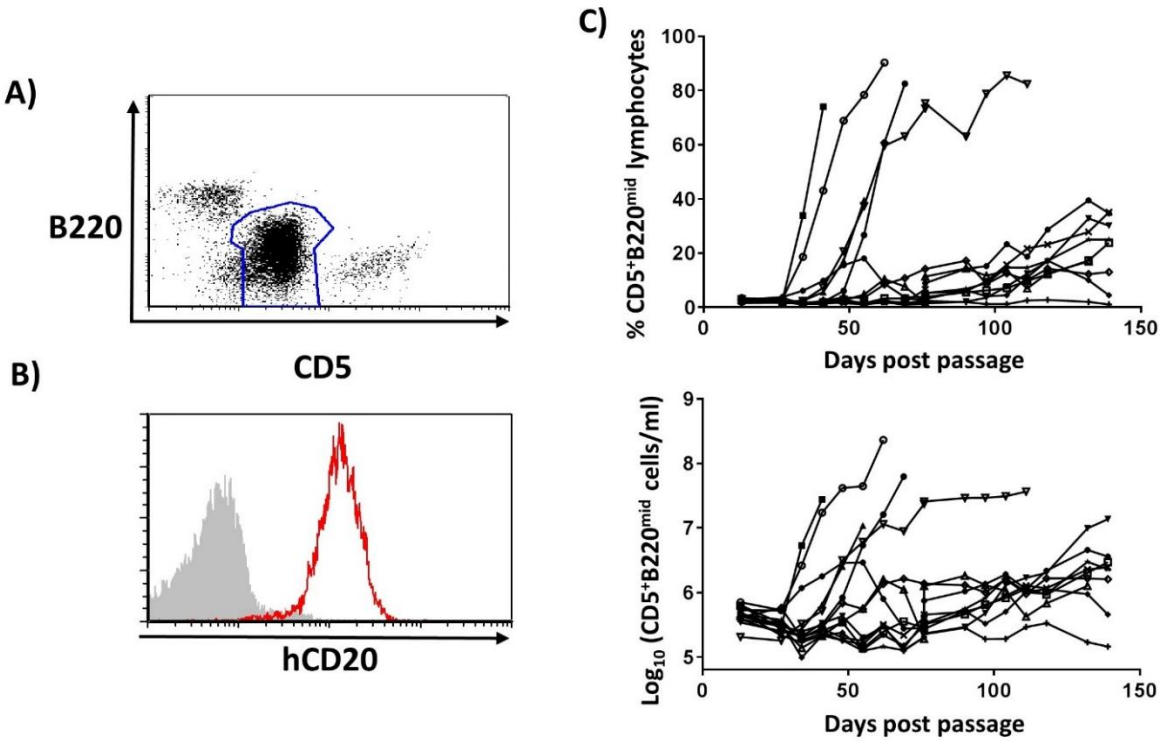

Figure 5.3 ***Passage of Tcl-1 hCD20 tumours into hCD20 +/- mice****.*
$1x10^7$ splenocytes from Tcl-1 hCD0 mice with spontaneous tumours were passaged into hCD20 mice, with cells injected i.p A) Peripheral blood was stained with fluorescently labelled mAbs against B220 and CD5 to identify the tumour cells by flow cytometry (blue gate). B) Tumour cells were stained with fluorescently labelled rituximab (red histogram) or isotype control (grey) demonstrating that circulating tumour cells expressed hCD20. C) 14 spontaneous tumours were passaged with the percentage tumour determined by flow cytometry (top panel). The number of tumour cells in the blood (bottom) was also measured. This indicates a number of tumours became established in recipient mice albeit at different rates. Some tumours did not become established whilst others were detectable in the blood before contracting.

Mice receiving these 14 Tcl-1 hCD20 tumours were monitored over time by serial bleeding. Figure 5.3c shows the percentage of tumour lymphocytes and the number of tumour cells in the peripheral blood for these recipient mice. These results demonstrate that five of the spontaneous tumours passaged presented quickly, with high tumour burden in the peripheral blood. Out of the remaining tumours some established detectable disease, whilst for others progression was slow with a low tumour burden maintained over several weeks. In some tumours, the burden fluctuated over the course of the experiment, with levels rising and falling. Overall, these results demonstrate that the choice of spontaneous tumour for passage is important, in order to select one giving rapidly establishing disease with a constant expansion of tumour cells expressing hCD20.

It has been demonstrated here that Tcl-1 hCD20 splenocytes can be transferred to hCD20 recipients where cells become established. Importantly, once established, these tumours maintain expression of hCD20; this will be important in order to use the model to investigate therapy using anti-hCD20 mAbs.

5.4 Immunotherapy of Tcl1 hCD20 tumours in immune competent mice

Having confirmed that Tcl-1 hCD20 tumours could become established in hCD20 Tg mice, experiments were performed in order to determine whether these tumours could be cleared using anti-hCD20 mAbs. $1x10^7$ Splenocytes from a single mouse with a spontaneous Tcl1-1 hCD20 tumour (tumour FU2) were transferred into hCD20 Tg recipients and monitored until tumour cells were detectable in the periphery. Mice were then randomised to be treated with 250µg of the type I anti-hCD20 mAb rituximab, the type II mAb BHH2 or the isotype control, Herceptin. As well as confirming whether this model is suitable for investigating anti-hCD20 immunotherapy, the two antibodies used were compared to determine whether they differed in their ability to clear tumour cells.

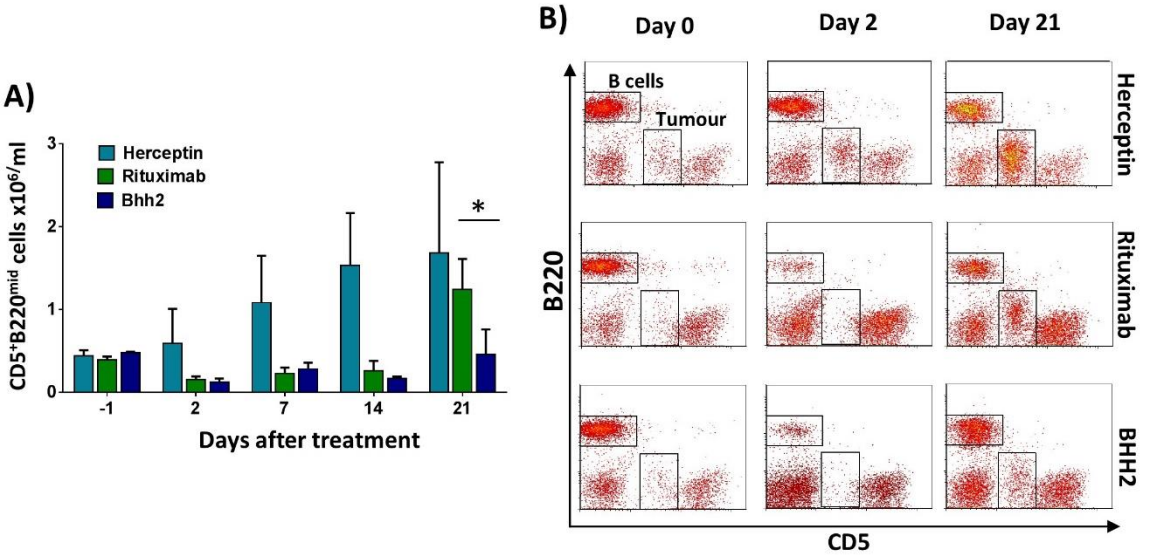

Figure 5.4 ***Anti-hCD20 therapy of Tcl-1 hCD20 tumours in hCD20 Tg mice***
$1x10^7$ Splenocytes from a mouse with a Tcl-1 hCD20 tumour were injected i.p. into hCD20 Tg mice. Presence of tumour cells ($B220^{lo}CD5^{lo}$) in the peripheral blood was monitored by flow cytometry and, once a tumour population detected, mice were treated with 250µg of rituximab, BHH2 or Herceptin i.v. A) mAb was given on day 0 and the number of tumour cells in the peripheral blood following treatment determined by flow cytometry and total WBC count. Rituximab and BHH2 depleted tumour cells within 48 hours, however tumour cells returned by day 21 after therapy. At day 21 peripheral blood of rituximab treated mice contained significantly more tumour cells than BHH2 treated (n=3 unpaired T-test $p<0.05$). B) Identification of cell populations by flow cytometry suggests that normal circulating B cells were cleared by rituximab and BHH2 as well as tumour cells. In Herceptin treated mice, the tumour population continued to expand following treatment.

Figure 5.4a demonstrates the effect of anti-hCD20 therapy on the clearance of Tcl-1 hCD20 tumours. These results suggest that the anti-hCD20 mAbs rituximab and BHH2 were able to deplete Tcl-1 hCD20 cells from the peripheral blood within 48 hours of treatment, whilst in Herceptin treated mice the tumour population continued to expand. The clearance of tumour cells was maintained for 14 days following administration of a single dose of mAb. By day 21 post treatment, there was an increase in tumour burden in the anti-hCD20 treated groups. However, at day 21 there were significantly fewer tumour cells in the peripheral blood of BHH2 treated mice compared to those treated with rituximab. This suggests that BHH2 affords prolonged clearance of tumour cells compared to rituximab. Importantly, this data suggests that Tcl-1 hCD20 tumour cells were susceptible to treatment with anti-hCD20 mAbs, making this model suitable for investigating anti-hCD20 immunotherapy.

In this model, the antigen hCD20 was expressed on normal circulating B cells as well as the tumour. Therefore, depletion of normal B cells was also expected, akin to anti-hCD20 therapy in humans. Figure 5.4b shows that normal B cells were easily identified alongside the tumour population. Furthermore, administration of rituximab or BHH2 was able to deplete this population. Figure 5.5 demonstrates that normal B cells were depleted within 24 hours of rituximab or BHH2 administration. By day 21 following mAb treatment, normal B cells began to return with more normal B cells in rituximab treated mice compared to BHH2 treated; this did not reach statistical significance, however the trend adds further weight to the suggestion that BHH2 may result in prolonged target cell clearance than rituximab. 21 days after mAb administration, there appeared to be a reduction in the number of normal B cells in the Herceptin treated group, however this was likely to be an artefact resulting from the increasing tumour burden in these mice.

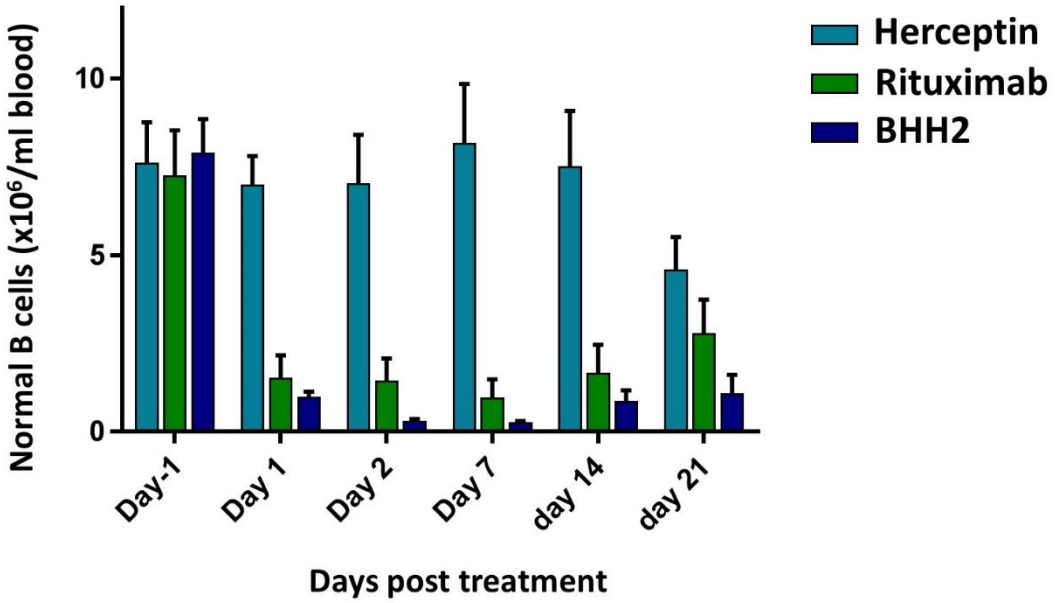

Figure 5.5 ***Clearance of normal B cells in Tcl-1 hCD20 bearing mice following anti-hCD20 treatment***
Mice bearing established Tcl-1 hCD20 tumours were treated with 250µg rituximab, BHH2 or Herceptin i.v. and the number of normal ($B220^+CD5^-$) B cells determined by WBC count and flow cytometry. Rituximab and BHH2 were able to deplete normal B cells within 24 hours of mAb treatment whereas Herceptin did not. At days 1-14 after mAb treatment there was significantly fewer normal B cells in anti-hCD20 compared to Herceptin treated (2-way ANOVA with multiple comparisons, P<0.001 for all comparisons). There were no significant differences between BHH2 and rituximab treatments at any time point. B cells began to return at day 21 after anti-hCD20 treatment. At day 21 there was a reduction in B cells in Herceptin treated mice as these animals reached a high tumour burden. n=3 per group +SEM.

One important observation from these experiments was that BHH2 resulted in a prolonged clearance of Tcl-1 hCD20 cells from the peripheral blood compared to rituximab; this was apparent 21 days after treatment. It is known that type I mAbs such as rituximab are internalised following engagement with CD20, something which does not occur to the same extent with type II mAbs.[254] This results in a greater mAb consumption by the tumour, therefore in order to further investigate the reason for this prolonged clearance the concentration of hIgG in the plasma was determined by ELISA. Figure 5.6 suggests that hIgG was detectable in the plasma of BHH2 treated mice 14 and 21 days after therapy. This is in contrast to rituximab treated mice, where hIgG was not detectable in the plasma by day 14 after mAb treatment. This increased persistence of BHH2 in the plasma could explain the improved clearance of tumour cells (Figure 5.4a) and normal B cells (Figure 5.5) previously observed with BHH2. The ELISA also suggests that rituximab and BHH2 were consumed at a faster rate than the control mAb Herceptin.

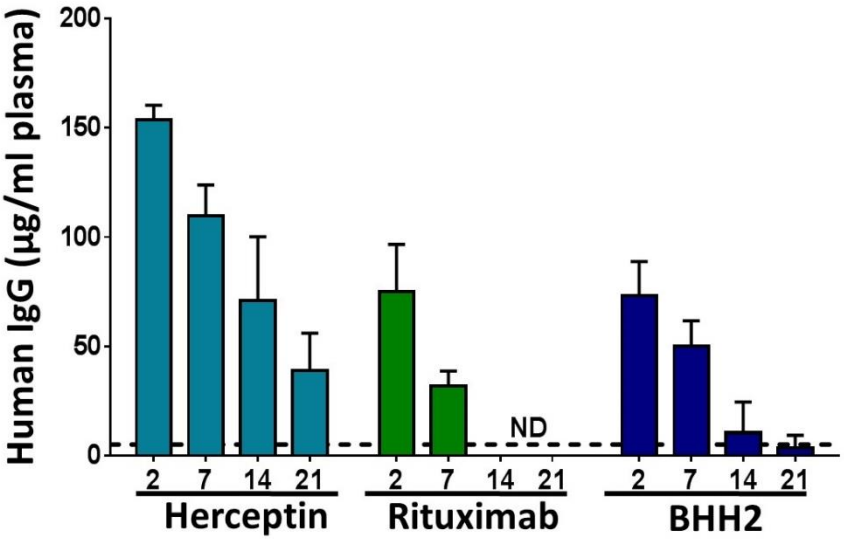

Figure 5.6 ***Plasma concentration of hIgG in anti-hCD20 treated Tcl-1 hCD20 bearing mice.***
Mice with established Tcl-1 hCD20 were treated with 250µg Herceptin, rituximab or BHH2. The concentration of human IgG in the plasma was measured by ELISA 2, 7, 14 and 21 days after therapy. Bars represent mean + SD (n=3-4 per group). By day 14 rituximab was no longer detectable in the plasma (ND), whereas at day 14 BHH2 concentration was above 5µg/ml (dotted line).

Overall, these experiments suggest that Tcl-1 hCD20 tumours can become established in hCD20 mice. Subsequently, circulating tumour cells can be transiently cleared using clinically relevant anti-hCD20 mAb. Normal circulating B cells were also cleared, akin to therapy in humans. Finally, the model can be used to investigate differences in therapy between mAbs targeting hCD20.

5.5 Immunotherapy of Eµ-Tcl1 hCD20 tumours in immune compromised mice

Whist passage of tumours into hCD20 mice provided a good model for investigating anti-hCD20 immunotherapy in a fully immune competent model, there remains a number of issues, not least that not all recipient mice develop disease with the rate typically between 60-70%. Additionally, the time to disease presentation was variable between mice. In order to increase the penetrance and rate of passage, Tcl-1 hCD20 experiments were performed in SCID mice. These mice carry a recessive mutation in the Prkdc gene, which results in the absence of functional B and T cells.

5.5.1 Immunotherapy in SCID mice

$1x10^7$ splenocytes from Tcl-1 hCD20 tumour EC2 were transferred into SCID mice; tumours typically became established in greater than 90% of recipients (data not shown). Once tumour ($CD19^+$ $CD5^{lo}$) was detectable in the peripheral blood, anti-hCD20 mAb was administered to mice (i.p) and the depletion of circulating tumour cells was monitored over time. The dose of mAb was reduced to 100μg per mouse to account for the lack of normal B cells and competing IgG in the recipient mice. In this experiment, the clinical candidate obinutuzumab was used which has been approved by the FDA. This mAb has a glycomodification, as detailed earlier, but has been demonstrated within the lab not to impact on murine effector cell functions (Dr T.Tipton, personal communication). Mice were assigned to groups that resulted in comparable average tumour burden prior to treatment.

Figure 5.7 suggests that the anti-hCD20 mAbs rituximab and obinutuzumab were able to deplete tumour cells in the periphery of SCID mice. 48 hours after mAb treatment, there were significantly fewer circulating tumour cells than before treatment, with both anti-CD20 mAbs (paired T-test on maximum depletion, $p<0.001$). A single dose of rituximab was able to prevent tumour cell expansion for approximately two weeks longer than control whereas for obinutuzumab this was extended to 3 weeks, similar to the results seen in immune competent mice. At day 20 after treatment, there were significantly more tumour cells in the periphery of rituximab treated mice (mean of $26.66x10^6$ $CD19^+CD5^{lo}$ cells/ml) compared to those treated with obinutuzumab ($3.17x10^6$ cells/ml). Furthermore, performing experiments in SCID mice was found to give more consistent tumour presentation. When coupled with comparable tumour clearance compared to hCD20 mice, data demonstrated that the passage of Tcl-1 hCD20 tumours into SCID mice was an appropriate model for investigating anti-hCD20 immunotherapy.

The concentration of human IgG in the serum was measured by ELISA in SCID mice following treatment. Figure 5.8 suggests that obinutuzumab was present at a higher concentration in the serum compared to rituximab. 14 days after treatment, there was significantly more human IgG in the serum of obinutuzumab treated mice (mean: 13.53μg/ml) than those treated with rituximab (6.45μg/ml).

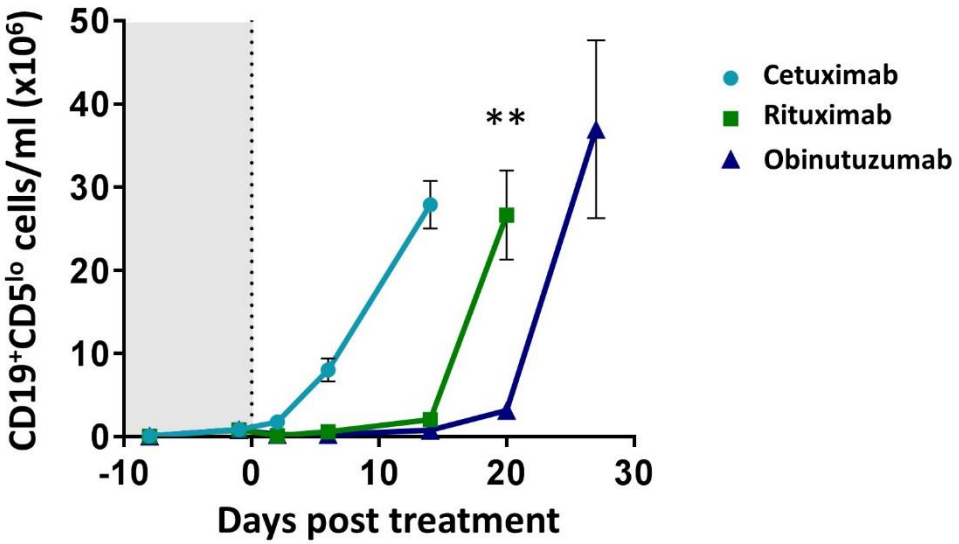

Figure 5.7 ***Anti-CD20 immunotherapy of Tcl-1 hCD20 tumours in SCID mice.***
$1x10^7$ Splenocytes from Tcl-1 hCD20 mice were passaged into SCID mice. Once tumours were detectable in the peripheral blood 100µg cetuximab, rituximab or obinutuzumab was administered i.p. and tumour cells monitored in the peripheral blood by flow cytometry ($CD19^+CD5^{lo}$) and WBC count to determine the number of tumour cells. Both anti-hCD20 mAbs were able to prevent the expansion of tumour cells. At day 20 obinutuzumab treated mice had significantly fewer circulating tumour cells than rituximab treated mice (paired T-test, p=0.003). n=8-10, mean ±SEM representative example from 2 independent experiments.

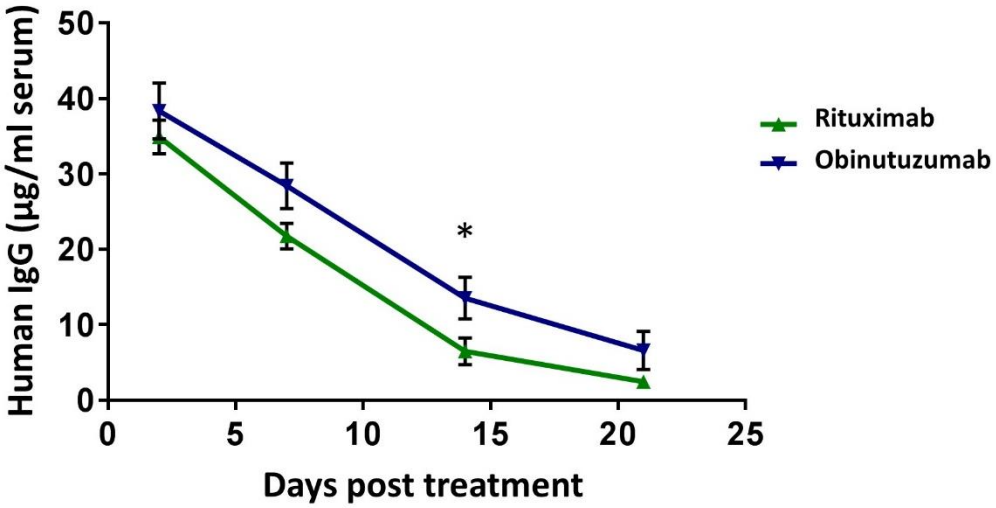

Figure 5.8 ***Human IgG concentration in the plasma of SCID mice following anti-CD20 immunotherapy****.*
*Tcl-1 hCD20 bearing SCID mice were treated with 100µg i.p. rituximab or obinutuzumab and the concentration of human IgG in the serum was determined by ELISA. Plates were coated with a goat anti-human IgG γ-chain and IgG was detected using an HRP conjugated $F(ab')_2$ goat anti-human IgG. 14 days after treatment there was significantly more human IgG in the serum of obinutuzumab treated mice compared to rituximab treated (multiple T tests on combined groups *=p<0.05). This suggests that obinutuzumab persists in the serum for longer than rituximab. N=8-10 mean ±SEM.*

5.5.2 Immunotherapy in NOD SCID mice

In addition to SCID mice, immunotherapy of Tcl-1 hCD20 tumours was investigated in NOD SCID mice. These mice carry polymorphisms in the ldd3 locus, one of the effects of which is severely impaired NK cell function and reduced NK cell numbers. Tcl-1 hCD20 splenocytes from tumour EC2 were transferred into NOD SCID mice and treated with 100μg rituximab, BHH2 or Herceptin once tumour was detectable in the peripheral blood. Figure 5.9 suggests that BHH2 and rituximab were able to deplete tumour cells in NOD SCID mice, compared to the irrelevant control Herceptin, despite the lack of functional NK cells in these mice. Points representing individual mice highlight the variability in the return of tumour cells; this is particularly apparent for BHH2 treated mice at day 7, where the number of tumour cells varied by over two orders of magnitude ($2.4x10^4$ and $3.3x10^6$ cells/ml blood). Despite initial therapy, tumour cells began to return in anti-hCD20 treated mice by day 7 following mAb treatment. Overall this suggests that anti-hCD20 mAbs are able to deplete Tcl-1 hCD20 tumours in NOD SCID mice despite the NK cell deficiency. However this depletion was less prolonged than that observed in SCID mice.

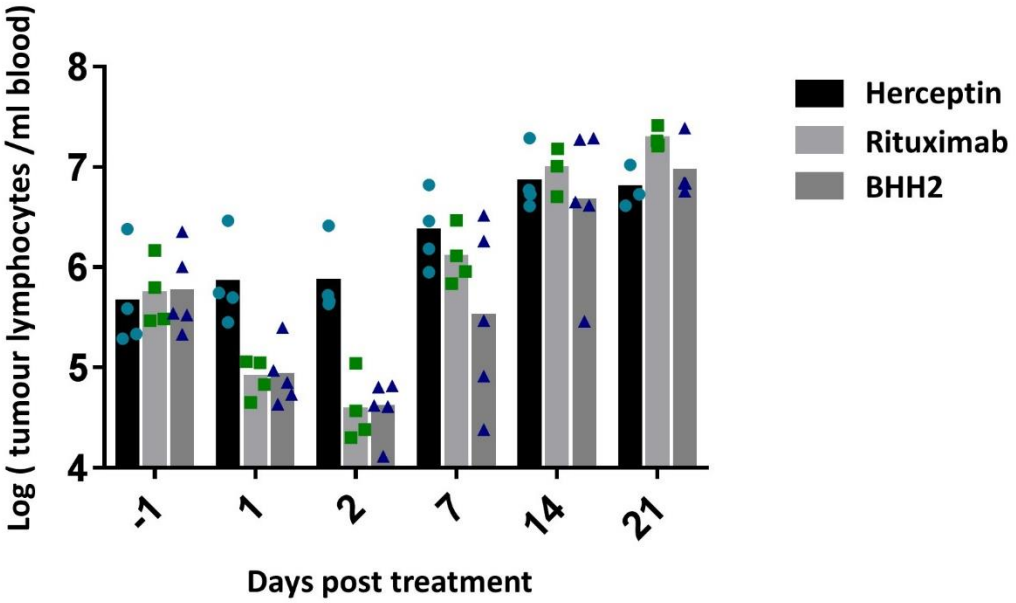

Figure 5.9 ***Anti-CD20 immunotherapy of Tcl-1 hCD20 tumours in NOD SCID mice.***
Splenocytes from Tcl-1 hCD20 mice with terminal disease were transferred i.p into sex matched NOD SCID mice and tumours allowed to develop. Once tumour cells ($CD19^+CD5^{lo}$) were detected in the peripheral blood, 100μg antibody was administered i.p. and the number of tumour cells in the peripheral blood monitored by flow cytometry and total WBC count. Rituximab and BHH2 depleted circulating tumour cells which began to return by day 7. The control antibody Herceptin did not result in any clearance of tumour cells as expected. n=4-5 per group bars show mean plus individual mice.

5.6 FcγR requirement for immunotherapy of Eμ-Tcl1 hCD20 tumours

Having established that the Tcl-1 hCD20 model is suitable for investigating the anti-tumour activity of anti-hCD20 mAbs in immune competent and immune deficient mice, the mechanism by which these clinically relevant mAbs exert their effect was investigated. Tcl-1 hCD20 splenocytes were transferred into SCID γ-/- mice; these mice are immune deficient, lacking B and T cells but retaining NK cells. However, they do not express the common FcR γ-chain, resulting in a lack of expression of activatory FcγRs. Tcl-1 hCD20 splenocytes were transferred into SCID and SCID γ-/- mice and tumours were allowed to establish. Once tumour cells were detectable in the peripheral blood, mice were treated with 100μg rituximab or obinutuzumab i.p.

Figure 5.10 demonstrates that at day 7 following treatment, there was a significantly lower percentage of tumour lymphocytes in obinutuzumab treated mice compared to controls. This suggests that obinutuzumab may have some therapeutic activity in the absence of the γ-chain. This benefit is short lived, however, with a comparable percentage tumour at day 14 between all groups. Additionally, the therapy observed is minimal compared to that observed previously. In contrast, there were no significant differences between rituximab treated mice and controls.

To put these results into context, therapy in SCID γ -/- was compared to that in SCID mice. When the number of tumour cells in the peripheral blood was investigated (Figure 5.11b), there was no significant differences between cetuximab treatment and anti-CD20 therapy in SCID γ-/- mice. This is in contrast to SCID mice, where at days 2 and 7 following treatment, there were significantly fewer circulating tumour cells compared to control or to the same treatment in SCID γ-/- mice. This result suggest that in order for rituximab and obinutuzumab to mediate effective anti-tumour activity, the γ-chain must be present. Additionally, when the survival of mice following anti-hCD20 therapy was investigated (Figure 5.11b), there were no significant differences in survival between the treatment groups in SCID γ-/- mice. Conversely, in SCID mice, rituximab improved survival compared to cetuximab treatment, whereas obinutuzumab resulted in significantly longer survival compared to both rituximab and cetuximab treatment.

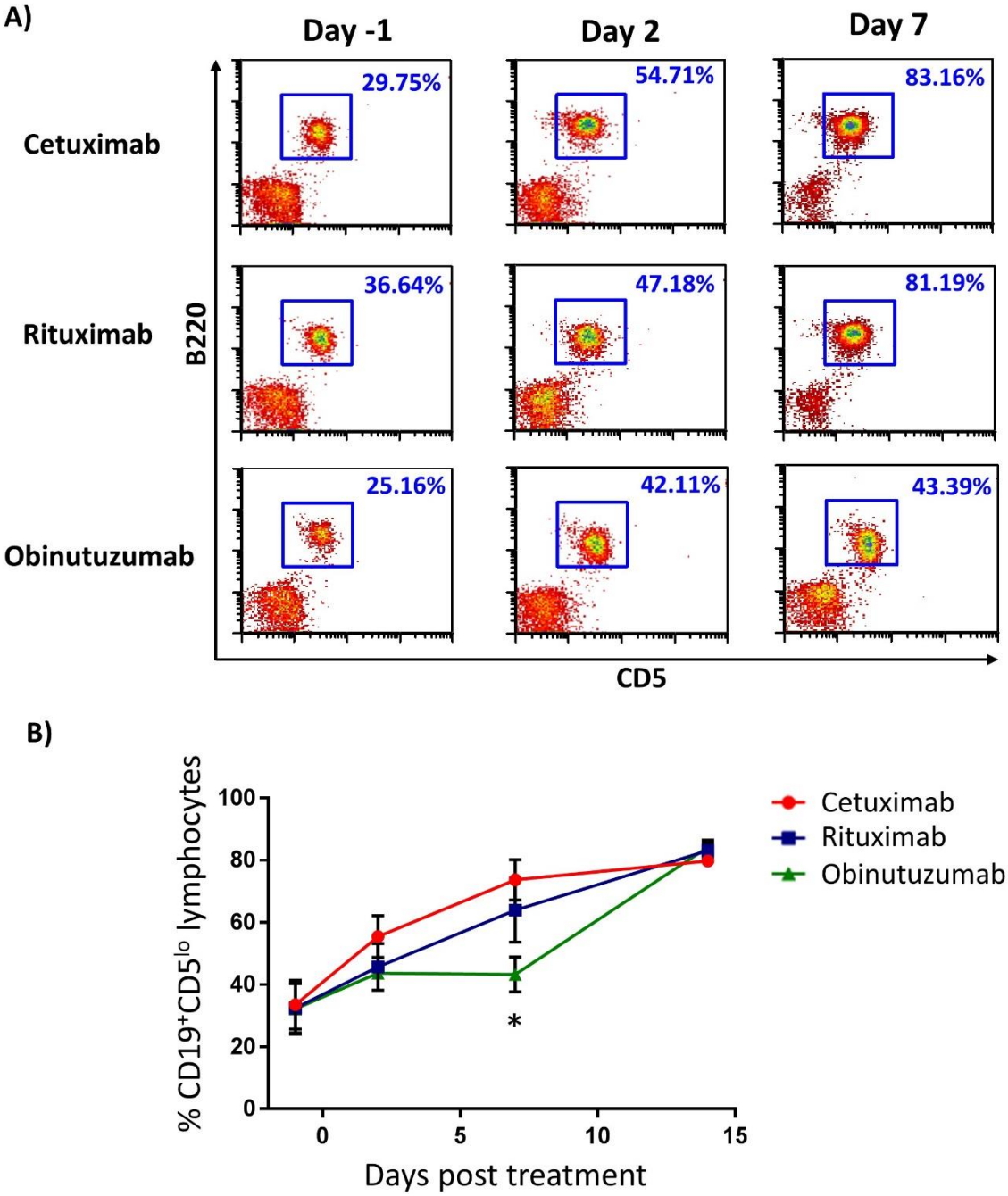

Figure 5.10 ***Anti-hCD20 therapy of Tcl-1 hCD20 tumours in SCID γ-/- mice.***

*$1x10^7$ Tcl-1 hCD20 splenocytes were transferred i.p. into SCID γ-/- mice. Once tumour cells ($CD19^+CD5^{lo}$) were detectable in the blood by flow cytometry, mice were treated with 100μg cetuximab, rituximab or obinutuzumab (i.p) and the % tumour lymphocytes in the peripheral blood determined over time by flow cytometry. A) representative flow cytometry plots for 1 mouse per treatment group with the percentage of tumour lymphocytes indicated. B) Combined data for all mice in the experiment. 7 days after treatment there was a significantly lower percentage at tumour lymphocytes in obinutuzumab treated mice compared to cetuximab treated controls (2-way ANOVA; *P<0.05). Mean +SEM N=4 per group*

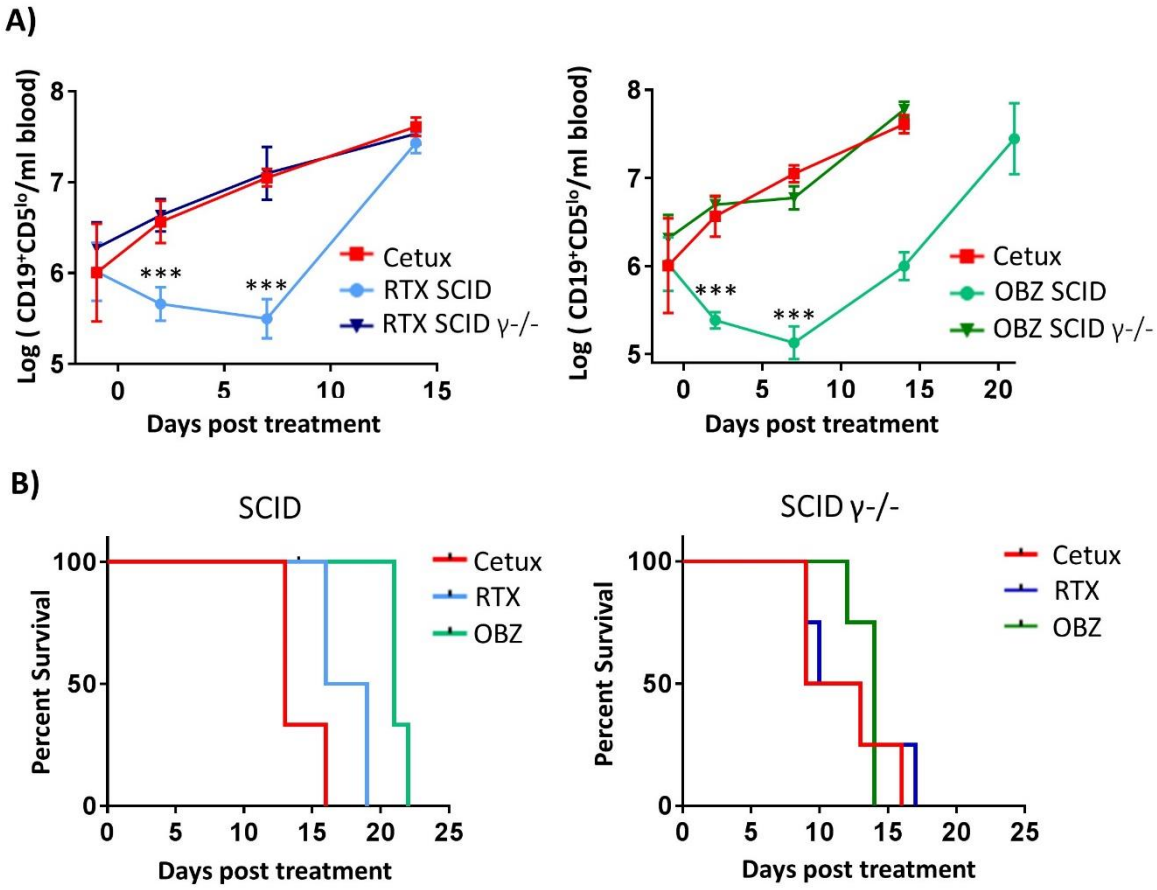

Figure 5.11 ***Anti-hCD20 therapy of Tcl-1 hCD20 tumours in SCID and SCID γ-/- mice.***
*$1x10^7$ Tcl-1 hCD20 splenocytes were injected i.p into SCID and SCID γ-/- mice. Once tumour ($CD19^+CD5^{lo}$) was detectable in the blood by flow cytometry, mice were treated with 100μg cetuximab (Cetux), rituximab (RTX) or obinutuzumab (OBZ) i.p. A) The number of tumour cells in the peripheral blood was determined from the WBC count and flow cytometry. Treatment with rituximab or obinutuzumab in SCID mice resulted in significantly fewer tumour cells compared to cetuximab treatment at day 2 and 7. There were no significant differences in between treatments in SCID γ-/- mice. (2-way ANOVA; ***P<0.001). Mean +SD N=4 per group. B) Survival plots following mAb therapy. In SCID mice survival was significantly longer following rituximab (P=0.0499) or obinutuzumab (P=o.0218) compared to cetuximab treatment. Survival was also longer for obinutuzumab treatment compared to rituximab (P=0.0259). There were no significant differences in survival between treatment groups in SCID γ-/- mice.*

5.7 Anti-hCD20 mAb therapy in combination with GS9820

Small molecule inhibitors of PI3Kδ are currently under clinical investigation for use in combination with anti-hCD20 mAbs. Here, it was investigated whether the Tcl-1 hCD20 model could be used to investigate the combination of small molecules and mAbs. Tcl-1 hCD20 splenocytes were transferred into hCD20 mice and the tumours were allowed to establish. Once tumour cells were detectable in the blood, treatment began. 100μg Rituximab or obinutuzumab was administered i.p weekly for 5 weeks. Additionally, mice received the PI3Kδ inhibitor GS9820 at 10mg/kg or vehicle only by oral gavage. For 14 days, the drug was administered twice daily for five days then

once a day for two days. In weeks 3-5, the drug was administered once a day for five days followed by two days off.

Figure 5.12a presents the number of tumour lymphocytes in the circulation for the mice in this experiment. There was a large amount of variation between mice within each group however, within each group, the trends for individual mice remained the same. For this reason, error bars have been excluded for clarity. The mAbs alone were able to deplete tumour cells in the short term, however tumour returned rapidly and the mice developed terminal disease within 35 days of treatment commencing. GS9820 alone was able to control the expansion of tumour cells. The addition of rituximab or obinutuzumab to GS9820 treatment resulted in a rapid initial depletion of tumour cells followed by prolonged suppression of tumour cell expansion.

The concentration of human IgG in the serum of treated mice was measured by ELISA. Again, there was a large variation in concentrations. Figure 5.12b suggests that, when given as a monotherapy, rituximab and obinutuzumab were rapidly consumed. In contrast, when given in combination with GS9820, both mAbs were detected in the serum for longer than in the comparable monotherapy. This result is consistent with the reduced tumour burden (and therefore mAb consumption) in combination treated mice. This data also suggests that obinutuzumab may persist for longer in the serum than rituximab in the combination treated groups. However this experiment showed that combination therapy is effective with either rituximab or obinutuzumab.

A)

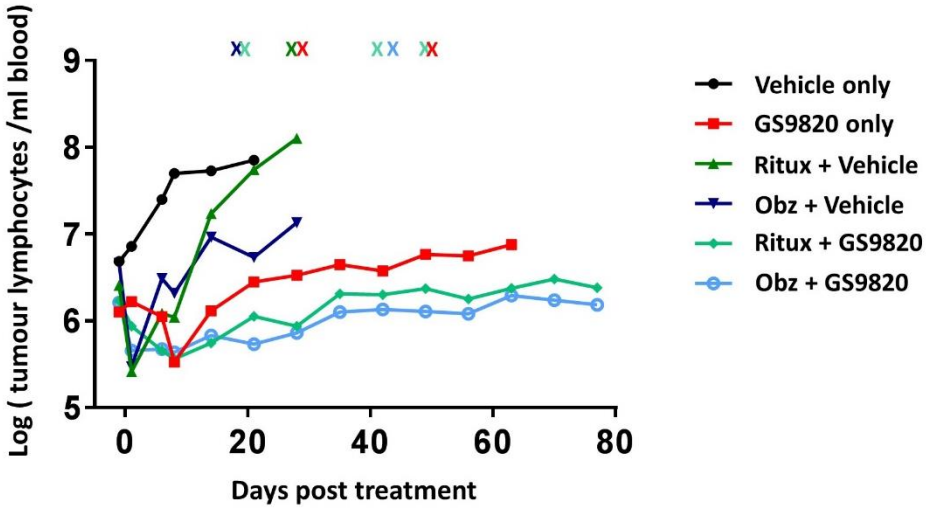

B)

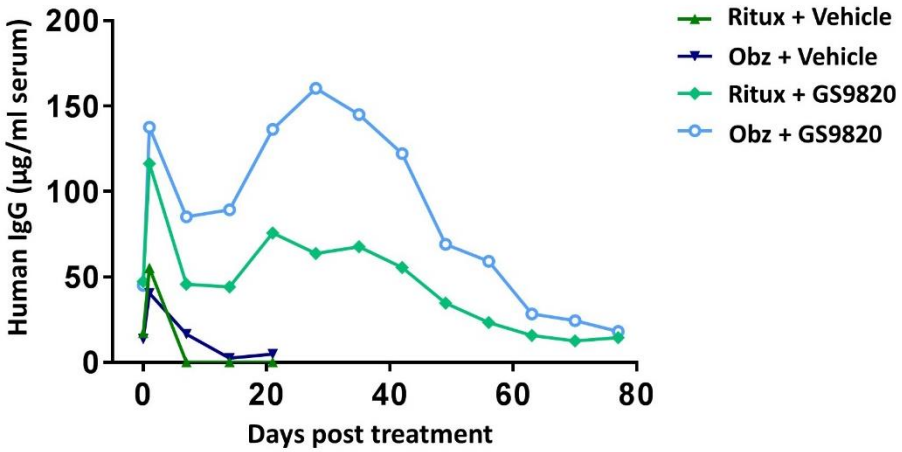

Figure 5.12 ***Combination therapy of Tcl-1 hCD20 tumours with anti-CD20 mAbs and GS9820.***
$1x10^7$ hCD20 splenocytes were transferred to hCD20 mice and tumours allowed to establish. Once tumour was detectable in the blood mice were treated with 100µg rituximab or obinutuzumab (Obz) i.p. weekly for 5 weeks. Additionally mice received 10mg/kg GS9820 or vehicle control by oral gavage. For 2 weeks drug was given twice a day for 5 days and once a day for 2 days, weeks 3-5 the drug was given once a day for 5 days with 2 days off. A) The number of tumour cells in the peripheral blood were measured by flow cytometry and total WBC count. The antibody only groups depleted tumour cells before they returned and mice developed terminal disease. GS9820 alone was able to slow the expansion of tumour cells. The combination of mAb and GS9830 was the most effective at slowing tumour expansion. Crosses demonstrate where deaths occurred before the end of the treatment group which may result in fluctuation in the number of tumour cells, lines were stopped when less than 3 mice remained in a given group. B) The concentration of human IgG in the serum was measured by ELISA. hIgG was detected for longer following treatment in the combination groups. Mean of N= 3-7 per group, error bars omitted for clarity due to large variation.

5.8 Chapter discussion

In this chapter, the Tcl-1 hCD20 model was developed, characterised and used to investigate anti-hCD20 immunotherapy. In the Eμ-Tcl-1 model the Tcl-1 gene is overexpressed under a B cell specific promoter, giving rise to CLL like disease.[407] In this study, Tcl-1 mice were crossed onto the hCD20 +/- background; the characterisation of spontaneous Tcl-1 hCD20 tumours was akin that originally described during the development of the Tcl-1 model.[407] This suggests that crossing Tcl-1 mice to express hCD20 does not fundamentally affect the biological features or survival of these mice. Mice were characterised by an expansion in $CD5^{lo}$ B cells in the peripheral blood, as well as splenomegaly and slight lymphadenopathy. An expansion in $CD5^{+}$ B cells is an important clinical characteristic of CLL suggesting that the tumour model shares a key feature of the human disease.[478] Interestingly expression of the Tcl-1 gene was found in 90% of CLL cases investigated, with increased expression associated with poor prognosis markers such as unmutated IgHV genes.[479]

The slow and variable time to disease presentation in Tcl-1 hCD20 mice was prohibitive to their use in therapy experiments. In order to adapt the tumour model to facilitate more rapid and robust analysis, splenocytes from mice with spontaneous Tcl-1 hCD20 tumours were transferred to recipient mice. It was initially observed that that the rate of passage into C57BL/6 mice was very low; for those tumours which did become established, expression of hCD20 was lost. This is likely to occur due to T cells in recipient mice not having developed tolerance to human CD20, meaning that only Tcl-1 cells that do not express the hCD20 transgene are able to evade immune detection and become established. It is unclear in this study if there is a subset of Tcl-1 cells not expressing the hCD20 transgene or if hCD20 becomes downregulated in a subset of cells, allowing escape from immune surveillance. In contrast, hCD20 mice should have developed tolerance to hCD20, yet even in these recipients only 50% of Tcl-1 hCD20 tumours reached terminal disease; this rate was much lower than that observed for Tcl-1 tumours (Dr M Carter, personal communication). The reason for this remains to be established; it is possible that that expression of the hCD20 transgene limits B cell growth, however there is no difference in the development of spontaneous Tcl-1 tumours compared to Tcl-1 hCD20 tumours. Nonetheless, several spontaneous Tcl-1 hCD20 tumours were identified which were capable of repassage and were used for subsequent immunotherapy investigation.

Initial experiments focused on the clearance of Tcl-1 hCD20 tumours in SCID and hCD20 Tg mice using the type I mAb rituximab or the type II mAb BHH2 and the glycomodified clinically used type II, obinutuzumab. Direct comparison has previously demonstrated that BHH2 and obinutuzumab elicit comparable levels of B cell depletion *in vivo,* suggesting that differences between mAbs are not due to their glycosylation state.[309] These studies demonstrated that clinically relevant anti-hCD20 mAbs were able to clear circulating Tcl-1 hCD20 cells in both recipient mouse strains investigated. The clearance of tumours was similar between hCD20 Tg and SCID mice; this suggests that T cells and normal B cells are not required to support the growth of tumour or in mediating anti-hCD20 mAb activity. Interestingly, BHH2/obinutuzumab treatment resulted in prolonged tumour clearance compared to rituximab in both recipient strains of mice, further suggesting that both recipient strains are suitable for exploring differences in efficacy between clinically relevant mAbs. This tumour clearance was consistent with ELISA data demonstrating that the type II mAbs were better able to persist in the circulation, offering a likely mechanism for prolonged therapeutic activity that applies to immune competent and immune deficient mice. This supports previous observations that rituximab is internalised to a greater extent by the tumour than type II mAbs, which can affect the effector mechanisms engaged by the mAb.[241, 309] This internalisation has been proposed to occur through cis binding of rituximab to CD32b on the tumour cell. Indeed, the amount of mAb internalisation has been found to be directly correlated to the expression level of CD32b on the tumour.[254] Further work found an anti-hCD32b blocking mAb was able to block rituximab internalisation and potentiate rituximab anti-tumour activity *in vivo*.[256] However, it is important to note that these studies used human tumour cells rather than the fully murine model used in this chapter. It is possible that type II mAbs are less sensitive to internalisation due to their inability to redistribute CD20 into lipid rafts, however this requires further investigation.

Importantly, the observations made in this study with regards to mAb efficacy are consistent with previous *in vivo* studies which found obinutuzumab to have greater anti-tumour activity compared to rituximab.[265] However, this previous study investigated subcutaneous tumour xenografts rather than the more clinically relevant syngeneic leukaemia model used in this project. Furthermore, mouse data is supported by clinical trials demonstrating that, when combined with chlorambucil, obinutuzumab prolonged progression free survival in CLL patients compared to rituximab. However, in this trial obinutuzumab was given at a higher dose than rituximab, whereas in the current study, obinutuzumab demonstrated superiority at the same dose as rituximab, albeit as a monotherapy. When taken together, the data presented here suggests that the Tcl-1 hCD20

model is able to faithfully replicate phenomena observed in patients, strengthening its use as a biologically relevant disease model.[263]

Additionally, here it is shown that normal B cells are efficiently depleted by both anti-hCD20 mAb in hCD20 mice. For the first time, this model allows the simultaneous depletion of both tumour cells and normal B cells following treatment with anti-hCD20 mAbs, making this the most biologically relevant model available for studying human disease. It was suggested by these results that 21 days after treatment, the number of normal B cells was reduced in Herceptin treated mice. This result could be due to the large number of tumour cells outgrowing and diluting the normal B cells present in the mice. Following mAb treatment, the normal B cells appear to return more slowly than the tumour cells; this is likely because the tumour cells have a faster rate of division compared to normal B cells. This could be confirmed through investigating the expression of proliferation markers such as Ki-67 or by investigating the incorporation of BrdU, a synthetic nucleoside. Tcl-1 hCD20 cells would be expected to divide at a faster rate than normal B cells due to the overexpression of the Tcl-1 gene. The Tcl-1 gene has been shown to be a coactivator of Akt, capable of facilitating its phosphorylation and nuclear translocation.[410, 480] Activation of Akt can impact on cell survival with activated Akt shown to phosphorylate BAD, suppressing its apoptotic effect.[411] Additionally, Akt can inhibit transcription factors such as FKHRL1, which would otherwise promote cell death through transcription of pro-apoptotic genes.[412] This activity through Akt offers a mechanism for the tumourogenesis induced in the Tcl-1 hCD20 model, as well as an explanation for the faster return of tumour cells following mAb therapy compared to normal B cells.

When depletion experiments were performed in NOD SCID mice, the initial tumour deletion was comparable to that observed in SCID mice. NOD SCID mice have a reduction in the frequency of NK cells compared to SCID mice; those cells that are present have been found to have significantly reduced ADCC activity.[418, 481] The comparable initial tumour depletion to that observed in SCID mice suggests NK cell mediated ADCC is not an essential mechanism for initial clearance of Tcl-1 hCD20 tumour by anti-hCD20 mAbs. There is limited evidence on the role of NK cells in anti-hCD20 therapy in humans, however the results here are consistent with previous experiments performed in mice. Depletion of NK cells using a specific antibody was found to have no effect on the capacity of rituximab to delete a $hCD20^+$ murine lymphoma cell line *in vivo*.[232] An additional observation from the experiments in NOD SCID mice was that tumour clearance was less prolonged compared to SCID mice. One possibility is that NK cells are required for longer term therapy, however as

discussed in the next chapter this is unlikely to be the case, with differences more likely to be due to differences in mAb consumption.

This study aimed to investigate the mechanism of action for anti-CD20 mAbs *in vivo.* One proposed mechanism for anti-hCD20 activity is through complement activation. Type I mAbs have been found to be more potent at inducing CDC than type II mAbs such as obinutuzumab.[180] The results in this study show that initial tumour depletion is comparable between rituximab and obinutuzumab, suggesting that enhanced CDC activity does not alter tumour clearance in mice and implying a limited role for CDC in general. This is supported by previous studies where mice deficient in components of the complement cascade did not have a reduction in rituximab activity.[199, 200]

The major mechanism that has been proposed for the *in vivo* activity of anti-CD20 mAbs is through the activity of FcγRs. Experiments here demonstrate that in γ-chain deficient mice, lacking FcγRs there was no effective depletion of Tcl-1 hCD20 cells following anti-hCD20 therapy. This strongly suggests that effector cell mechanisms mediated through activatory FcγRs are the primary mechanisms by which rituximab and obinutuzumab act. This supported previous results, which demonstrated that the activity of rituximab was dependent on activatory FcγRs.[200, 222] When experiments were performed in NOTAM mice, which express FcγRs that are signalling deficient, rituximab did not induce any significant anti-tumour activity.[214] Further experiments have previously shown that the major FcγR expressing effector cell responsible for rituximab activity is macrophages, deduced through the use of clodronate vesicles to deplete phagocytes.[241] These previous experiments focused on depletion of human xenografts or cell lines; in contrast, here the FcγR requirement has been in investigated using a syngeneic murine tumour model. It would be interesting to pursue this work further to identify the relative contributions of individual FcγRs through the use of knock-out mice.

It has been widely reported previously that anti-hCD20 mAbs are able to induce direct cell death through the transmission of intracellular signals.[205] However, rituximab requires cross-linking in order to induce potent direct cell killing *in vitro*, whereas type II anti-hCD20 mAbs such as obinutuzumab do not require further cross-linking.[185, 191, 482] This is consistent with the results in this chapter where there was no evidence for rituximab activity in the absence of the γ-chain, suggesting that the mAb could not significantly deplete tumour cells by inducing direct cell death or indeed CDC. The type II mAb obinutuzumab has been demonstrated *in vitro* to result in the death of CLL cell lines through induction of homotypic adhesion and actin-dependent cell death.[138]

Experiments performed here in γ-chain deficient mice found that there was a small reduction in the percentage of tumour lymphocytes seven days after obinutuzumab treatment. Given that these mice do not express functional FcγRs, and that obinutuzumab is known not to potently activate CDC, this suggests some induction of direct cell death could be occurring. However, there was no significant difference in the total number of circulating tumour cells following obinutuzumab treatment and no improvement in survival compared to controls. This suggests that the role of direct cell death in obinutuzumab activity is likely to be very minimal, with FcγR mediated mechanisms dominating.

Whilst anti-CD20 mAbs such as rituximab have no doubt proven successful in the treatment of B cell malignancies, there are a significant number of patients who do not reach a complete response.[483] For example, in follicular lymphoma, rituximab plus chemotherapy achieved a complete response rate of 87%; nine years later just under 50% of patients remained progression free.[484] This highlights how rituximab treatment provides significant patient benefit whilst underlining the need for further improvement in therapy. One strategy has been the introduction of newer anti-hCD20 mAbs such as obinutuzumab, as has already been discussed. Another approach has been to combine anti-hCD20 therapy with targeted small molecules; this includes the δ isoform selective PI3K inhibitor idelalisib. In this current study, GS9820 was used in combination with anti-hCD20 mAbs; this molecule has been shown to be a potent and highly selective inhibitor of PI3K δ.[485] The results presented here suggest that as a monotherapy, GS9820 is able to slow tumour growth in the Tcl-1 hCD20 model, an effect which is more pronounced when combined with anti-hCD20. This supports *in vitro* data demonstrating that GS9820 induced the death of Tcl-1 cells and patient CLL cells (Carter et al. manuscript in preparation). This is something which has been demonstrated previously in the structurally related molecule idelalisib.[486] A trial in previously untreated SLL and CLL patients found the response rate for rituximab plus idelalisib to be 97%, demonstrating an improvement over rituximab alone.[487] Given that results in this chapter have proposed that obinutuzumab offers more prolonged tumour clearance compared to rituximab, it will be interesting to see if therapy in humans can be improved by the combination of obinutuzumab with a PI3Kδ inhibitor. The results here suggest that anti-hCD20 mAb is detectable in the plasma for longer after treatment when used in combination with GS9820. This result is based on a single experiment using only one tumour and should therefore be treated with caution. However, were this result to be corroborated it could offer a useful, additional mechanism by which GS9820 improves anti-tumour therapy. The finer details on how this effect

occurs would also need dissecting to determine whether GS9820 impairs mAb turnover or if prolonged reduction in tumour burden is responsible for reduced mAb consumption.

In this chapter, it has been demonstrated that Tcl-1 hCD20 tumours offer a model of CLL like disease which maintains expression of human CD20 even after transfer of tumours into hCD20 transgenic or immune compromised recipients. Tcl-1 hCD20 tumours can be efficiently deleted using clinically relevant anti-hCD20 mAbs, with results suggesting that obinutuzumab induces more prolonged tumour clearance than rituximab due to its improved persistence in the plasma. The transfer to tumour cells into hCD20 transgenic mice has allowed anti-hCD20 mAbs to be investigated in a fully syngeneic system where the target antigen is present on malignant and non-malignant B cells. Additionally, this model can be used to investigate novel combination therapies which are currently under clinical investigation. Finally, the Tcl-1 hCD20 model has been used to investigate the mechanism of action for anti-hCD20 mAbs. Importantly, this revealed that activatory FcγRs are essential for the efficient anti-tumour activity of these mAbs *in vivo.*

Chapter 6 Investigating abnormal antibody depletion in NOD SCID mice

6.1 Chapter introduction

As discussed in the previous chapter, *in vivo* modelling is vital in the development of new immunotherapy approaches, as well as understanding the mechanisms by which these therapies work. NOD SCID mice are an immune compromised strain of mouse widely used for investigating immunotherapy. The SCID mutation results from a single base pair change in the Prkdc gene, which impairs V(D)J recombination and leads to a absence of functional T and B cells.[415, 417] The NOD phenotype has been used for studying type 1 diabetes, however when combined with the SCID mutation produces mice with reduced NK cell frequency and NK cell activity on top of the SCID phenotype, as well as having no hemeolytic complement activity.[417, 418] The severe immune deficiency in NOD SCID mice makes them attractive recipients for human tumour xenografts, allowing the treatment of human cancers to be modelled in a living organism. The NOD SCID mice have subsequently been used as the background for additional mutations to give further immune deficiency. NSG mice lack expression of the IL2 γ-chain which completely prevents development of NK cells, overcoming one of the drawbacks of NOD SCID mice.[488] Furthermore, in order to better support the grown of human xenografts, particularly AML cells, NSGS mice have been developed which express human IL3, GM-CSF and stem cell factor (SCF).[489] Despite these advances to improve engraftment, all these widely used models rely on the NOD background and carry its associated genetic defects.

The use of tumour xenografts often means investigating the anti-tumour activity of mAbs; the majority of the mAbs investigated for use in humans are of the IgG1 (hIgG1) isotype. However, there is little understanding or consideration as to how the pharmacokinetics of mAbs, particularly hIG1 vary between strains of mice. This is a particularly important consideration if results are to be compared between different models using alternative genetic backgrounds.

The clearance and turnover of antibodies is primarily controlled by the neonatal fc receptor (FcRn) in both humans and mice. This receptor is more closely related to MHC I than to the FcγRs. It binds IgG avidly in an acidic environment, such as the lysosome and releases it in a neutral pH.[395, 490] This allows for IgG to escape degradation by being scavenged from the lysosome, helping to maintain

serum IgG concentration. Importantly, FcRn in mice displays a degree of promiscuity, mouse FcRn maintains binding to hIgG1 albeit with a reduced affinity compared to mouse IgG.[491]

The experiments in this chapter were initiated based on the results observed in Figure 6.1a. Tcl-1 tumours were passaged into SCID and NOD SCID mice before being treated with rituximab or obinutuzumab. The initial depletion of tumour cells was comparable between the strains, however 14 days after treatment, SCID mice had significantly fewer tumour cells in their peripheral blood compared to NOD SCID mice. In order to determine why this occurs, the concentration of antibody in the plasma of treated mice was investigated. The most striking results were observed with the isotype control mAb as shown in Figure 6.1b. Seven days after mAb treatment, there was significantly less human IgG in the plasma of NOD SCID mice compared to SCID mice. Similar results were also observed for the hCD20 targeting antibodies, with NOD SCID mice having a lower plasma concentration that SCID mice (data not shown). These results suggest that mAb therapy was less effective in NOD SCID mice due to the faster clearance of hIgG1 from the plasma. Importantly, this faster clearance was observed with the isotype control, suggesting it was not a result of mAb binding to the tumour. However, this observation is based on experiments that were not performed side by side and with small group sizes for the ELISA data. Therefore in this chapter the phenomenon was investigated further.

Previously, there has been very little work investigating the abnormal clearance of human IgG from the circulation of NOD SCID mice, with only one limited report which described shorter human IgG half-life in NOD SCID mice.[492] This study sequenced the FcRn gene and found no differences between the sequence in NOD SCID mice and other common strains. Instead, the abnormal mAb half-life was attributed to FcγRs on macrophages in NOD SCID mice. In this chapter, the abnormal clearance of IgG from the circulation of NOD SCID mice was studied in depth with a focus on understanding the mechanisms behind this phenomenon.

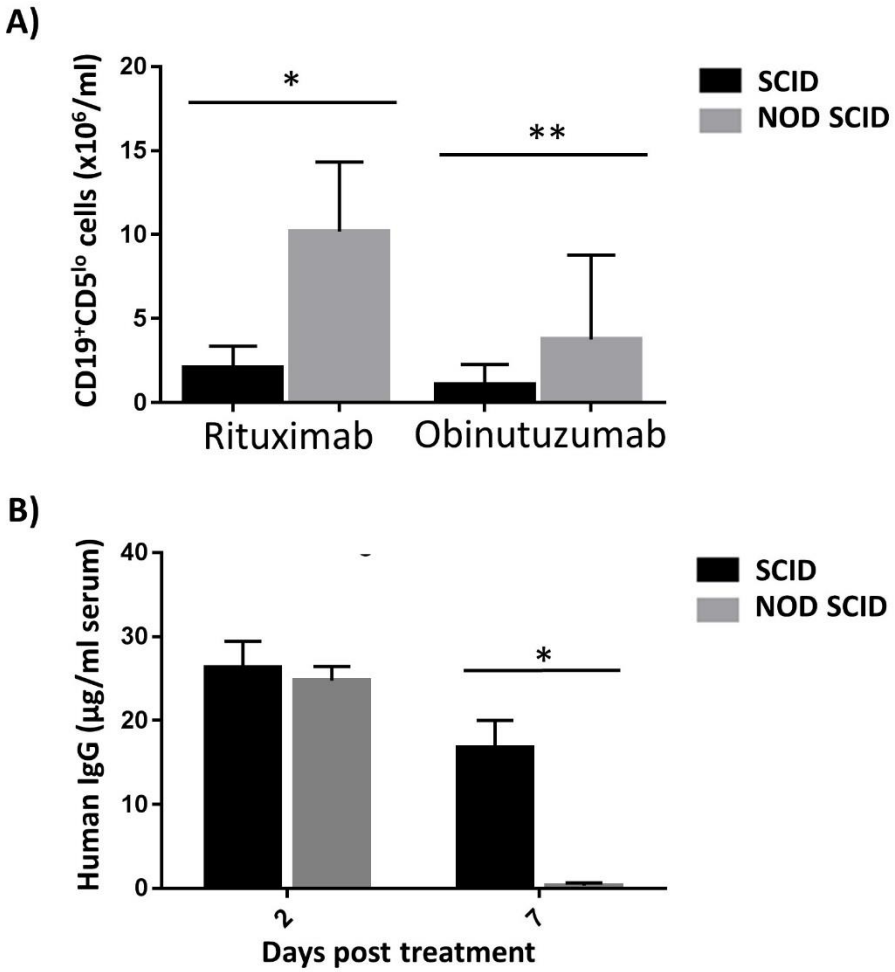

Figure 6.1 ***Tumour clearance and human IgG concentration in SCID and NOD SCID mice.***
*$1x10^7$ splenocytes from Tcl-1 hCD20 mice were injected i.p. into SCID or NOD SCID mice. Once tumour cells ($CD19^+CD5^{low}$) were detectable in the blood by flow cytometry mice were treated with 100µg rituximab, obinutuzumab or herceptin. A) 14 days after mAb treatment SCID mice had significantly fewer tumour cells in their blood compared to NOD SCID mice (one-way ANOVA with multiple comparisons *p<0.05; **p<0.01) mean +SD N=4-10. B) The concentration of human IgG in the plasma was determined by ELISA for the herceptin treated mice. 7 days after treatment NOD SCID mice had a significantly lower human IgG plasma concentration compared to SCID (T-test *p<0.05) mean + range N=2-3).*

6.2 NOD SCID mice have faster hIgG1 clearance from the plasma.

Following the preliminary observations in the Tcl-1 hCD20 model, the clearance of irrelevant i.e. non-binding hIgG1 mAbs from the plasma of NOD SCID mice was investigated further. Initially, 100µg of the anti-human EGFR specific mAb cetuximab was administered i.v. to male SCID, BALB/c and NOD mice before the concentration of human IgG in the plasma was determined by ELISA. Figure 6.2 demonstrates that seven days after administration of cetuximab there was no significant difference in the concentration of human IgG in the plasma of BALB/c, SCID or NOD

mice. This suggests that the NOD or SCID mutations in isolation do not alter hIgG1 mAb persistence. Furthermore, results suggest SCID mice are a suitable control for future experiments.

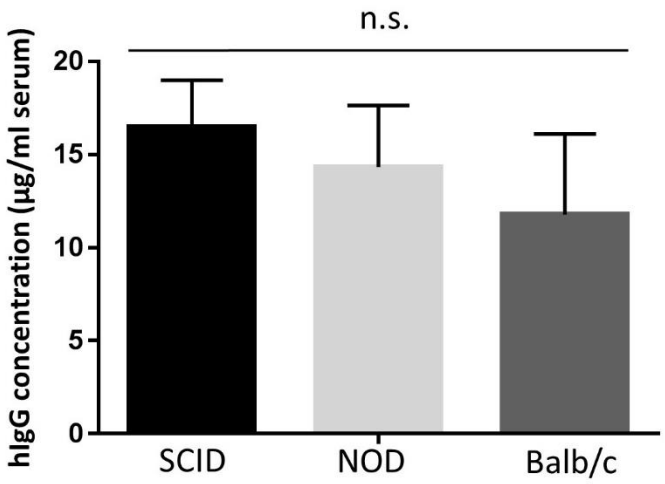

Figure 6.2 **Human IgG (hIgG) concentration in SCID, NOD SCID and BALB/c mice 7 days after mAb.** 100µg cetuximab was administered i.v. to male SCID, NOD SCID and BALB/c mice. 7 days after mAb administration plasma was collected and the concentration of hIgG determined by ELISA. Results were not significantly different between strains (one–way ANOVA). Bars represent mean + SD, N=4-6 per group.

The clearance of human IgG from the plasma of SCID and NOD SCID mice was investigated using two different human IgG1 mAbs. Additionally both male and female mice were used to confirm that the observations were not restricted to a single mAb and were not sex dependent. 100µg of the anti-human Her2 specific mAb Herceptin was administered i.v. to female SCID or NOD SCID mice (Figure 6.3a) whilst 100µg cetuximab was given to male mice (Figure 6.3b) and the concentration of human IgG in the plasma determined by ELISA. These results indicate that in female mice from day seven onwards, and in male mice at all time points, there was a significantly lower concentration of hIgG in the plasma of NOD SCID mice compared to SCID mice. These results suggest that hIgG was cleared from the plasma of NOD SCID mice faster than in SCID mice in the absence binding to any target molecules (such as the hCD20 on the tumour cells and normal B cells described in the experiments performed previously). This observation appears to be true for both Herceptin and cetuximab and was not affected by the gender of the mice used.

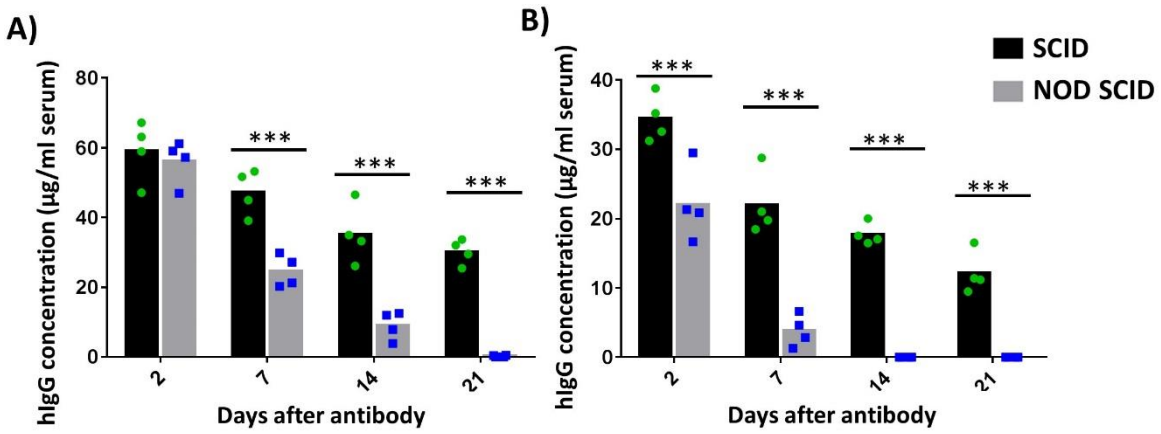

Figure 6.3 ***Clearance of hIgG from the plasma of SCID and NOD SCID mice.***

*mAb was administered i.v. either herceptin to female mice (A) or cetuximab to male mice (B). Mice were bled 2, 7, 14 and 21 days after mAb and the concentration of hIgG in the plasma determined by ELISA. In female mice from day 7 onwards, and in male mice at all time points, SCID mice had a significantly higher plasma IgG concentration than NOD SCID mice (2-way ANOVA with multiple comparisons; ***P<0.001). Bars represent mean with points for individual animals, N=4 per group.*

6.3 The Impact of isotype on mAb clearance in NOD SCID mice

With hIgG1 found to be cleared more quickly from NOD SCID mice, it was next investigated if this observation also applied to other IgG isotypes. Accordingly SCID and NOD SCID mice were injected i.v. with 100µg rituximab hIgG2, mIgG1 or mIgG2a and the concentration of either hIgG or mIgG determined by ELISA. Importantly rituximab does not bind to mouse CD20 and is therefore an irrelevant, non-binding mAb in this context.

Figure 6.4 suggests that there was no difference in the clearance of mIgG1 or hIgG2 between SCID and NOD SCID mice, with IgG of each of these isotypes still detectable in the plasma 28 days after administration. In contrast, there were significant differences in the concentration of mIgG2a in the plasma of SCID and NOD SCID mice. At all of the time points investigated, there was significantly less mouse IgG in the plasma of NOD SCID mice receiving mIgG2a compared to SCID mice. 14 days after mAb, there was no mIgG detectable in NOD SCID mice whereas in SCID mice the average concentration was 15µg/ml. These results suggest that NOD SCID mice had a faster clearance of mIgG2a from their plasma than SCID mice, but that there was no difference in the clearance of hIgG2 or mIgG1 between the two strains.

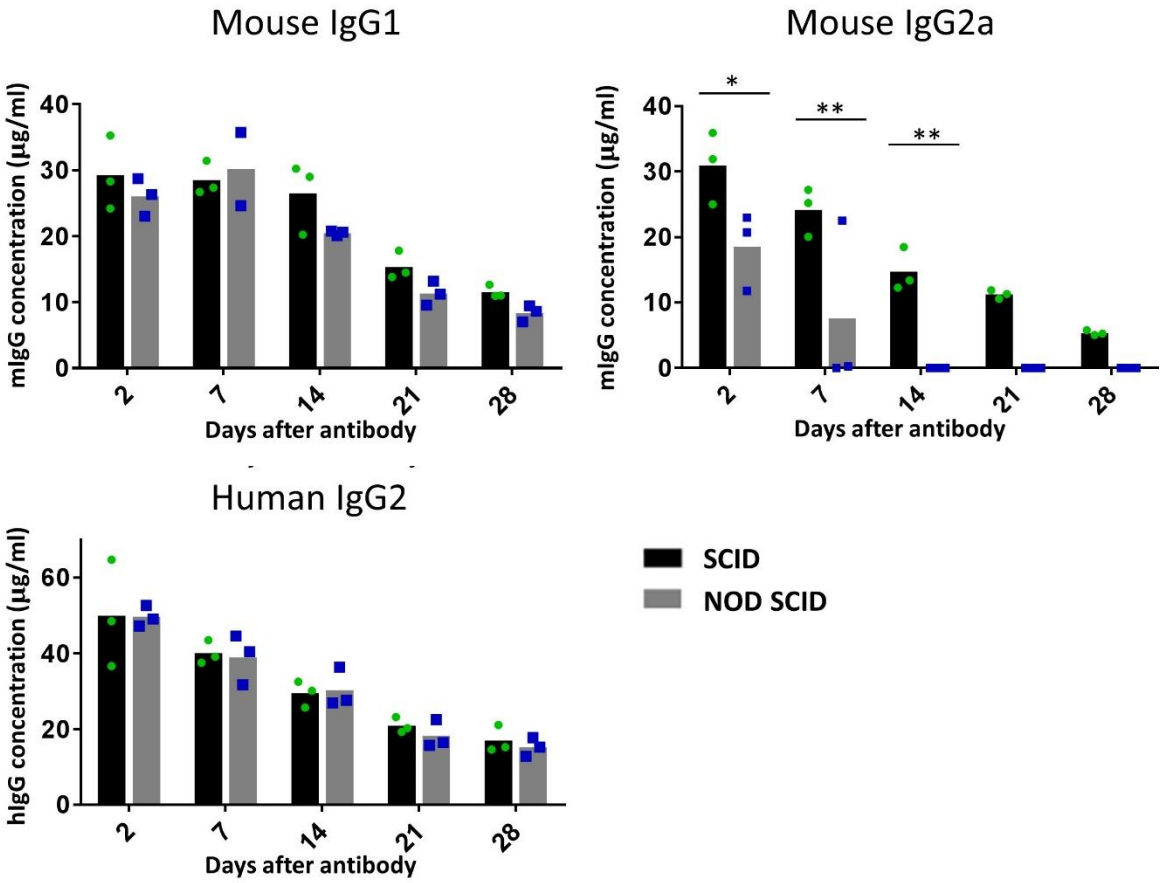

Figure 6.4 ***Clearance of mIgG1, mIgG2a and hIgG2 from the serum of SCID and NOD SCID mice.***

*100µg Rituximab mouse IgG1, mouse IgG2a or human IgG2 was injected i.v into sex matched SCID or NOD SCID mice. Animals were bled 2, 7, 14, 21 and 28 days after mAb treatment and serum collected. The concentration of IgG in the serum was measured using an anti-human IgG or anti-mouse IgG ELISA. There was no differences in antibody concentration between SCID and NOD SCID mice at any time point for mouse IgG1 and human IgG2. However, SCID mice had a significantly higher concentration of mouse IgG2a 2, 7 and 14 days after mAb, compared to NOD SCID mice. (2-way ANOVA with multiple comparisons; *P<0.05, **P<0.01) N=3 per group. Bars show mean with points for individual mice.*

6.4 Bead phagocytosis to assess absolute phagocytic capacity

Having established that the clearance of hIgG1 and mIgG2a was faster in NOD SCID mice, the underlying mechanisms for this was investigated. A previous study suggested than NOD SCID macrophages were responsible for abnormal half-life, therefore the phagocytic potential of BMDMs was investigated.[492] BMDMs from SCID and NOD SCID mice were differentiated over seven days in the presence of L929 conditioned media before the assay was performed. BMDMS were incubated with BSA-Alexafluor488 labelled 3µm beads for 1 hour at differing bead:BMDM ratios. Microscopy in Figure 6.5a demonstrates that beads were taken up by the BMDMs, as can

be seen by light (left panels) and fluorescence microscopy (right panels); additionally, a greater number of beads appeared to be taken up at higher bead:BMDM ratios. Quantification of the percentage bead positive BMDMs was determined by flow cytometry; Figure 6.5b indicates that, at bead ratios above 20 beads per BMDM, more SCID BMDMs were bead positive.

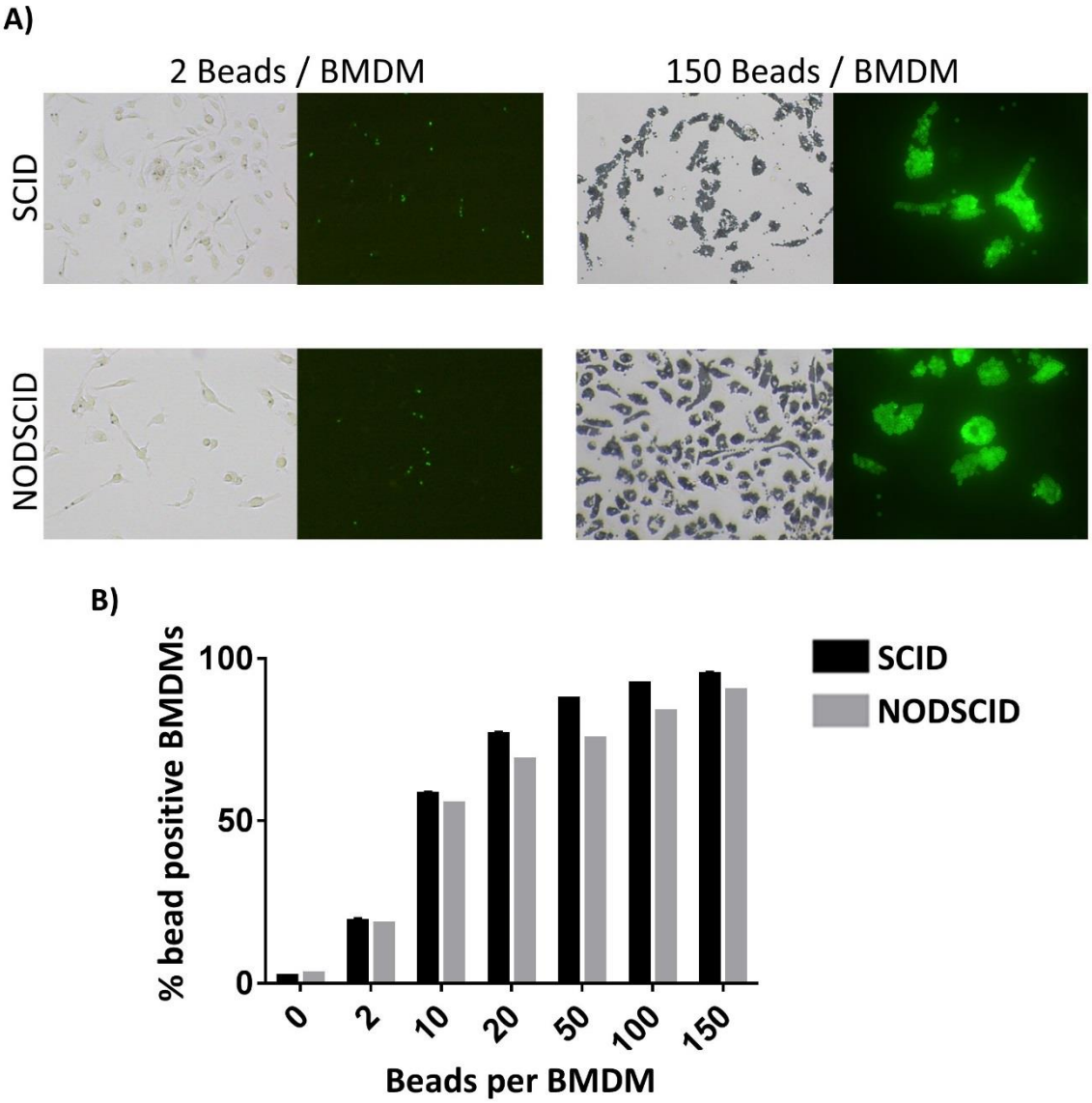

Figure 6.5 ***Bead phagocytosis assay to determine phagocytic potential of SCID and NOD SCID BMDMs.***
BMDMs from SCID and NOD SCID mice were harvested and plated at 5x10^4 cells per well in a 96 well plate and incubated overnight. Alexafluor 488-BSA coated 3µm latex beads were diluted in PBS and added to the beads at the bead:BMDM ratios indicated. Cells with beads were incubated for 1 hour at 37°C. A) representative light microscopy (left images) and fluorescence (right images) following bead phagocytosis assay using SCID and NOD SCID BMDMs at 2 or 150 beads per BMDM. B) The percentage of BMDMs positive for Alexafluor-488 beads was determined by flow cytometry. Results show mean + range for duplicates and are representative of three independent experiments. BMDMs from SCID mice appear to have a higher percentage bead positive at ratios greater than 20 beads per BMDM.

NOD SCID BMDMs appear to have a slightly reduced phagocytic potential compared to cells from SCID mice. This is the inverse of the expectation that phagocytic capability was responsible for the shortened persistence of antibody in NOD SCID mice. However, it should be noted that this

experiment investigated the non-specific uptake by BMDMs rather than specific internalisation of antibody through FcγRs, which would be more relevant to clearance of antibody.

6.5 Internalisation of human IgG1 by SCID and NOD SCID BMDMs

To determine whether specific antibody internalisation differed between SCID and NOD SCID macrophages, and could explain differences in antibody clearance, internalisation assays were performed. BMDMs were differentiated from SCID and NOD SCID mice before Alexafluor488 (A488) labelled mAb of different isotypes were added to the cells and incubated for 16 hours. Following incubation, the cells were harvested; to half of the cells, an anti-A488 quenching antibody was added. The schema for the assay is presented in Figure 6.6a, unquenched samples allowed the total bound mAb to be determined whilst the quenched sample allowed the quantification of only internalised mAb as presented in Figure 6.6b.

SB2H2 mIgG1 showed very little fluorescence with BMDMs from either strain with virtually no difference between quenched and unquenched samples, suggesting only a small amount of mAb has bound and the majority of this is internalised. BHH2 hIgG2 resulted in the highest MFI, suggesting that this isotype was bound to the highest extent by BMDMs, with the majority of the mAb internalised by BMDMs from both strains of mice. For BHH2 mIgG2a, the unquenched MFI was significantly higher for SCID BMDMs compared to NOD SCID, suggesting that more mAb was bound to cells from SCID mice. Additionally, quenched MFI was significantly higher for SCID mice than NOD SCID with BHH2 m2a indicating that there may be more mAb internalised by SCID BMDMs. For Herceptin hIgG1, there was a trend towards increased fluorescence in quenched and unquenched samples with NOD SCID BMDMs, suggesting increased mAb binding to NOD SCID BMDMs compared to those from SCID mice. However, this did not reach significance.

There was a high degree of variability in the maximum fluorescence obtained for individual mice following incubation with mAb. Therefore, the ratio of quenched to unquenched MFI was calculated with the averages from two independent experiments presented in Figure 6.6c. A higher ratio indicates a greater proportion of mAb is has been internalised. For BHH2 mIgG2a, BHH2 hIgG2 and Herceptin hIgG1 the ratio was lower for NOD SCID BMDMs than for SCID BMDMs, suggesting that for NOD SCID BMDMs a smaller proportion of bound antibody was internalised. This is despite Figure 6.6b suggesting that, for Herceptin hIgG1 NOD SCID, BMDMs were capable

of binding mAb to a greater extent than SCID BMDMs, evidenced by an increased MFI. These results suggest that there were differences in IgG binding to SCID and NOD SCID BMDMs, with a greater proportion of mAb internalised by SCID BMDMs. However, this result does not explain why human IgG1 and mouse IgG2a were cleared more quickly from the serum of NOD SCID mice compared to SCID.

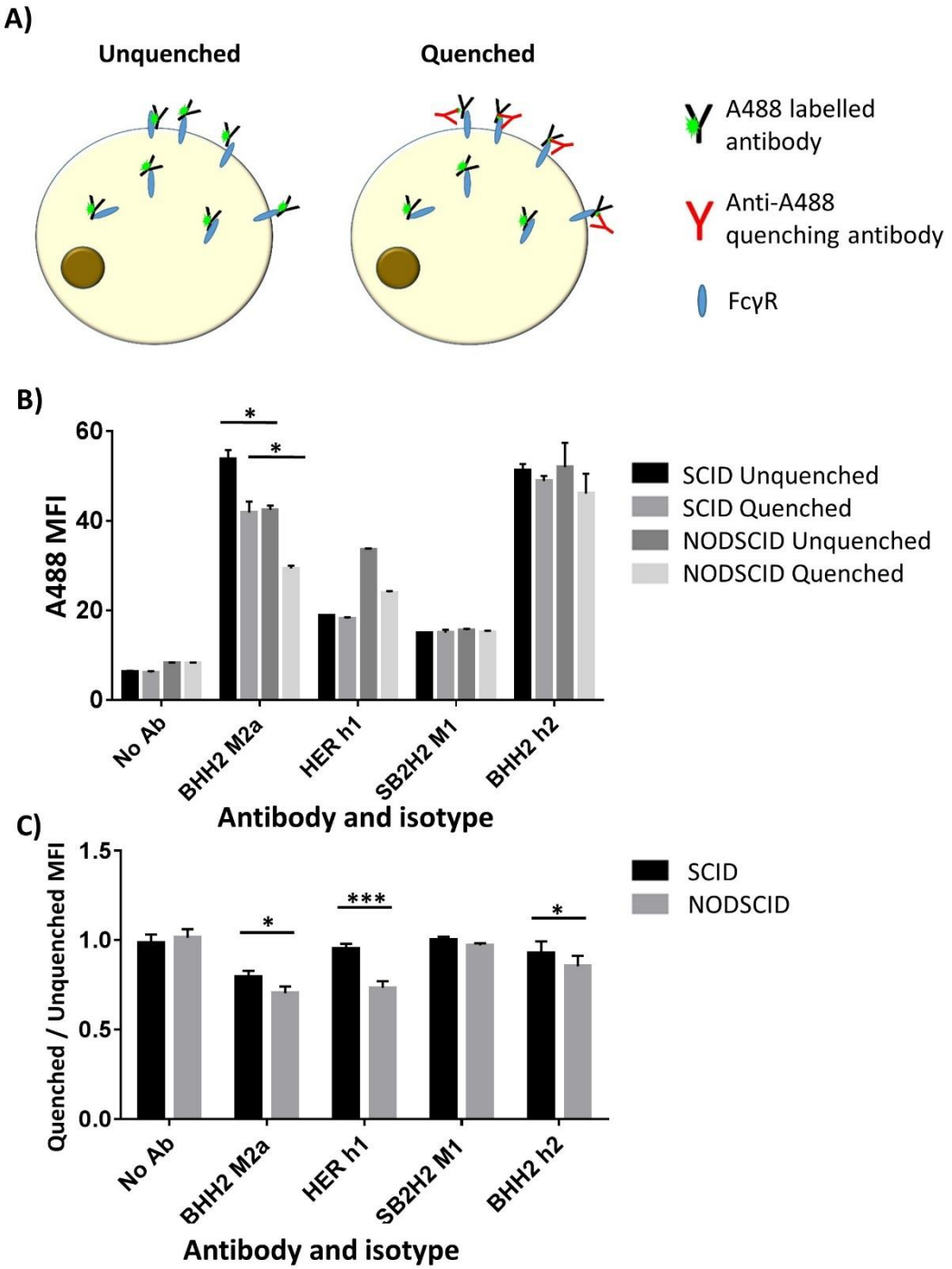

Figure 6.6 ***Antibody internalisation assays.***

*BMDMs were differentiated from the bone marrow of SCID and NOD SCID mice for 7 days. 2 x10^5 BMDMs were plated per well in a 96-well plate and incubated overnight. A488 labelled mAbs were added at 5µg/ml: BHH2 mouse IgG2a (BHH2 M2a,) Herceptin (HeER h1), SB2H2 mouse IgG1 (SB2H2 M1) or BHH2 human IgG2 (BHH2 h2) and incubated for 16 hours. Cells were removed by scraping and washed before half of each sample was treated with 2.5µl anti-A488 mAb for 30 minutes at 4°C then washed. A) Schematic for analysis with unquenched fluorescence from total mAb at the surface and internalised mAb. Fluorescence from quenched samples reflected that from internalised mAb. B) MFI values obtained for quenched and unquenched samples using BMDMs from both strains. MFI was significantly higher for unquenched BHH2 m2a on SCID compared to NOD SCID BMDMs as well as quenched samples with the same mAb (2-way ANOVA with multiple comparisons, *P<0.05. B) Ratio of quenched to unquenched MFI from internalisation assays. NOD SCID BMDMs had a significantly lower ratio compared to SCID mice for BHH2 M2a, HER h1 and BHH2 h2 (2-way ANOVA with multiple comparisons *P<0.05, ***P<0.001. Results using 3 mice split between 2 independent experiments, bars represent mean +SD.*

6.6 Altered antibody clearance is FcγR dependent and can be overcome with IgG reconstitution

FcγRs are the major class of receptor responsible for IgG binding, and so the role of these receptors in the clearance of mAb from the plasma of NOD SCID mice was investigated. To determine whether interaction with FcγRs mediated abnormal mAb persistence, the clearance of an antibody with the N297Q (NQ) mutation was investigated; this mutation prevents efficient interaction with FcγRs but not FcRn.[104] 100µg rituximab hIgG1 or rituximab hIgG1 NQ was administered to NOD SCID mice and their concentration in the plasma was measured over time. Figure 6.7 shows that rituximab hIgG1 NQ was found at a significantly higher concentration in the plasma of mice compared to unmodified rituximab seven days after administration. Additionally, rituximab NQ was detectable in the plasma 21 days after injection, whereas unmodified rituximab was undetectable by day 14. This suggests that preventing Fc-FcγR interaction could prolong hIgG1 persistence in the plasma of NOD SCID mice to levels equivalent to those seen in SCID mice. Therefore, FcγRs may, at least in part, be responsible for abnormal mAb clearance in NOD SCID mice.

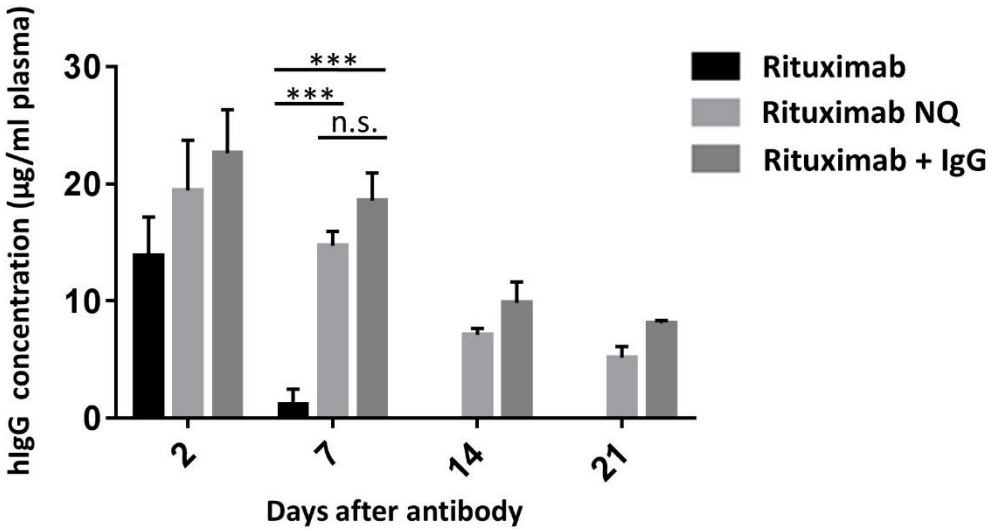

Figure 6.7 ***Clearance of rituximab NQ or rituximab in the presence of mouse IgG in NOD SCID mice***. *100µg rituximab or rituximab N297Q (NQ) was given i.v. to NOD SCID mice and the concentration of hIgG in the plasma determined by ELISA. Additionally one group (rituximab +IgG) were also given 400µg mIgG2a and 500µg mIgG1 with an additional 200µg mIgG2a i.p. every 3 days for 15 days. 7 days after mAb there was significantly less hIgG in the plasma of mice receiving rituximab compared to those receiving rituximab NQ or rituximab +IgG (2-way ANOVA with multiple comparisons ***P<0.001). Bars represent mean + SD, N= 3-4 per group.*

NOD SCID mice do not produce any endogenous IgG as a result of the SCID mutation, therefore the effect of reconstitution with mouse IgG on clearance of hIgG1 in NOD SCID mice was

investigated. As such, 100µg rituximab was administered with the addition of 400µg mIgG2a (WR17) and 500µg mIgG1 (3G8), due to its rapid clearance, an additional 200µg mIgG2a was administered on days 3, 6, 9, 12 and 15. This dosing regime was determined based on earlier observations as to the clearance rate of mIgG1 and mIgG2a in SCID mice with the aim of maintaining a serum IgG concentration to that in BALB/c mice. The concentration of mIgG in the plasma of NOD SCID mice following reconstitution was determined by ELISA, which found that concentrations were comparable to that in BALB/c mice (Figure 6.8). Figure 6.7 demonstrates that seven days after mAb there was a significantly higher concentration of hIgG in the plasma of NOD SCID mice reconstituted with mIgG compared to those receiving rituximab only. 14 and 21 days after mAb, rituximab was still detectable in the plasma of the mIgG reconstituted mice, but not those receiving rituximab only.

These results demonstrate that the rapid clearance of hIgG from the plasma of NOD SCID mice could be overcome by preventing mAb binding to FcγRs or through reconstitution with mIgG. Both of these results suggest that FcγRs play an important role in abnormal mAb half-life in NOD SCID mice.

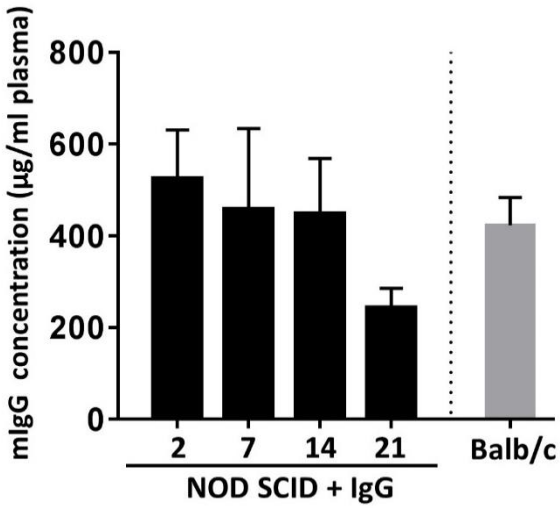

Figure 6.8 ***Concentration of mouse IgG in the serum of NOD SCID mice receiving IgG or BALB/c mice.***

NOD SCID mice were reconstituted with mouse 400µg mIgG2a and 500µg mIgG1 on day 0, with an additional 200µg mIgG2a on days 3, 6, 9 and 12. The concentration of mIgG in the plasma was determined by ELISA. Additionally the concentration of mIgG in BALB/c mice was investigated. Bars represent mean +SD n=4 per group.

6.7 FcγR phenotyping

Given the differences that were observed in IgG clearance between SCID and NOD SCID mice, coupled with the results using rituximab NQ, the FcγR repertoire on monocytes and macrophages in the blood and spleen was investigated. Spleens were harvested from SCID or NOD SCID mice and a single cell suspension was obtained by passing the tissue through a 100µm cell strainer. Additionally, peripheral blood was taken. Blood and spleen suspension were stained with fluorescently labelled antibodies to identify monocyte and macrophage populations. Figure 6.9 demonstrates the gating strategy with live cells first being gated, based on forward and side scatter, before identifying the $CD11b^{+}$ cells and subsequently, $Ly6G^{-}Ly6C^{Hi}$ and $Ly6G^{-}Ly6C^{Lo}$ monocytes. Neutrophils were also identified as $Ly6G^{Hi}Ly6C^{Mid}$. The plots in Figure 6.9 are for a spleen sample, however the same gating strategy was used for blood where the main difference was the relative proportions of each cell type.

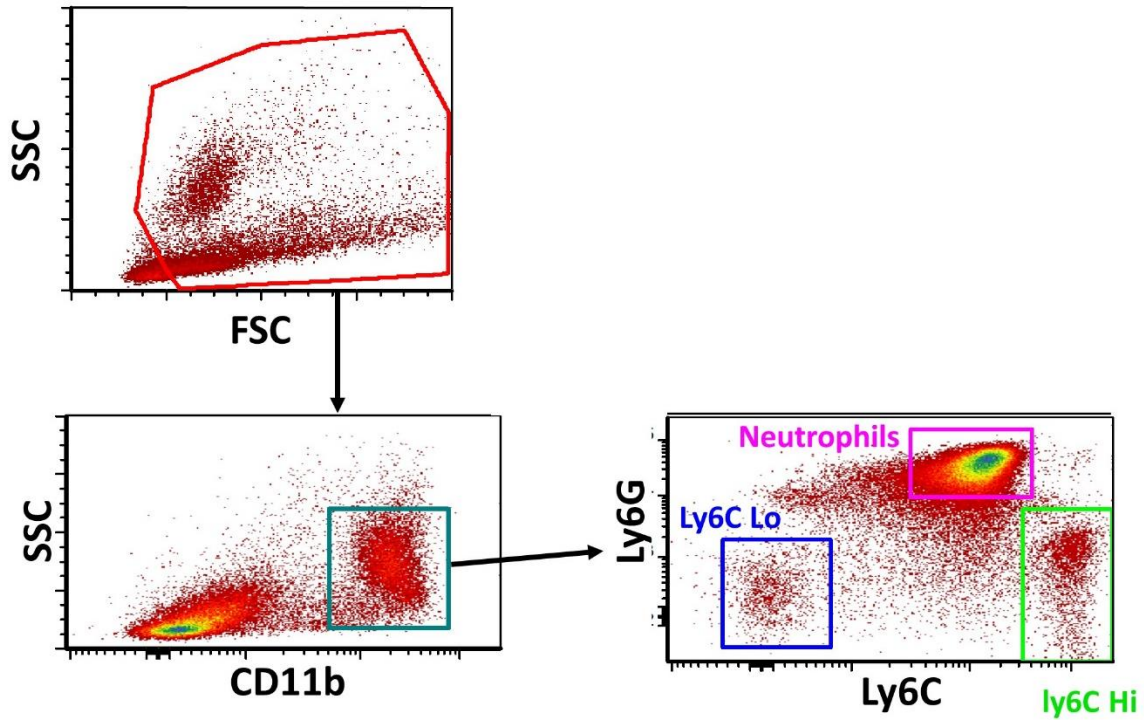

Figure 6.9 ***Gating strategy used to identify monocytes subsets in spleen and blood.*** *were identified.*
Spleens and peripheral blood were harvested from SCID and NOD SCID mice. Single cells suspensions were obtained by passing spleens through a 100µm cell strainer. Spleens were resuspended in 5ml PBS and 200µl cell suspension or 20µl blood stained with the following antibodies: anti-CD11b pacific blue, anti-F4/80 APC, anti-Ly6G APC-Cy7 and anti-Ly6C PerCP-Cy5.5. Figure shows the gating a sample of spleen cells with the same strategy used for blood samples. Live cells were identified by forward (FSC) and side (SSC) scatter. From the live cells CD11b+F4/80- monocytes, Ly6C+Ly6G- monocytes and F4/80+ macrophages were identified.

The FcγR expression on the three populations identified was investigated by staining with receptor specific FITC labelled $F(ab')_2$ fragments. These results in Figure 6.10 show that the expression of CD32 was higher on both monocyte populations in SCID mice in the spleen and the blood. Additionally, the expression of FcγRIV appeared lower on $ly6C^{lo}$ monocytes in SCID blood compared to NOD SCID mice. When investigating neutrophils, the expression of CD16 was found to be higher in the blood and spleen of SCID mice. In addition to the three populations identified above, $F4/80^{+}$ splenic macrophages were also identified, where similar differences in CD16 expression was seen. Additionally, FcγRIV was more highly expressed on splenic macrophages in SCID mice compared to NOD SCID. The expression of CD64 was also investigated, where it appeared that expression was higher in SCID mice for all cell populations investigated. However, NOD SCID mice contain a polymoprhic variation in CD64, which has previously been reported not to affect expression level. It is therefore possible that the low expression observed here for CD64 in NOD SCID mice was as a result of the polymorphism preventing binding of the CD64 specific $F(ab')_2$.

In addition to spleen and blood, BMDMs were also differentiated by culturing bone marrow from SCID and NOD SCID mice with L929 conditioned media for 7 days. Following differentiation, BMDMs were stained with receptor specific FITC labelled $F(ab')_2$ and the expression of FcγRs assessed by flow cytometry. These results in Figure 6.11 suggest that CD16, CD32 and FcRIV expression was comparable between BMDMs from SCID and NOD SCID mice. It also appeared that CD64 expression was lower on BMDMs from NOD SCID mice. However, as previously mentioned, this could be a result of a polymorphism in CD64 in NOD SCID mice. Overall, these results suggest that there are few major differences in FcγR expression between the two strains of mice; it is therefore unlikely that FcγR expression was responsible for faster antibody clearance in NOD SCID mice.

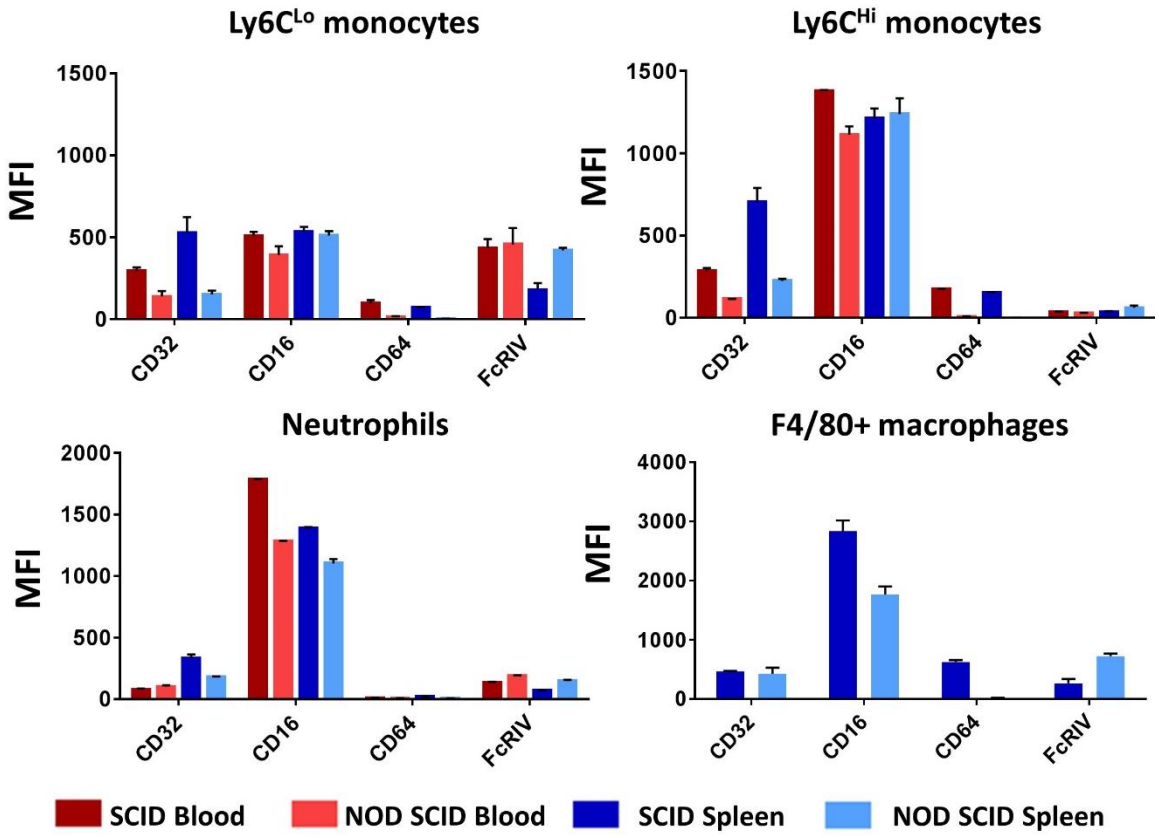

Figure 6.10 ***Expression of FcγRs on monocytes, neutrophils and macrophages from SCID and NOD SCID mice.***

Using the gating strategy described previously, spleen and blood from SCID and NOD SCID mice were stained for FcγR expression using receptor specific FITC labelled $F(ab')_2$ at 10μg/ml final concentration. Results show mean and range from 2 mice per strain, representative of 2 independent experiments. Results suggests SCID mice have a higher expression of CD32 on monocytes as well as a higher expression of CD16 on neutrophils. The CD64 expression level cannot be fully interpreted due to the possibility that polymorphic variation may affect $F(ab')_2$ binding.

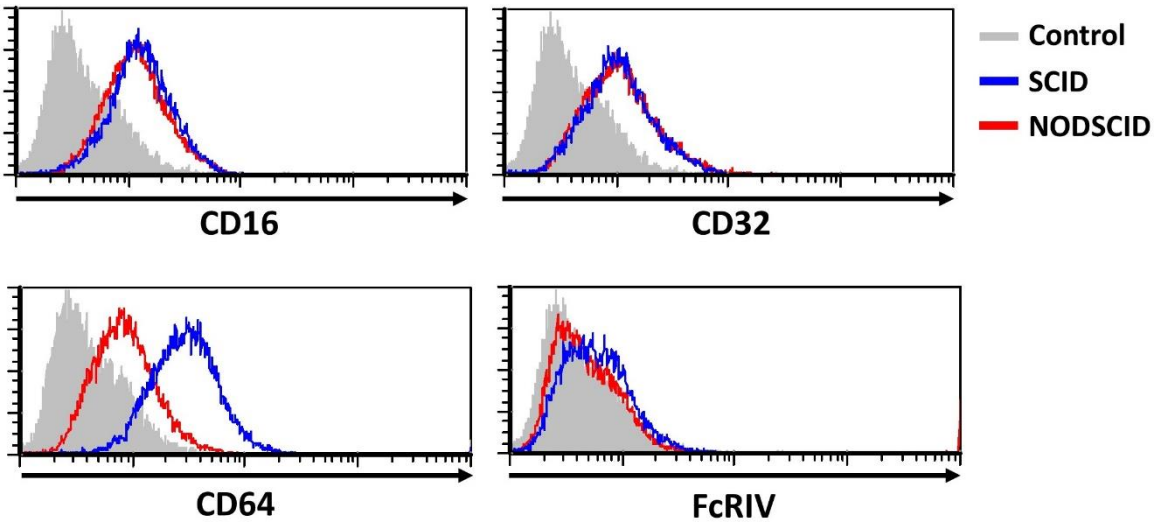

Figure 6.11 ***FcγR expression on SCID and NOD SCID BMDMs.***
Bone marrow was extracted from the hind legs of SCID and NOD SCID mice. Cells were cultured at 4x10^6 cells/well in a 6-well plate with 20% L929 conditioned media. After 7 days BMDMs were harvested by incubating with PBS +2mM EDTA and light scraping. BMDMs were resuspended at 1x10^6 cells/ml and 200µl cell suspension stained with receptor specific FITC labelled F(ab')$_2$ or irrelevant control. Results are representative of 3 independent experiments and demonstrate that CD16, CD32 and FcRIV was comparable between SCID and NOD SCID mice. CD64 expression appears to be lower in NOD SCID mice however this could be due to polymorphic variation limiting F(ab')$_2$ binding to NOD SCID CD64.

6.8 FcγR requirement for altered antibody clearance in NOD SCID mice

Having established that FcγRs are important for antibody clearance in NOD SCID mice, further investigations were conducted to determine which specific receptors were responsible. Initially, the clearance of antibody in NOD SCID mice lacking expression of the FcR γ-chain was investigated. These mice do not express activatory FcγRs but maintain expression of the inhibitory FcγR, CD32. 100µg Herceptin hIgG1 was administered to NOD SCID γ-/- mice i.v. and the concentration of hIgG in the plasma was determined by ELISA. The results in Figure 6.12 show that there were no significant differences in hIgG concentration between NOD SCID and NOD SCID γ-/- mice, with both strains having a rapid clearance of Herceptin hIgG1 from the plasma. As mice lacking the FcR γ-chain do not express activatory FcγRs on the cell surface, this result suggested that activatory FcγRs are not responsible for the altered clearance of Herceptin by NOD SCID mice.

Mice lacking the FcR γ-chain still maintain the expression of the inhibitory FcγR, CD32; to confirm whether this receptor was able to alter the clearance of hIgG1, experiments were performed in NOD SCID CD32-/- mice. Additionally, experiments were performed in NOD SCID CD32-/- hFcγRIIb +/- mice where the human transgene for the inhibitory FcγR is expressed in place of the mouse.

Mice were injected with 100µg cetuximab i.v. and the concentration of human IgG determined in the plasma by ELISA.

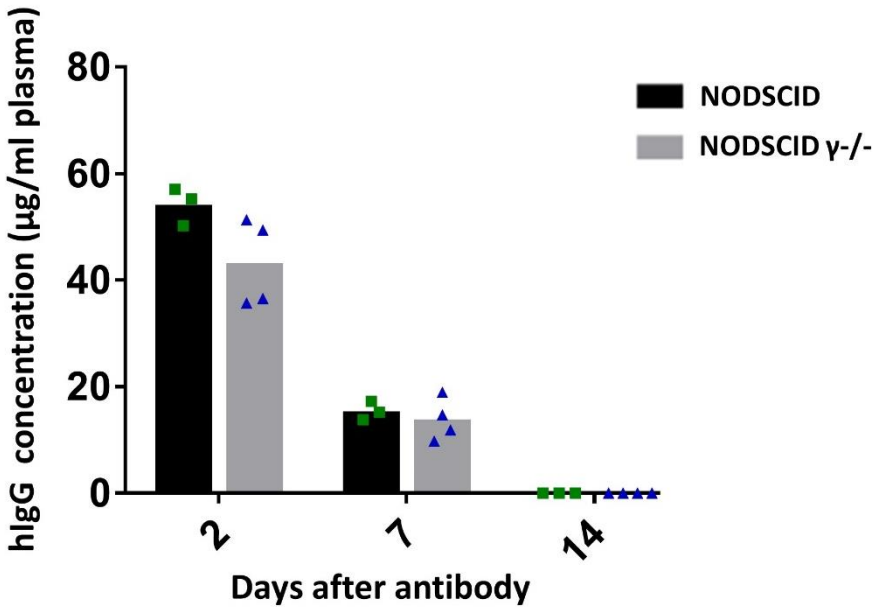

Figure 6.12 ***Herceptin clearance in NOD SCID and NOD SCID γ-/- mice.***
100µg Herceptin was injected i.v. into NOD SCID or NOD SCID γ-/- mice. The concentration of hIgG in the plasma of these mice was determined by ELISA. Concentrations were not significantly different between strains at any time point (2-way ANOVA with multiple comparisons). Bars represent mean with points for individual mice, N=4 per group.

Results in Figure 6.13a were from a single experiment with the absolute concentration of hIgG presented with points for individual mice. Figure 6.13b shows combined data from two independent experiments; one where cetuximab hIgG1 was administered and one with Herceptin hIgG1, with the data normalised so that concentrations of hIgG on day two were 100%. Both of these results confirm those seen previously, that seven days after mAb there was a higher concentration of hIgG in the plasma of SCID mice compared to NOD SCID. At the same time point, mice lacking mCD32 had a significantly higher concentration of hIgG in their plasma than NOD SCID mice, whilst values in NOD SCID CD32-/- mice are not significantly different to those from SCID mice. By day 14 after mAb administration, hIgG was no longer detectable in the plasma of NOD SCID mice whilst It was still detectable in mice lacking mCD32. Furthermore, when the mouse CD32 gene was absent but the human FcγRIIb (CD32b) transgene was expressed, hIgG levels were still significantly higher than in NOD SCID mice. These results suggest that expression of mCD32 in NOD SCID mice reduced the persistence of antibody in NOD SCID mice. This increased antibody clearance does not occur when mouse CD32 is replaced by the hFcγRIIb transgene, suggesting that the effect is specific to the CD32 gene in NOD SCID mice rather than a general property of inhibitory FcγR expression on the NOD SCID background.

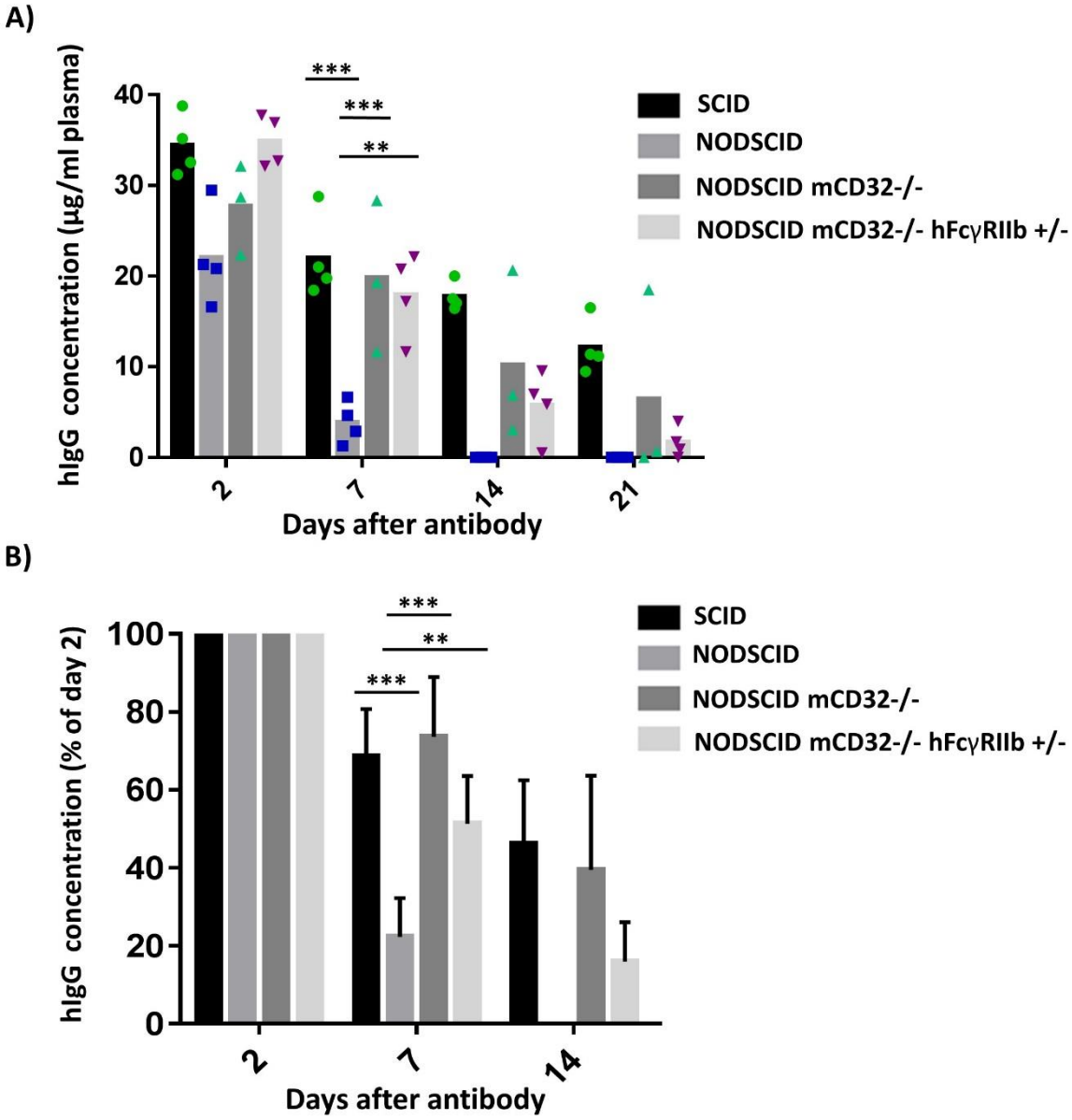

Figure 6.13 ***Clearance of hIgG1 in mice lacking mCD32.***

*100µg cetuximab was injected i.v. into SCID, NOD SCID, NOD SCID mCD32-/- or NOD SCID mCD32-/- hFcγRIIb+/- mice. Mice were bled and plasma collected, the concentration of human IgG in the plasma was determined by ELISA. A) Results for a single experiment, bars represent mean with points for individual mice (N=3-4 per group). At day 7 NOD SCID mice had a significantly lower concentration of hIgG in the plasma compared to SCID, NOD SCID mCD32-/- or NOD SCID mCD32-/- hFcγRIIb+/- mice. (2-way ANOVA with multiple comparisons; **P<0.01, ***P<0.001). By day 14 the concentration of hIgG in the plasma of NOD SCID mice was below the detectable limit for the assay. B) Normalised results from 2 independent experiments one using cetuximab and one with Herceptin. The concentration of plasma hIgG was normalised to the concentration at day 2 for each mouse. At day 7 the proportion of hIgG in the plasma was significantly lower in NOD SCID mice than in the other strains investigated. mean±SD.*

6.9 Sequencing of mouse CD32; gene and promoter

Previous studies identified a haplotype present in mCD32; strains such as C57BL/6 and BALB/c express the ly17.2 haplotype whilst strains including NOD express the ly17.1 haplotype.[306] In order to confirm the haplotypes of CD32 in SCID and NOD SCID mice, mRNA was isolated from BMDMs differentiated from SCID and NOD SCID mice before being converted to cDNA. Gene specific primers were used to amplify the CD32 gene from both mice by PCR with the reaction run on an agarose gel (Figure 6.14). As can be seen, bands were present at approximately 1kb, corresponding to CD32, suggesting that the gene was successfully isolated from both strains. There are two bands present in each lane which are likely to correspond to CD32b1 and CD32b2, with the b1 isoform containing an additional 141bp.

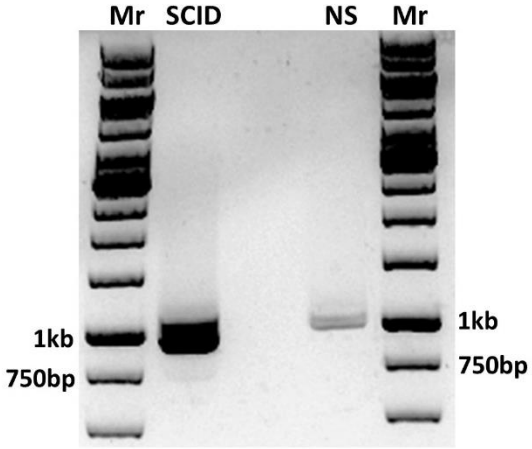

Figure 6.14 ***PCR to isolate CD32 gene from SCID and NOD SCID mice.***
BMDMs were derived from SCID and NOD SCID (NS) mice and mRNA isolated using poly(A) resin, reverse transcription was performed to generate a cDNA library for both mice. PCR was performed using cDNA and gene specific primers to amplify CD32. The PCR products were run on a 0.7% agarose gel giving bands at approximately 1kb, corresponding to the CD32 gene.

The bands corresponding to CD32 in SCID and NOD SCID mice were excised from the gel and the DNA was extracted before being blunt-end ligated into the pCR BluntII-TOPO. The genes were subsequently sequenced using the T7 and SP6 primers. Sequencing confirmed that SCID mice express the ly17.2 haplotype of CD32 whilst NOD SCID mice express the ly17.1 haplotype. The amino acid substitutions in the two variants are summarised in Figure 6.15. This demonstrates that sequence differences result in four amino acid substitutions; three are extracellular and one is in the cytoplasmic domain. With no previous studies describing this polymorphism affecting IgG binding, this variation was further investigated as a possible reason for altered mAb clearance in NOD SCID mice.

Amino acid	116	161	166	258
Ly17.1 (NOD SCID)	Pro	Gln	Thr	Ile
Ly17.2 (SCID)	Leu	Leu	Pro	Ser

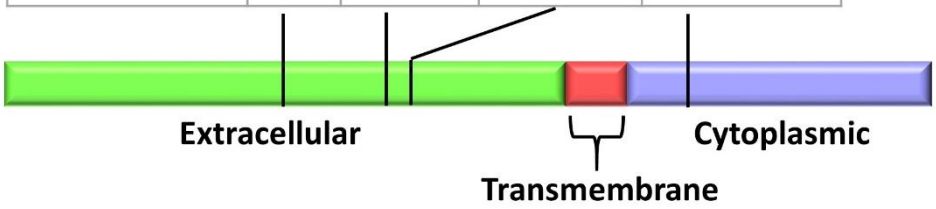

Figure 6.15 ***Ly17 haplotype in mouse CD32****.*
The mouse CD32 gene was isolated from BMDMs from SCID and NOD SCID mice and blunt end ligated into pCR BluntII TOPO before Sanger sequencing was performed using the T7 forward and SP6 primers. This confirmed that NOD SCID mice contained the ly17.1 haplotype whilst SCID mice were ly17.2. The 2 haplotypes differ by 4 amino acids, 3 in the extracellular region and 1 in the cytoplasmic domain.

6.10 Aggregated and monomeric IgG binding to mCD32

With sequencing confirming polymorphic variation in CD32 between SCID and NOD SCID mice, further investigation was carried out on the receptors in isolation in order to understand how variation could contribute to the observed differences in mAb clearance. The primary function of CD32 is to bind to IgG; given that three of the identified polymorphisms are in the extracellular region of the receptor, it is possible that variation may alter IgG binding. The previously isolated mCD32 genes were therefore subcloned into the expression vector pcDNA3 and transiently transfected into 293F cells. Transfection was confirmed using AT130-2 $F(ab')_2$ and the binding of aggregated or monomeric IgG investigated using a range of concentrations. Whilst mouse CD32 normally binds to mIgG, this study focuses on the clearance of hIgG mAbs, therefore the binding of monomeric and aggregated hIgG to mCD32 was investigated. Pooled human IgG was heat aggregated, with the monomeric and aggregated fractions separated by size exclusion chromatography; with both fractions subsequently fluorescently labelled with Alexafluor488.

The transfection was variable between the two haplotypes of mCD32, therefore results were normalised so that MFI obtained with AT130-2 $F(ab')_2$ was set as 100%. To account for this variability, Figure 6.16 presents a representative example from three independent transfections, with the same trends observed on each occasion. The binding of monomeric IgG (Figure 6.16a)

appeared to be higher to cells transfected with the NOD SCID (ly17.1) variant of CD32 than to the SCID (ly17.2) form. This was particularly apparent at concentrations between 0.5 and 10 µg/ml. Similarly, aggregated hIgG (Figure 6.16b) appeared to bind to NOD SCID mCD32 more efficiently than to the SCID variant. This suggests that CD32 in NOD SCID mice may be able to bind to hIgG more efficiently than that in SCID mice, which could have an effect on the persistence of mAb within the mice.

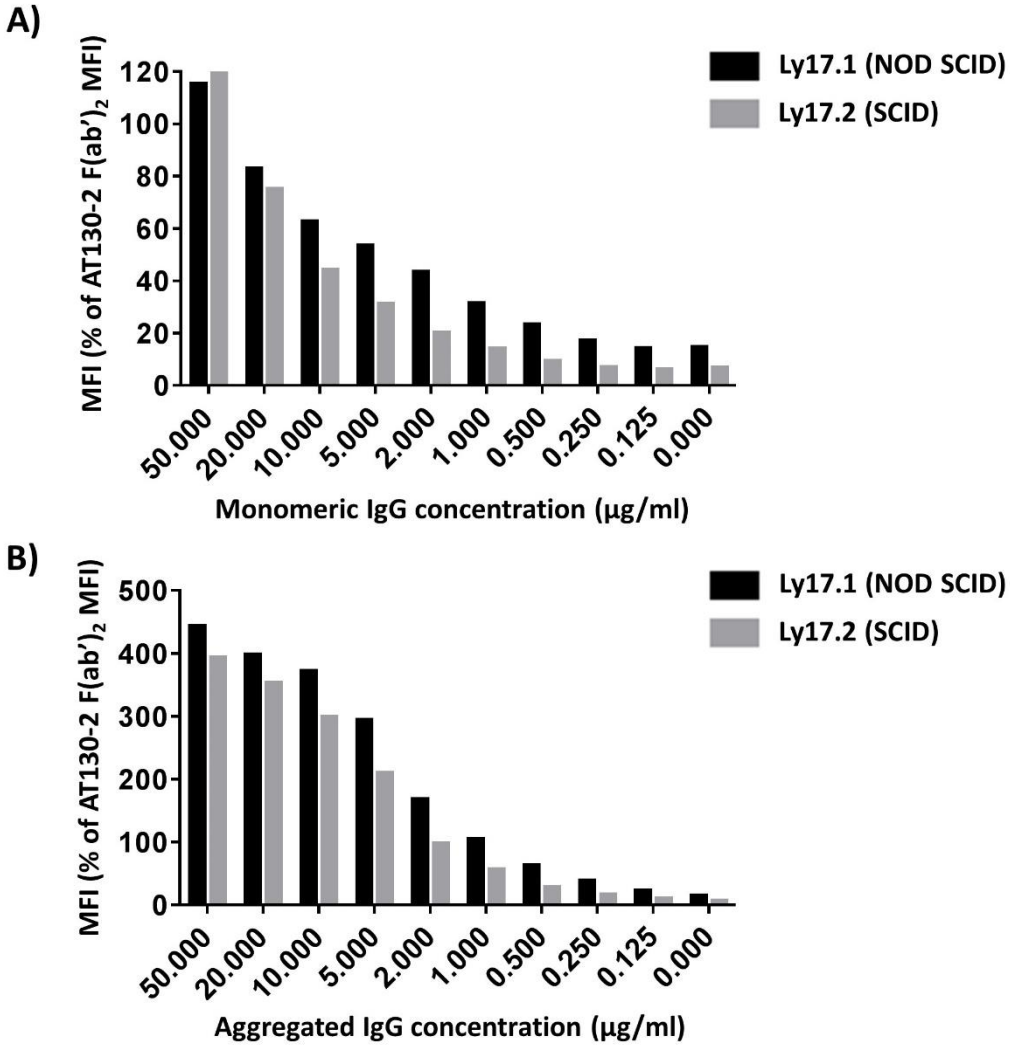

Figure 6.16 ***Binding of hIgG to 293F cells expressing mCD32 polymorphic variants.***

293F cells were transiently transfected with the polymorphic variants of mCD32 (ly17.1 and ly17.2) 48 hours after transfection the binding of A488 labelled monomeric (A) or aggregated (B) pooled hIgG was incubated with transfected cells for 15 minutes at room temperature at the concentrations indicated. Cells were washed once and binding determined by flow cytometry. Results were normalised so the MFI obtained by staining with AT130-2 F(ab')$_2$ was set at 100%. Results are representative of 3 independent experiments and suggest that a higher relative MFI was obtained when monomeric or aggregated IgG is incubated with cells expressing ly17.1 compared to the same concentration on ly17.2 transfected cells. This implies more efficient binding to this polymorphic variant of mCD32.

6.11 Generating soluble mouse CD32

The results obtained here suggest that the polymorphic variants of mCD32 vary in their binding to hIgG when expressed on the cell's surface. In order to further investigate binding, purified mCD32 was required. As the protein is normally membrane bound, only the extracellular region (residues 1-207) was produced.

6.11.1 Expression and purification of mCD32

PCR was performed on the previously isolated full length mCD32 gene in the pcDNA3 vector. PCR was performed with specific primers in order to amplify the region of the gene encoding for amino acids 1-207 representing the extracellular domain. The resulting PCR product was cloned into the pDSG-IBA vector incorporating a C-terminal 6xHIS tag. The constructs were then transfected into MEXI 293E cells using PEI as a transfection reagent and incubated for seven days to allow for protein production, after which the supernatant was harvested by centrifugation and filtration before being stored at 4°C. mCD32 was purified from the supernatant using a HisTrap HP column. Following column washing, HIS tagged protein was eluted using 250mM imidazole. Figure 6.7 shows the trace from the purification of ly17.1 with the blue line showing the absorbance at 280nm. This demonstrates that a high absorbance was seen for the flow though when the supernatant was loaded with a small peak during washing with 20mM imidazole. Finally, a peak in A_{280} was observed following addition of 250mM imidazole, indicating that protein specifically bound to the column was eluted. A similar plot was obtained for the purification of ly1.2 (data not shown) suggesting that both variants of mCD32 had been produced.

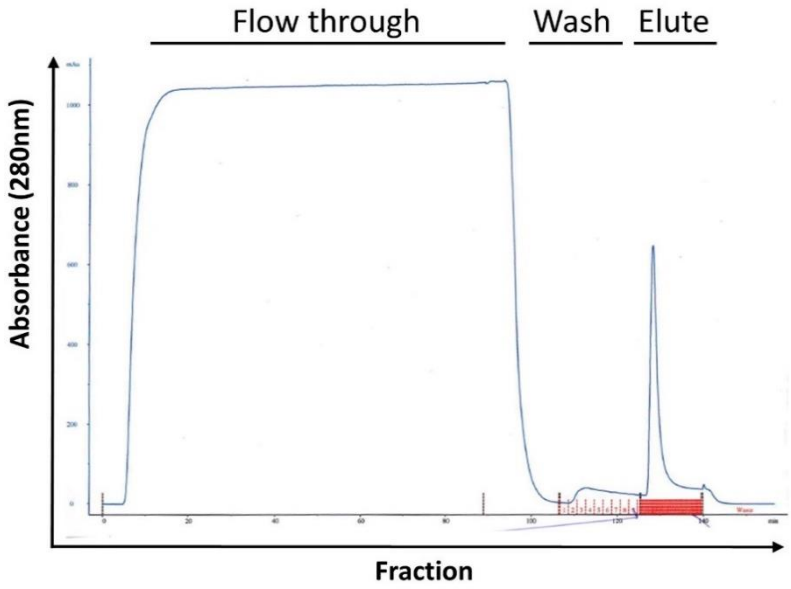

Figure 6.17 ***Purification of mCD32, extracellular domain****.*
Plasmid DNA encoding for the extracellular region of mCD32 (residues 1-207) was transfected into MEXI 293E cells using PEI. 7 days after transfection and once cell viability had dropped below 75%, supernatant was harvested by centrifugation and filtration. Imidazole was added to the supernatant at a final concentration of 10mM. The supernatant was flowed through a 1ml HisTrap HP column before being washed with 20mM imidazole. Bound protein was eluted with 250mM Imidazole at the point indicated by a tight peak corresponding to protein specifically bound to the column.

In order to confirm the purity of the protein, several fractions were run on a 12% SDS-PAGE gel along with a sample of supernatant (starting), flow through (FT) and material from the wash of the column. The gel was stained with coomassie blue and destained to allow the protein bands to be visualised. The expected molecular weight of the processed HIS tagged protein was 21.1 kDa (determined from sequence by ProtParam, ExPASy; http://web.expasy.org/protparam). Figure 6.18 shows that there was a smear visible on the gel between 30-40kDa for both ly17.1 and ly17.2. This was present in the purified fractions and, to a lesser extent, in the flow through and wash sample. This smear was the only species visible in the unpurified culture supernatant, suggesting that it was present in a large quantity. Following purification, the fractions corresponding to the eluted protein were pooled and concentrated to a volume of 4-5ml using a spin concentrator before dialysis into PBS, the total purified protein yield was 4.8mg for ly17.1 and 3.2mg for ly17.2 as determined by nanodrop.

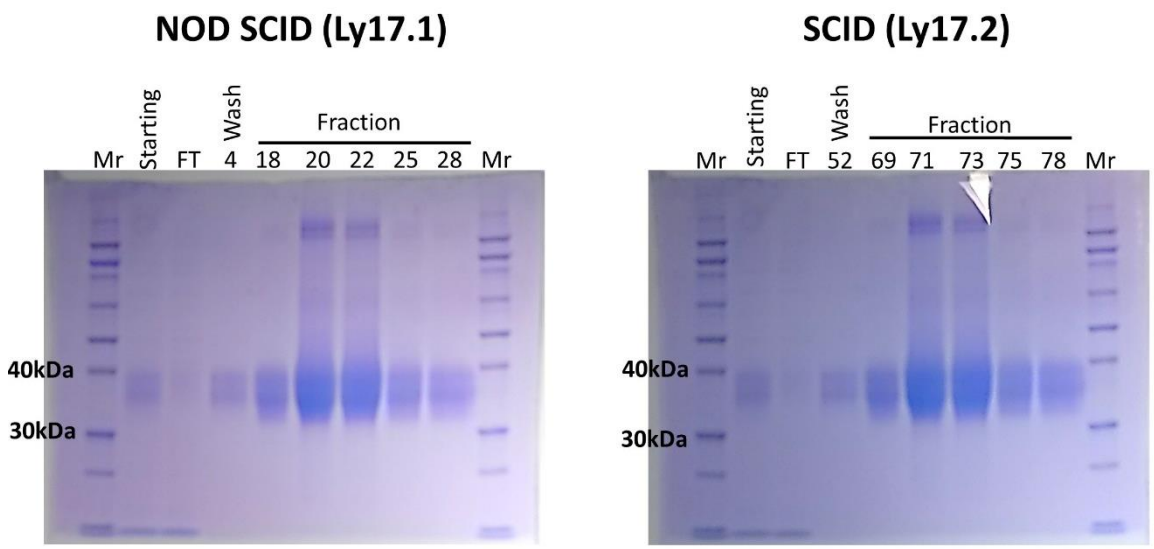

Figure 6.18 ***SDS-PAGE gel of purified mCD32 polymorphic variants.***
Following purification samples of were run on a 12% SDS-PAGE gel. A sample of the culture supernatant (starting), column flow through (FT) a fraction corresponding to the wash step and several fractions of the eluted protein were loaded onto the gel and run at 100v. The gel was stained with coomassie blue and detained. A smear was observed between 30-40kDA for both variants of mCD32 in the eluted fractions. A fainter band was seen at the same molecular weight in the starting material, FT and collected wash buffer.

6.11.2 Deglycosylation of purified mCD32

It is clear from the SDS-PAGE gel in Figure 6.8 that the major band present in the purified protein was at a higher molecular weight than the expected 21kDa and was a smear rather than a tight band. This discrepancy could have been due to glycosylation of the receptor, therefore the purified protein was enzymatically deglycosylated.

Deglycosylation of mCD32 was performed using PNGase F under reducing conditions; this enzyme is able to cleave N-linked glycans from the receptor. Following PNGase treatment for 2 hours, samples of both variants of mCD32 were run on a 12% SDS-PAGE gel along with a sample of untreated material as well as flow through from the purification. Figure 6.19 demonstrates that, following N-glycan removal, a band was present at approximately 21kDa, corresponding to the calculated molecular weight of mCD32. An additional band was seen at a weight of approximately 35 kDa; this is likely to correspond to the PNGase F which was not removed from the reaction before analysis. The smear between 30-40 kDa present in the untreated, purified material was no longer visible after PNGase treatment. This suggests that the smear was caused by N-linked glycomodifications to mCD32, giving rise to species with a range of molecular weight. Upon removal, a species was obtained with the expected molecular weight. Following PNGase

treatment, an additional band was observed at approximately 29kDa for ly17.1 as well as a few minor contaminants. However, the major species present was at a molecular weight corresponding to mouse CD32.

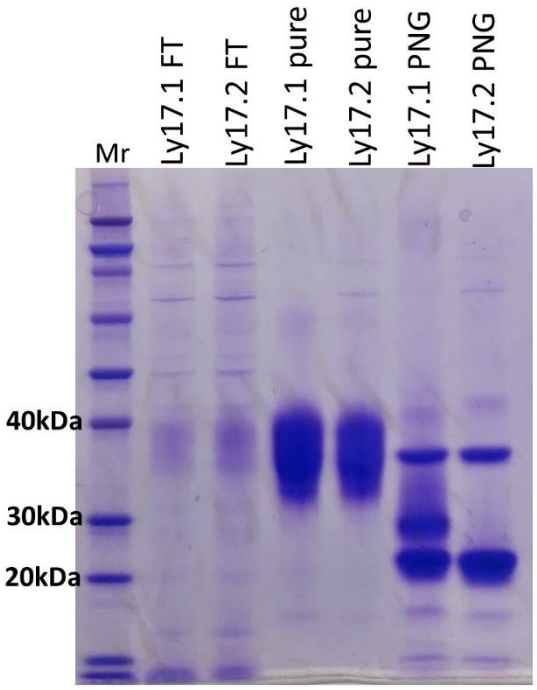

Figure 6.19 ***PNGase F treatment of purified mCD32.***
Purified mCD32 of both ly17.1 and ly17.2 haplotypes was treated overnight with PNGase F under reducing conditions before being run on a 12% SDS-PAGE gel under reducing conditions. Flow through (FT) from the purification and untreated purified protein were also run on the gel (pure). Following PNGase F treatment bands were seen at 21kDa corresponding to deglycosylated mCD32 in contrast to the band seen in the pure sample containing several glycovariants. A band was also observed at 35kDa corresponding to PNGase F with an unknown band at 28kDa in the ly17.1 PNGase treated sample.

6.12 Surface plasmon resonance (SPR) analysis of IgG binding to mouse CD32

In order to better understand the interaction between polymorphic variants of mCD32 and IgG, analysis of binding affinity was carried out by SPR. Initial experiments aimed to confirm that the purified proteins, comprising the extracellular regions of mCD32, could be recognised by receptor specific $F(ab')_2$. For all experiments, an anti-HIS capture antibody was immobilised on a CM5 Biacore chip. The purified receptor was flowed over the capture antibody at 10µg/ml. Following this the receptor specific $F(ab')_2$ AT130-2 or irrelevant control was flowed over the immobilised receptor and binding measured with the background binding subtracted. Figure 6.20 demonstrates that binding to mCD32, as determined by an increase in response units, only occurs

when using AT130-2 F(ab')$_2$ and not with the irrelevant control. This suggests that the protein produced was correctly folded and is capable of being recognised by specific reagents.

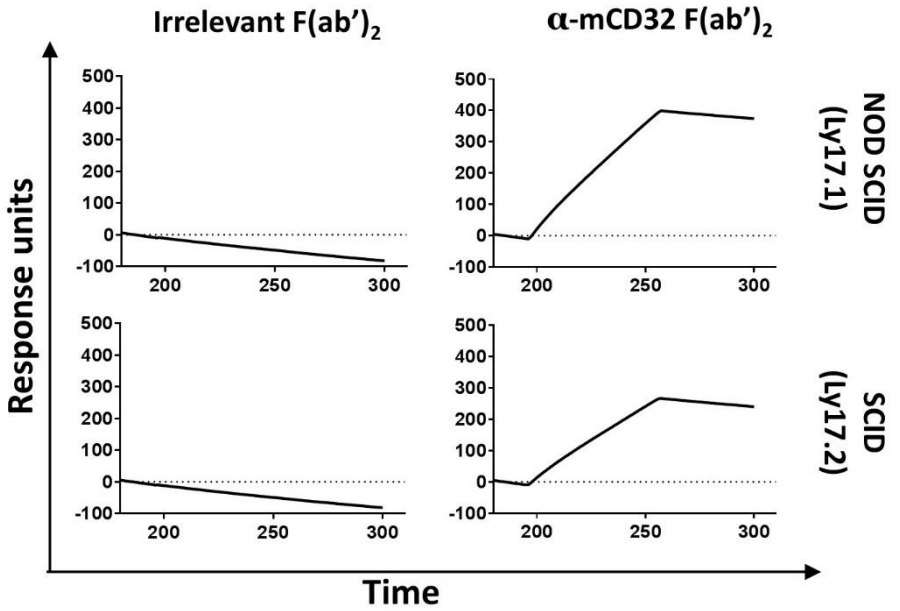

Figure 6.20 ***Biacore results for receptor specific binding to mCD32.***
Purified mouse CD32 (ly17.1 or ly17.2) was captured on a CM5 chip using an immobilised anti-HIS antibody. Receptor specific F(ab')$_2$ (AT130-2) or an irrelevant control were flowed over the chip and response measure on a Biacore T100 instrument. Only AT130-2 gave an increase in response units, representative of binding. This was seen with both variants of mCD32.

Having established that the binding of receptor specific reagents to mCD32 could be detected, next the interaction between mCD32 and IgG was investigated. As before mCD32 was captured on the Biacore sensor chip via its HIS tag, IgG was then flowed over the chip at concentrations ranging from 3000-187.25nM. Figure 6.21a presents representative sensograms for the binding of cetuximab hIgG1 to both variants of mCD32. This indicates that with increasing mAb concentration, a greater response is seen; the overall response also appears to be higher for NOD SCID than for SCID mCD32. Subsequently, the binding of aggregated, pooled human IgG1 was investigated (Figure 6.21b). The KD was found to be slightly higher for aggregated IgG binding to SCID than to NOD SCID mCD32 (1.519 x10^{-7}M v 1.311 x10^{-7}M) suggesting NOD SCID variant may have an increased affinity for aggregated IgG. Additionally, the affinity of each receptor variant for IgG of defined isotypes was also investigated (Figure 6.21c). NOD SCID mCD32 was found to have a higher affinity for the IgG1 than the SCID variant as determined by the KD for cetuximab (4.380 x10^{-6}M v 5.424 x10^{-6}M) and rituximab (2.500 x10^{-6}M v 3.138 x10^{-6}M). This suggests that mCD32 in NOD SCID mice may have a higher affinity for hIgG1 the receptor expressed in SCID mice. However, it will need to be confirmed if this result is reproducible across multiple experiments. The

differences observed between the receptor variants were more minimal for all other observed IgG isotypes investigated.

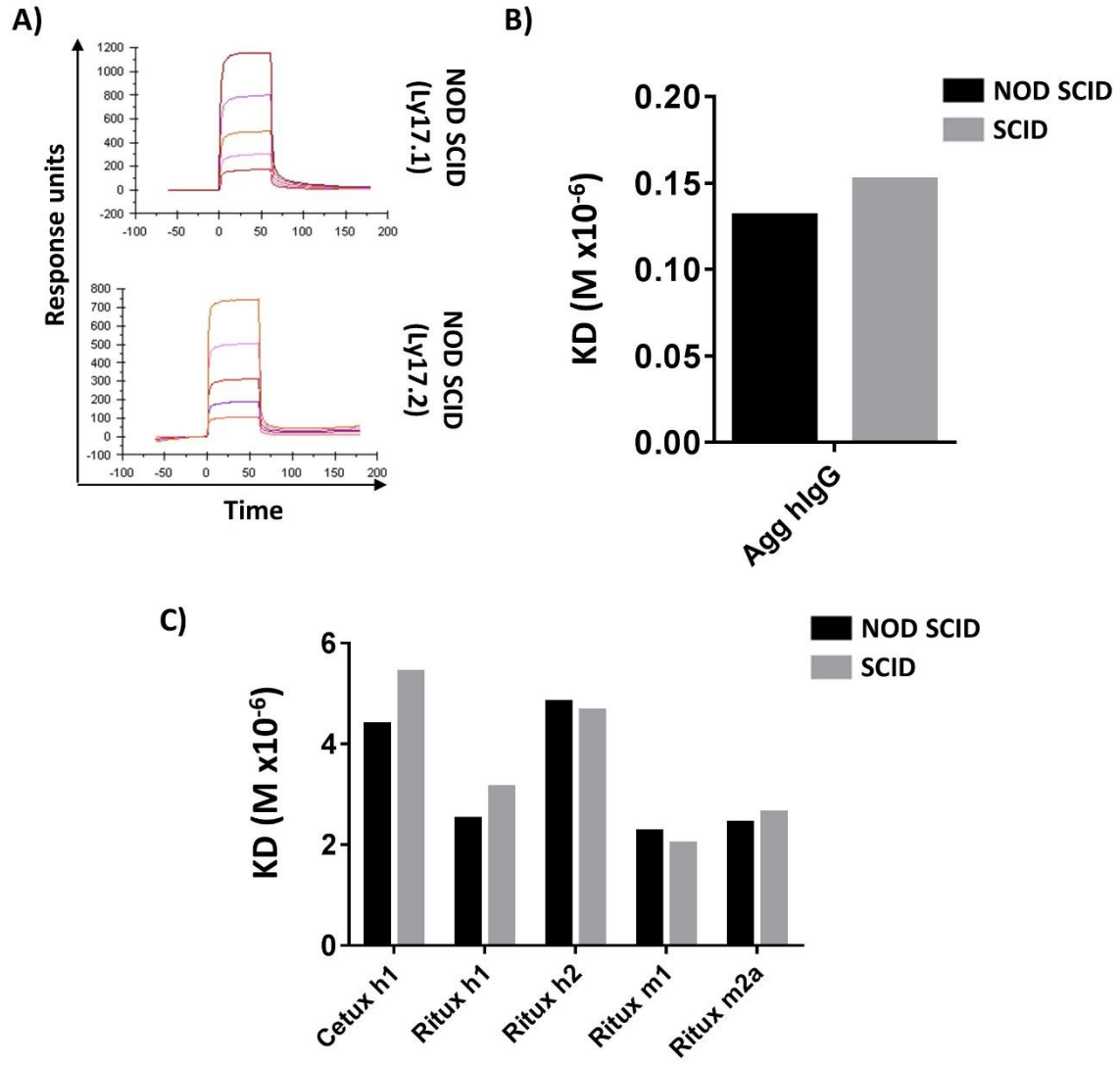

Figure 6.21 ***Biacore analysis of IgG binding to mCD32 variants****.*

Polymorphic variants of mCD32 (ly17.1 or ly17.2) were captured on a Biacore CM5 sensor chip using an immobilised anti-HIS antibody. Monomeric or aggregated IgG was then flowed over the chip and used to calculate the KD. A) Example sensograms for the addition of cetuximab to captured mCD32. Cetuximab was used at (from top down) 3000, 1500, 750, 375 and 187.5nM. B) Binding of pooled aggregated human IgG (agg hIgG) which was used at 2000, 1000, 500, 250 and 125nM with the steady state affinity calculated. C) Steady state affinities for monomeric IgG, cetuximab (cetux) or rituximab (ritux) were used as human IgG1 (h1), human IgG2 (h2), mouse IgG1 (m1) or mouse IgG2a (m2a) at the same concentrations as in panel A.

6.13 Bone marrow chimera

With polymorphic variation in mCD32 established as the most likely candidate for the abnormal mAb clearance observed in NOD SCID mice, the cell populations responsible for the clearance were investigated by generating the bone marrow chimera. The aim of this was to differentiate between CD32 present on haematopoietic and non-haematopoietic cells.

6.13.1 Design, generation and phenotyping of mCD32-/- chimeric mice

The chimera was designed with the aim of generating mice that expressed NOD SCID mCD32 (Ly17.1) on their non-haematopoietic cells with no CD32 expression on haematopoietic cells. The schematic for the generation of the bone marrow chimera can be seen in Figure 6.22. NOD SCID mice were sedated and irradiated with 1.5Gy X-ray radiation on day -1 and 0. After recovery, mice were injected with $6x10^6$ bone marrow cells taken from BALB/c CD32-/- donors. Mice were allowed to recover before being screened to confirm bone marrow engraftment 6-8 weeks later.

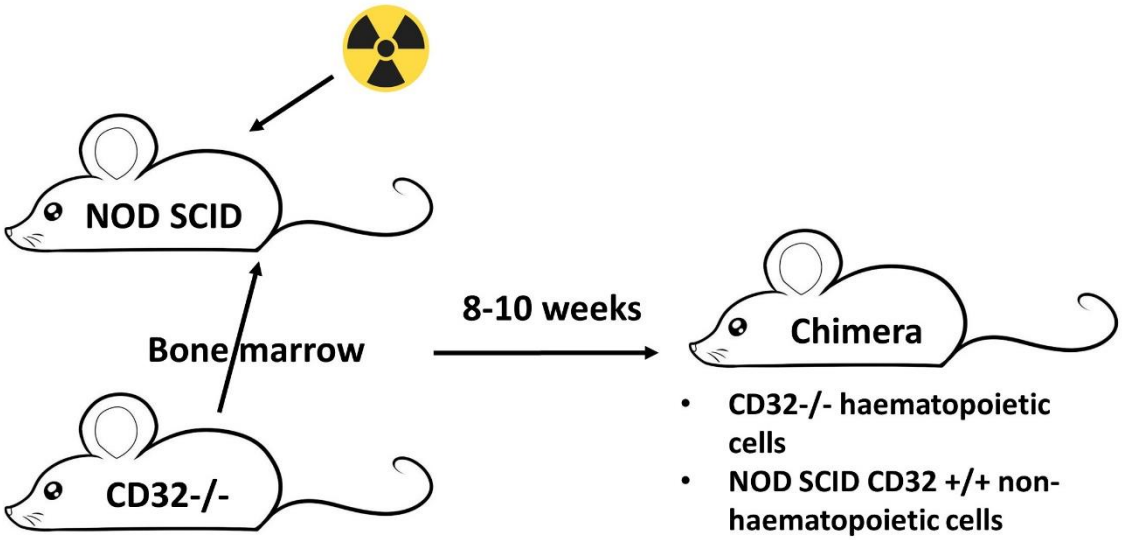

Figure 6.22 ***Design of mouse CD32 bone marrow chimera.***
NOD SCID mice were sedated and given 1.5Gy X-ray radiation on day -1 and 0. Bone marrow was harvested from the hind legs of BALB/c CD32-/- and a single cells suspension obtained, $6x10^6$ cells were injected i.v. into irradiated NOD SCID mice. Bone marrow was allowed to engraft for 8-10 weeks before mice were screened to confirm engraftment.

To determine whether donor bone marrow had engrafted in NOD SCID mice, chimera were bled and stained with fluorescently labelled mAbs against CD14, CD19 and CD32, before being analysed

by flow cytometry. Figure 6.23a shows that B cells ($CD19^+$) were detectable in the blood of chimera mice but were not present in NOD SCID mice. Importantly, these B cells did not have expression of CD32. Furthermore, $CD14^+$ monocytes were also present with no detectable expression of CD32 (Figure 6.23b). This is in contrast to NOD mice which had clear expression of CD32 on B cells and monocytes. Taken together, these results suggest that the bone marrow chimera were generated successfully with CD32-/- haematopoietic cells engrafted into NOD SCID mice.

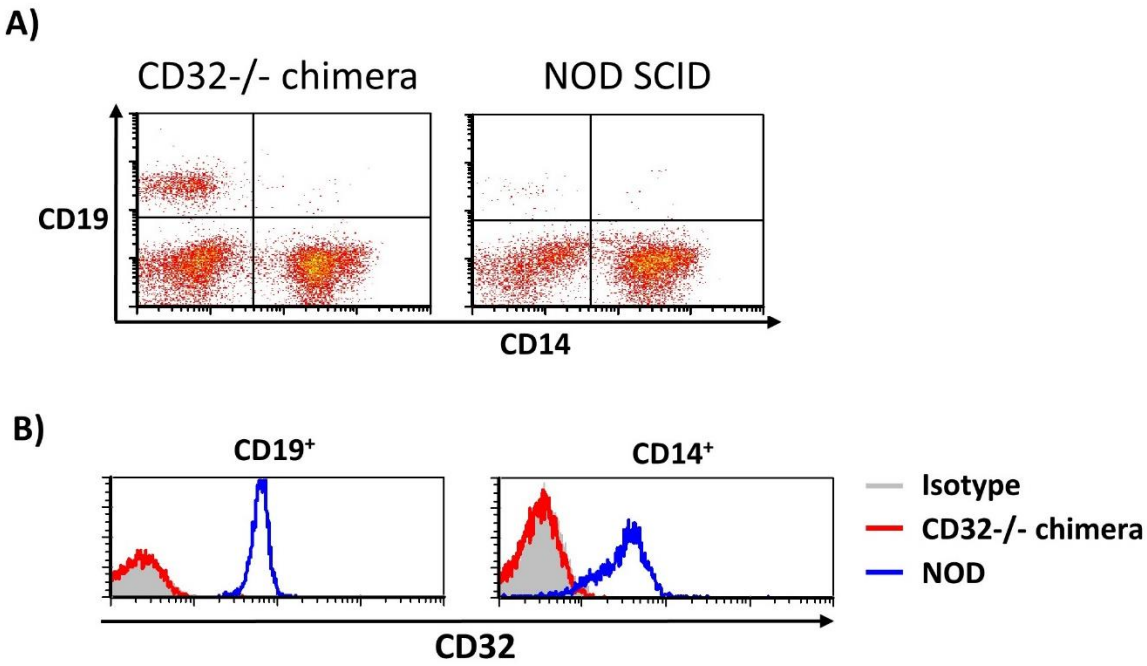

Figure 6.23 ***Flow cytometry analysis of bone marrow chimera.***
Blood was collected from NOD SCID mice 8 weeks after reconstitution with CD32-/- bone marrow. Blood was stained with fluorescently labelled mAbs against CD19, CD14 and CD32 before being analysed by flow cytometry. Live cells were gated based on forward and side scatter as before. A) staining for CD19 and CD14 from a NOD SID and CD32-/- chimera mouse. B) The expression of CD32 on the surface of $CD19^+$ B cells and $CD14^+$ monocytes from a CD32-/- chimera and a NOD mouse. Plots are representative of all chimera generated.

6.13.2 Antibody clearance in bone marrow chimera

To investigate the clearance of hIgG1 from the plasma of these chimeric mice and to investigate the cell types responsible for abnormal clearance in NOD SCID mice, 100µg cetuximab hIgG1 was injected i.v. into SCID, NOD SCID and CD32-/- chimera mice. The concentration of hIgG in the plasma was determined by ELISA, with the results presented in Figure 6.24. This shows that, at day seven, chimera mice had a significantly higher concentration of hIgG in their plasma than NOD SCID mice. This suggests that generating a chimera was able to overcome the faster mAb clearance observed in NOD SCID mice. Interestingly, chimera mice had significantly less circulating IgG at day

seven than SCID mice; suggesting that the chimera is unable to fully restore mAb persistence to that observed in SCID mice. However, there was one major confounding factor in these experiments; quantification of mouse IgG in chimera mice revealed a high concentration of mIgG. Figure 6.25 demonstrates that the average concentration of mIgG in BALB/c mice was 423µg/ml compared to 1735µg/ml in CD32-/- chimera mice. In one mouse, the concentration of mIgG was as high as 3584µg/ml. Additionally, chimera mice displayed symptoms of autoimmunity, likely to be due to the high mIgG titre. This result means that there were two variables between NOD SCID mice and chimera; the altered CD32 expression pattern and elevated mIgG, making it difficult to deduce the mechanisms behind the changed phenotype in the chimera.

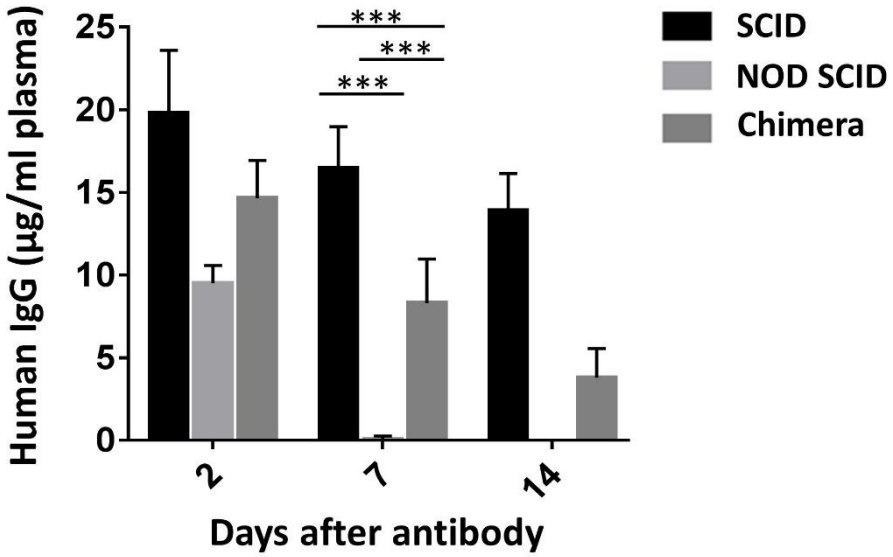

Figure 6.24 ***Clearance of antibody from CD32 bone marrow chimera.***
*100µg cetuximab was injected i.v. into SCID, NOD SCID or CD32 bone marrow chimera mice. Mice were bled and plasma collected, the concentration of hIgG in the plasma was determined by ELISA. At day 7 NOD SCID mice had a significantly lower concentration of hIgG in their plasma than SCID or Chimera mice. Chimera mice also had a significantly lower concentration than SCID mice (2-way ANOVA with multiple comparisons; ***P<0.001). Bars present mean +SD, N= 4-8 per group.*

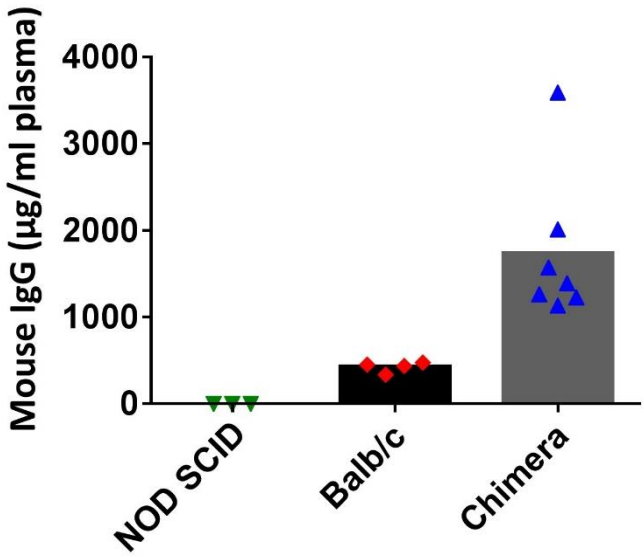

Figure 6.25 ***Concentration of mouse IgG in the plasma of bone marrow chimera mice.*** *Following the generation of bone marrow chimera, plasma was collected from chimera mice, BALB/c and NOD SCID mice. The concentration of mIgG in the plasma was determined by ELISA. There was no detectable mIgG in NOD SCID mice. Bars show mean with points for individual mice N=3-7.*

6.14 Chapter discussion

In this chapter, the abnormally rapid clearance of certain mAb isotypes from the plasma of NOD SCID mice was investigated. This was based on the initial observation in the Tcl-1 hCD20 model where, 14 days after anti-hCD20 therapy, tumour cells had returned in NOD SCID mice but not in SCID mice. Investigating the concentration of the isotype control found that it was present at a significantly lower concentration in the plasma of NOD SCID mice compared to SCID mice seven days after treatment, with similar observations for tumour targeting anti-hCD20 mAbs. The occurrence of this phenomenon, with the isotype control Herceptin antibody, suggested that the abnormal clearance was not related to the mAb binding its antigen on the tumour. This has been briefly reported previously where human IgG1 or chimeric mAbs with a hIgG1 Fc were found to have a shorter half-life in NOD SCID mice. [492]

Subsequent experiments revealed that this abnormal clearance occurred in the absence of tumour cells and suggested that it was isotype dependent. All hIgG1 mAbs investigated throughout this chapter (cetuximab, rituximab and Herceptin) were cleared rapidly from the plasma of NOD SCID mice as well as mIgG2a whereas hIgG2 and mIgG1 were cleared at comparable rates between SCID and NOD SCID mice. This grouping of mAb isotypes was perhaps not surprising, with hIgG1 and

mIgG2a displaying similar functionality; both are efficient isotypes for direct targeting and have been demonstrated to have comparable binding to mouse FcγRs.[493, 494] mIgG1 has been found to be restricted in only binding efficiently to mCD32 and mCD16. In comparison, competition assays demonstrated that hIgG2 could compete with mouse IgG for binding to mCD32 and mCD16, comparable to results with mIgG1.[494] However, SPR has since revealed that hIgG2 displays very little binding to mFcγRs.[98] These results gave the first suggestion that altered mAb clearance in NOD SCID mice may be related to FcγR binding.

Previous data suggested that hIgG had a higher *in vitro* binding to macrophages from NOD SCID mice than those from other strains.[492] This previous work only constitutes a poster abstract so methodologies used to draw these conclusions are not clear, however based on this, the possible role of BMDMs in abnormal mAb half-life was explored. Initially non-specific uptake was investigated with bead phagocytosis assays suggesting that BMDMs from SCID mice had greater potential for non-specific uptake of material, the reverse of the pattern observed with mAb clearance *in vivo.* This result implies that non-specific phagocytosis of material was not responsible for abnormal mAb clearance in NOD SCID mice. Results from mAb internalisation assays suggest that the proportion of mAb internalised was greater for BMDMs from SCID mice than NOD SCID with mouse IgG2a, human IgG1 and human IgG2. However, this result was compounded by differences in the absolute binding levels to the cell surface (MFI), suggesting that there may be differences in the binding capacity of different BMDMs for IgG. This was particularly true for mouse IgG2a, where fluorescence was higher for SCID BMDMs, and additionally for human IgG1, where binding was found to be higher on NOD SCID BMDMs. This latter result was consistent with the previous study reporting abnormal IgG1 half-life in NOD SCID mice, stating that IgG has a higher *in vitro* binding to FcγRs on macrophages of NOD SCID mice, however the strains of mice used for comparison were not detailed. [492] However, the same study also suggested that there was no difference in the half-life of murine IgG, whereas here mouse IgG2a was found to be cleared more rapidly from the plasma of NOD SCID mice. The previous study did not state the methodologies used or the isotypes of mouse IgG investigated, which may account for the discrepancies regarding mouse IgG to the data reported here.

The requirement of FcγRs to facilitate abnormal mAb clearance was confirmed by using an N297Q mutant of rituximab. This mutation prevents N-linked glycosylation at amino acid 297, which inhibits binding to FcγRs and prevents Fc dependent effector mechanisms.[104] The effect of this mutation on binding to FcRn is less clear, this is the major receptor responsible for transporting IgG across the placenta as well as for extending the half-life of IgG in the serum.[387] Efficient

interaction with FcRn is essential for maintaining the serum concentration of IgG; the receptor scavenges IgG from the lysosome by way of having a high affinity in acidic environments before releasing IgG at a neutral pH.[395, 490] Crystal structures of hFcγRs and hFcRn with hIgG1 Fc identified hFcRn as binding to Fc between its C_H2 and C_H3 domains.[495] In contrast structural and mutational studies have identified residues clustered around the C_H2 domain and lower hinge as being important in the Fc:FcγR interaction.[496, 497] It is in this region where residue N297 is found, taken together this suggests hFcRn interacts with hIgG1 away from the mutated N297 residue. Importantly *in vivo* studies have demonstrated that the N297Q mutation does not alter hIgG half-life in mice In this chapter, when compared to wild type rituximab, the NQ mutant was cleared from the plasma of NOD SCID mice significantly slower than the wild type mAb.[104] Given that the mutation does not appear to alter the FcRn mediated half-life, this result suggests that abnormally fast hIgG clearance is dependent on the interaction between mAb Fc and FcγRs in NOD SCID mice.

One interesting observation was made previously regarding FcRn that hIgG1 retains binding to mouse FcRn at a neutral pH, albeit with a significantly lower affinity than at pH6.[498] This is in contrast to hFcRn, where binding to hIgG was virtually non-existent at pH7.2. Experiments should be performed to understand the affinity of the mouse and human IgG isotypes used here for mouse FcRn at different pH. This could help to explain the variation in half-life between different isotypes. Importantly, FcRn has been previously been shown in NOD SCID mice to contain no polymorphisms and to have no difference in hIgG binding compared to BALB/c mice.[492] This suggests that, whilst hIgG1 may interact differently between human and mouse FcRn, there is unlikely to be differences between binding in SCID and NOD SCID mice. Despite this, it will be important to investigate the expression level of FcRn and tissue distribution in NOD SCID mice to determine whether this has any influence on abnormal hIgG1 clearance. It is possible that reduced expression of FcRn could contribute to less efficient recycling of hIgG1, resulting in faster degradation. Whilst results using mCD32 knock-out mice suggest that abnormal clearance is not mediated by FcRn, further work is required to confirm that this is the case.

Furthermore, the reconstitution of NOD SCID mice with mIgG at concentrations found in BALB/c mice was also able to prevent abnormal hIgG1 clearance. The addition of mIgG to NOD SCID mice mimics the situation in NOD mice, which have normal mAb clearance, suggesting that the presence of circulating IgG can overcome abnormal mAb clearance, possibly through engaging and saturating FcγRs. This mechanism would be similar to one of the proposed mechanisms for the action of IVIG, where in autoimmunity the treatment has been proposed to act by inhibiting the binding of autoreactive antibodies to FcγRs, although this is still widely debated.[499, 500]

Having established that abnormal mAb clearance in NOD SCID mice was likely to be FcγR dependent, the expression levels of FcγRs was explored in SCID and NOD SCID mice. With previous studies suggesting that macrophages were the cell type responsible for the abnormal half-life of hIgG1, BMDMs and splenic macrophages were phenotyped, as well as monocytes and neutrophils. Two major subsets of mouse monocytes were investigated. Ly6C^{Hi} monocytes are considered to be proinflammatory with a high capacity for phagocytosis and potent TNFα production.[501, 502] In contrast, Ly6C^{Lo} monocytes patrol the luminal side of the endothelium in blood vessels and secrete the anti-inflammatory cytokine IL-10 following bacterial infection.[501, 503] FcγR phenotyping indicated splenic macrophages from SCID mice to have a higher expression of CD16 compared to NOD SCID, whilst FcγRIV had the opposite trend. It is possible that these differences are compensatory and do not result in any net change in the expression of activatory FcγRs. There was very low expression of CD64 on all cell types investigated from NOD SCID mice, especially when compared to expression in SCID mice. One explanation for this phenomenon is that NOD mice (and by association NOD SCID) contain a variant of mCD64 that differs from the canonical mCD64 sequence by 17 amino acids.[504] These mutations are spread throughout the protein an include a four amino acid insertion at the interface between extracellular domains two and three.[505] These extensive mutations are therefore likely to prevent recognition of the receptor by the reagents used for phenotyoping.[506] This variation in mCD64 has been found to result in a gain of function of CD64 in NOD mice, allowing increased binding to mIgG2b and mIgG3 compared to BALB/c CD64. This mutation was not found to alter mIgG2a binding; although affinity of the variant for hIgG1 has not been determined, the use of the γ-chain -/- mice here suggests that the variation in mCD64 is not responsible for the abnormal hIgG1 clearance.

Furthermore, the expression of mCD32 appeared substantially lower on monocytes from NOD SCID mice compared to SCID. The likely explanation for this is that NOD mice (and therefore NOD SCID) contain a promoter haplotype in mCD32. A 13bp deletion results in the loss of two putative transcription factor binding sites upstream of the CD32 gene; this was found to result in a lower expression of mCD32.[507] However, this previous study used the mAb 2.4G2, which binds both mCD32 and mCD16. Despite this, in this current work the results suggest that mCD32 expression was reduced in splenic and circulating monocytes in NOD SCID mice, supporting previous work where promoter polymorphisms resulted in reduced mCD32 surface expression. Given that knocking-out mCD32 in NOD SCID mice extended hIgG1 half-life it is unlikely that the lower mCD32 expression in NOD SCID mice was responsible for abnormal mAb clearance.

When mCD32 was genetically deleted in NOD SCID mice, the persistence of mAb was restored to the levels observed in SCID mice. This result was confirmed using two different hIgG1 mAb, suggesting that the phenomenon observed was a result of the isotype rather than the mAb target. This result implies that the expression of mCD32 in NOD SCID mice is responsible for the faster clearance of hIgG1 from the plasma. This is a surprising result, given the previous indication that the NOD SCID mice have a reduced expression of mCD32 due to a promoter haplotype.

Polymorphisms in the translated mCD32 gene have been identified with 2 distinct haplotypes.[306, 508] As has been confirmed in this chapter, SCID mice possess the ly17.2 haplotype whilst NOD SCID mice are ly17.1. These variants differ by four amino acids; three in the extracellular domain and one intracellular, with the ly17.1 haplotype more common in autoimmune prone strains of mice.[508-510] Despite this, there have, so far, been no reports to suggest that this haplotype alters the affinity for IgG or affects the biological function of mCD32.[306] In this chapter, evidence has been presented to suggest that ly17.1, the variant of mCD32 found in NOD SCID mice, may have a slightly increased affinity for hIgG. The first evidence for this came from the binding of monomeric and aggregated hIgG to Ly17.1 and Ly17.2 expressing 293F cells. When normalised to transfection, cells expressing the NOD SCID variant of mCD32 were able to more efficiently bind both monomeric and aggregated pooled hIgG. This system does not represent physiological levels of receptor expression with receptors overexpressed. Additionally, entirely comparable receptor expression could not be obtained for both variants, making normalisation necessary. Another important consideration from these experiments was the use of pooled hIgG; this will contain mixture of all possible human IgG isotypes. IgG1 and IgG2 are the primary subclasses in pooled IgG, although IgG3 and IgG4 will be present to a lesser extent, with reports suggesting preparations from some suppliers contain small amounts of IgA.[511, 512] Additionally, it is possible that certain subclasses aggregate more efficiently and may therefore be overrepresented in either the aggregated on monomeric fractions. Whilst these experiments suggest that IgG is binding more efficiently to NOD SCID mCD32, it is hard to conclude which subclasses are responsible for binding. Producing subclass-specific samples of aggregated and monomeric IgG would useful to confirm whether binding follows the *in vivo* pattern, where only certain subclasses resulted in abnormal mAb clearance.

Biacore analysis addressed this further following generation and purification of soluble forms of the extracellular portion of both variants. Results for aggregated hIgG binding correlated with FACS experiments, suggesting that NOD SCID mCD32 has a higher affinity for aggregated hIgG, as before the subclasses present in the aggregated IgG are unknown. When investigating monomeric

hIgG binding, both mAbs investigated suggested a similar increase in hIgG1 affinity with KD for ly17.1 1.24 fold lower for cetuximab and 1.26 fold lower for rituximab, compared to ly17.2. Whether this increase in affinity is enough to fully explain the abnormal mAb clearance in NOD SCID mice appears unlikely. However, the observation that normal mIgG levels can prevent rapid clearance suggests a subtle difference may be responsible.

One question left by these experiments is why mIgG1 has a normal clearance from NOD SCID mice. As shown by the Biacore data presented here, mCD32 has a high affinity for mIgG1, higher than the affinity of either mCD32 variant for hIgG1. This result is surprising as, if the increase in NOD SCID CD32 affinity was responsible for fast clearance of hIgG1, it would be expected that mIgG1 would also be cleared quickly due to mCD32 having an even higher affinity for this isotype. Yet as demonstrated here, mIgG1 was cleared more slowly from the plasma with no differences between SCID and NOD SCID mice; the reason for this anomaly is so far not understood. Additionally, mIgG2a was cleared rapidly from NOD SCID mice despite NOD SCID and SCID mCD32 having a similar affinity for mIgG2a. It is important to note that the clearance of mIgG2a has not been investigated in NOD SCID mCD32-/- mice and therefore this receptor may not be responsible for the fast clearance of this isotype in NOD SCID mice.

The basis for the higher affinity of mCD32 for hIgG1 is not known. There is currently no crystal structure for mCD32, either alone or in complex with IgG. It would be beneficial to determine the crystal structure of the receptor in order to locate residues that vary between the isoforms of mCD32. This would allow their likely impact on the interaction with IgG to be investigated. Structural prediction of the extracellular region of mCD32 using the Phyre2 investigator predicted the polymorphism at position 116 to be in the linker between the two extracellular domains. Furthermore, residues 161 and 166, the other extracellular polymorphic residues were predicted to be in the membrane distal extracellular domain (Phyre 2 http://www.sbg.bio.ic.ac.uk/phyre2/phyre2_output/f5a2d5ad3f08fa59/summary.html).[513] This structural prediction was modelled on the structure of human CD32b (PDB: 1E4J); using it as a template for interface prediction by PiSITE, which suggested that residue 161 may be at the Fc interface with residue 166 adjacent to interface residues.[514] Whilst this data is predictive and would require confirming through a crystal structure, it suggests that there may be some structural basis for the difference in affinity observed in this study. As well as the residues mutated in the extracellular region of mCD32 between SCID and NOD SCID mice, there is also a polymorphism intracellularly. It is possible that this intracellular I258S polymorphism could impact on the internalisation of the receptor, however this requires further investigation.

Finally, bone marrow chimera were generated in order to obtain mice where ly17.1 (NOD SCID) mCD32 was expressed on the non-haematopoietic cells and no CD32 was expressed on haematopoietic cells. Normal hIgG clearance was observed in these mice, which suggested that haematopoietic mCD32 was responsible for the abnormal mAb clearance. However, these mice were revealed to have very high levels of mIgG in the plasma. Although some mIgG would be expected after reconstituting the NOD SCID mice with splenocytes capable of generating B cells (and hence plasma cells and antibodies) this high level may reflect some graft versus host disease (GVHD), as mice also displayed signs of colitis. Given previous results in this chapter that IgG can overcome abnormal mAb clearance, it is impossible to deduce if the results of the chimera experiment are due to the mCD32 expression pattern or simply a result of elevated mIgG. This complication could be overcome by transferring bone marrow from NOD SCID CD32-/- mice; this would prevent the production of mIgG in the recipient mice as there would be no reconstitution with B cells. Alternatively, the cell types responsible for the abnormal hIgG1 clearance could be investigated by deleting specific populations. Clodronate vesicles can be used to deplete macrophages whilst monocytes can be deleted with specific antibodies, this can be used to identify if removing cell populations can restore normal hIgG half-life without the need to generate chimera.

Despite some limitations, this chapter has clearly identified that hIgG1 and mIgG2a are cleared abnormally quickly from the plasma of NOD SCID mice. The evidence strongly suggests that this is dependent on the Fc portion of the mAb and is mediated by CD32b. Whilst further work is required to fully deduce the mechanism by which mCD32 exerts this effect, this work identifies a small increase in affinity for hIgG1 by the ly17.1 haplotype of mCD32, the variant expressed in NOD SCID mice. Importantly, this abnormal clearance can be overcome by restoring mIgG levels. The NOD SCID mouse strain is widely used for studying immunotherapy. However, the implications for the findings in the chapter could be wider reaching; NOD SCID mice are used as the background for a number or more highly immune compromised strains it should be investigated if these derivative strains also have abnormal mAb half-life. One example is NSG mice lacking expression of the IL-2 γ-chain.[488] These have been used as the hosts for PDX models for studying a number of human cancers including B cell lymphoma. Amongst other applications, these PDX mice are utilised to investigate immunotherapy.[515] Given the results here, the mAb half-life and therapy duration obtained in these models should be treated with caution. The alternative is to use immune deficient strains on a different background or to reconstitute recipients with mIgG prior to mAb administration. The results in this chapter highlight the need for careful consideration when

interpreting results from NOD SCID mice or those on a NOD SCID background, particularly when comparing results between strains. It is important to consider reconstituting NOD SCID mice with IgG when using the strain for immunotherapy in order to restore normal antibody kinetics.

Chapter 7 Discussion and future work

The aim of this thesis was to investigate the role of FcγRs in mAb therapy. FcγRs are expressed throughout the body on immune and epithelial cells where they bind to the Fc of antibodies through their extracellular immunoglobulin domain.[218] Despite this general similarity, it is clear from the work here that this family of receptors are responsible for a diverse range of activities. There are three roles for FcγRs discussed in this work: mAb mediated receptor cross-linking, effector cell activation and modulating mAb half-life. These are three distinct functions, which all contribute to the activity, efficacy and persistence of therapeutic mAb.

Initially, cell lines were generated expressing polymorphic variants of hFcγRs and characterised for their ability to bind to IgG and IC before being used as feeder cells in T cell proliferation and cytokine release assays. It was their use in these proliferation assays that dictated the decision to use an adherent cell line as the basis for transfected cells. The rationale was that previous assays had identified cross-linking of TGN1412 as being vital for its activity, however this was achieved by immobilising the mAb on plastic or using a secondary mAb.[158, 159] The use of FcγR transfected cells provided a more biologically relevant method for mAb and receptor cross-linking. Moreover, these CHO-K1 based proliferation assays revealed that CD32b expressing CHO-K1 cells facilitated T cell proliferation following stimulation with TGN1412. This result is perhaps not surprising given that several other immune stimulatory mAbs have been described to require cross-linking via CD32b for activity. For example, the anti-CD40 mAb 3/23 was found to require trans cross-linking via CD32b in order to have a stimulatory effect *in vivo*.[434] Similarly, agonistic mAbs directed to death receptor 5 (DR5) have been shown to require cross-linking through CD32b to induce death of the target cell.[516] Together these results, added to those described here with TGN1412, suggest an important role for CD32b cross-linking in the activity of agonistic mAbs that require higher order receptor cross-linking for function. Moreover, this is consistent with results from PBMC assays where high density pre-culture was required to allow TGN1412 to induce proliferation, with the same process resulting in an upregulation of CD32b.[161] The results presented here suggest that this upregulation may be directly responsible for the proliferation observed in PBMC assays. This is in contrast to the postulation made my Römer et al who proposed that high density culture resulted in sub-threshold T cell stimulation through contact with monocytes.[160] Overall, assays such as those presented here, as well as an increased understanding of toxicity, have led to

development of TGN1412 (now called TAB08) being restarted, albeit at much lower concentrations, with promising early results in rheumatoid arthritis.[517]

The results in this thesis go beyond demonstrating the requirement for CD32b for TGN1412 induced proliferation. CD32a transfected cells were also able to induce TGN1412 mediated proliferation. This is perhaps not surprising given that CD32a and CD32b have a high degree of sequence similarity. What will be interesting is to investigate if CD32a cross-linking is able to facilitate cross-linking of agonistic mAbs *in vivo*. Perhaps more surprising was that CD64 transfected cells were able to facilitate TGN1412 induced proliferation, however this was to a lesser extent than that from CD32b, despite CD64 having a 150 fold higher affinity for IgG4 than CD32b.[290] Whilst it is possible that the higher expression level of CD32b on the CHO-K1 cells was responsible for this difference, it seems more likely, particularly given results with other mAbs (3/23 and anti-DR5), that CD32b and CD32a have an innate property which makes it optimally suited for mAb cross-linking. One possibility is that the receptor dimerises at the cell surface. This has been reported to occur with CD32a, with the dimerization motif identified.[302] This motif is not well conserved among FcγRs but is present in CD32b, raising the possibility that this could be the shared mechanism by which CD32a and CD32b efficiently cross-link agonistic mAbs, clustering the target receptor on the cell surface.[302] The proliferation assays performed here only used cells transfected with the I232 allele of CD32b. It would be interesting to perform the experiments with cells expressing the T232 variant. This allele is known to prevent receptor redistribution into lipid rafts and may therefore prevent the clustering of TGN1412 required to induce proliferation.[359]

One surprising set of results from these experiments were those achieved with CD16a transfected cells. It is widely known that the low affinity FcγRs, of which CD16a is one, have a higher affinity for IC and aggregated IgG than they do for monomeric IgG.[290] This was observed for CD32a and CD32b but not for CD16a where transfected cells only had low binding to aggregated IgG, as determined by FACS. As has previously been discussed, this could be related to preferential aggregation of IgG isotypes, however CD16a was also unable to facilitate TGN1412 induced proliferation. This is despite the receptor having a similar affinity for IgG4 as CD32a.[290] In isolation, this latter result could be explained by the dimerization of CD32a (and potentially CD32b) previously discussed. Yet when coupled with the low aggregated IgG binding, these results suggest that CD16a may not be binding to IgG as expected, despite the sequence of the transfected receptor being confirmed. One factor which could explain both these results is glycosylation of the CD16a receptor; CD32a contains two N-linked glycosylation sites with glycosylation reported not to have an effect on IgG binding.[518] In contrast CD16a has five potential N-linked glycosylation sites.

Importantly these glycans have been shown to influence IgG binding; removal of the glycan from N162 reduced the binding of IgG1 to the receptor.[519] It stands to reason that similar differences in binding to IgG4 may result from altered glycosylation. Crucially, earlier work has demonstrated that CD16a is differentially glycosylated depending on the cells in which it is produced and that this can influence the IgG binding kinetics.[520] This offers an explanation for the unexpected results using CD16a transfected CHO-K1 cells however it is an area that requires further investigation.

With CD32b extensively shown to regulate the immune response via signalling initiated by its ITIM motif the results from the proliferation assays and elsewhere demonstrate how the role of CD32b is far more complex than was initially thought.[218, 306] As a result, the loss or reduced expression of CD32b, may impact on therapy with direct targeting mAb, with the potential to improve agonistic mAb responses if strategies can be developed to increase CD32b expression. Key to manipulating the expression of CD32b in each context, is understanding the underpinning regulation of the receptor. As such, work set out to understand the lack of CD32b expression by Ramos cells. This identified that the absence of CD32b expression in Ramos cells occurs at the transcriptional level, despite their being no significant differences in either the gene or promoter sequences. Furthermore, expression could not be induced using epigenetic inhibitors, which prevent the methylation of DNA. As a result the mechanism for this lack of CD32b expression is still unclear and requires further investigation as has been discussed earlier. Ramos cells are derived from a Burkitt's lymphoma patient. It seems plausible that the loss of CD32b expression reduces inhibitory signalling and therefore allows clonal outgrowth.[444] There is evidence for CD32b dysregulation *in vivo* with variable expression between tumour types; DLBCL and FL were found to have a significantly lower CD32b expression than CLL cells and normal B cells.[254] Furthermore, studies have identified translocations resulting in an increased expression of CD32b in cases of NHL and FL, further identifying the variability in CD32b expression levels which could impact on mAb therapy.[467, 521]

On the other hand, elevated CD32b expression can have its drawbacks, particularly when it comes to the activity of the anti-CD20 mAb rituximab. It has been demonstrated in two independent clinical trials that increased expression of CD32b on target cells negatively effects the response to rituximab.[254, 255] Further experiments have shown that this occurs due to the cis binding of rituximab on the target cell, promoting internalisation.[253] Moreover, it has been demonstrated here that the type II mAb obinutuzumab, which is not internalised to the same extent, results in improved therapy in a mouse tumour model and persists in the circulation for longer than

rituximab. Overall, these data efficiently demonstrate the opposing roles for CD32b interactions between direct targeting and agonistic immune modulatory mAbs.

Building from the observations that hCD32b binding influences rituximab half-life *in vivo* through internalisation; this work also identified a direct role for mouse CD32 in altering mAb half-life as a result of a polymorphic variant in NOD SCID mice. The reduction in mAb half-life in a NOD SCID mouse was sufficient to give a significantly shortened therapy with rituximab and obinutuzumab compared to effects in SCID mice. Further experiments found that this altered mAb clearance applied to hIgG1 and mIgG2a but not to mIgG1 and hIgG2. The isotype restricted nature of this phenomena suggested that it could due to a specific receptor interaction. This deduction was supported by the single previous study describing the abnormal half-life of hIgG1 mAbs in NOD SCID mice, which identified interaction with FcγRs on macrophages as being responsible.[492] Based on this, experiments were performed in various FcγR deficient mice. NOD SCID mice lacking the expression of activatory FcγRs had no alteration in mAb clearance whereas when mCD32 was absent, mAb persistence was restored to the same level as in SCID mice. A role for mCD32 in mAb clearance would not be unusual given the internalisation of rituximab mediated by cis binding to hCD32b as previously discussed.[253, 254] However the mechanism of mAb consumption in the current study is likely to be different as increased mAb clearance occurs in the absence of target B cells. Phenotyping performed here demonstrated that mCD32 was expressed on splenic macrophages and BMDMs, consistent with the previous study identifying macrophage FcγRs as mediating the abnormal half-life. In order to confirm if macrophages were responsible for the increased mAb clearance, hIgG1 clearance could be investigated in mice treated with clodronate vesicles to deplete macrophages. However, there are other tissues on which mCD32 is expressed in mice, even despite NOD SCID mice lacking B cells, a major source of mCD32 expression. It has been demonstrated that mCD32 is expressed in the intestinal epithelia where it is associated with IgG.[522] Furthermore, expression of mCD32 has been seen on liver sinusoidal endothelial cells where has been shown to facilitate the clearance of small immune complexes.[523] Due to these observations, bone marrow chimera were generated to deduce the source of mCD32 expression responsible for the abnormal mAb half-life. However these mice had a high concentration of serum IgG which was demonstrated to restore normal mAb-half life, preventing these chimera from being useful to elucidate the mechanism of reduced half life in NOD SCID mice. As a result experiments are ongoing to generate chimera using bone marrow from NOD SCID mCD32 -/- mice.

Further investigations suggested that the variant of mCD32 expressed by NOD SCID mice had a higher affinity for hIgG1 than SCID mCD32. However, whether the modest increase in affinity can

account for the dramatic reduction in mAb half-life remains to be seen. This is especially true given that mCD32 was found to have a higher affinity for mIgG1 than for hIgG1, yet mIgG1 had a normal half-life in NOD SCID mice. One way to investigate this would be to use a hIgG1 mAb engineered to have a reduced affinity for mCD32 to determine if a modest decrease in mCD32 affinity is capable of restoring normal mAb clearance. Sequencing of mCD32 from SCID and NOD SCID mice revealed the expected ly17 polymorphic variation in the NOD SCID mice. The two variants of mCD32 vary be four amino acids, three of which are extracellular (P116L, Q161L, T166P) and one intracellular (I258S). Crystallographic studies are required to determine if these polymorphisms occur in the tertiary structure of the Fc binding region of the receptor in order to deduce if these residues are responsible for the altered hIgG1 affinity.

The results of these experiments into mAb half-life are likely to have an increased significance and be applicable to a number of strains. NOD SCID mice are severely immune compromised and are widely used in their own right as well as forming the background for NSG mice.[417, 419] It will be important to confirm if the abnormal half-life of mIgG2a and hIgG1 also occurs in NSG mice. These strains are extensively used, particularly as recipients for patient xenografts and are rapidly becoming a widely used model for pre-clinical testing, including for investigation into novel immunotherapies.[515] Where the abnormal half-life in NOD SCID mice becomes a challenge is in comparing results between strains. In these cases real consideration should be made as to the strain specific effects on mAb half life and efficacy. Furthermore, it has been shown here that isotype has a significant effect on mAb half-life in NOD SCID mice, therefore caution should be exercised when comparing results of mAbs of different isotypes in these strains.

There is also a significant question as to whether NOD SCID mice and their related sub-strains are a suitable model for studying agonistic immune modulatory mAbs. As well as the abnormal half-life, work presented here plus that of others (White[434], Wilson[516] and Li[524]) has demonstrated a clear requirement for cross-linking by inhibitory FcγRs for the activity of these mAbs. With mCD32 polymorphisms affecting affinity for IgG, this could have a significant impact on the activity of agonistic mAbs in these strains. For example, studies have been performed in NSG mice to investigate anti-CD40 mAb, known to require cross-linking via CD32b.[434, 525] However without direct comparison to therapy in strains not expressing the NOD SCID variant of mCD32 it is difficult to determine the effect of the polymorphism on therapy. Furthermore, xenograft mice are reconstituted with a human immune system, the extent to which this alters the mAb half-life requires further investigation. Understanding the tissue localisation of CD32 responsible for abnormal mAb half-life should go some way towards understanding this question.

One strategy that was found here to extend mAb half-life in NOD SCID mice without the need for genetic manipulation was to reconstitute the mouse with mIgG at levels comparable to that in BALB/c mice. This implied that the polymorphisms in mCD32 were responsible for the abnormal mAb clearance in NOD SCID mice but only in the absence of normal circulating IgG. This suggests a mechanism whereby serum IgG can bind to mCD32, preventing the therapeutic mAb from doing so and extending its half-life. Moreover, this offers a practical method by which abnormal half-life in NOD SCID mice can be overcome. As well as prolonging half-life, restoring biological IgG levels is more physiologically relevant; with serum IgG found to have a profound effect on mAb activity. Initial experiments using *ex vivo* cynomolgus monkey samples postulated that IgG was having an inhibitory effect on rituximab killing.[526] Subsequently, experiments found that human serum inhibited Herceptin mediated ADCC, an effect that could be overcome by removal of IgG from serum.[527] Moreover, this inhibitory effect of IgG could be overcome by using an afucosylated mAb which could displace serum IgG from CD16a due to its higher affinity for the receptor.[528] Taken together these results suggest that the benefits of reconstituting NOD SCID mice with IgG goes beyond restoring normal half-life, they also provide a more relevant model for studying effector cell mechanisms and efficacy. This is applicable to experiments in the Tcl-1 model where a number of experiments were performed in SCID mice, also lacking endogenous IgG. However the results from SCID mice displayed the same trends as those performed in immune competent mice, suggesting a lack of IgG did not significantly alter therapy in this system. It is possible that the inhibitory effects of serum IgG are reduced in a murine system. An alternative explanation is that a higher amount of mAb was used in immune competent mice, which could overcome the inhibitory IgG effects as has been reported previously.[527]

Despite the lack of serum IgG in SCID recipients, the Tcl-1 model was been shown to provide a murine model of B cell malignancy which replicates features of human disease. When splenocytes from Tcl-1 tumour bearing mice were transferred into hCD20 Tg or immune deficient mice, hCD20 expression was maintained and tumours could be effectively treated with anti-CD20 mAbs. Investigations into the effector mechanisms required for anti-CD20 mAb activity found that activatory FcγRs were an absolute requirement for rituximab activity whilst obinutuzumab only had residual activity. Taken together these results agree with those previously demonstrating the importance of activatory FcγRs for anti-CD20 mAb activity, with the results presented here showing this for the first time in a fully murine model of disease. [200, 222]

Whilst not all mice innoculated with Tcl-1 hCD20 splenocytes developed disease, the model is unique in that both malignant and non-malignant B cells are present, with both expressing the

target human CD20 antigen. This system is most akin to that in humans and was used to model anti-CD20 therapy in combination with the PI3Kδ inhibitor GS9820. Furthermore, these experiments used multiple doses of mAb, similar to the cycles of treatment received by patients.[127] These experiments found that, as before, mAb monotherapy gave effective tumour clearance which was more prolonged for obinutuzumab compared to rituximab, consistent with previous results.[309] Moreover, when combined with GS9820, the therapy was more prolonged, with the inhibitor alone also having a profound anti-tumour effect. It was demonstrated that GS9820 was able to prolong the half-life of anti-CD20 mAbs in the Tcl-1 model. It is possible that the anti-tumour activity of GS9820 reduces the tumour burden and extends mAb half-life by reducing the consumption of mAb either tumour binding, binding to effector cells or mAb internalisation via CD32. Alternatively GS9820 could be having a more direct effect on prolonging mAb half-life through an as yet unknown mechanism. Overall it is clear that the combination therapy improves mAb half-life and leads to a prolonged tumour cell clearance in the Tcl-1 hCD20 model. These results were comparable to those observed in patients, where the combination of rituximab with the related PI3Kδ inhibitor idelalisib improved progression free survival in CLL patients compared to rituximab alone.[49]

Overall there are two major themes that have emerged from this work. The first is the role of hCD32b in modulating functions beyond negative signalling in immune effector cells. The work presented here has demonstrated that hCD32b cross-linking is required for the activity of the anti-CD28 mAb TGN1412. Furthermore, this cross-linking is capable of inducing the cytokine release observed in humans following TGN1412 infusion. Additional work into understanding the regulation of hCD32b expression such as in Ramos cells could lead to effective ways to modulate hCD32b expression for immune modulatory or direct targeting mAb therapy. On the other hand, mCD32 has also been shown to play a role in mAb half-life, at least in some strains of mice. In particular, the polymorphic variant of mCD32 found in NOD SCID mice was shown to result in a shorter mAb half-life for mIgG2a and hIgG1, the two most commonly used isotypes of mAb. The importance of half-life on mAb therapy is the second major theme from this work. The shorter mAb half-life in NOD SCID mice was found to result in a less prolonged tumour clearance following rituximab or obinutuzumab therapy. Additionally, the persistence of these mAbs in the circulation was found to be increased following combination therapy in the Tcl-1 model. Together these results suggest that mAb half-life is an important variable in the efficacy of therapeutic antibodies and that careful consideration should be made as to the differences in half-life between mouse strains.

Appendices

Appendix A: Primer sequences used during this project

Primer Name	Purpose	Sequence
CD32a H→R	CD32a mutagenesis	CCAGAAATTCTCCCATTTGGATCCCACCTTCTCC
CD16a V→F	CD16a mutagenesis	CTTCTGCAGGGGGCTTGTTGGGAGTAAAAATGTGTC
T7	Sequencing (pcDNA3, pCI-Puro, TOPO)	TAATACGACTCACTATAGGG
T3	Sequencing (pCI-PURO)	ATTAACCCTCACTAAAGGGA
BGH rev	Sequencing (pcDNA3)	TAGAAGGCACAGTCGAGG
SP6	Sequencing (TOPO)	ATTTAGGTGACACTATAG
CD16a 350R	CD16a sequencing	TATCTGGAAACTTAAAGTTCC

Appendix B Vector maps

pcDNA3

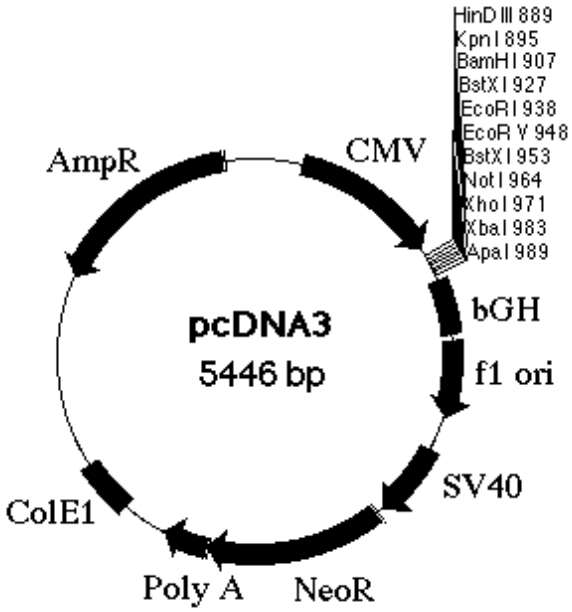

pCI-neo

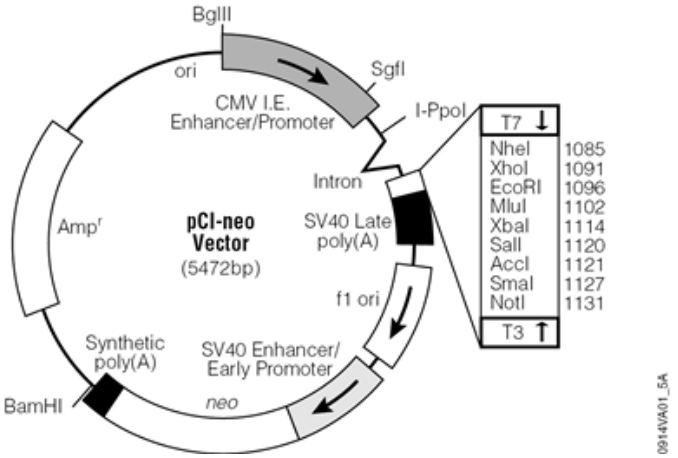

pCI-puro was created by replacing the neomycin cassette with the puromycin resistance cassette from pPURO

pCR-Blunt II-TOPO

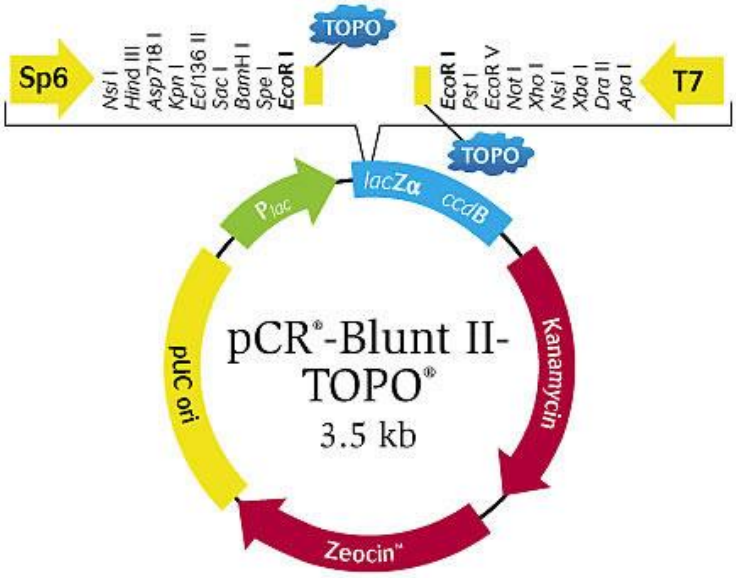

pDSG-IBA

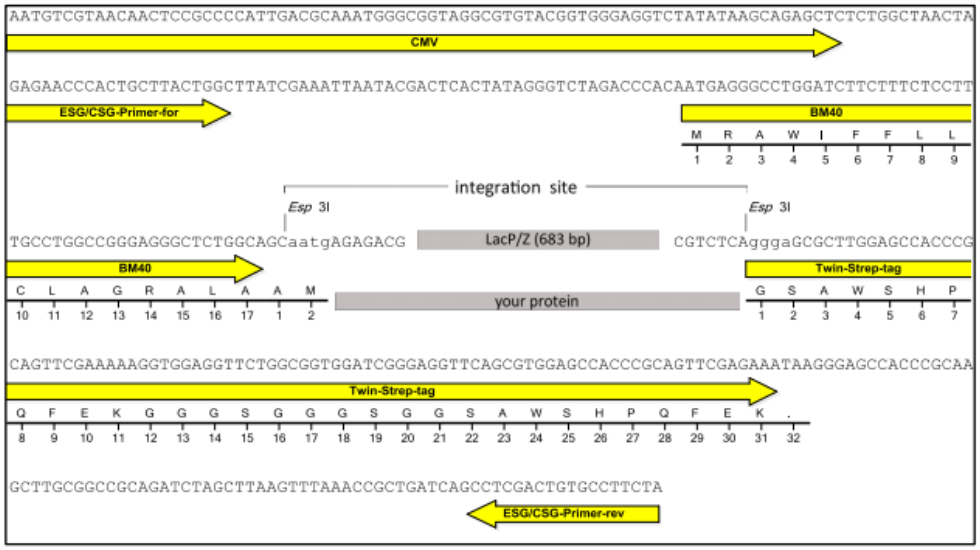

LacP/Z cassette = contains LacZ alpha fragment under control of a separate promoter, which allows alpha complementation of *LacZ* mutations such as *LacZΔM15* as in *E. coli* DH5α or TOP10.

your protein = after StarGate cloning using *Esp*3I your gene of interest will be located here

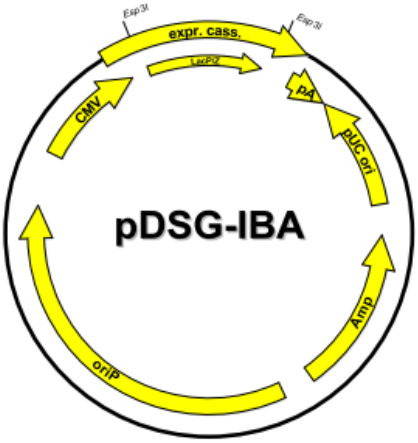

References

1. Cancer Research UK - Cancer Stats: Cancer Statistics for the UK 2015 [26/01/2015]. Available from: http://www.cancerresearchuk.org/cancer-info/cancerstats/.
2. Cancer Research UK - Cancer statistics report - Cancer survival 2014 [16/02/2015]. Available from: http://publications.cancerresearchuk.org/downloads/Product/CS_REPORT_SURVIVAL.pdf.
3. National cancer institute - staging 2015 [06/09/2016]. Available from: http://www.cancer.gov/about-cancer/diagnosis-staging/staging.
4. Cancer Research UK - Cancer incidence by age 2016 [22/08/2016]. Available from: http://www.cancerresearchuk.org/health-professional/cancer-statistics/incidence/age#heading-Zero.
5. Venkitaraman AR. Functions of BRCA1 and BRCA2 in the biological response to DNA damage. Journal Of Cell Science. 2001;114(20):3591-8.
6. Harvey Lodish AB, S. Lawrence Zipursky, Paul Matsudaira, David Baltimore and James Darnell. Molecular Cell Biology (4th edition). New York, NY: Freeman & Co; 2001.
7. World Health Organisation - HPV and cervical cancer 2016 [22/08/2016]. Available from: http://www.who.int/mediacentre/factsheets/fs380/en/.
8. Jones DL, Thompson DA, Münger K. Destabilization of the RB Tumor Suppressor Protein and Stabilization of p53 Contribute to HPV Type 16 E7-Induced Apoptosis. Virology. 1997;239(1):97-107.
9. Münger K, Baldwin A, Edwards KM, Hayakawa H, Nguyen CL, Owens M, et al. Mechanisms of Human Papillomavirus-Induced Oncogenesis. Journal of Virology. 2004;78(21):11451-60.
10. Hanahan D, Weinberg RA. The hallmarks of cancer. Cell. 2000;100(1):57-70.
11. Bartram CR, de Klein A, Hagemeijer A, van Agthoven T, van Kessel AG, Bootsma D, et al. Translocation of c-abl oncogene correlates with the presence of a Philadelphia chromosome in chronic myelocytic leukaemia. Nature. 1983;306(5940):277-80.
12. Jonuleit T, Peschel C, Schwab R, Kuip Hvd, Buchdunger E, Fischer T, et al. Bcr-Abl kinase promotes cell cycle entry of primary myeloid CML cells in the absence of growth factors. British Journal of Haematology. 1998;100(2):295-303.
13. Ouyang L, Shi Z, Zhao S, Wang FT, Zhou TT, Liu B, et al. Programmed cell death pathways in cancer: a review of apoptosis, autophagy and programmed necrosis. Cell proliferation. 2012;45(6):487-98.
14. Tsujimoto Y, Croce CM. Analysis of the structure, transcripts, and protein products of bcl-2, the gene involved in human follicular lymphoma. Proceedings of the National Academy of Sciences. 1986;83(14):5214-8.
15. Tas F, Duranyildiz D, Oguz H, Camlica H, Yasasever V, Topuz E. Circulating levels of vascular endothelial growth factor (VEGF), matrix metalloproteinase-3 (MMP-3), and BCL-2 in malignant melanoma. Medical Oncology. 2008;25(4):431-6.
16. Kim J-w, Dang CV. Cancer's Molecular Sweet Tooth and the Warburg Effect. Cancer Research. 2006;66(18):8927-30.
17. Senyilmaz D, Teleman AA. Chicken or the egg: Warburg effect and mitochondrial dysfunction. F1000Prime Reports. 2015;7:41.
18. Lane DP. Cancer. p53, guardian of the genome. Nature. 1992;358(6381):15-6.
19. Zilfou JT, Lowe SW. Tumor Suppressive Functions of p53. Cold Spring Harbor Perspectives in Biology. 2009;1(5):a001883.
20. Kastan MB, Onyekwere O, Sidransky D, Vogelstein B, Craig RW. Participation of p53 Protein in the Cellular Response to DNA Damage. Cancer Research. 1991;51(23 Part 1):6304-11.

21. Walerych D, Napoli M, Collavin L, Del Sal G. The rebel angel: mutant p53 as the driving oncogene in breast cancer. Carcinogenesis. 2012;33(11):2007-17.
22. Iacopetta B. TP53 mutation in colorectal cancer. Human Mutation. 2003;21(3):271-6.
23. Kranenburg O. The KRAS oncogene: past, present, and future. Biochim Biophys Acta. 2005;1756(2):81-2.
24. Hanahan D, Weinberg Robert A. Hallmarks of Cancer: The Next Generation. Cell. 2011;144(5):646-74.
25. Grivennikov SI, Greten FR, Karin M. Immunity, inflammation, and cancer. Cell. 2010;140(6):883-99.
26. Boleij A, Hechenbleikner EM, Goodwin AC, Badani R, Stein EM, Lazarev MG, et al. The Bacteroides fragilis toxin gene is prevalent in the colon mucosa of colorectal cancer patients. Clinical Infectious Diseases. 2015;60(2):208-15.
27. Wu S, Rhee K-J, Albesiano E, Rabizadeh S, Wu X, Yen H-R, et al. A human colonic commensal promotes colon tumorigenesis via activation of T helper type 17 T cell responses. Nat Med. 2009;15(9):1016-22.
28. Nissinen L, Kähäri V-M. Matrix metalloproteinases in inflammation. Biochimica et Biophysica Acta. 2014;1840(8):2571-80.
29. Masson R, Lefebvre O, Noël A, Fahime ME, Chenard M-P, Wendling C, et al. In Vivo Evidence That the Stromelysin-3 Metalloproteinase Contributes in a Paracrine Manner to Epithelial Cell Malignancy. The Journal of Cell Biology. 1998;140(6):1535-41.
30. Shankaran V, Ikeda H, Bruce AT, White JM, Swanson PE, Old LJ, et al. IFN[gamma] and lymphocytes prevent primary tumour development and shape tumour immunogenicity. Nature. 2001;410(6832):1107-11.
31. Naito Y, Saito K, Shiiba K, Ohuchi A, Saigenji K, Nagura H, et al. CD8+ T Cells Infiltrated within Cancer Cell Nests as a Prognostic Factor in Human Colorectal Cancer. Cancer Research. 1998;58(16):3491-4.
32. Watson NFS, Ramage JM, Madjd Z, Spendlove I, Ellis IO, Scholefield JH, et al. Immunosurveillance is active in colorectal cancer as downregulation but not complete loss of MHC class I expression correlates with a poor prognosis. International Journal of Cancer. 2006;118(1):6-10.
33. Smyth MJ, Dunn GP, Schreiber RD. Cancer immunosurveillance and immunoediting: the roles of immunity in suppressing tumor development and shaping tumor immunogenicity. Advances in Immunology. 2006;90:1-50.
34. Hiddemann W, Cheson BD. How we manage follicular lymphoma. Leukemia. 2014;28(7):1388-95.
35. Inamdar KV, Bueso-Ramos CE. Pathology of chronic lymphocytic leukemia: an update. Annals of Diagnostic Pathology. 2007;11(5):363-89.
36. Ghia P, Ferreri AM, Caligaris-Cappio F. Chronic lymphocytic leukemia. Critical Reviews in Oncology/Hematology. 2007;64(3):234-46.
37. Hunt KE, Reichard KK. Diffuse Large B-Cell Lymphoma. Archives of Pathology & Laboratory Medicine. 2008;132(1):118-24.
38. Gatter K, Pezzella F. Diffuse large B-cell lymphoma. Diagnostic Histopathology. 2010;16(2):69-81.
39. Begg AC, Stewart FA, Vens C. Strategies to improve radiotherapy with targeted drugs. Nature Reviews Cancer. 2011;11(4):239-53.
40. Graeber TG, Osmanian C, Jacks T, Housman DE, Koch CJ, Lowe SW, et al. Hypoxia-mediated selection of cells with diminished apoptotic potential in solid tumours. Nature. 1996;379(6560):88-91.
41. Olcina MM, Hammond ME. Hypoxia and the DNA Damage Response. In: Melillo G, editor. Hypoxia and Cancer: Biological Implications and Therapeutic Opportunities. New York, NY: Springer New York; 2014. p. 21-41.

42. Dawson LA, Jaffray DA. Advances in image-guided radiation therapy. Journal of Clinical Oncology. 2007;25(8):938-46.
43. Hall AG, Tilby MJ. Mechanisms of action of, and modes of resistance to, alkylating agents used in the treatment of haematological malignancies. Blood Reviews. 1992;6(3):163-73.
44. Plunkett W, Peterson BL. Nucleoside analogs: cellular pharmacology, mechanism of action, and trategies for combination therapy. In: Cheson BD, JM K, Plunkett W, editors. Nucleosides in cancer therapy. New York: Marcel Dekker; 1997. p. 1-36.
45. Pettitt AR. Mechanism of action of purine analogues in chronic lymphocytic leukaemia. British Journal of Haematology. 2003;121(5):692-702.
46. NHS Choices, Chemotherapy 2013 [26/01/2015]. Available from: http://www.nhs.uk/Conditions/Chemotherapy/Pages/Definition.aspx.
47. Vanhaesebroeck B, Welham MJ, Kotani K, Stein R, Warne PH, Zvelebil MJ, et al. p110δ, a novel phosphoinositide 3-kinase in leukocytes. Proceedings of the National Academy of Sciences. 1997;94(9):4330-5.
48. Jennifer R. Brown RRF, Ian Flinn, Steven E. Coutre, Nina D. Wagner-Johnston, Brad S. Kahl, Stephen Edward Forbes Spurgeon, Don M. Benson, Sissy Peterman, David Michael Johnson, Daniel Li, Roger D. Dansey, Thomas Michael Jahn, John C. Byrd; . Final results of a phase I study of idelalisib (GS-1101) a selective inhibitor of PI3Kδ, in patients with relapsed or refractory CLL. 2013 ASCO Annual Meeting (J Clin Oncol 31, 2013 (suppl; abstr 7003))2013.
49. Furman RR, Sharman JP, Coutre SE, Cheson BD, Pagel JM, Hillmen P, et al. Idelalisib and Rituximab in Relapsed Chronic Lymphocytic Leukemia. New England Journal of Medicine. 2014;370(11):997-1007.
50. Seda V, Mraz M. B-cell receptor signalling and its crosstalk with other pathways in normal and malignant cells. European Journal of Haematology. 2015;94(3):193-205.
51. Schuster SJ, Neelapu SS, Gause BL, Janik JE, Muggia FM, Gockerman JP, et al. Vaccination With Patient-Specific Tumor-Derived Antigen in First Remission Improves Disease-Free Survival in Follicular Lymphoma. Journal of Clinical Oncology. 2011;29(20):2787-94.
52. Hemmi H, Takeuchi O, Kawai T, Kaisho T, Sato S, Sanjo H, et al. A Toll-like receptor recognizes bacterial DNA. Nature. 2000;408(6813):740-5.
53. Stevenson FK. DNA vaccines and adjuvants. Immunological Reviews. 2004;199(1):5-8.
54. Yu JS, Liu G, Ying H, Yong WH, Black KL, Wheeler CJ. Vaccination with Tumor Lysate-Pulsed Dendritic Cells Elicits Antigen-Specific, Cytotoxic T-Cells in Patients with Malignant Glioma. Cancer Research. 2004;64(14):4973-9.
55. Wheeler CM, Castellsagué X, Garland SM, Szarewski A, Paavonen J, Naud P, et al. Cross-protective efficacy of HPV-16/18 AS04-adjuvanted vaccine against cervical infection and precancer caused by non-vaccine oncogenic HPV types: 4-year end-of-study analysis of the randomised, double-blind PATRICIA trial. The Lancet Oncology. 2012;13(1):100-10.
56. Markowitz LE, Liu G, Hariri S, Steinau M, Dunne EF, Unger ER. Prevalence of HPV After Introduction of the Vaccination Program in the United States. Pediatrics. 2016;137(3):Epub.
57. Gaffen SL, Liu KD. Overview of interleukin-2 function, production and clinical applications. Cytokine. 2004;28(3):109-23.
58. Smith FO, Downey SG, Klapper JA, Yang JC, Sherry RM, Royal RE, et al. Treatment of Metastatic Melanoma Using Interleukin-2 Alone or in Conjunction with Vaccines. Clinical Cancer Research. 2008;14(17):5610-8.
59. June C, Maus M, Plesa G, Johnson L, Zhao Y, Levine B, et al. Engineered T cells for cancer therapy. Cancer Immunology, Immunotherapy. 2014;63(9):969-75.
60. Maude SL, Frey N, Shaw PA, Aplenc R, Barrett DM, Bunin NJ, et al. Chimeric Antigen Receptor T Cells for Sustained Remissions in Leukemia. New England Journal of Medicine. 2014;371(16):1507-17.

61. Porter DL, Hwang W-T, Frey NV, Lacey SF, Shaw PA, Loren AW, et al. Chimeric antigen receptor T cells persist and induce sustained remissions in relapsed refractory chronic lymphocytic leukemia. Science Translational Medicine. 2015;7(303):303ra139.
62. Kochenderfer JN, Dudley ME, Feldman SA, Wilson WH, Spaner DE, Maric I, et al. B-cell depletion and remissions of malignancy along with cytokine-associated toxicity in a clinical trial of anti-CD19 chimeric-antigen-receptor–transduced T cells. Blood. 2012;119(12):2709-20.
63. Brentjens R, Yeh R, Bernal Y, Riviere I, Sadelain M. Treatment of Chronic Lymphocytic Leukemia With Genetically Targeted Autologous T Cells: Case Report of an Unforeseen Adverse Event in a Phase I Clinical Trial. Molecular Therapeutics. 2010;18(4):666-8.
64. Sotillo E, Barrett DM, Black KL, Bagashev A, Oldridge D, Wu G, et al. Convergence of Acquired Mutations and Alternative Splicing of CD19 Enables Resistance to CART-19 Immunotherapy. Cancer Discovery. 2015;Epub.
65. Senzer NN, Kaufman HL, Amatruda T, Nemunaitis M, Reid T, Daniels G, et al. Phase II Clinical Trial of a Granulocyte-Macrophage Colony-Stimulating Factor–Encoding, Second-Generation Oncolytic Herpesvirus in Patients With Unresectable Metastatic Melanoma. Journal of Clinical Oncology. 2009;27(34):5763-71.
66. Korn EL, Liu P-Y, Lee SJ, Chapman J-AW, Niedzwiecki D, Suman VJ, et al. Meta-Analysis of Phase II Cooperative Group Trials in Metastatic Stage IV Melanoma to Determine Progression-Free and Overall Survival Benchmarks for Future Phase II Trials. Journal of Clinical Oncology. 2008;26(4):527-34.
67. Liu BL, Robinson M, Han ZQ, Branston RH, English C, Reay P, et al. ICP34.5 deleted herpes simplex virus with enhanced oncolytic, immune stimulating, and anti-tumour properties. Gene Ther. 2003;10(4):292-303.
68. Murphy K, Travers P, Walport M, Janeway C. Janeway's immunobiology. New York: Garland Science; 2012.
69. Kumar V, McNerney ME. A new self: MHC-class-I-independent Natural-killer-cell self-tolerance. Nature Reviews Immunology. 2005;5(5):363-74.
70. Karre K, Ljunggren HG, Piontek G, Kiessling R. Selective rejection of H-2-deficient lymphoma variants suggests alternative immune defence strategy. Nature. 1986;319(6055):675-8.
71. Guermonprez P, Valladeau J, Zitvogel L, Thery C, Amigorena S. Antigen presentation and T cell stimulation by dendritic cells. Annual Review of Immunology. 2002;20:621-67.
72. Chen L, Flies DB. Molecular mechanisms of T cell co-stimulation and co-inhibition. Nature Reviews Immunology. 2013;13(4):227-42.
73. Francisco LM, Sage PT, Sharpe AH. The PD-1 Pathway in Tolerance and Autoimmunity. Immunological Reviews. 2010;236:219-42.
74. Ahmadzadeh M, Johnson LA, Heemskerk B, Wunderlich JR, Dudley ME, White DE, et al. Tumor antigen–specific CD8 T cells infiltrating the tumor express high levels of PD-1 and are functionally impaired. Blood. 2009;114(8):1537-44.
75. Alberts B, Wilson J, Hunt T. Molecular biology of the cell. New York: Garland Science; 2008.
76. Matsuuchi L, Gold MR. New views of BCR structure and organization. Current Opinion in Immunology. 2001;13(3):270-7.
77. Paul WE. Fundamental Immunology. 7th ed. Philadelphia, USA: Lippincott Williams and Wilkins; 2012.
78. Tonegawa S. Somatic generation of antibody diversity. Nature. 1983;302(5909):575-81.
79. Bassing CH, Swat W, Alt FW. The Mechanism and Regulation of Chromosomal V(D)J Recombination. Cell. 2002;109(2, Supplement 1):S45-S55.
80. Fugmann SD, Lee AI, Shockett PE, Villey IJ, Schatz DG. The RAG Proteins and V(D)J Recombination: Complexes, Ends, and Transposition. Annual Review of Immunology. 2000;18(1):495-527.

81. Sadofsky MJ. The RAG proteins in V(D)J recombination: more than just a nuclease. Nucleic Acids Research. 2001;29(7):1399-409.
82. Komori T, Okada A, Stewart V, Alt F. Lack of N regions in antigen receptor variable region genes of TdT-deficient lymphocytes. Science. 1993;261(5125):1171-5.
83. Keim C, Kazadi D, Rothschild G, Basu U. Regulation of AID, the B-cell genome mutator. Genes & Development. 2013;27(1):1-17.
84. Revy P, Muto T, Levy Y, Geissmann F, Plebani A, Sanal O, et al. Activation-Induced Cytidine Deaminase (AID) Deficiency Causes the Autosomal Recessive Form of the Hyper-IgM Syndrome (HIGM2). Cell. 2000;102(5):565-75.
85. Larson E, Maizels N. Transcription-coupled mutagenesis by the DNA deaminase AID. Genome Biology. 2004;5(3):211.
86. Burnet FM. A modification of Jerne's theory of antibody production using the concept of clonal selection. CA: a cancer journal for clinicians. 1976;26(2):119-21.
87. Melchers F, Ten Boekel E, Seidl T, Kong XC, Yamagami T, Onishi K, et al. Repertoire selection by pre-B-cell receptors and B-cell receptors, and genetic control of B-cell development from immature to mature B cells. Immunological Reviews. 2000;175(1):33-46.
88. Levine MH, Haberman AM, Sant'Angelo DB, Hannum LG, Cancro MP, Janeway CA, et al. A B-cell receptor-specific selection step governs immature to mature B cell differentiation. Proceedings of the National Academy of Sciences. 2000;97(6):2743-8.
89. Hartley SB, Cooke MP, Fulcher DA, Harris AW, Cory S, Basten A, et al. Elimination of self-reactive B lymphocytes proceeds in two stages: Arrested development and cell death. Cell. 1993;72(3):325-35.
90. Pelanda R, Torres RM. Central B-Cell Tolerance: Where Selection Begins. Cold Spring Harbor Perspectives in Biology. 2012;4(4):a007146.
91. Gay D, Saunders T, Camper S, Weigert M. Receptor editing: an approach by autoreactive B cells to escape tolerance. The Journal of Experimental Medicine. 1993;177(4):999-1008.
92. Chen C, Nagy Z, Prak EL, Weigert M. Immunoglobulin heavy chain gene replacement: a mechanism of receptor editing. Immunity. 1995;3(6):747-55.
93. Esser C, Radbruch A. Immunoglobulin Class Switching: Molecular and Cellular Analysis. Annual Review of Immunology. 1990;8(1):717-35.
94. Heise N, De Silva NS, Silva K, Carette A, Simonetti G, Pasparakis M, et al. Germinal center B cell maintenance and differentiation are controlled by distinct NF-κB transcription factor subunits. The Journal of Experimental Medicine. 2014;211(10):2103-18.
95. Muramatsu M, Kinoshita K, Fagarasan S, Yamada S, Shinkai Y, Honjo T. Class Switch Recombination and Hypermutation Require Activation-Induced Cytidine Deaminase (AID), a Potential RNA Editing Enzyme. Cell. 2000;102(5):553-63.
96. Stavnezer J, Guikema JE, Schrader CE. Mechanism and regulation of class switch recombination. Annual review of immunology. 2008;26:261-92.
97. Roux KH, Strelets L, Michaelsen TE. Flexibility of human IgG subclasses. The Journal of Immunology. 1997;159(7):3372-82.
98. White AL, Chan HT, French RR, Willoughby J, Mockridge CI, Roghanian A, et al. Conformation of the human immunoglobulin G2 hinge imparts superagonistic properties to immunostimulatory anticancer antibodies. Cancer Cell. 2015;27(1):138-48.
99. Luster MI, Armen RC, Hallum JV, Leslie GA. Measles virus-specific IgD antibodies in patients with subacute sclerosing panencephalitis. Proceedings of the National Academy of Sciences of the United States of America. 1976;73(4):1297-9.
100. Chen K, Cerutti A. New Insights into the Enigma of Immunoglobulin D. Immunological Reviews. 2010;237(1):160-79.
101. Woof JM, Russell MW. Structure and function relationships in IgA. Mucosal Immunology. 2011;4(6):590-7.

102. Erb KJ. Helminths, allergic disorders and IgE-mediated immune responses: Where do we stand? European Journal of Immunology. 2007;37(5):1170-3.
103. Arnold JN, Wormald MR, Sim RB, Rudd PM, Dwek RA. The impact of glycosylation on the biological function and structure of human immunoglobulins. Annual review of immunology. 2007;25:21-50.
104. Tao MH, Morrison SL. Studies of aglycosylated chimeric mouse-human IgG. Role of carbohydrate in the structure and effector functions mediated by the human IgG constant region. The Journal of Immunology. 1989;143(8):2595-601.
105. Lifely MR, Hale C, Boyce S, Keen MJ, Phillips J. Glycosylation and biological activity of CAMPATH-1H expressed in different cell lines and grown under different culture conditions. Glycobiology. 1995;5(8):813-22.
106. Kohler G, Milstein C. Continuous cultures of fused cells secreting antibody of predefined specificity. Nature. 1975;256(5517):495-7.
107. Norman DJ, Kahana L, Stuart FP, Jr., Thistlethwaite JR, Jr., Shield CF, 3rd, Monaco A, et al. A randomized clinical trial of induction therapy with OKT3 in kidney transplantation. Transplantation. 1993;55(1):44-50.
108. Webster AC, Pankhurst T, Rinaldi F, Chapman JR, Craig JC. Monoclonal and Polyclonal Antibody Therapy for Treating Acute Rejection in Kidney Transplant Recipients: A Systematic Review of Randomized Trial Data. Transplantation. 2006;81(7):953-65.
109. Petrovsky N, Aguilar JC. Vaccine adjuvants: Current state and future trends. Immunology and Cell Biology. 2004;82(5):488-96.
110. Cox JC, Coulter AR. Adjuvants--a classification and review of their modes of action. Vaccine. 1997;15(3):248-56.
111. Billiau A, Matthys P. Modes of action of Freund's adjuvants in experimental models of autoimmune diseases. Journal of Leukocyte Biology. 2001;70(6):849-60.
112. Partridge L. The Production of Monoclonal Antibodies to Membrane Proteins. Biomembrane Protocols. Methods in Molecular Biology. 27: Springer New York; 1994. p. 65-86.
113. Mayes JT, Thistlethwaite JR, Jr., Stuart JK, Buckingham MR, Stuart FP. Reexposure to OKT3 in renal allograft recipients. Transplantation. 1988;45(2).
114. Oldham RK, Dillman RO. Monoclonal Antibodies in Cancer Therapy: 25 Years of Progress. Journal of Clinical Oncology. 2008;26(11):1774-7.
115. Saito K, Nawata M, Iwata S, Tokunaga M, Tanaka Y. Extremely high titer of anti-human chimeric antibody following re-treatment with rituximab in a patient with active systemic lupus erythematosus. Rheumatology. 2005;44(11):1462-4.
116. Lunardon L, Payne AS. Inhibitory human anti-chimeric antibodies to rituximab in a pemphigus patient. The Journal of allergy and clinical immunology. 2012;130(3):800-3.
117. Clackson T, Hoogenboom HR, Griffiths AD, Winter G. Making antibody fragments using phage display libraries. Nature. 1991;352(6336):624-8.
118. Riechmann L, Clark M, Waldmann H, Winter G. Reshaping human antibodies for therapy. Nature. 1988;332(6162):323-7.
119. Breitling F, Dübel S, Seehaus T, Klewinghaus I, Little M. A surface expression vector for antibody screening. Gene. 1991;104(2):147-53.
120. Hammers CM, Stanley JR. Antibody Phage Display: Technique and Applications. The Journal of Investigative Dermatology. 2014;134(2):e17.
121. Thie H, Voedisch B, Dubel S, Hust M, Schirrmann T. Affinity maturation by phage display. Methods in Molecular Biology. 2009;525:309-22.
122. Taylor LD, Carmack CE, Schramm SR, Mashayekh R, Higgins KM, Kuo C-C, et al. A transgenic mouse that expresses a diversity of human sequence heavy and light chain immunoglobulins. Nucleic Acids Research. 1992;20(23):6287-95.

123. Lee EC, Liang Q, Ali H, Bayliss L, Beasley A, Bloomfield-Gerdes T, et al. Complete humanization of the mouse immunoglobulin loci enables efficient therapeutic antibody discovery. Nature Biotechnology. 2014;32(4):356-63.
124. Becker PD, Legrand N, van Geelen CMM, Noerder M, Huntington ND, Lim A, et al. Generation of Human Antigen-Specific Monoclonal IgM Antibodies Using Vaccinated "Human Immune System" Mice. PLoS ONE. 2010;5(10):e13137.
125. Reichart J. Therapeutic monoclonal antibodies approved or in review in the European Union or the United States 2015. Available from: http://tandf.co.uk/journals/pdf/announcements/kmab-antibodies.pdf.
126. Scott AM, Wolchok JD, Old LJ. Antibody therapy of cancer. Nature Reviews Cancer. 2012;12(4):278-87.
127. Rituxan - Established dosing regimens for treatment settings in NHL and CLL 2016 [13/09/2016]. Available from: http://www.rituxan.com/hem/hcp/non-hodgkins/rituxan-dosing#untreated-nhl.
128. Oldham RJ, Cleary KLS, Cragg MS. CD20 and Its Antibodies: Past, Present, and Future. Forum on Immunopathological Diseases and Therapeutics. 2014;5(1-2):7-23.
129. Herceptin website [18/02/2015]. Available from: http://www.herceptin.com/.
130. Hudis CA. Trastuzumab — Mechanism of Action and Use in Clinical Practice. New England Journal of Medicine. 2007;357(1):39-51.
131. Erbitux website [18/02/15]. Available from: https://www.erbitux-international.com/en/index.html.
132. Bou-Assaly W, Mukherji S. Cetuximab (Erbitux). American Journal of Neuroradiology. 2010;31(4):626-7.
133. Avastin information website [18/02/15]. Available from: http://www.avastin.com/patient.
134. Mukherji SK. Bevacizumab (Avastin). American Journal of Neuroradiology. 2010;31(2):235-6.
135. Campath information website [18/02/15]. Available from: http://www.campath.com/.
136. Alinari L, Lapalombella R, Andritsos L, Baiocchi RA, Lin TS, Byrd JC. Alemtuzumab (Campath-1H) in the treatment of chronic lymphocytic leukemia. Oncogene. 2007;26(25):3644-53.
137. Gazyva information website [18/02/15]. Available from: http://www.gazyva.com/.
138. Alduaij W, Ivanov A, Honeychurch J, Cheadle EJ, Potluri S, Lim SH, et al. Novel type II anti-CD20 monoclonal antibody (GA101) evokes homotypic adhesion and actin-dependent, lysosome-mediated cell death in B-cell malignancies. Blood. 2011;117(17):4519-29.
139. Yervoy information website [25/08/2016]. Available from: http://www.yervoy.com/.
140. Tarhini A, Lo E, Minor DR. Releasing the Brake on the Immune System: Ipilimumab in Melanoma and Other Tumors. Cancer Biotherapy & Radiopharmaceuticals. 2010;25(6):601-13.
141. Opdivo information site [25/08/2016]. Available from: http://www.opdivo.bmscustomerconnect.com/gateway.
142. Raedler LA. Opdivo (Nivolumab): Second PD-1 Inhibitor Receives FDA Approval for Unresectable or Metastatic Melanoma. American Health & Drug Benefits. 2015;8(Spec Feature):180-3.
143. Kirkpatrick P, Graham J, Muhsin M. Cetuximab. Nature Reviews Drug Discovery. 2004;3(7):549-50.
144. Goldstein NI, Prewett M, Zuklys K, Rockwell P, Mendelsohn J. Biological efficacy of a chimeric antibody to the epidermal growth factor receptor in a human tumor xenograft model. Clinical Cancer Research. 1995;1(11):1311-8.
145. Baselga J. The EGFR as a target for anticancer therapy--focus on cetuximab. European Journal of Cancer. 2001;37 Suppl 4:S16-22.

146. Zhang W, Liu HT. MAPK signal pathways in the regulation of cell proliferation in mammalian cells. Cell Research. 2002;12(1):9-18.
147. Amati B, Alevizopoulos K, Vlach J. Myc and the cell cycle. Frontiers in Bioscience. 1998;3:d250-68.
148. Sato JD, Kawamoto T, Le AD, Mendelsohn J, Polikoff J, Sato GH. Biological effects in vitro of monoclonal antibodies to human epidermal growth factor receptors. Molecular biology & medicine. 1983;1(5):511-29.
149. Prewett MC, Hooper AT, Bassi R, Ellis LM, Waksal HW, Hicklin DJ. Enhanced antitumor activity of anti-epidermal growth factor receptor monoclonal antibody IMC-C225 in combination with irinotecan (CPT-11) against human colorectal tumor xenografts. Clinical Cancer Research. 2002;8(5):994-1003.
150. Sobrero AF, Maurel J, Fehrenbacher L, Scheithauer W, Abubakr YA, Lutz MP, et al. EPIC: Phase III Trial of Cetuximab Plus Irinotecan After Fluoropyrimidine and Oxaliplatin Failure in Patients With Metastatic Colorectal Cancer. Journal of Clinical Oncology. 2008;26(14):2311-9.
151. Cunningham D, Lang I, Marcuello E, Lorusso V, Ocvirk J, Shin DB, et al. Bevacizumab plus capecitabine versus capecitabine alone in elderly patients with previously untreated metastatic colorectal cancer (AVEX): an open-label, randomised phase 3 trial. The Lancet Oncology. 2013;14(11):1077-85.
152. Nunès JA, Truneh A, Olive D, Cantrell DA. Signal Transduction by CD28 Costimulatory Receptor on T Cells: B7-1 and B7-2 REGULATION OF TYROSINE KINASE ADAPTOR MOLECULES. Journal of Biological Chemistry. 1996;271(3):1591-8.
153. Reif K, Cantrell DA. Networking Rho Family GTPases in Lymphocytes. Immunity. 1998;8(4):395-401.
154. Elflein K, Rodriguez-Palmero M, Kerkau T, Hünig T. Rapid recovery from T lymphopenia by CD28 superagonist therapy. Blood. 2003;102(5):1764-70.
155. TeGenero Ag Investigator's Brochure. TGN1412 agonistic anti-CD28 monoclonal antibody. [29/01/2015]. 1.1:[Available from: http://www.circare.org/foia5/tgn1412investigatorbrochure.pdf.
156. Attarwala H. TGN1412: From Discovery to Disaster. Journal of Young Pharmacists. 2010;2(3):332-6.
157. Suntharalingam G, Perry MR, Ward S, Brett SJ, Castello-Cortes A, Brunner MD, et al. Cytokine storm in a phase 1 trial of the anti-CD28 monoclonal antibody TGN1412. N Engl J Med. 2006;355(10):1018-28.
158. Eastwood D, Findlay L, Poole S, Bird C, Wadhwa M, Moore M, et al. Monoclonal antibody TGN1412 trial failure explained by species differences in CD28 expression on CD4(+) effector memory T-cells. British Journal of Pharmacology. 2010;161(3):512-26.
159. Stebbings R, Findlay L, Edwards C, Eastwood D, Bird C, North D, et al. "Cytokine Storm" in the Phase I Trial of Monoclonal Antibody TGN1412: Better Understanding the Causes to Improve PreClinical Testing of Immunotherapeutics. The Journal of Immunology. 2007;179(5):3325-31.
160. Römer PS, Berr S, Avota E, Na S-Y, Battaglia M, ten Berge I, et al. Preculture of PBMCs at high cell density increases sensitivity of T-cell responses, revealing cytokine release by CD28 superagonist TGN1412. Blood. 2011;118(26):6772-82.
161. Hussain K, Hargreaves CE, Roghanian A, Oldham RJ, Chan HT, Mockridge CI, et al. Upregulation of FcgammaRIIb on monocytes is necessary to promote the superagonist activity of TGN1412. Blood. 2015;125(1):102-10.
162. Vu T, Claret FX. Trastuzumab: Updated Mechanisms of Action and Resistance in Breast Cancer. Frontiers in Oncology. 2012;2:62.
163. Arnould L, Gelly M, Penault-Llorca F, Benoit L, Bonnetain F, Migeon C, et al. Trastuzumab-based treatment of HER2-positive breast cancer: an antibody-dependent cellular cytotoxicity mechanism? British Journal of Cancer. 2006;94(2):259-67.

164. Stashenko P, Nadler LM, Hardy R, Schlossman SF. Characterization of a human B lymphocyte-specific antigen. The Journal of Immunology. 1980;125(4):1678-85.
165. Beers SA, Chan CH, French RR, Cragg MS, Glennie MJ. CD20 as a target for therapeutic type I and II monoclonal antibodies. Seminars in Hematology. 2010;47(2):107-14.
166. Tedder TF, Engel P. CD20: a regulator of cell-cycle progression of B lymphocytes. Immunology Today. 1994;15(9):450-4.
167. Cragg MS, Walshe CA, Ivanov AO, Glennie MJ. The biology of CD20 and its potential as a target for mAb therapy. Current directions in autoimmunity. 2005;8:140-74.
168. Gulbis JM, Zhou M, Mann S, MacKinnon R. Structure of the Cytoplasmic β Subunit--T1 Assembly of Voltage-Dependent K+ Channels. Science. 2000;289(5476):123-7.
169. Polyak MJ, Li H, Shariat N, Deans JP. CD20 Homo-oligomers Physically Associate with the B Cell Antigen Receptor: dissociation upon receptor engagement and recruitment of phosphoproteins and calmodulin-binding proteins. Journal of Biological Chemistry. 2008;283(27):18545-52.
170. Polyak MJ, Tailor SH, Deans JP. Identification of a Cytoplasmic Region of CD20 Required for Its Redistribution to a Detergent-Insoluble Membrane Compartment. The Journal of Immunology. 1998;161(7):3242-8.
171. Bubien JK, Zhou LJ, Bell PD, Frizzell RA, Tedder TF. Transfection of the CD20 cell surface molecule into ectopic cell types generates a Ca2+ conductance found constitutively in B lymphocytes. The Journal of Cell Biology. 1993;121(5):1121-32.
172. Petrie RJ, Deans JP. Colocalization of the B Cell Receptor and CD20 Followed by Activation-Dependent Dissociation in Distinct Lipid Rafts. The Journal of Immunology. 2002;169(6):2886-91.
173. O'Keefe TL, Williams GT, Davies SL, Neuberger MS. Mice carrying a CD20 gene disruption. Immunogenetics. 1998;48(2):125-32.
174. Uchida J, Lee Y, Hasegawa M, Liang Y, Bradney A, Oliver JA, et al. Mouse CD20 expression and function. International Immunology. 2004;16(1):119-29.
175. Kuijpers TW, Bende RJ, Baars PA, Grummels A, Derks IAM, Dolman KM, et al. CD20 deficiency in humans results in impaired T cell–independent antibody responses. The Journal of Clinical Investigation. 2010;120(1):214-22.
176. Golay JT, Clark EA, Beverley PC. The CD20 (Bp35) antigen is involved in activation of B cells from the G0 to the G1 phase of the cell cycle. The Journal of Immunology. 1985;135(6):3795-801.
177. Polyak MJ, Deans JP. Alanine-170 and proline-172 are critical determinants for extracellular CD20 epitopes; heterogeneity in the fine specificity of CD20 monoclonal antibodies is defined by additional requirements imposed by both amino acid sequence and quaternary structure. Blood. 2002;99(9):3256-62.
178. Deans JP, Robbins SM, Polyak MJ, Savage JA. Rapid Redistribution of CD20 to a Low Density Detergent-insoluble Membrane Compartment. Journal of Biological Chemistry. 1998;273(1):344-8.
179. Lim SH, Beers SA, French RR, Johnson PW, Glennie MJ, Cragg MS. Anti-CD20 monoclonal antibodies: historical and future perspectives. Haematologica. 2010;95(1):135-43.
180. Cragg MS, Morgan SM, Chan HT, Morgan BP, Filatov AV, Johnson PW, et al. Complement-mediated lysis by anti-CD20 mAb correlates with segregation into lipid rafts. Blood. 2003;101(3):1045-52.
181. Teeling JL, French RR, Cragg MS, van den Brakel J, Pluyter M, Huang H, et al. Characterization of new human CD20 monoclonal antibodies with potent cytolytic activity against non-Hodgkin lymphomas. Blood. 2004;104(6):1793-800.
182. Niederfellner G, Lammens A, Mundigl O, Georges GJ, Schaefer W, Schwaiger M, et al. Epitope characterization and crystal structure of GA101 provide insights into the molecular basis for type I/II distinction of CD20 antibodies. Blood. 2011;118(2):358-67.

183. Du J, Yang H, Guo Y, Ding J. Structure of the Fab fragment of therapeutic antibody Ofatumumab provides insights into the recognition mechanism with CD20. Molecular Immunology. 2009;46(11-12):2419-23.
184. Cragg MS. CD20 antibodies: doing the time warp. Blood. 2011;118(2):219-20.
185. Mossner E, Brunker P, Moser S, Puntener U, Schmidt C, Herter S, et al. Increasing the efficacy of CD20 antibody therapy through the engineering of a new type II anti-CD20 antibody with enhanced direct and immune effector cell-mediated B-cell cytotoxicity. Blood. 2010;115(22):4393-402.
186. Cragg MS, Glennie MJ. Antibody specificity controls in vivo effector mechanisms of anti-CD20 reagents. Blood. 2004;103(7):2738-43.
187. Marder SR, Chenoweth DE, Goldstein IM, Perez HD. Chemotactic responses of human peripheral blood monocytes to the complement-derived peptides C5a and C5a des Arg. The Journal of Immunology. 1985;134(5):3325-31.
188. Guo R-F, Ward PA. Role of C5a in Inflammatory Responses. Annual Review of Immunology. 2005;23(1):821-52.
189. Shushakova N, Skokowa J, Schulman J, Baumann U, Zwirner J, Schmidt RE, et al. C5a anaphylatoxin is a major regulator of activating versus inhibitory FcγRs in immune complex–induced lung disease. The Journal of Clinical Investigation. 2002;110(12):1823-30.
190. Derer S, Beurskens FJ, Rosner T, Peipp M, Valerius T. Complement in antibody-based tumor therapy. Critical reviews in immunology. 2014;34(3):199-214.
191. Chan HTC, Hughes D, French RR, Tutt AL, Walshe CA, Teeling JL, et al. CD20-induced Lymphoma Cell Death Is Independent of Both Caspases and Its Redistribution into Triton X-100 Insoluble Membrane Rafts. Cancer Research. 2003;63(17):5480-9.
192. Natsume A, Shimizu-Yokoyama Y, Satoh M, Shitara K, Niwa R. Engineered anti-CD20 antibodies with enhanced complement-activating capacity mediate potent anti-lymphoma activity. Cancer Science. 2009;100(12):2411-8.
193. Golay J, Zaffaroni L, Vaccari T, Lazzari M, Borleri G-M, Bernasconi S, et al. Biologic response of B lymphoma cells to anti-CD20 monoclonal antibody rituximab in vitro: CD55 and CD59 regulate complement-mediated cell lysis. Blood. 2000;95(12):3900-8.
194. Teeling JL, Mackus WJ, Wiegman LJ, van den Brakel JH, Beers SA, French RR, et al. The biological activity of human CD20 monoclonal antibodies is linked to unique epitopes on CD20. The Journal of Immunology. 2006;177(1):362-71.
195. Treon SP, Mitsiades C, Mitsiades N, Young G, Doss D, Schlossman R, et al. Tumor Cell Expression of CD59 Is Associated With Resistance to CD20 Serotherapy in Patients With B-Cell Malignancies. Journal of Immunotherapy. 2001;24(3):263-71.
196. Terui Y, Sakurai T, Mishima Y, Mishima Y, Sugimura N, Sasaoka C, et al. Blockade of bulky lymphoma-associated CD55 expression by RNA interference overcomes resistance to complement-dependent cytotoxicity with rituximab. Cancer Science. 2006;97(1):72-9.
197. Weng W-K, Levy R. Expression of complement inhibitors CD46, CD55, and CD59 on tumor cells does not predict clinical outcome after rituximab treatment in follicular non-Hodgkin lymphoma. Blood. 2001;98(5):1352-7.
198. Cittera E, Leidi M, Buracchi C, Pasqualini F, Sozzani S, Vecchi A, et al. The CCL3 family of chemokines and innate immunity cooperate in vivo in the eradication of an established lymphoma xenograft by rituximab. Journal of Immunology. 2007;178(10):6616-23.
199. Beers SA, Chan CH, James S, French RR, Attfield KE, Brennan CM, et al. Type II (tositumomab) anti-CD20 monoclonal antibody out performs type I (rituximab-like) reagents in B-cell depletion regardless of complement activation. Blood. 2008;112(10):4170-7.
200. Minard-Colin V, Xiu Y, Poe JC, Horikawa M, Magro CM, Hamaguchi Y, et al. Lymphoma depletion during CD20 immunotherapy in mice is mediated by macrophage FcgammaRI, FcgammaRIII, and FcgammaRIV. Blood. 2008;112(4):1205-13.

201. Wang S-Y, Racila E, Taylor RP, Weiner GJ. NK-cell activation and antibody-dependent cellular cytotoxicity induced by rituximab-coated target cells is inhibited by the C3b component of complement. Blood. 2008;111(3):1456-63.
202. Kennedy AD, Beum PV, Solga MD, DiLillo DJ, Lindorfer MA, Hess CE, et al. Rituximab Infusion Promotes Rapid Complement Depletion and Acute CD20 Loss in Chronic Lymphocytic Leukemia. The Journal of Immunology. 2004;172(5):3280-8.
203. van der Kolk LE, Grillo-Lopez AJ, Baars JW, Hack CE, van Oers MH. Complement activation plays a key role in the side-effects of rituximab treatment. British Journal of Haematology. 2001;115(4):807-11.
204. Racila E, Link BK, Weng WK, Witzig TE, Ansell S, Maurer MJ, et al. A polymorphism in the complement component C1qA correlates with prolonged response following rituximab therapy of follicular lymphoma. Clinical Cancer Research. 2008;14(20):6697-703.
205. Shan D, Ledbetter JA, Press OW. Apoptosis of Malignant Human B Cells by Ligation of CD20 With Monoclonal Antibodies. Blood. 1998;91(5):1644-52.
206. Janas E, Priest R, Wilde JI, White JH, Malhotra R. Rituxan (anti-CD20 antibody)-induced translocation of CD20 into lipid rafts is crucial for calcium influx and apoptosis. Clinical and experimental immunology. 2005;139(3):439-46.
207. Olejniczak SH, Hernandez-Ilizaliturri FJ, Clements JL, Czuczman MS. Acquired resistance to rituximab is associated with chemotherapy resistance resulting from decreased Bax and Bak expression. Clinical Cancer Research. 2008;14(5):1550-60.
208. Czuczman MS, Olejniczak S, Gowda A, Kotowski A, Binder A, Kaur H, et al. Acquirement of rituximab resistance in lymphoma cell lines is associated with both global CD20 gene and protein down-regulation regulated at the pretranscriptional and posttranscriptional levels. Clinical Cancer Research. 2008;14(5):1561-70.
209. Li H, Ayer LM, Lytton J, Deans JP. Store-operated Cation Entry Mediated by CD20 in Membrane Rafts. Journal of Biological Chemistry. 2003;278(43):42427-34.
210. Walshe CA, Beers SA, French RR, Chan CHT, Johnson PW, Packham GK, et al. Induction of Cytosolic Calcium Flux by CD20 Is Dependent upon B Cell Antigen Receptor Signaling. Journal of Biological Chemistry. 2008;283(25):16971-84.
211. Byrd JC, Kitada S, Flinn IW, Aron JL, Pearson M, Lucas D, et al. The mechanism of tumor cell clearance by rituximab in vivo in patients with B-cell chronic lymphocytic leukemia: evidence of caspase activation and apoptosis induction. Blood. 2002;99(3):1038-43.
212. Eeva J, Nuutinen U, Ropponen A, Matto M, Eray M, Pellinen R, et al. The involvement of mitochondria and the caspase-9 activation pathway in rituximab-induced apoptosis in FL cells. Apoptosis. 2009;14(5):687-98.
213. van der Kolk LE, Evers LM, Omene C, Lens SM, Lederman S, van Lier RA, et al. CD20-induced B cell death can bypass mitochondria and caspase activation. Leukemia. 2002;16(9):1735-44.
214. de Haij S, Jansen JHM, Boross P, Beurskens FJ, Bakema JE, Bos DL, et al. In vivo Cytotoxicity of Type I CD20 Antibodies Critically Depends on Fc Receptor ITAM Signaling. Cancer Research. 2010;70(8):3209-17.
215. Overdijk MB, Jansen JHM, Nederend M, Lammerts van Bueren JJ, Groen RWJ, Parren PWHI, et al. The Therapeutic CD38 Monoclonal Antibody Daratumumab Induces Programmed Cell Death via Fcγ Receptor–Mediated Cross-Linking. The Journal of Immunology. 2016;197(3):807-13.
216. Smith MR. Rituximab (monoclonal anti-CD20 antibody): mechanisms of action and resistance. Oncogene. 2003;22(47):7359-68.
217. Raghavan M, Bjorkman PJ. Fc receptors and their interactions with immunoglobulins. Annu Rev Cell Dev Biol. 1996;12:181-220.
218. Nimmerjahn F, Ravetch JV. Fcgamma receptors as regulators of immune responses. Nature Reviews Immunology. 2008;8(1):34-47.

219. Muta T, Kurosaki T, Misulovin Z, Sanchez M, Nussenzweig MC, Ravetch JV. A 13-amino-acid motif in the cytoplasmic domain of Fc gamma RIIB modulates B-cell receptor signalling. Nature. 1994;368(6466):70-3.
220. Ravetch JV, Bolland S. IgG Fc receptors. Annual review of immunology. 2001;19:275-90.
221. Clynes RA, Towers TL, Presta LG, Ravetch JV. Inhibitory Fc receptors modulate in vivo cytoxicity against tumor targets. Nature Medicine. 2000;6(4):443-6.
222. Uchida J, Hamaguchi Y, Oliver JA, Ravetch JV, Poe JC, Haas KM, et al. The Innate Mononuclear Phagocyte Network Depletes B Lymphocytes through Fc Receptor–dependent Mechanisms during Anti-CD20 Antibody Immunotherapy. The Journal of Experimental Medicine. 2004;199(12):1659-69.
223. Cartron G, Dacheux L, Salles G, Solal-Celigny P, Bardos P, Colombat P, et al. Therapeutic activity of humanized anti-CD20 monoclonal antibody and polymorphism in IgG Fc receptor FcgammaRIIIa gene. Blood. 2002;99(3):754-8.
224. Weng W-K, Levy R. Two Immunoglobulin G Fragment C Receptor Polymorphisms Independently Predict Response to Rituximab in Patients With Follicular Lymphoma. Journal of Clinical Oncology. 2003;21(21):3940-7.
225. Keane C, Nourse J, Crooks P, Nguyen-Van D, Mutsando H, Mollee P, et al. Homozygous FCGR3A-158V alleles predispose to late onset neutropenia after CHOP-R for diffuse large B-cell lymphoma. Internal Medicine Journal. 2012;42(10):1113-9.
226. Mellor JD, Brown MP, Irving HR, Zalcberg JR, Dobrovic A. A critical review of the role of Fc gamma receptor polymorphisms in the response to monoclonal antibodies in cancer. Journal of Hematology & Oncology. 2013;6(1):1.
227. Farag SS, Flinn IW, Modali R, Lehman TA, Young D, Byrd JC. Fc gamma RIIIa and Fc gamma RIIa polymorphisms do not predict response to rituximab in B-cell chronic lymphocytic leukemia. Blood. 2004;103(4):1472-4.
228. Abdullah N, Greenman J, Pimenidou A, Topping KP, Monson JR. The role of monocytes and natural killer cells in mediating antibody-dependent lysis of colorectal tumour cells. Cancer immunology, immunotherapy : CII. 1999;48(9):517-24.
229. Manches O, Lui G, Chaperot L, Gressin R, Molens J-P, Jacob M-C, et al. In vitro mechanisms of action of rituximab on primary non-Hodgkin lymphomas. Blood. 2003;101(3):949-54.
230. Shinkai Y, Yoshida MC, Maeda K, Kobata T, Maruyama K, Yodoi J, et al. Molecular cloning and chromosomal assignment of a human perforin (PFP) gene. Immunogenetics. 1989;30(6):452-7.
231. Cullen SP, Martin SJ. Mechanisms of granule-dependent killing. Cell Death Differ. 2007;15(2):251-62.
232. Di Gaetano N, Cittera E, Nota R, Vecchi A, Grieco V, Scanziani E, et al. Complement activation determines the therapeutic activity of rituximab in vivo. The Journal of Immunology. 2003;171(3):1581-7.
233. Perdiguero EG, Klapproth K, Schulz C, Busch K, Azzoni E, Crozet L, et al. Tissue-resident macrophages originate from yolk-sac-derived erythro-myeloid progenitors. Nature. 2014;518(7540):547-51.
234. Martinez FO, Gordon S. The M1 and M2 paradigm of macrophage activation: time for reassessment. F1000prime reports. 2014;6:13.
235. Mantovani A, Sica A, Sozzani S, Allavena P, Vecchi A, Locati M. The chemokine system in diverse forms of macrophage activation and polarization. Trends in Immunology. 2004;25(12):677-86.
236. Mantovani A, Biswas SK, Galdiero MR, Sica A, Locati M. Macrophage plasticity and polarization in tissue repair and remodelling. The Journal of pathology. 2013;229(2):176-85.
237. Davies LC, Jenkins SJ, Allen JE, Taylor PR. Tissue-resident macrophages. Nature Immunology. 2013;14(10):986-95.

238. Roszer T. Understanding the Mysterious M2 Macrophage through Activation Markers and Effector Mechanisms. Mediators of Inflammation. 2015;2015:16.
239. Leidi M, Gotti E, Bologna L, Miranda E, Rimoldi M, Sica A, et al. M2 macrophages phagocytose rituximab-opsonized leukemic targets more efficiently than m1 cells in vitro. The Journal of Immunology. 2009;182(7):4415-22.
240. Herter S, Birk MC, Klein C, Gerdes C, Umana P, Bacac M. Glycoengineering of Therapeutic Antibodies Enhances Monocyte/Macrophage-Mediated Phagocytosis and Cytotoxicity. The Journal of Immunology. 2014;192(5):2252-60.
241. Beers S, French R, Chan H, Lim S, Jarrett T, Vidal R, et al. Antigenic modulation limits the efficacy of anti-CD20 antibodies: implications for antibody selection. Blood. 2010;115(25):5191-201.
242. Gong Q, Ou Q, Ye S, Lee WP, Cornelius J, Diehl L, et al. Importance of Cellular Microenvironment and Circulatory Dynamics in B Cell Immunotherapy. The Journal of Immunology. 2005;174(2):817-26.
243. Otten MA, van der Bij GJ, Verbeek SJ, Nimmerjahn F, Ravetch JV, Beelen RHJ, et al. Experimental Antibody Therapy of Liver Metastases Reveals Functional Redundancy between FcγRI and FcγRIV. The Journal of Immunology. 2008;181(10):6829-36.
244. Montalvao F, Garcia Z, Celli S, Breart B, xE, atrice, et al. The mechanism of anti-CD20–mediated B cell depletion revealed by intravital imaging. The Journal of Clinical Investigation. 2013;123(12):5098-103.
245. Gül N, Babes L, Siegmund K, Korthouwer R, Bögels M, Braster R, et al. Macrophages eliminate circulating tumor cells after monoclonal antibody therapy. The Journal of Clinical Investigation. 2014;124(2):812-23.
246. Lacey DC, Achuthan A, Fleetwood AJ, Dinh H, Roiniotis J, Scholz GM, et al. Defining GM-CSF- and macrophage-CSF-dependent macrophage responses by in vitro models. The Journal of Immunology. 2012;188(11):5752-65.
247. Cartron G, Zhao-Yang L, Baudard M, Kanouni T, Rouillé V, Quittet P, et al. Granulocyte-Macrophage Colony-Stimulating Factor Potentiates Rituximab in Patients With Relapsed Follicular Lymphoma: Results of a Phase II Study. Journal of Clinical Oncology. 2008;26(16):2725-31.
248. Strati P, Tong WG, Vitale C, Wierda WG, O'Brien S, Brown JR, et al. A phase II study of the combination of rituximab and granulocyte macrophage colony stimulating factor as treatment of patients with chronic lymphocytic leukemia. Leuk Lymphoma. 2014:1-3.
249. Haidar JH, Shamseddine A, Salem Z, Mrad YA, Nasr MR, Zaatari G, et al. Loss of CD20 expression in relapsed lymphomas after rituximab therapy. European Journal of Haematology. 2003;70(5):330-2.
250. Press OW, Appelbaum F, Ledbetter JA, Martin PJ, Zarling J, Kidd P, et al. Monoclonal antibody 1F5 (anti-CD20) serotherapy of human B cell lymphomas. Blood. 1987;69(2):584-91.
251. Beers SA, French RR, Chan HTC, Lim SH, Jarrett TC, Vidal RM, et al. Antigenic modulation limits the efficacy of anti-CD20 antibodies: implications for antibody selection. Blood. 2010;115(25):5191-201.
252. Beum PV, Kennedy AD, Williams ME, Lindorfer MA, Taylor RP. The Shaving Reaction: Rituximab/CD20 Complexes Are Removed from Mantle Cell Lymphoma and Chronic Lymphocytic Leukemia Cells by THP-1 Monocytes. The Journal of Immunology. 2006;176(4):2600-9.
253. Vaughan AT, Iriyama C, Beers SA, Chan CHT, Lim SH, Williams EL, et al. Inhibitory FcγRIIb (CD32b) becomes activated by therapeutic mAb in both cis and trans and drives internalization according to antibody specificity. Blood. 2014;123(5):669-77.
254. Lim SH, Vaughan AT, Ashton-Key M, Williams EL, Dixon SV, Chan HTC, et al. Fc gamma receptor IIb on target B cells promotes rituximab internalization and reduces clinical efficacy. Blood. 2011;118(9):2530-40.

255. Lee CS, Ashton-Key M, Cogliatti S, Rondeau S, Schmitz S-FH, Ghielmini M, et al. Expression of the inhibitory Fc gamma receptor IIB (FCGR2B, CD32B) on follicular lymphoma cells lowers the response rate to rituximab monotherapy (SAKK 35/98). British Journal of Haematology. 2015;168(1):145-8.
256. Roghanian A, Teige I, Martensson L, Cox KL, Kovacek M, Ljungars A, et al. Antagonistic human FcgammaRIIB (CD32B) antibodies have anti-tumor activity and overcome resistance to antibody therapy in vivo. Cancer Cell. 2015;27(4):473-88.
257. Shimizu R, Kikuchi J, Wada T, Ozawa K, Kano Y, Furukawa Y. HDAC inhibitors augment cytotoxic activity of rituximab by upregulating CD20 expression on lymphoma cells. Leukemia. 2010;24(10):1760-8.
258. Zinzani PL, Khuageva NK, Wang H, Garicochea B, Walewski J, Van Hoof A, et al. Bortezomib plus rituximab versus rituximab in patients with high-risk, relapsed, rituximab-naïve or rituximab-sensitive follicular lymphoma: subgroup analysis of a randomized phase 3 trial. Journal of Hematology & Oncology. 2012;5:67-.
259. Bil J, Winiarska M, Nowis D, Bojarczuk K, Dabrowska-Iwanicka A, Basak GW, et al. Bortezomib modulates surface CD20 in B-cell malignancies and affects rituximab-mediated complement-dependent cytotoxicity. Blood. 2010;115(18):3745-55.
260. Hagenbeek A, Fayad L, Delwail V, Rossi JF, Jacobsen E, Kuliczkowski K, et al. Evaluation of Ofatumumab, a Novel Human CD20 Monoclonal Antibody, as Single Agent Therapy in Rituximab-Refractory Follicular Lymphoma. ASH Annual Meeting Abstracts. 2009;114(22):935.
261. Morschhauser F, Marlton P, Vitolo U, Linden O, Seymour JF, Crump M, et al. Results of a phase I/II study of ocrelizumab, a fully humanized anti-CD20 mAb, in patients with relapsed/refractory follicular lymphoma. Annals of Oncology. 2010;21(9):1870-6.
262. Sehn LH, Assouline SE, Stewart DA, Mangel J, Gascoyne RD, Fine G, et al. A phase 1 study of obinutuzumab induction followed by 2 years of maintenance in patients with relapsed CD20-positive B-cell malignancies. Blood. 2012;119(22):5118-25.
263. Goede V, Fischer K, Busch R, Engelke A, Eichhorst B, Wendtner CM, et al. Obinutuzumab plus Chlorambucil in Patients with CLL and Coexisting Conditions. New England Journal of Medicine. 2014;370(12):1101-10.
264. Shields RL, Lai J, Keck R, O'Connell LY, Hong K, Meng YG, et al. Lack of Fucose on Human IgG1 N-Linked Oligosaccharide Improves Binding to Human FcγRIII and Antibody-dependent Cellular Toxicity. Journal of Biological Chemistry. 2002;277(30):26733-40.
265. Herter S, Herting F, Mundigl O, Waldhauer I, Weinzierl T, Fauti T, et al. Preclinical Activity of the Type II CD20 Antibody GA101 (Obinutuzumab) Compared with Rituximab and Ofatumumab In Vitro and in Xenograft Models. Molecular Cancer Therapeutics. 2013;12(10):2031-42.
266. Chanan-Khan A, Porter CW. Immunomodulating drugs for chronic lymphocytic leukaemia. The Lancet Oncology. 2006;7(6):480-8.
267. Badoux XC, Keating MJ, Wen S, Lee B-N, Sivina M, Reuben J, et al. Lenalidomide as initial therapy of elderly patients with chronic lymphocytic leukemia. Blood. 2011;118(13):3489-98.
268. Chen CI, Bergsagel PL, Paul H, Xu W, Lau A, Dave N, et al. Single-Agent Lenalidomide in the Treatment of Previously Untreated Chronic Lymphocytic Leukemia. Journal of Clinical Oncology. 2011;29(9):1175-81.
269. Chanan-Khan A, Miller KC, Musial L, Lawrence D, Padmanabhan S, Takeshita K, et al. Clinical Efficacy of Lenalidomide in Patients With Relapsed or Refractory Chronic Lymphocytic Leukemia: Results of a Phase II Study. Journal of Clinical Oncology. 2006;24(34):5343-9.
270. Ferrajoli A, Lee B-N, Schlette EJ, O'Brien SM, Gao H, Wen S, et al. Lenalidomide induces complete and partial remissions in patients with relapsed and refractory chronic lymphocytic leukemia. Blood. 2008;111(11):5291-7.
271. Ramsay AG, Johnson AJ, Lee AM, Gorgun G, Le Dieu R, Blum W, et al. Chronic lymphocytic leukemia T cells show impaired immunological synapse formation that can be

reversed with an immunomodulating drug. Journal of Clinical Investigation. 2008;118(7):2427-37.
272. Reddy N, Hernandez-Ilizaliturri FJ, Deeb G, Roth M, Vaughn M, Knight J, et al. Immunomodulatory drugs stimulate natural killer-cell function, alter cytokine production by dendritic cells, and inhibit angiogenesis enhancing the anti-tumour activity of rituximab in vivo. British Journal of Haematology. 2008;140(1):36-45.
273. Wu L, Adams M, Carter T, Chen R, Muller G, Stirling D, et al. Lenalidomide Enhances Natural Killer Cell and Monocyte-Mediated Antibody-Dependent Cellular Cytotoxicity of Rituximab-Treated CD20+ Tumor Cells. Clinical Cancer Research. 2008;14(14):4650-7.
274. Thompson PA, Keating MJ, Hinojosa C, Smith SC, Daver NG, Jain N, et al. Lenalidomide and Rituximab in Combination As Initial Treatment of Chronic Lymphocytic Leukemia: Initial Results of a Phase II Study. Blood. 2014;124(21):1988-.
275. Kim ES, Dhillon S. Ibrutinib: a review of its use in patients with mantle cell lymphoma or chronic lymphocytic leukaemia. Drugs. 2015;75(7):769-76.
276. Herman SE, Gordon AL, Hertlein E, Ramanunni A, Zhang X, Jaglowski S, et al. Bruton tyrosine kinase represents a promising therapeutic target for treatment of chronic lymphocytic leukemia and is effectively targeted by PCI-32765. Blood. 2011;117(23):6287-96.
277. Ponader S, Chen SS, Buggy JJ, Balakrishnan K, Gandhi V, Wierda WG, et al. The Bruton tyrosine kinase inhibitor PCI-32765 thwarts chronic lymphocytic leukemia cell survival and tissue homing in vitro and in vivo. Blood. 2012;119(5):1182-9.
278. Byrd JC, Furman RR, Coutre SE, Burger JA, Blum KA, Coleman M, et al. Three-year follow-up of treatment-naïve and previously treated patients with CLL and SLL receiving single-agent ibrutinib. Blood. 2015;125(16):2497-506.
279. Jain P, Keating MJ, Wierda W, Sivina M, Thompson PA, Ferrajoli A, et al. Long term follow up of treatment with ibrutinib and rituximab (IR) in patients with high-risk Chronic Lymphocytic Leukemia (CLL). Clinical Cancer Research. 2016.
280. Hoellenriegel J, Meadows SA, Sivina M, Wierda WG, Kantarjian H, Keating MJ, et al. The phosphoinositide 3'-kinase delta inhibitor, CAL-101, inhibits B-cell receptor signaling and chemokine networks in chronic lymphocytic leukemia. Blood. 2011;118(13):3603-12.
281. Lannutti BJ, Meadows SA, Herman SEM, Kashishian A, Steiner B, Johnson AJ, et al. CAL-101, a p110δ selective phosphatidylinositol-3-kinase inhibitor for the treatment of B-cell malignancies, inhibits PI3K signaling and cellular viability. Blood. 2011;117(2):591-4.
282. Ren Z, Guo J, Liao J, Luan Y, Liu Z, Sun Z, et al. CTLA-4 limits anti-CD20-mediated tumor regression. Clinical Cancer Research. 2016.
283. Brusa D, Serra S, Coscia M, Rossi D, D'Arena G, Laurenti L, et al. The PD-1/PD-L1 axis contributes to T-cell dysfunction in chronic lymphocytic leukemia. Haematologica. 2013;98(6):953-63.
284. Westin JR, Chu F, Zhang M, Fayad LE, Kwak LW, Fowler N, et al. Safety and activity of PD1 blockade by pidilizumab in combination with rituximab in patients with relapsed follicular lymphoma: a single group, open-label, phase 2 trial. The Lancet Oncology. 2014;15(1):69-77.
285. Gillis C, Gouel-Chéron A, Jönsson F, Bruhns P. Contribution of Human FcγRs to Disease with Evidence from Human Polymorphisms and Transgenic Animal Studies. Frontiers in Immunology. 2014;5(254):00254.
286. Pincetic A, Bournazos S, DiLillo DJ, Maamary J, Wang TT, Dahan R, et al. Type I and type II Fc receptors regulate innate and adaptive immunity. Nature Immunology. 2014;15(8):707-16.
287. Woolf JM, Burton DR. Human antibody-Fc receptor interactions illuminated by crystal structures. Nature Reviews Immunology. 2004;4(2):89-99.
288. Meknache N, Jönsson F, Laurent J, Guinnepain M-T, Daëron M. Human basophils express the glycosylphosphatidylinositol-anchored low-affinity IgG receptor FcgammaRIIIB (CD16B). The Journal of Immunology. 2009;182(4):2542-50.

289. Guilliams M, Bruhns P, Saeys Y, Hammad H, Lambrecht BN. The function of Fc[gamma] receptors in dendritic cells and macrophages. Nature Reviews Immunology. 2014;14(2):94-108.
290. Bruhns P, Iannascoli B, England P, Mancardi DA, Fernandez N, Jorieux S, et al. Specificity and affinity of human Fcγ receptors and their polymorphic variants for human IgG subclasses. Blood. 2009;113(16):3716-25.
291. Cambier JC. Antigen and Fc receptor signaling. The awesome power of the immunoreceptor tyrosine-based activation motif (ITAM). The Journal of Immunology. 1995;155(7):3281-5.
292. Fernandes Maria J G, Rollet-Labelle E, Paré G, Marois S, Tremblay M-L, Teillaud J-L, et al. CD16b associates with high-density, detergent-resistant membranes in human neutrophils. Biochemical Journal. 2006;393(Pt 1):351-9.
293. Kiyoshi M, Caaveiro JMM, Kawai T, Tashiro S, Ide T, Asaoka Y, et al. Structural basis for binding of human IgG1 to its high-affinity human receptor Fc[gamma]RI. Nature Communications. 2015;6.
294. Lu J, Chu J, Zou Z, Hamacher NB, Rixon MW, Sun PD. Structure of FcγRI in complex with Fc reveals the importance of glycan recognition for high-affinity IgG binding. Proceedings of the National Academy of Sciences. 2015;112(3):833-8.
295. van der Poel CE, Spaapen RM, van de Winkel JG, Leusen JH. Functional characteristics of the high affinity IgG receptor, FcgammaRI. The Journal of Immunology. 2011;186(5):2699-704.
296. Mancardi DA, Albanesi M, Jonsson F, Iannascoli B, Van Rooijen N, Kang X, et al. The high-affinity human IgG receptor FcgammaRI (CD64) promotes IgG-mediated inflammation, anaphylaxis, and antitumor immunotherapy. Blood. 2013;121(9):1563-73.
297. James ND, Atherton PJ, Jones J, Howie AJ, Tchekmedyian S, Curnow RT. A phase II study of the bispecific antibody MDX-H210 (anti-HER2 [times] CD64) with GM-CSF in HER2+ advanced prostate cancer. British Journal of Cancer. 2001;85(2):152-6.
298. van der Poel CE, Karssemeijer RA, Boross P, van der Linden JA, Blokland M, van de Winkel JGJ, et al. Cytokine-induced immune complex binding to the high-affinity IgG receptor, FcγRI, in the presence of monomeric IgG. Blood. 2010;116(24):5327-33.
299. Rollet-Labelle E, Marois S, Barbeau K, Malawista S, Naccache P. Recruitment of the cross-linked opsonic receptor CD32A (FcgammaRIIA) to high-density detergent-resistant membrane domains in human neutrophils. The Biochemical Journal. 2004;381(3):919-28.
300. Golay J, Da Roit F, Bologna L, Ferrara C, Leusen JH, Rambaldi A, et al. Glycoengineered CD20 antibody obinutuzumab activates neutrophils and mediates phagocytosis through CD16B more efficiently than rituximab. Blood. 2013;122(20):3482-91.
301. Richards JO, Karki S, Lazar GA, Chen H, Dang W, Desjarlais JR. Optimization of antibody binding to FcγRIIa enhances macrophage phagocytosis of tumor cells. Molecular Cancer Therapeutics. 2008;7(8):2517-27.
302. Powell MS, Barnes NC, Bradford TM, Musgrave IF, Wines BD, Cambier JC, et al. Alteration of the FcγRIIa Dimer Interface Affects Receptor Signaling but Not Ligand Binding. The Journal of Immunology. 2006;176(12):7489-94.
303. Sardjono CT, Mottram PL, Velde NCvd, Powell MS, Power D, Slocombe RF, et al. Development of spontaneous multisystem autoimmune disease and hypersensitivity to antibody-induced inflammation in Fcγ receptor IIa–transgenic mice. Arthritis & Rheumatism. 2005;52(10):3220-9.
304. Yuasa T, Kubo S, Yoshino T, Ujike A, Matsumura K, Ono M, et al. Deletion of fcgamma receptor IIB renders H-2(b) mice susceptible to collagen-induced arthritis. Journal of Experimental Medicine. 1999;189(1):187-94.
305. Qin D, Wu J, Vora KA, Ravetch JV, Szakal AK, Manser T, et al. Fc gamma receptor IIB on follicular dendritic cells regulates the B cell recall response. The Journal of Immunology. 2000;164(12):6268-75.

306. Smith KGC, Clatworthy MR. Fc[gamma]RIIB in autoimmunity and infection: evolutionary and therapeutic implications. Nature Reviews Immunology. 2010;10(5):328-43.
307. Brooks DG, Qiu WQ, Luster AD, Ravetch JV. Structure and expression of human IgG FcRII(CD32). Functional heterogeneity is encoded by the alternatively spliced products of multiple genes. J Exp Med. 1989;170(4):1369-85.
308. Miettinen HM, Matter K, Hunziker W, Rose JK, Mellman I. Fc receptor endocytosis is controlled by a cytoplasmic domain determinant that actively prevents coated pit localization. The Journal of Cell Biology. 1992;116(4):875-88.
309. Tipton TR, Roghanian A, Oldham RJ, Carter MJ, Cox KL, Mockridge CI, et al. Antigenic modulation limits the effector cell mechanisms employed by type I anti-CD20 monoclonal antibodies. Blood. 2015;125(12):1901-9.
310. Willcocks LC, Carr EJ, Niederer HA, Rayner TF, Williams TN, Yang W, et al. A defunctioning polymorphism in FCGR2B is associated with protection against malaria but susceptibility to systemic lupus erythematosus. Proceedings of the National Academy of Sciences. 2010;107(17):7881-5.
311. Su K, Yang H, Li X, Li X, Gibson AW, Cafardi JM, et al. Expression profile of FcgammaRIIb on leukocytes and its dysregulation in systemic lupus erythematosus. The Journal of Immunology. 2007;178(5):3272-80.
312. van der Heijden J, Breunis WB, Geissler J, de Boer M, van den Berg TK, Kuijpers TW. Phenotypic variation in IgG receptors by nonclassical FCGR2C alleles. The Journal of Immunology. 2012;188(3):1318-24.
313. Su K, Wu J, Edberg JC, McKenzie SE, Kimberly RP. Genomic organization of classical human low-affinity Fcγ receptor genes. Genes Immun. 2002;3(S1):S51-S6.
314. Li X, Wu J, Ptacek T, Redden DT, Brown EE, Alarcón GS, et al. Allelic-Dependent Expression of an Activating Fc Receptor on B Cells Enhances Humoral Immune Responses. Science Translational Medicine. 2013;5(216):216-175.
315. Ernst L, Metes D, Herberman R, Morel P. Allelic polymorphisms in the FcγRIIC gene can influence its function on normal human natural killer cells. J Mol Med. 2002;80(4):248-57.
316. Nagler A, Lanier LL, Cwirla S, Phillips JH. Comparative studies of human FcRIII-positive and negative natural killer cells. The Journal of Immunology. 1989;143(10):3183-91.
317. Park JG, Isaacs RE, Chien P, Schreiber AD. In the absence of other Fc receptors, Fc gamma RIIIA transmits a phagocytic signal that requires the cytoplasmic domain of its gamma subunit. Journal of Clinical Investigation. 1993;92(4):1967-73.
318. Golay J, Leidi M, Palumbo GA, Introna M. Human Macrophages Phagocytose Rituximab Opsonised Leukemic Cells Via CD16, CD32 and CD64 but Do Not Mediate ADCC. ASH Annual Meeting Abstracts. 2006;108(11):2507.
319. McKinney C, Merriman TR. Meta-analysis confirms a role for deletion in FCGR3B in autoimmune phenotypes. Human Molecular Genetics. 2012;21(10):2370-6.
320. Davies KA, Peters AM, Beynon HL, Walport MJ. Immune complex processing in patients with systemic lupus erythematosus. In vivo imaging and clearance studies. The Journal of Clinical Investigation. 1992;90(5):2075-83.
321. Mancardi DA, Iannascoli B, Hoos S, England P, Daeron M, Bruhns P. FcgammaRIV is a mouse IgE receptor that resembles macrophage FcepsilonRI in humans and promotes IgE-induced lung inflammation. Journal of Clinical Investigation. 2008;118(11):3738-50.
322. Daeron M. Fc receptor biology. Annual review of immunology. 1997;15:203-34.
323. Nimmerjahn F, Ravetch JV. Fcγ Receptors: Old Friends and New Family Members. Immunity. 2006;24(1):19-28.
324. Bruhns P. Properties of mouse and human IgG receptors and their contribution to disease models. Blood. 2012;119(24):5640-9.
325. Pitcher LA, van Oers NSC. T-cell receptor signal transmission: who gives an ITAM? Trends in Immunology. 2003;24(10):554-60.

326. Reth M. Antigen receptor tail clue. Nature. 1989;338(6214):383-4.
327. Isakov N. Immunoreceptor tyrosine-based activation motif (ITAM), a unique module linking antigen and Fc receptors to their signaling cascades. J Leukoc Biol. 1997;61(1):6-16.
328. Romeo C, Amiot M, Seed B. Sequence requirements for induction of cytolysis by the T cell antigenFc receptor ζ chain. Cell. 1992;68(5):889-97.
329. Suzuki T, Kono H, Hirose N, Okada M, Yamamoto T, Yamamoto K, et al. Differential involvement of Src family kinases in Fc gamma receptor-mediated phagocytosis. The Journal of Immunology. 2000;165(1):473-82.
330. Crowley MT, Costello PS, Fitzer-Attas CJ, Turner M, Meng F, Lowell C, et al. A Critical Role for Syk in Signal Transduction and Phagocytosis Mediated by Fcγ Receptors on Macrophages. The Journal of Experimental Medicine. 1997;186(7):1027-39.
331. Lowell CA. Src-family and Syk Kinases in Activating and Inhibitory Pathways in Innate Immune Cells – Signaling Crosstalk. Cold Spring Harbor Perspectives in Biology. 2011;3(3).
332. Catalina MI, Fischer MJE, Dekker FJ, Liskamp RMJ, Heck AJR. Binding of a Diphosphorylated-ITAM Peptide to Spleen Tyrosine Kinase (Syk) Induces Distal Conformational Changes: A Hydrogen Exchange Mass Spectrometry Study. Journal of the American Society for Mass Spectrometry. 2005;16(7):1039-51.
333. Furlong MT, Mahrenholz AM, Kim K-H, Ashendel CL, Harrison ML, Geahlen RL. Identification of the major sites of autophosphorylation of the murine protein-tyrosine kinase Syk. Biochimica et Biophysica Acta. 1997;1355(2):177-90.
334. Milella M, Gismondi A, Roncaioli P, Bisogno L, Palmieri G, Frati L, et al. CD16 cross-linking induces both secretory and extracellular signal-regulated kinase (ERK)-dependent cytosolic phospholipase A2 (PLA2) activity in human natural killer cells: involvement of ERK, but not PLA2, in CD16-triggered granule exocytosis. The Journal of Immunology. 1997;158(7):3148-54.
335. Luo Y, Pollard JW, Casadevall A. Fcgamma receptor cross-linking stimulates cell proliferation of macrophages via the ERK pathway. The Journal of biological chemistry. 2010;285(6):4232-42.
336. Araki N, Johnson, M. T., Swanson, J. A. A role for phosphoinositide 3-kinase in the completion of macropinocytosis and phagocytosis by macrophages. The Journal of Cell Biology. 1996;135(5):1249-60.
337. Swanson JA, Hoppe AD. The coordination of signaling during Fc receptor-mediated phagocytosis. Journal of Leukocyte Biology. 2004;76(6):1093-103.
338. Kanakaraj P, Duckworth B, Azzoni L, Kamoun M, Cantley LC, Perussia B. Phosphatidylinositol-3 kinase activation induced upon Fc gamma RIIIA-ligand interaction. The Journal of Experimental Medicine. 1994;179(2):551-8.
339. Larsen EC, DiGennaro JA, Saito N, Mehta S, Loegering DJ, Mazurkiewicz JE, et al. Differential requirement for classic and novel PKC isoforms in respiratory burst and phagocytosis in RAW 264.7 cells. The Journal of Immunology. 2000;165(5):2809-17.
340. Di Virgilio F, Meyer BC, Greenberg S, Silverstein SC. Fc receptor-mediated phagocytosis occurs in macrophages at exceedingly low cytosolic Ca2+ levels. J Cell Biol. 1988;106(3):657-66.
341. Mao Y, Finnemann SC. Regulation of phagocytosis by Rho GTPases. Small GTPases. 2015;6(2):89-99.
342. Caron E, Hall A. Identification of two distinct mechanisms of phagocytosis controlled by different Rho GTPases. Science. 1998;282(5394):1717-21.
343. Dart AE, Donnelly SK, Holden DW, Way M, Caron E. Nck and Cdc42 co-operate to recruit N-WASP to promote FcgammaR-mediated phagocytosis. Journal of cell science. 2012;125(12):2825-30.
344. Unkeless JC, Jin J. Inhibitory receptors, ITIM sequences and phosphatases. Current Opinion in Immunology. 1997;9(3):338-43.

345. Malbec O, Fong DC, Turner M, Tybulewicz VL, Cambier JC, Fridman WH, et al. Fc epsilon receptor I-associated lyn-dependent phosphorylation of Fc gamma receptor IIB during negative regulation of mast cell activation. The Journal of Immunology. 1998;160(4):1647-58.
346. Getahun A, Cambier JC. Of ITIMs, ITAMs, and ITAMis: revisiting immunoglobulin Fc receptor signaling. Immunological Reviews. 2015;268(1):66-73.
347. March M, Ravichandran K. Regulation of the immune response by SHIP. Seminars in Immunology. 2002;14(1):37-47.
348. Ming-Lum A, Shojania S, So E, McCarrell E, Shaw E, Vu D, et al. A pleckstrin homology-related domain in SHIP1 mediates membrane localization during Fcγ receptor-induced phagocytosis. The FASEB Journal. 2012;26(8):3163-77.
349. Mashima R, Hishida Y, Tezuka T, Yamanashi Y. The roles of Dok family adapters in immunoreceptor signaling. Immunological Reviews. 2009;232(1):273-85.
350. Pritchard NR, Smith KGC. B cell inhibitory receptors and autoimmunity. Immunology. 2003;108(3):263-73.
351. Bolland S, Ravetch JV. Inhibitory pathways triggered by ITIM-containing receptors. Adv Immunol. 1999;72:149-77.
352. Nimmerjahn F. Activating and inhibitory FcγRs in autoimmune disorders. Springer Seminars in Immunopathology. 2006;28(4):305-19.
353. Hippen KL, Buhl AM, D'Ambrosio D, Nakamura K, Persin C, Cambier JC. FcγRIIB1 Inhibition of BCR-Mediated Phosphoinositide Hydrolysis and Ca2+ Mobilization Is Integrated by CD19 Dephosphorylation. Immunity. 1997;7(1):49-58.
354. Van Sorge NM, Van Der Pol WL, Van De Winkel JGJ. FcγR polymorphisms: Implications for function, disease susceptibility and immunotherapy. Tissue Antigens. 2003;61(3):189-202.
355. van der Pol WL, van den Berg LH, Scheepers RH, van der Bom JG, van Doorn PA, van Koningsveld R, et al. IgG receptor IIa alleles determine susceptibility and severity of Guillain-Barre syndrome. Neurology. 2000;54(8):1661-5.
356. Duan J, Lou J, Zhang Q, Ke J, Qi Y, Shen N, et al. A Genetic Variant rs1801274 in FCGR2A as a Potential Risk Marker for Kawasaki Disease: A Case-Control Study and Meta-Analysis. PLoS ONE. 2014;9(8):e103329.
357. Zhu X-W, Wang Y, Wei Y-H, Zhao P-P, Wang X-B, Rong J-J, et al. Comprehensive Assessment of the Association between FCGRs polymorphisms and the risk of systemic lupus erythematosus: Evidence from a Meta-Analysis. Scientific Reports. 2016;6:31617.
358. Wang D, Hu S-L, Cheng X-L, Yang J-Y. FCGR2A rs1801274 polymorphism is associated with risk of childhood-onset idiopathic (immune) thrombocytopenic purpura: Evidence from a meta-analysis. Thrombosis Research. 2014;134(6):1323-7.
359. Kono H, Kyogoku C, Suzuki T, Tsuchiya N, Honda H, Yamamoto K, et al. FcgammaRIIB Ile232Thr transmembrane polymorphism associated with human systemic lupus erythematosus decreases affinity to lipid rafts and attenuates inhibitory effects on B cell receptor signaling. Human Molecular Genetics. 2005;14(19):2881-92.
360. Bournazos S, Bournazou I, Murchison JT, Wallace WA, McFarlane P, Hirani N, et al. Fcγ Receptor IIIb (CD16b) Polymorphisms are Associated with Susceptibility to Idiopathic Pulmonary Fibrosis. Lung. 2010;188(6):475-81.
361. Paiva M, Marques H, Martins Â, Ferreira P, Catarino R, Medeiros R. FcγRIIa polymorphism and clinical response to rituximab in non-Hodgkin lymphoma patients. Cancer Genetics and Cytogenetics. 2008;183(1):35-40.
362. Mitrovic Z, Aurer I, Radman I, Ajdukovic R, Sertic J, Labar B. FCgammaRIIIA and FCgammaRIIA polymorphisms are not associated with response to rituximab and CHOP in patients with diffuse large B-cell lymphoma. Haematologica. 2007;92(7):998-9.
363. Kyogoku C, Dijstelbloem HM, Tsuchiya N, Hatta Y, Kato H, Yamaguchi A, et al. Fcγ receptor gene polymorphisms in Japanese patients with systemic lupus erythematosus: Contribution of FCGR2B to genetic susceptibility. Arthritis & Rheumatism. 2002;46(5):1242-54.

364. Kyogoku C, Tsuchiya N, Matsuta K, Tokunaga K. Studies on the association of Fc gamma receptor IIA, IIB, IIIA and IIIB polymorphisms with rheumatoid arthritis in the Japanese: evidence for a genetic interaction between HLA-DRB1 and FCGR3A. Genes and Immunity. 2002;3(8):488-93.
365. Li X, Wu J, Carter RH, Edberg JC, Su K, Cooper GS, et al. A novel polymorphism in the Fcgamma receptor IIB (CD32B) transmembrane region alters receptor signaling. Arthritis and Rheumatism. 2003;48(11):3242-52.
366. Radstake TR, Franke B, Wenink MH, Nabbe KC, Coenen MJ, Welsing P, et al. The functional variant of the inhibitory Fcgamma receptor IIb (CD32B) is associated with the rate of radiologic joint damage and dendritic cell function in rheumatoid arthritis. Arthritis and Rheumatism. 2006;54(12):3828-37.
367. Mo N, Lai R, Luo S, Xie J, Wang X, Liu L, et al. A Transmembrane Polymorphism of Fcgamma Receptor IIb Is Associated with Kidney Deficiency Syndrome in Rheumatoid Arthritis. Evidence-Based Complementary and Alternative Medicine. 2016;2016:7.
368. Floto RA, Clatworthy MR, Heilbronn KR, Rosner DR, MacAry PA, Rankin A, et al. Loss of function of a lupus-associated Fc[gamma]RIIb polymorphism through exclusion from lipid rafts. Nature Medicine. 2005;11(10):1056-8.
369. Weng W-K, Levy R. Genetic polymorphism of the inhibitory IgG Fc receptor FcγRIIb is not associated with clinical outcome in patients with follicular lymphoma treated with rituximab. Leukemia & lymphoma. 2009;50(5):723-7.
370. Salmon JE, Edberg JC, Brogle NL, Kimberly RP. Allelic polymorphisms of human Fc gamma receptor IIA and Fc gamma receptor IIIB. Independent mechanisms for differences in human phagocyte function. Journal of Clinical Investigation. 1992;89(4):1274-81.
371. Cartron G, Ohresser M, Salles G, Solal-Celigny P, Colombat P, Watier H. Neutrophil role in in vivo anti-lymphoma activity of rituximab: FCGR3B-NA1/NA2 polymorphism does not influence response and survival after rituximab treatment. Annals of Oncology. 2008;19(8):1485-7.
372. Wu J, Edberg JC, Redecha PB, Bansal V, Guyre PM, Coleman K, et al. A novel polymorphism of FcgammaRIIIa (CD16) alters receptor function and predisposes to autoimmune disease. The Journal of Clinical Investigation. 1997;100(5):1059-70.
373. Edberg JC, Langefeld CD, Wu J, Moser KL, Kaufman KM, Kelly J, et al. Genetic linkage and association of Fcγ receptor IIIA (CD16A) on chromosome 1q23 with human systemic lupus erythematosus. Arthritis & Rheumatism. 2002;46(8):2132-40.
374. Persky DO, Dornan D, Goldman BH, Braziel RM, Fisher RI, Leblanc M, et al. Fc gamma receptor 3a genotype predicts overall survival in follicular lymphoma patients treated on SWOG trials with combined monoclonal antibody plus chemotherapy but not chemotherapy alone. Haematologica. 2012;97(6):937-42.
375. Ghesquieres H, Cartron G, Seymour JF, Delfau-Larue MH, Offner F, Soubeyran P, et al. Clinical outcome of patients with follicular lymphoma receiving chemoimmunotherapy in the PRIMA study is not affected by FCGR3A and FCGR2A polymorphisms. Blood. 2012;120(13):2650-7.
376. Bibeau F, Lopez-Crapez E, Di Fiore F, Thezenas S, Ychou M, Blanchard F, et al. Impact of FcγRIIa-FcγRIIIa Polymorphisms and KRAS Mutations on the Clinical Outcome of Patients With Metastatic Colorectal Cancer Treated With Cetuximab Plus Irinotecan. Journal of Clinical Oncology. 2009;27(7):1122-9.
377. Rodríguez J, Zarate R, Bandres E, Boni V, Hernández A, Sola JJ, et al. Fc gamma receptor polymorphisms as predictive markers of Cetuximab efficacy in epidermal growth factor receptor downstream-mutated metastatic colorectal cancer. European Journal of Cancer. 2012;48(12):1774-80.
378. Etienne-Grimaldi MC, Bennouna J, Formento JL, Douillard JY, Francoual M, Hennebelle I, et al. Multifactorial pharmacogenetic analysis in colorectal cancer patients receiving 5-

fluorouracil-based therapy together with cetuximab-irinotecan. British Journal of Clinical Pharmacology. 2012;73(5):776-85.
379. Cao R, Zhang Y. The functions of E(Z)/EZH2-mediated methylation of lysine 27 in histone H3. Current Opinion in Genetics & Development. 2004;14(2):155-64.
380. Dahan L, Norguet E, Etienne-Grimaldi MC, Formento JL, Gasmi M, Nanni I, et al. Pharmacogenetic profiling and cetuximab outcome in patients with advanced colorectal cancer. BMC cancer. 2011;11:496.
381. Zhang W, Gordon M, Schultheis AM, Yang DY, Nagashima F, Azuma M, et al. FCGR2A and FCGR3A Polymorphisms Associated With Clinical Outcome of Epidermal Growth Factor Receptor–Expressing Metastatic Colorectal Cancer Patients Treated With Single-Agent Cetuximab. Journal of Clinical Oncology. 2007;25(24):3712-8.
382. Ying HQ, Wang F, Chen XL, He BS, Pan YQ, Jie C, et al. FCGR2A, FCGR3A polymorphisms and therapeutic efficacy of anti-EGFR monoclonal antibody in metastatic colorectal cancer. Oncotarget. 2015;6(29):28071-83.
383. Bournazos S, Woof JM, Hart SP, Dransfield I. Functional and clinical consequences of Fc receptor polymorphic and copy number variants. Clinical and Experimental Immunology. 2009;157(2):244-54.
384. Willcocks LC, Lyons PA, Clatworthy MR, Robinson JI, Yang W, Newland SA, et al. Copy number of FCGR3B, which is associated with systemic lupus erythematosus, correlates with protein expression and immune complex uptake. The Journal of Experimental Medicine. 2008;205(7):1573-82.
385. Franke L, el Bannoudi H, Jansen DT, Kok K, Trynka G, Diogo D, et al. Association analysis of copy numbers of FC-gamma receptor genes for rheumatoid arthritis and other immune-mediated phenotypes. European Journal of Human Genetics. 2016;24(2):263-70.
386. Breunis WB, van Mirre E, Geissler J, Laddach N, Wolbink G, van der Schoot E, et al. Copy number variation at the FCGR locus includes FCGR3A, FCGR2C and FCGR3B but not FCGR2A and FCGR2B. Human Mutation. 2009;30(5):E640-E50.
387. Roopenian DC, Akilesh S. FcRn: the neonatal Fc receptor comes of age. Nature Reviews Immunology. 2007;7(9):715-25.
388. Burmeister WP, Gastinel LN, Simister NE, Blum ML, Bjorkman PJ. Crystal structure at 2.2 A resolution of the MHC-related neonatal Fc receptor. Nature. 1994;372(6504):336-43.
389. Rodewald R. pH-dependent binding of immunoglobulins to intestinal cells of the neonatal rat. The Journal of Cell Biology. 1976;71(2):666-9.
390. Mitragotri S, Burke PA, Langer R. Overcoming the challenges in administering biopharmaceuticals: formulation and delivery strategies. Nature Reviews Drug Discovery. 2014;13(9):655-72.
391. Leach JL, Sedmak DD, Osborne JM, Rahill B, Lairmore MD, Anderson CL. Isolation from human placenta of the IgG transporter, FcRn, and localization to the syncytiotrophoblast: implications for maternal-fetal antibody transport. The Journal of Immunology. 1996;157(8):3317-22.
392. Kristoffersen EK. Human placental Fc gamma-binding proteins in the maternofetal transfer of IgG. APMIS Supplementum. 1996;64:5-36.
393. Jones EA, Waldmann TA. The mechanism of intestinal uptake and transcellular transport of IgG in the neonatal rat. Journal of Clinical Investigation. 1972;51(11):2916-27.
394. Vaughn DE, Bjorkman PJ. Structural basis of pH-dependent antibody binding by the neonatal Fc receptor. Structure. 1998;6(1):63-73.
395. Raghavan M, Bonagura VR, Morrison SL, Bjorkman PJ. Analysis of the pH Dependence of the Neonatal Fc Receptor/Immunoglobulin G Interaction Using Antibody and Receptor Variants. Biochemistry. 1995;34(45):14649-57.

396. Kim JK, Firan M, Radu CG, Kim CH, Ghetie V, Ward ES. Mapping the site on human IgG for binding of the MHC class I-related receptor, FcRn. European Journal of Immunology. 1999;29(9):2819-25.
397. Roopenian DC, Christianson GJ, Sproule TJ, Brown AC, Akilesh S, Jung N, et al. The MHC Class I-Like IgG Receptor Controls Perinatal IgG Transport, IgG Homeostasis, and Fate of IgG-Fc-Coupled Drugs. The Journal of Immunology. 2003;170(7):3528-33.
398. Petkova SB, Akilesh S, Sproule TJ, Christianson GJ, Al Khabbaz H, Brown AC, et al. Enhanced half-life of genetically engineered human IgG1 antibodies in a humanized FcRn mouse model: potential application in humorally mediated autoimmune disease. International Immunology. 2006;18(12):1759-69.
399. Kenanova V, Olafsen T, Crow DM, Sundaresan G, Subbarayan M, Carter NH, et al. Tailoring the pharmacokinetics and positron emission tomography imaging properties of anti-carcinoembryonic antigen single-chain Fv-Fc antibody fragments. Cancer Res. 2005;65(2):622-31.
400. Yu Z, Lennon VA. Mechanism of Intravenous Immune Globulin Therapy in Antibody-Mediated Autoimmune Diseases. New England Journal of Medicine. 1999;340(3):227-8.
401. Wall RJ, Shani M. Are animal models as good as we think? Theriogenology. 2008;69(1):2-9.
402. Ahuja A, Shupe J, Dunn R, Kashgarian M, Kehry MR, Shlomchik MJ. Depletion of B Cells in Murine Lupus: Efficacy and Resistance. The Journal of Immunology. 2007;179(5):3351-61.
403. Döhner H, Stilgenbauer S, Benner A, Leupolt E, Kröber A, Bullinger L, et al. Genomic Aberrations and Survival in Chronic Lymphocytic Leukemia. New England Journal of Medicine. 2000;343(26):1910-6.
404. Klein U, Lia M, Crespo M, Siegel R, Shen Q, Mo T, et al. The DLEU2/miR-15a/16-1 Cluster Controls B Cell Proliferation and Its Deletion Leads to Chronic Lymphocytic Leukemia. Cancer Cell. 2010;17(1):28-40.
405. Virgilio L, Narducci MG, Isobe M, Billips LG, Cooper MD, Croce CM, et al. Identification of the TCL1 gene involved in T-cell malignancies. Proceedings of the National Academy of Sciences of the United States of America. 1994;91(26):12530-4.
406. Narducci MG, Pescarmona E, Lazzeri C, Signoretti S, Lavinia AM, Remotti D, et al. Regulation of TCL1 Expression in B- and T-Cell Lymphomas and Reactive Lymphoid Tissues. Cancer Research. 2000;60(8):2095-100.
407. Bichi R, Shinton SA, Martin ES, Koval A, Calin GA, Cesari R, et al. Human chronic lymphocytic leukemia modeled in mouse by targeted TCL1 expression. Proceedings of the National Academy of Sciences. 2002;99(10):6955-60.
408. Kantor AB, Herzenberg LA. Origin of murine B cell lineages. Annual review of immunology. 1993;11:501-38.
409. Johnson A, Lucas D, Muthusamy N, Smith L, Edwards R, De Lay M, et al. Characterization of the TCL-1 transgenic mouse as a preclinical drug development tool for human chronic lymphocytic leukemia. Blood. 2006;108(4):1334-8.
410. Pekarsky Y, Koval A, Hallas C, Bichi R, Tresini M, Malstrom S, et al. Tcl1 enhances Akt kinase activity and mediates its nuclear translocation. Proceedings of the National Academy of Sciences. 2000;97(7):3028-33.
411. Datta SR, Dudek H, Tao X, Masters S, Fu H, Gotoh Y, et al. Akt Phosphorylation of BAD Couples Survival Signals to the Cell-Intrinsic Death Machinery. Cell. 1997;91(2):231-41.
412. Brunet A, Bonni A, Zigmond MJ, Lin MZ, Juo P, Hu LS, et al. Akt Promotes Cell Survival by Phosphorylating and Inhibiting a Forkhead Transcription Factor. Cell. 1999;96(6):857-68.
413. Zanesi N, Balatti V, Riordan J, Burch A, Rizzotto L, Palamarchuk A, et al. A Sleeping Beauty screen reveals NF-kB activation in CLL mouse model. Blood. 2013;121(21):4355-8.
414. Hewamana S, Alghazal S, Lin TT, Clement M, Jenkins C, Guzman ML, et al. The NF-κB subunit Rel A is associated with in vitro survival and clinical disease progression in chronic lymphocytic leukemia and represents a promising therapeutic target. Blood. 2008;111(9):4681-9.

415. Blunt T, Finnie NJ, Taccioli GE, Smith GC, Demengeot J, Gottlieb TM, et al. Defective DNA-dependent protein kinase activity is linked to V(D)J recombination and DNA repair defects associated with the murine scid mutation. Cell. 1995;80(5):813-23.
416. Meyerrose TE, Herrbrich P, Hess DA, Nolta JA. Immune-deficient mouse models for analysis of human stem cells. Biotechniques. 2003;35(6):1262-72.
417. Mouse strain datasheet-001303 NOD scid: The Jackson Laboratory; 2015 [02/08/2016]. Available from: https://www.jax.org/strain/001303.
418. Shultz LD, Schweitzer PA, Christianson SW, Gott B, Schweitzer IB, Tennent B, et al. Multiple defects in innate and adaptive immunologic function in NOD/LtSz-scid mice. The Journal of Immunology. 1995;154(1):180-91.
419. Ito M, Hiramatsu H, Kobayashi K, Suzue K, Kawahata M, Hioki K, et al. NOD/SCID/γc^{null} mouse: an excellent recipient mouse model for engraftment of human cells. Blood. 2002;100(9):3175-82.
420. Futrega K, Lott WB, Doran MR. Direct bone marrow HSC transplantation enhances local engraftment at the expense of systemic engraftment in NSG mice. Scientific Reports. 2016;6:23886.
421. Tentler JJ, Tan AC, Weekes CD, Jimeno A, Leong S, Pitts TM, et al. Patient-derived tumour xenografts as models for oncology drug development. Nat Rev Clin Oncol. 2012;9(6):338-50.
422. Garralda E, Paz K, López-Casas PP, Jones S, Katz A, Kann LM, et al. Integrated Next-Generation Sequencing and Avatar Mouse Models for Personalized Cancer Treatment. Clinical Cancer Research. 2014;20(9):2476-84.
423. Richmond A, Su Y. Mouse xenograft models vs GEM models for human cancer therapeutics. Disease Models & Mechanisms. 2008;1(2-3):78-82.
424. Vilches C, Castaño J, Muñoz P, Peñalver J. Simple genotyping of functional polymorphisms of the human immunoglobulin G receptors CD16A and CD32A: a reference cell panel. Tissue Antigens. 2008;71(3):242-6.
425. Böttcher S, Ritgen M, Brüggemann M, Raff T, Lüschen S, Humpe A, et al. Flow cytometric assay for determination of FcγRIIIA-158 V/F polymorphism. Journal of Immunological Methods. 2005;306(1–2):128-36.
426. Cooper MA, Fehniger TA, Caligiuri MA. The biology of human natural killer-cell subsets. Trends in Immunology. 2001;22(11):633-40.
427. Ziegler-Heitbrock L, Ancuta P, Crowe S, Dalod M, Grau V, Hart DN, et al. Nomenclature of monocytes and dendritic cells in blood. Blood. 2010;116(16):e74-e80.
428. Waibler Z, Sender LY, Merten C, Hartig R, Kliche S, Gunzer M, et al. Signaling Signatures and Functional Properties of Anti-Human CD28 Superagonistic Antibodies. PLoS ONE. 2008;3(3):e1708.
429. Chowdhury F, Williams A, Johnson P. Validation and comparison of two multiplex technologies, Luminex and Mesoscale Discovery, for human cytokine profiling. Journal of Immunological Methods. 2009;340(1):55-64.
430. Lanier LL, Le AM, Civin CI, Loken MR, Phillips JH. The relationship of CD16 (Leu-11) and Leu-19 (NKH-1) antigen expression on human peripheral blood NK cells and cytotoxic T lymphocytes. Journal of Immunology. 1986;136(12):4480-6.
431. Romee R, Foley B, Lenvik T, Wang Y, Zhang B, Ankarlo D, et al. NK cell CD16 surface expression and function is regulated by a disintegrin and metalloprotease-17 (ADAM17). Blood. 2013;121(18):3599-608.
432. Herndon TM, Pirone DM, Tsokos GC, Chen CS. T cell-to-T cell clustering enhances NF-κB activity by a PI3K signal mediated by Cbl-b and Rho. Biochemical and Biophysical Research Communications. 2005;332(4):1133-9.
433. Bartholomaeus P, Semmler LY, Bukur T, Boisguerin V, Romer PS, Tabares P, et al. Cell contact-dependent priming and Fc interaction with CD32+ immune cells contribute to the TGN1412-triggered cytokine response. The Journal of Immunology. 2014;192(5):2091-8.

434. White AL, Chan HTC, Roghanian A, French RR, Mockridge CI, Tutt AL, et al. Interaction with FcγRIIB Is Critical for the Agonistic Activity of Anti-CD40 Monoclonal Antibody. The Journal of Immunology. 2011;187(4):1754-63.
435. Larkin MA, Blackshields G, Brown NP, Chenna R, McGettigan PA, McWilliam H, et al. Clustal W and Clustal X version 2.0. Bioinformatics. 2007;23(21):2947-8.
436. Ebert EC, Roberts AI. Costimulation of the CD3 Pathway by CD28 Ligation in Human Intestinal Lymphocytes. Cellular Immunology. 1996;171(2):211-6.
437. Geppert TD, Lipsky PE. Activation of T lymphocytes by immobilized monoclonal antibodies to CD3. Regulatory influences of monoclonal antibodies to additional T cell surface determinants. Journal of Clinical Investigation. 1988;81(5):1497-505.
438. Ceuppens JL, Bloemmen FJ, Van Wauwe JP. T cell unresponsiveness to the mitogenic activity of OKT3 antibody results from a deficiency of monocyte Fc gamma receptors for murine IgG2a and inability to cross-link the T3-Ti complex. The Journal of Immunology. 1985;135(6):3882-6.
439. Notter M, Ludwig W, Bremer S, Thiel E. Selective targeting of human lymphokine-activated killer cells by CD3 monoclonal antibody against the interferon-inducible high-affinity Fc gamma RI receptor (CD64) on autologous acute myeloid leukemic blast cells. Blood. 1993;82(10):3113-24.
440. Wing MG, Moreau T, Greenwood J, Smith RM, Hale G, Isaacs J, et al. Mechanism of first-dose cytokine-release syndrome by CAMPATH 1-H: involvement of CD16 (FcgammaRIII) and CD11a/CD18 (LFA-1) on NK cells. Journal of Clinical Investigation. 1996;98(12):2819-26.
441. Hu Y, Turner MJ, Shields J, Gale MS, Hutto E, Roberts BL, et al. Investigation of the mechanism of action of alemtuzumab in a human CD52 transgenic mouse model. Immunology. 2009;128(2):260-70.
442. Sancéau J, Falcoff R, Beranger F, Carter DB, Wietzerbin J. Secretion of interleukin-6 (IL-6) by human monocytes stimulated by muramyl dipeptide and tumour necrosis factor alpha. Immunology. 1990;69(1):52-6.
443. Budde P, Bewarder N, Weinrich V, Schulzeck O, Frey J. Tyrosine-containing sequence motifs of the human immunoglobulin G receptors FcRIIb1 and FcRIIb2 essential for endocytosis and regulation of calcium flux in B cells. Journal of Biological Chemistry. 1994;269(48):30636-44.
444. ATCC-Ramos datasheet [cited 2016 19/8/2016]. Available from: https://www.lgcstandards-atcc.org/Products/All/CRL-1596.aspx.
445. ATCC - Raji datasheet [cited 2016 19/08/2016]. Available from: https://www.lgcstandards-atcc.org/Products/All/CCL-86.aspx.
446. Heider K-H, Kiefer K, Zenz T, Volden M, Stilgenbauer S, Ostermann E, et al. A novel Fc-engineered monoclonal antibody to CD37 with enhanced ADCC and high proapoptotic activity for treatment of B-cell malignancies. Blood. 2011;118(15):4159-68.
447. Chen D, Frezza M, Schmitt S, Kanwar J, Dou QP. Bortezomib as the First Proteasome Inhibitor Anticancer Drug: Current Status and Future Perspectives. Current Cancer Drug Targets. 2011;11(3):239-53.
448. Adams J, Palombella VJ, Sausville EA, Johnson J, Destree A, Lazarus DD, et al. Proteasome inhibitors: a novel class of potent and effective antitumor agents. Cancer Research. 1999;59(11):2615-22.
449. Kikuchi J, Takashina T, Kinoshita I, Kikuchi E, Shimizu Y, Sakakibara-Konishi J, et al. Epigenetic therapy with 3-deazaneplanocin A, an inhibitor of the histone methyltransferase EZH2, inhibits growth of non-small cell lung cancer cells. Lung Cancer. 2012;78(2):138-43.
450. Jones PA, Taylor SM. Cellular differentiation, cytidine analogs and DNA methylation. Cell. 1980;20(1):85-93.
451. Stresemann C, Lyko F. Modes of action of the DNA methyltransferase inhibitors azacytidine and decitabine. International Journal of Cancer. 2008;123(1):8-13.

452. Bonvini P, Zorzi E, Basso G, Rosolen A. Bortezomib-mediated 26S proteasome inhibition causes cell-cycle arrest and induces apoptosis in CD-30+ anaplastic large cell lymphoma. Leukemia. 2007;21(4):838-42.
453. Cooper GM. The Cell - A Molecular Approach 2nd Edition: Sunderland (MA): Sinauer Associates; 2000.
454. Blank M, Stefanescu R, Masuda E, Marti F, King P, Redecha P, et al. Decreased transcription of the human FCGR2B gene mediated by the -343 G/C promoter polymorphism and association with systemic lupus erythematosus. Human Genetics. 2005;117(2-3):220-7.
455. Nishimura T, Narita T, Miyazaki E, Ito T, Nishimoto N, Yoshizaki K, et al. Characterization of the human FcγRIIB gene promoter: human zinc-finger proteins (ZNF140 and ZNF91) that bind to different regions function as transcription repressors. International Immunology. 2001;13(8):1075-84.
456. Yusufzai TM, Tagami H, Nakatani Y, Felsenfeld G. CTCF Tethers an Insulator to Subnuclear Sites, Suggesting Shared Insulator Mechanisms across Species. Molecular Cell. 2004;13(2):291-8.
457. Phillips JE, Corces VG. CTCF: Master Weaver of the Genome. Cell. 2009;137(7):1194-211.
458. Oti M, Falck J, Huynen MA, Zhou H. CTCF-mediated chromatin loops enclose inducible gene regulatory domains. BMC Genomics. 2016;17(1):1-16.
459. Santi DV, Norment A, Garrett CE. Covalent bond formation between a DNA-cytosine methyltransferase and DNA containing 5-azacytosine. Proceedings of the National Academy of Sciences. 1984;81(22):6993-7.
460. Goll MG, Bestor TH. Eukaryotic cytosine methyltransferases. Annual Review of Biochemistry. 2005;74(1):481-514.
461. Kiziltepe T, Hideshima T, Catley L, Raje N, Yasui H, Shiraishi N, et al. 5-Azacytidine, a DNA methyltransferase inhibitor, induces ATR-mediated DNA double-strand break responses, apoptosis, and synergistic cytotoxicity with doxorubicin and bortezomib against multiple myeloma cells. American Association for Cancer Research. 2007;6(6):1718-27.
462. Miranda TB, Cortez CC, Yoo CB, Liang G, Abe M, Kelly TK, et al. DZNep is a global histone methylation inhibitor that reactivates developmental genes not silenced by DNA methylation. American Association for Cancer Research. 2009;8(6):1579-88.
463. Venkatesh S, Workman JL. Histone exchange, chromatin structure and the regulation of transcription. Nat Rev Mol Cell Biol. 2015;16(3):178-89.
464. Grunstein M. Histone acetylation in chromatin structure and transcription. Nature. 1997;389(6649):349-52.
465. Kuo M-H, Allis CD. Roles of histone acetyltransferases and deacetylases in gene regulation. BioEssays. 1998;20(8):615-26.
466. Greer WL, Lee CLY, Callanan MB, Zayed E, Sadek I. Case of acute lymphoblastic leukemia presenting with t(14;18)/BCL2, t(8;14)/cMYC, and t(1;2)/FCGR2B. American Journal of Hematology. 2003;74(2):112-8.
467. Chen W, Palanisamy N, Schmidt H, Teruya-Feldstein J, Jhanwar SC, Zelenetz AD, et al. Deregulation of FCGR2B expression by 1q21 rearrangements in follicular lymphomas. Oncogene. 2001;20(52):7686-93.
468. Ambros V. The functions of animal microRNAs. Nature. 2004;431(7006):350-5.
469. Pedersen JS, Bejerano G, Siepel A, Rosenbloom K, Lindblad-Toh K, Lander ES, et al. Identification and Classification of Conserved RNA Secondary Structures in the Human Genome. PLOS Computational Biology. 2006;2(4):e33.
470. Chen C, Zhang H, Broitman SL, Reiche M, Farrell I, Cooperman BS, et al. Dynamics of translation by single ribosomes through mRNA secondary structures. Nat Struct Mol Biol. 2013;20(5):582-8.

471. Grillo-Lopez AJ, White CA, Varns C, Shen D, Wei A, McClure A, et al. Overview of the clinical development of rituximab: first monoclonal antibody approved for the treatment of lymphoma. Seminars in Oncology. 1999;26(5 Suppl 14):66-73.
472. National Cancer Institute - Idelalisib [updated 26/09/2016; cited 2016 17/08/2016]. Available from: http://www.cancer.gov/about-cancer/treatment/drugs/idelalisib.
473. Grillo-López AJ. Zevalin: the first radioimmunotherapy approved for the treatment of lymphoma. Expert Review of Anticancer Therapy. 2002;2(5):485-93.
474. Mentrik Biotech AME-133v pipeline [17/08/2016]. Available from: http://mentrik.com/.
475. U.S. FDA grants Breakthrough Therapy Designation for Roche's investigational medicine ocrelizumab in primary progressive multiple sclerosis 2016 [17/08/2016]. Available from: http://www.roche.com/investors/updates/inv-update-2016-02-17.htm.
476. Immunomedics - Veltuzumab pipeline [17/08/2016]. Available from: http://www.immunomedics.com/veltuzumab.shtml.
477. Hamblin TJ. The TCL1 mouse as a model for chronic lymphocytic leukemia. Leukemia Research. 2010;34(2):135-6.
478. Dighiero G, Hamblin TJ. Chronic lymphocytic leukaemia. The Lancet. 2008;371(9617):1017-29.
479. Herling M, Patel KA, Khalili J, Schlette E, Kobayashi R, Medeiros LJ, et al. TCL1 shows a regulated expression pattern in chronic lymphocytic leukemia that correlates with molecular subtypes and proliferative state. Leukemia. 2005;20(2):280-5.
480. Laine J, Künstle G, Obata T, Sha M, Noguchi M. The Protooncogene TCL1 Is an Akt Kinase Coactivator. Molecular Cell. 2000;6(2):395-407.
481. Shultz LD, Ishikawa F, Greiner DL. Humanized mice in translational biomedical research. Nature Reviews Immunology. 2007;7(2):118-30.
482. Mathas S, Rickers A, Bommert K, Dörken B, Mapara MY. Anti-CD20- and B-cell Receptor-mediated Apoptosis: Evidence for Shared Intracellular Signaling Pathways. Cancer Research. 2000;60(24):7170-6.
483. Hauptrock B, Hess G. Rituximab in the treatment of non-Hodgkin's lymphoma. Biologics : Targets & Therapy. 2008;2(4):619-33.
484. Czuczman MS, Weaver R, Alkuzweny B, Berlfein J, Grillo-López AJ. Prolonged Clinical and Molecular Remission in Patients With Low-Grade or Follicular Non-Hodgkin's Lymphoma Treated With Rituximab Plus CHOP Chemotherapy: 9-Year Follow-Up. Journal of Clinical Oncology. 2004;22(23):4711-6.
485. Shugg RPP, Thomson A, Tanabe N, Kashishian A, Steiner BH, Puri KD, et al. Effects of Isoform-selective Phosphatidylinositol 3-Kinase Inhibitors on Osteoclasts: ACTIONS ON CYTOSKELETAL ORGANIZATION, SURVIVAL, AND RESORPTION. Journal of Biological Chemistry. 2013;288(49):35346-57.
486. Fiorcari S, Brown WS, McIntyre BW, Estrov Z, Maffei R, O'Brien S, et al. The PI3-Kinase Delta Inhibitor Idelalisib (GS-1101) Targets Integrin-Mediated Adhesion of Chronic Lymphocytic Leukemia (CLL) Cell to Endothelial and Marrow Stromal Cells. PLoS ONE. 2013;8(12):e83830.
487. O'Brien S, Lamanna N, Kipps TJ, Flinn IW, Zelenetz AD, Burger JA, et al. Update on a Phase 2 Study of Idelalisib in Combination with Rituximab in Treatment-Naïve Patients ≥65 Years with Chronic Lymphocytic Leukemia (CLL) or Small Lymphocytic Lymphoma (SLL). 56th ASH Annual Meeting and Exposition; 2014-12-06 2014. p. 1994.
488. Shultz LD, Lyons BL, Burzenski LM, Gott B, Chen X, Chaleff S, et al. Human Lymphoid and Myeloid Cell Development in NOD/LtSz-scid IL2Rγnull Mice Engrafted with Mobilized Human Hemopoietic Stem Cells. The Journal of Immunology. 2005;174(10):6477-89.
489. Wunderlich M, Chou FS, Link KA, Mizukawa B, Perry RL, Carroll M, et al. AML xenograft efficiency is significantly improved in NOD/SCID-IL2RG mice constitutively expressing human SCF, GM-CSF and IL-3. Leukemia. 2010;24(10):1785-8.

490. Kuo TT, Baker K, Yoshida M, Qiao SW, Aveson VG, Lencer WI, et al. Neonatal Fc receptor: from immunity to therapeutics. J Clin Immunol. 2010;30(6):777-89.
491. Ober RJ, Radu CG, Ghetie V, Ward ES. Differences in promiscuity for antibody–FcRn interactions across species: implications for therapeutic antibodies. International Immunology. 2001;13(12):1551-9.
492. Pop L, Liu X-y, Pop I, Vitetta E. Abnormally short serum half-lives of chimeric and human IgGs in NOD-SCID mice (P4184). The Journal of Immunology. 2013;190(1 Supplement):48.2.
493. Nimmerjahn F, Ravetch JV. Divergent Immunoglobulin G Subclass Activity Through Selective Fc Receptor Binding. Science. 2005;310(5753):1510-2.
494. Overdijk MB, Verploegen S, Ortiz Buijsse A, Vink T, Leusen JH, Bleeker WK, et al. Crosstalk between human IgG isotypes and murine effector cells. The Journal of Immunology. 2012;189(7):3430-8.
495. Oganesyan V, Damschroder MM, Cook KE, Li Q, Gao C, Wu H, et al. Structural Insights into Neonatal Fc Receptor-based Recycling Mechanisms. Journal of Biological Chemistry. 2014;289(11):7812-24.
496. Shields RL, Namenuk AK, Hong K, Meng YG, Rae J, Briggs J, et al. High Resolution Mapping of the Binding Site on Human IgG1 for FcγRI, FcγRII, FcγRIII, and FcRn and Design of IgG1 Variants with Improved Binding to the FcγR. Journal of Biological Chemistry. 2001;276(9):6591-604.
497. Ramsland PA, Farrugia W, Bradford TM, Sardjono CT, Esparon S, Trist HM, et al. Structural basis for Fc gammaRIIa recognition of human IgG and formation of inflammatory signaling complexes. The Journal of Immunology. 2011;187(6):3208-17.
498. Neuber T, Frese K, Jaehrling J, Jäger S, Daubert D, Felderer K, et al. Characterization and screening of IgG binding to the neonatal Fc receptor. mAbs. 2014;6(4):928-42.
499. Nagelkerke SQ, Dekkers G, Kustiawan I, van de Bovenkamp FS, Geissler J, Plomp R, et al. Inhibition of FcγR-mediated phagocytosis by IVIg is independent of IgG-Fc sialylation and FcγRIIb in human macrophages. Blood. 2014;124(25):3709-18.
500. Nagelkerke SQ, Kuijpers TW. Immunomodulation by IVIg and the Role of Fc-Gamma Receptors: Classic Mechanisms of Action after all? Frontiers in Immunology. 2014;5:674.
501. Yang J, Zhang L, Yu C, Yang X-F, Wang H. Monocyte and macrophage differentiation: circulation inflammatory monocyte as biomarker for inflammatory diseases. Biomarker Research. 2014;2:1-.
502. Geissmann F, Jung S, Littman DR. Blood Monocytes Consist of Two Principal Subsets with Distinct Migratory Properties. Immunity. 2003;19(1):71-82.
503. Auffray C, Fogg D, Garfa M, Elain G, Join-Lambert O, Kayal S, et al. Monitoring of blood vessels and tissues by a population of monocytes with patrolling behavior. Science. 2007;317(5838):666-70.
504. Prins J, Todd J, Rodrigues N, Ghosh S, Hogarth P, Wicker L, et al. Linkage on chromosome 3 of autoimmune diabetes and defective Fc receptor for IgG in NOD mice. Science. 1993;260(5108):695-8.
505. Gavin AL, Leiter EH, Hogarth PM. Mouse FcgammaRI: identification and functional characterization of five new alleles. Immunogenetics. 2000;51(3):206-11.
506. Gavin AL, Tan PS, Hogarth PM. Gain-of-function mutations in FcgammaRI of NOD mice: implications for the evolution of the Ig superfamily. The EMBO Journal. 1998;17(14):3850-7.
507. Pritchard NR, Cutler AJ, Uribe S, Chadban SJ, Morley BJ, Smith KGC. Autoimmune-prone mice share a promoter haplotype associated with reduced expression and function of the Fc receptor FcγRII. Current Biology. 2000;10(4):227-30.
508. Hibbs ML, Hogarth PM, McKenzie IF. The mouse Ly-17 locus identifies a polymorphism of the Fc receptor. Immunogenetics. 1985;22(4):335-48.

509. Holmes KL, Palfree RG, Hammerling U, Morse HC, 3rd. Alleles of the Ly-17 alloantigen define polymorphisms of the murine IgG Fc receptor. Proceedings of the National Academy of Sciences. 1985;82(22):7706-10.
510. Slingsby JH, Hogarth MB, Walport MJ, Morley BJ. Polymorphism in the Ly-17 alloantigenic system of the mouse FcgRII gene. Immunogenetics. 1997;46(4):361-2.
511. Schwab I, Nimmerjahn F. Intravenous immunoglobulin therapy: how does IgG modulate the immune system? Nature Reviews Immunology. 2013;13(3):176-89.
512. Gelfand EW. Differences between IGIV products: Impact on clinical outcome. International Immunopharmacology. 2006;6(4):592-9.
513. Kelley LA, Mezulis S, Yates CM, Wass MN, Sternberg MJ. The Phyre2 web portal for protein modeling, prediction and analysis. Nature Protocols. 2015;10(6):845-58.
514. Higurashi M, Ishida T, Kinoshita K. PiSite: a database of protein interaction sites using multiple binding states in the PDB. Nucleic Acids Research. 2009;37(suppl 1):D360-D4.
515. Chao MP, Alizadeh AA, Tang C, Myklebust JH, Varghese B, Gill S, et al. Anti-CD47 antibody synergizes with rituximab to promote phagocytosis and eradicate non-Hodgkin lymphoma. Cell. 2010;142(5):699-713.
516. Wilson NS, Yang B, Yang A, Loeser S, Marsters S, Lawrence D, et al. An Fcgamma receptor-dependent mechanism drives antibody-mediated target-receptor signaling in cancer cells. Cancer Cell. 2011;19(1):101-13.
517. Tyrsin D, Chuvpilo S, Matskevich A, Nemenov D, Romer PS, Tabares P, et al. From TGN1412 to TAB08: the return of CD28 superagonist therapy to clinical development for the treatment of rheumatoid arthritis. Clinical and experimental rheumatology. 2016;34(4 Suppl 98):45-8.
518. Hayes JM, Cosgrave EF, Struwe WB, Wormald M, Davey GP, Jefferis R, et al. Glycosylation and Fc receptors. Current topics in microbiology and immunology. 2014;382:165-99.
519. Ferrara C, Grau S, Jager C, Sondermann P, Brunker P, Waldhauer I, et al. Unique carbohydrate-carbohydrate interactions are required for high affinity binding between FcgammaRIII and antibodies lacking core fucose. Proceedings of the National Academy of Sciences. 2011;108(31):12669-74.
520. Zeck A, Pohlentz G, Schlothauer T, Peter-Katalinić J, Regula JT. Cell Type-Specific and Site Directed N-Glycosylation Pattern of FcγRIIIa. Journal of Proteome Research. 2011;10(7):3031-9.
521. Callanan MB, Le Baccon P, Mossuz P, Duley S, Bastard C, Hamoudi R, et al. The IgG Fc receptor, FcγRIIB, is a target for deregulation by chromosomal translocation in malignant lymphoma. Proceedings of the National Academy of Sciences. 2000;97(1):309-14.
522. Moreno-Fierros L, Verdin-Teran SL, Garcia-Hernandez AL. Intraperitoneal Immunization with Cry1Ac Protoxin from Bacillus thuringiensis Provokes Upregulation of Fc-Gamma-II/and Fc-Gamma-III Receptors Associated with IgG in the Intestinal Epithelium of Mice. Scandinavian journal of immunology. 2015;82(1):35-47.
523. Ganesan LP, Kim J, Wu Y, Mohanty S, Phillips GS, Birmingham DJ, et al. FcγRIIb on Liver Sinusoidal Endothelium Clears Small Immune Complexes. The Journal of Immunology. 2012.
524. Li F, Ravetch JV. Apoptotic and antitumor activity of death receptor antibodies require inhibitory Fcγ receptor engagement. Proceedings of the National Academy of Sciences. 2012;109(27):10966-71.
525. Mangsbo SM, Broos S, Fletcher E, Veitonmaki N, Furebring C, Dahlen E, et al. The human agonistic CD40 antibody ADC-1013 eradicates bladder tumors and generates T-cell-dependent tumor immunity. Clinical Cancer Research. 2015;21(5):1115-26.
526. Vugmeyster Y, Howell K. Rituximab-mediated depletion of cynomolgus monkey B cells in vitro in different matrices: possible inhibitory effect of IgG. International Immunopharmacology. 2004;4(8):1117-24.

527. Preithner S, Elm S, Lippold S, Locher M, Wolf A, Silva AJd, et al. High concentrations of therapeutic IgG1 antibodies are needed to compensate for inhibition of antibody-dependent cellular cytotoxicity by excess endogenous immunoglobulin G. Molecular Immunology. 2006;43(8):1183-93.
528. Iida S, Misaka H, Inoue M, Shibata M, Nakano R, Yamane-Ohnuki N, et al. Nonfucosylated Therapeutic IgG1 Antibody Can Evade the Inhibitory Effect of Serum Immunoglobulin G on Antibody-Dependent Cellular Cytotoxicity through its High Binding to FcγRIIIa. Clinical Cancer Research. 2006;12(9):2879-87.